Factorization and Precision Calculations in Particle Physics

Factorization and Precision Calculations in Particle Physics

A thesis presented

by

Ilya Eric Alexander Feige

to

The Department of Physics

in partial fulfillment of the requirements

for the degree of

Doctor of Philosophy

in the subject of

Physics

Harvard University

Cambridge, Massachusetts

March 2015

Thesis advisor

Matthew D. Schwartz

Author

Ilya Eric Alexander Feige

Factorization and Precision Calculations in Particle Physics

Abstract

We state and prove to all orders in perturbation theory a factorization theorem in Quantum Chromodynamics that concisely describes the separation of the physics associated with jet formation from that associated with the hard-scattering in high-energy particle collisions. We show how the factorization theorem, which provides an equality between amplitudes in gauge theories, can be readily applied to precision calculations of cross-sections. In the resulting factorized cross sections, the components relevant to jet production are universal and perturbatively calculable. Their renormalization group evolution can be used to sum large logarithms of scale ratios to all orders in perturbation theory, thus enabling quantitive predictions in the regime of disparate scales relevant to many important collider-physics observables. As an application, we calculate the observable 2-subjettiness at next-to-next-to-next-to-leading-logarithmic order for the decay of boosted heavy color-singlet particles such as Electroweak bosons. Our calculation is the first analytic calculation of a jet substructure observable.

Contents

Citations to previously published work

Parts of this dissertation cover research reported in the following articles:

1. "Removing phase-space restrictions in factorized cross sections," I. Feige, M.D.. Schwartz and K. Yan. accepted *Phys.Rev.* **D** (2015)

2. "Hard-Soft-Collinear Factorization to All Orders," I. Feige and M.D. Schwartz. *Phys.Rev.* **D90**, no. 10 (2014) 105020

3. "An on-shell approach to factorization," I. Feige and M.D. Schwartz. *Phys.Rev.* **D88**, no. 6 (2013) 065021

4. "Precision Jet Substructure from Boosted Event Shapes," I. Feige, M.D. Schwartz, I. W. Stewart, and J. Thaler. *Phys.Rev.Lett.* **109** (2012) 092001

Acknowledgments

The past four and a half years at Harvard have been formative and incredibly enjoyable. My PhD research was, for me, the perfect blend of formal and applied questions that were compellingly topical in particle physics. For that I would like to thank my advisor, Matt Schwartz. The work that we did together was always at the right level for me, from my wonderfully clean and simple first project on jet substructure to the wide-open saga of all-orders factorization proofs that eventually followed. Matt spent a great deal of one-on-one time with me, from which I learned above all how to think about physics problems.

I learned a great deal from my colleagues, most of which were fellow grad students. David Farhi was always a great sounding board for ideas in research and in classes. Yang-Ting Chien helped me learn Soft-Collinear Effective Theory. Eric Kramer was a great translator from Weinberg to English. Peter Komar and Debanjan Chowdhury were excellent classmates to work with early on in my PhD. Working with these people, among others, during my PhD was a pleasure, and I am grateful for it.

Finally, I would like to thank my wife, Lauren Forbes, who perhaps contributed the most to my PhD by being a pillar of virtue and support for me every single day.

Acknowledgements of Financial Support

This thesis is based on work funded by NSERC, both PGS M and PGS D fellowships, by the Center for the Fundamental Laws of Nature at Harvard University and by Matthew D. Schwartz' grant DE-SC003916 from the Department of Energy.

May we always be curious.

Chapter 1

Introduction

1.1 What is particle physics?

We begin by putting particle physics into the broader picture of science as a whole. Science is the body of knowledge that predicts observations we have made in our natural world. The boundary can be drawn through the concept of prediction, often referred to as the scientific method; objective observations that cannot be objectively predicted are not part of the body of science, though eventually they may be. This definition of science is intentionally human, as we cannot describe observations without existing.

Science can be subdivided in many ways. Since this thesis concerns high-energy particle physics, the most natural way to break science down is into the energy scales at which different phenomena take place. For example, many biological processes in humans take place around body temperature, which is on the order of tens of milli-electronvolts (meV). In Figure 1.1 some fundamental energy scales in science

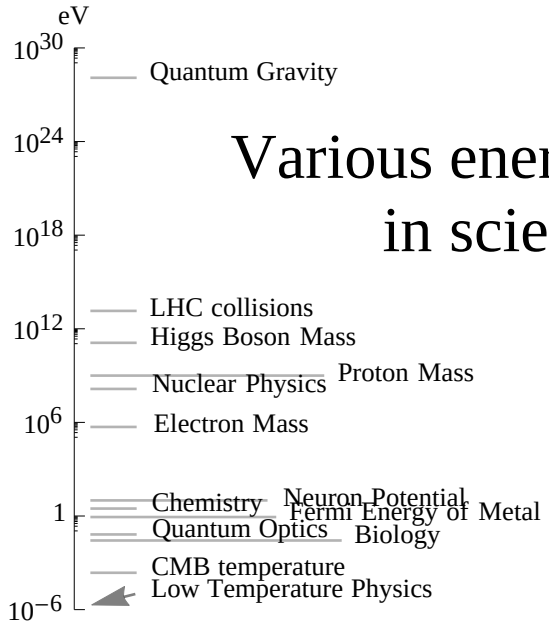

Figure 1.1: A depiction of some interesting energy scales in science

are displayed. There are many important fields of science near the biological energy scale, since this is not only important to human medicine and technology, but also because the environment in which we live must be sufficiently complex at these energy scales in order to support large-scale life.

Particle physics, or high-energy physics, is the study of phenomena that take place in nature at energies larger than approximately the electron mass, shown in Figure 1.1. Alternatively stated, these are phenomena that take place over distance scales less than around 10^{-13} meters. The incredible thing about particle physics is that our model, known as the Standard Model, is consistent with all measured phenomena on Earth. It predicts all of the non-collective phenomena that take place in our experiments probing energies from the mass of the Electron up to the highest-ever energy experiment, the Large Hadron Collider (LHC). Moreover, these predictions are made to some of the highest degree of accuracy ever achieved in science. There are

observations of phenomena in the universe that the Standard Model does not describe, most notable Dark Matter, which is an active subfield of particle physics. However, in this thesis, we will focus on direct observations produced by experiments on Earth, meaning particle collider experiments.

Though the Standard Model of particle physics seems to be consistent with observations that involve collective phenomena, like in condensed matter physics, chemistry and biology, it is impossible to use it to predict the observations in these regimes. Unfortunately for particle physics, it is these low-energy collective phenomena that are most interesting to humans, since they are most relevant to medicine and technology which are what drives our ever-increasing standards of living.

Therefore, particle physics should be thought of as the study of high-energy physics that involves only a few degrees of freedom, namely particles, at a time. The framework of particle physics and the Standard Model itself are beautiful and robust theories that describe the most fundamental and the simplest systems to incredible accuracy.

1.2 What is important in particle physics?

The landscape of particle physics at present is that the Standard Model predicts all of the direct observations that are made in collider-physics experiments. This has only been the case for about the last two years. The highly anticipated final piece of the Standard Model, the Higgs Boson, was discovered in 2012 at the LHC [1, 2]. The discovery resulted in the 2013 Nobel Prize in Physics being awarded to Peter Higgs and Francois Englert for their contribution to the development of the theoretical

underpinnings of the Higgs boson.

Since then, particle physics at colliders has been focused on precision measurements of components of the Standard Model as well as the search for new physics beyond the Standard Model. In the latter case, the new physics could be seen in clean channels, such as those with leptons in their final states, which are easy to identify with certainty. Or, it could manifest itself in messy channels, such as those with jets from Quantum Chromodynamics (QCD), a subset of the Standard Model. Measurements in the messy channels are much more inconclusive and require many more measurements to make a confident conclusion, if one can be made at all. To date, no new physics has been found in the so-called clean channels, forcing us to study the messy channels, which by virtue of their messiness, require precision measurements for discoveries to be made. Consequently, precision measurements have become a necessity for new physics searches as well as for improving our understanding of the Standard Model.

To understand precision measurements involving QCD processes in colliders, precision calculations of such processes are required. Therefore, precision calculations in QCD are critical to the advancement of particle collider physics, and are the topic of this thesis.

1.3 How to do precision calculations in QCD

Precision calculations in physics are often difficult because the easy calculations are all done and therefore, not considered precision calculations. This is true in QCD as well. However, there is another reason that precision calculations in QCD

are hard: QCD is a confining theory. That is, at low enough energy scales, around $\Lambda_{\text{QCD}} \sim 200$ MeV, the coupling constant of QCD, $\alpha_s(\mu)$, diverges and perturbation theory is no longer applicable to calculations. This is the statement of Asymptotic Freedom; alternatively said, at high energies the coupling constant asymptotically vanishes. So, we can do perturbation theory in QCD at high energies but not at low energies.

So why not just do experiments at high energies where the coupling constant is always a small parameter? The reason is that we live in a low-energy world. At the LHC, protons are taken from a little bottle of hydrogen and then accelerated to the highest energies ever achieved in a laboratory. When two protons collide, quarks and gluons go from a confined state within the proton to a high-energy free state during the scattering and then they confine again as they travel over long distances and are detected. Thus, any calculation that describes QCD processes in colliders must deal with a large range of energies over which perturbation theory does not always work.

Moreover, in between the confinement energy, Λ_{QCD}, and the hard-scattering energy, Q, the process of jet production occurs. Jets are collimated streams of particles originating from a single high-energy particle due to the collinear structure of QCD. A multi-jet event, as measured by the CMS detector, is shown in Figure 1.2 where each jet is composed of many different particle tracks, shown in green. Jet production involves intermediate scales, $\Lambda_{\text{QCD}} \ll \mu_{\text{jet}} \ll Q$, where the coupling constant is still small, but large logarithms of ratios of scales destroy the convergence of perturbation theory. That is:

$$\alpha_s(\mu_{\text{jet}}) \ll 1 \qquad \text{but} \qquad \alpha_s(\mu_{\text{jet}}) \log^2 \frac{\mu_{\text{jet}}}{Q} \sim \mathcal{O}(1) \tag{1.1}$$

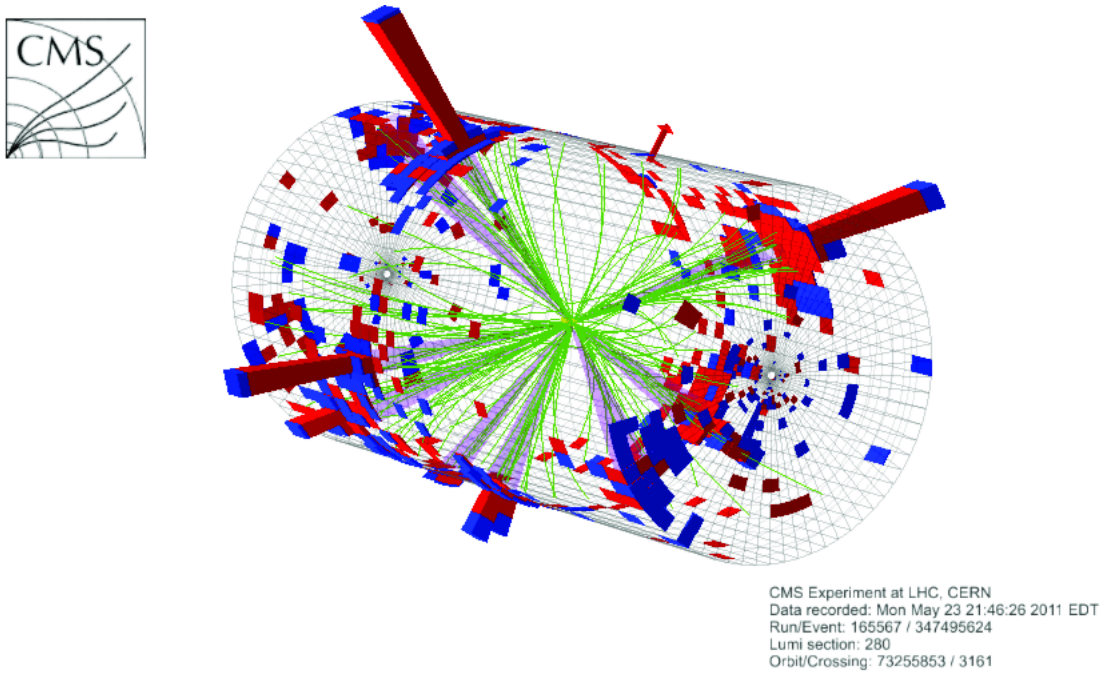

Figure 1.2: A proton-proton collision as seen by the CMS detector at the Large Hadron Collider. Image courtesy of CERN.

and the expansion of a cross section schematically might look like:

$$\sigma = 1 + \underbrace{\alpha_s(\mu_{\text{jet}})\, \log^2 \frac{\mu_{\text{jet}}}{Q}}_{\mathcal{O}(1)} + \underbrace{\alpha_s^2(\mu_{\text{jet}})\, \log^4 \frac{\mu_{\text{jet}}}{Q}}_{\mathcal{O}(1)} + \underbrace{\ldots}_{\mathcal{O}(1)} \tag{1.2}$$

Consequently a calculation at any fixed order in perturbation theory will not be a good approximation to the entire sum.

Both the problem of confinement (large coupling constant, α_s, at low energies) and the problem of large logarithms in collider physics observables can be solved by *factorization*. Factorization is the general idea that physics at one scale decouples from physics at another, much different scale. For example, to solve the Hydrogen atom in quantum mechanics, one does not need to model the dynamics of the quarks and gluons inside the proton. Instead, the proton can be treated as a static, point

charge. This is justified by the fact that the electronic energy scales in the hydrogen atom are around the Rydberg energy, -13.6 eV, which corresponds to approximately the size of the hydrogen atom, namely, $\sim 10^{-8}$ m. On the other hand the energy scale of the dynamics of the proton is around $\Lambda_{\rm QCD} \sim 200$ MeV or $\sim 10^{-15}$ m. So the electron in the hydrogen atom sees none of the structure of the proton, only its net charge. Thus, the dynamics of the electron in a Hydrogen atom and the quarks and gluons inside the proton factorize, and can be describe independently from each other.

Factorization solves the problem of confinement by stating that the confining physics does not influence the high-energy scattering, namely the two are factorized. The most common example of this is the statement that the probability to get a certain high-energy scattering event in proton-proton collisions is equal to the probability of the high-energy scattering on its own, times the probability that a particle came out of the proton to take part in the scattering. For example, if the two protons have momentum P_1 and P_2 and we are trying to calculate the probability that a pair of leptons, Y, will be produced along with some unmeasured QCD particles, X, we would write this as:

$$\sigma\big(p(P_1)+p(P_2)\to Y+X\big) = \int_0^1 dx_1\, dx_2 \sum_i f_i(x_1)\, f_{\bar{i}}(x_2)\, \hat{\sigma}\big(q_i(x_1P_1)+\bar{q}_i(x_2P_2)\to Y\big) \tag{1.3}$$

where $f_i(x)$ is the Parton Distribution Function (PDF) for producing a quark of flavor i and momentum fraction x out of the proton. In Eq. (1.3), $\hat{\sigma}$ is the parton-level cross-section for the process of quark-anti-quark annihilation to Y; it represents the high-energy process and is perturbatively calculable. The PDFs are not calculable

because of the large coupling constant at the energy scales of the proton, however, they are universal functions which can be measured in one process and used to predict any other.

The factorization of non-perturbative physics from perturbative physics, as outlined in the previous paragraph, is critical to our ability to make theoretical predictions at hadron colliders. It is also much more difficult to prove rigorously, since we have little handle on the objects involved because they are not amenable to a perturbative analysis. In this thesis, we will focus on the second type of factorization needed for precision collider-physics calculations. Namely, the factorization of jet production from the underlying hard process. This factorization also gives rise to universal functions which describe the soft and collinear physics associated with jet production. However, in this case they are perturbatively calculable and can be used to sum the large logarithms described in Eq. (1.2) to all orders in α_s. Thus, factorization renders the perturbative expansion convergent and makes precision QCD in collider physics possible.

1.4 Outline

This thesis is organized as follows. We begin the discussion of factorization in Ch. 2 where we provide a precise statement of factorization with any number of particles and prove it at tree-level in perturbation theory. The discussion at tree level is simple enough to understand how the main arguments work without the quagmire of making all-loop-order arguments. Ch. 2 closely follows the author and collaborators' paper [3]. In Ch. 3, we augment the arguments of Ch. 2 into an all-orders

proof of factorization. Some new pieces arise at loop level that modify the statement of factorization in Ch. 2, which are discussed in detail. As a consequence of our general proof, this chapter provides a first proof of the all-orders universality of the so-called collinear splitting functions and the soft current. Ch. 3 closely follows [4], a paper by the author and collaborators. With factorization proved at the amplitude level in Chs. 2 and 3, we turn to the structure of factorized cross sections in Ch. 4. In this chapter, which follows the author and collaborators' paper [5], we see that a phase-space subtraction procedure is required to fully exploit the simplifications of the amplitude-level factorization formulas at the cross-section level. Then, in Ch. 5 we make use of factorization to carry out the first analytic calculation of a jet-substructure observable. In particular, we calculate 2-subjettiness for massive color-singlet decays and compare the result to simulation. This chapter follows the author and collaborators' paper [6]. Finally, we provide our conclusions in Ch. 6.

Chapter 2

Tree-level factorization for e^+e^- annihilation

2.1 Introduction

That perturbative calculations in a strongly coupled theory like quantum chromodynamics (QCD) can ever be related to experimental data is due to two remarkable properties: asymptotic freedom and factorization. Of these, asymptotic freedom is much better understood. Indeed, the asymptotic behavior of a theory can usually be established from the ultraviolet divergences in 1-loop amplitudes. It is a short distance property. Factorization, on the other hand, is a long-distance property. In its most intuitive, and most useful form, factorization states that cross sections in QCD can be calculated up to power corrections in some small scale λ by convolutions of universal (and often nonperturbative) objects, such as parton-distribution functions, and perturbative, but process-dependent matrix elements.

There are both nonperturbative and pertubative aspects to factorization. On the nonperturbative side, one would ideally like to prove that factorization holds up to corrections in $\lambda = m_P/Q$ with m_P the proton (or some other particle) mass and $Q \gg m_P$ some high-energy scale. Unfortunately, to have access to m_P, which is a nonperturbative quantity in QCD, one needs access to nonperturbative physics. Instead, most approaches to factorization simply assume that operator matrix elements in hadronic states, and final-state hadronization effects, do not violate naive scaling expectations. Then they use perturbation theory and scaling arguments to relate those matrix elements among different processes. The most familiar example of this approach is the universality of the parton distribution functions (PDFs). Factorization implies (or should imply, if it were proven generally) that the same operator matrix elements representing the PDFs appear in the calculation of a great variety of physical processes. Since a preponderance of experimental evidence confirms this universality, providing a general proof seems almost academic.

On the other hand, there are purely perturbative aspects to factorization with great practical importance. For example, factorization is a first step in performing resummation which is necessary to reproduce even qualitative features of certain distributions. Classic examples are event shapes, particularly at e^+e^- colliders [7–12], and processes with hard well-separated objects at hadron colliders (such as photon plus jet production). In these cases, having a precise statement of factorization, with operator definitions of all the objects involved, allows one to compute distributions to all orders in α_s in certain singular regions, or to provide approximate fixed-order calculations for inclusive cross sections. Since exact calculations in QCD beyond next-

to-leading order can be extraordinarily challenging, having an alternative approach to produce numerically precise results has proven valuable. For example, the most accurate calculations of the Higgs-boson cross section includes contributions from logarithmically enhanced terms derived using a factorization formula [13, 14]. Other examples are the inclusive photon [15–18] or W-boson [19, 20] transverse momentum spectrum, the $t\bar{t}$ cross section [21, 22], and jet shapes such as jet mass [23–25] or n-subjettiness [6, 26].

Even at fixed order in perturbation theory, factorization is useful. When computing cross sections beyond leading order in perturbation theory, infrared divergences must cancel between real emission and loop diagrams. Imposing a simple infrared cutoff is not useful for numerical evaluation, since it requires the cancellation of large positive and negative contributions. It is more efficient to evaluate these cross sections using a subtraction scheme based on the universal behavior in the infrared singular limits, as described by a factorization formula. For example, DGLAP splitting functions describe analytically the behavior of cross sections in collinear limits. Spin-dependent expressions for tree-level collinear, soft and soft-collinear singular regions of cross sections can be found in [27].

In addition to being phenomenologically important, factorization formulae can elucidate profound structures hidden in quantum field theories. Factorization is related to the universality of the infrared structure of gauge theories. While this universality has been explored for decades [27–34], it is still not completely understood and an active area of contemporary research [35–38]. With the recent resurgence of interest in on-shell approaches to scattering amplitudes [39, 40], it is natural to ask

whether an on-shell approach can shed light new light on factorization. In this chapter, we give a preliminary affirmative answer to this question. Although we only work at tree-level, considering on-shell final-state particles using spinor helicity methods, we will see that the on-shell approach clarifies some aspects of factorization which are buried in the formalism of other approaches.

The Collins-Soper-Sterman approach to factorization (which is entirely perturbative) begins by identifying regions of real or virtual phase space which can produce singularities in Feynman diagrams [41–44]. These singularities, sometimes called pinch singular surfaces, are the solutions to the Landau equations [45]. They come from vanishing denominators of Feynman amplitudes, dependent on the topology of the graph, but largely independent of the theory. Since these singularities are due to long-distance physics, compartmentalizing them into sectors which are separately finite implies that there is no long-distance communication among sectors, the hallmark of factorization. In this approach, jets are abstract objects identified with a small region of size λ around nonzero-momentum solutions to the Landau equations. With factorization proven, hard, jet, and soft functions, as well as nonperturbative objects, such as parton-distribution and fragmentation functions, can be defined precisely. However, it appears not to be critical to connect the operator definitions for these objects to the factorization proof itself.

An alternative approach to factorization is provided by Soft-Collinear Effective Theory (SCET) [46–49]. In SCET, at least as applied to collider physics, the procedure has so far been more practical. In SCET one assumes, often without a completely rigorous proof, that factorization holds and then derives formulae for cross

sections in terms of gauge-invariant matrix elements of effective-theory fields with interactions different from those of full QCD. The Lagrangian for SCET is derived by power-counting at the level of operators, rather than diagrams (as with the Landau-equations). Then one uses similar power counting to derive factorization formulae, with the appropriate operators coming out automatically.

Unfortunately, some of the steps in the derivation of SCET are unintuitive and perhaps-unnecessary. For example, suppose we are interested in a process with a jet going in the n^μ direction. Then an energetic gluon in this jet should have a momentum p^μ which is collinear to n^μ, so, $p^\mu \sim En^\mu$ for some E. However, Lagrangians are expressed in terms of fields, not momenta. Thus, the *label-formalism* approach to SCET [46–48] begins by assigning scaling behavior to quark and gluon fields.[1] In [47], it is argued that a gauge field $A^\mu(x)$ associated with a collinear direction should scale like a collinear momentum $A^\mu(x) \sim p^\mu$. Indeed, if the effective theory is to be gauge invariant at some order in a power counting parameter, both terms in $D^\mu = \partial^\mu - igA^\mu$ should have the same power counting, so this is a natural choice. On the other hand, the gauge field acts on a gluon state $|p, h\rangle$ with momentum p^μ and helicity h as

$$\langle 0| A^\mu(x) |p, h\rangle = e^{-ip\cdot x}\, \epsilon_h^\mu(p) \tag{2.1}$$

with ϵ_h^μ the polarization vector. Thus, assigning the scaling behavior $A^\mu \sim p^\mu$ forces the polarization vector to scale like a collinear momentum $\epsilon^\mu \sim p^\mu$. This is the scaling of an unphysical, longitudinal polarization! Moreover, the gauge transformations $A_\mu \to A_\mu + \partial_\mu \alpha + \cdots$ which are consistent with the scaling $A^\mu \sim p^\mu$ are the limited set for which $\partial_\mu \alpha(x) \sim p^\mu$. Thus, the derivation of SCET in [47] takes place in a

[1] The alternative *multipole expansion* approach [49, 50], position space rather than momentum space takes a more prominent role.

particular subset of gauges. As we will see in Section 2.4, this set of gauges, where polarizations are nearly longitudinal, is the only one where an intuitive, semi-classical picture of gauge-boson emission does *not* apply. Of course, there is nothing wrong with considering a reduced class of gauge transformations in deriving an effective theory. However, such a strange gauge limits our ability to apply semi-classical intuition to see why factorization holds.

In contrast, traditional approaches to QCD, such as [27], tend to discuss factorization in "physical gauges", where the polarization vectors are not nearly longitudinal. In physical gauges, semi-classical intuition does apply. However, why factorization should hold in an unphysical gauge, such as the ones used in SCET, is not obvious in the traditional approach. Also, these traditional approaches tend to describe universality at the cross-section, rather than amplitude level. In summing over outgoing polarizations, the fact that factorization holds at the amplitude level is obscured.

The goal of this chapter is to give a more transparent derivation of factorized forms for matrix elements in perturbative QCD. We focus on finite real-emission graphs with physical on-shell states (rather than on the singularities of loops which are connected only indirectly to real-emission graphs through unitarity). Although gauge-invariance will play a critical role, we will not have to choose a particular gauge, and we will not have to assign a scaling behavior to unphysical fields.

The main result of this chapter is a rigorous and self-contained tree-level derivation of a factorization formula in perturbative QCD in which all the objects involved as well as the expansion parameter λ have transparent definitions from the beginning.

What we will show is that

$$\langle X_1 \cdots X_N; X_s | \, \bar{\psi} \cdots \psi \, |0\rangle \cong \langle X_1 | \, \bar{\psi} W_1 \, |0\rangle \cdots \langle X_N | \, W_N^\dagger \psi \, |0\rangle \, \langle X_s | \, Y_1^\dagger \cdots Y_N \, |0\rangle \quad (2.2)$$

Here, $\langle X_j|$ are states involving collinear momenta, all traveling in cones of opening angle λ, and $\langle X_s|$ are states involving soft momenta satisfying $k^\mu \lesssim \lambda^2 Q$, where Q is the center-of-mass energy of the entire state $\langle X_1 \cdots X_N; X_s|$. The W_j and Y_j are Wilson lines which we define in Section 2.2.3. All fields are evaluated at a common point $x = 0$. The $\cong$ symbol indicates that the two sides agree at leading non-vanishing order in a series expansion in λ. Color indices are suppressed. All matrix elements are taken in full QCD. We will prove Eq. (2.2), and its generalizations, rigorously at tree level at leading non-vanishing order in λ.

A tree-level factorization of collinear and soft states similar to Eq. (2.2) was discussed in [27], writing the result instead for the squared matrix element in terms of splitting functions and soft currents. However, a factorization formula in terms of matrix elements of gauge-invariant QCD operators in a form close to that of Eq. (2.2) has only appeared in the literature rather recently [51,52]. Earlier incarnations, where fields are not QCD fields but effective field theory fields, sprinkle the SCET literature. Indeed, once Eq. (2.2) is proven, the derivation of SCET (or rather, a theory which is equivalent to SCET at leading power) is almost trivial. We define the effective theory Lagrangian as $N + 1$ copies of the QCD Lagrangian

$$\mathcal{L}_{\rm EFT} = \mathcal{L}_1 + \cdots \mathcal{L}_N + \mathcal{L}_{\rm soft} \quad (2.3)$$

This decoupled Lagrangian is the one proposed in the simplified formulation of SCET in [51]. Then, assigning quantum numbers to the states in the different sectors one

can collapse the various matrix elements back to a simple form

$$\langle X_1 \cdots X_N; X_s | \, \bar{\psi}_1 \cdots \psi_N \, |0\rangle_{\mathcal{L}_{\rm QCD}} \cong \langle X_1 \cdots X_N; X_s | \, \left(\bar{\psi}_1 W_1 Y_1^\dagger\right) \cdots \left(Y_N W_N^\dagger \psi_N\right) |0\rangle_{\mathcal{L}_{\rm EFT}} \tag{2.4}$$

The advantage of doing this is that now one has an equivalence of a matrix element in QCD and a matrix element of a single operator in an effective theory. Thus, for example, one can compute the anomalous dimension of this operator to resum logarithms.

Returning to Eq. (2.2), we want to emphasize that this factorization formula is a statement about amplitudes in perturbative QCD. Although effective field theory techniques can be used to make formulae like this extremely predictive and powerful, they are not critical to understanding factorization or expressing it in a concise form.

To prove Eq. (2.2), which we do at tree-level, we will not have to make any assumptions about the spins of external states, or the scaling behavior of fields. A key tool which makes this possible is the spinor-helicity formalism. With spinor-helicity methods, lightlike four-momenta can be written as an outer product of spinors, $p^\mu = p\rangle[p$. Polarization vectors, $\epsilon^\mu(p)$, of definite helicity are also lightlike and can be written as an outer product of a spinor associated with their momentum, $p]$ or $p\rangle$, and a spinor, $r\rangle$ or $r]$, associated with any other lightlike four-vector r^μ called the *reference vector*. The reference vector r^μ and the momentum p^μ define a plane to which the polarization vector is orthogonal $p \cdot \epsilon = r \cdot \epsilon = 0$. Since the reference vector can be chosen to be some momentum in the external state of interest, we can write any matrix element in QCD in terms of helicity spinors associated with physical on-shell momentum. This lets us use only the scaling of external momenta to simplify

matrix elements at leading power.

An additional advantage of spinor-helicity methods is that one can choose reference vectors differently for different external states. Matrix elements are invariant under choice of reference vector r^μ if and only if they satisfy the Ward identity. The choice of reference vectors r^μ is in a way similar to a choice of gauge. For example, different r^μ can move dominant contributions from one Feynman diagram to another, and only the sum is r^μ-independent (as only the sum of diagrams is gauge invariant). However, gauge choices are associated with fields. For example, trying to have $n_j \cdot A = 0$ for fields associated with gluons collinear to different n_j directions, becomes a highly nonlocal[2] constraint on A_μ. In contrast, there is nothing awkward about choosing r^μ differently in different collinear sectors. Indeed, this freedom of choosing r^μ dramatically simplifies the calculation of even the simplest gluon scattering amplitudes. It will also simplify our proof of Eq. (2.2).

The on-shell approach to factorization clarifies the role played by the different ingredients, such as the soft and collinear Wilson lines, in Eq. (2.2). We therefore have organized this chapter by considering factorization in field theories of increasing complexity. Section 2.2 provides an orientation to our approach. It includes a motivation of why soft and collinear states are relevant, from the point of view of on-shell states, and reviews spinor-helicity methods and power-counting. We also provide a review of the Wilson lines in this orientation. In Section 2.3 we explain why scalar field theories do not factorize. The simplest theory that does admit a factorization formula like Eq. (2.2) is scalar QED, which is the subject of Section 2.4. Scalar QED

[2]If one changes to radial coordinates, this particular gauge choice becomes local; it is just Coulomb gauge in AdS [53].

already contains much of the relevant physics that goes into the soft and collinear limits, so we pause to discuss the physical picture of soft-collinear factorization in Section 2.4.4. To the extent that factorization can be understood from the tree-level considerations in this chapter, it can be understood in scalar QED. With the general result proven for matrix elements of a specific operator, we show how it applies to any hard process, including those with identical particles, in Section 2.5.

Going from scalars to spinors in Section 2.6 is straightforward and elucidates some new elements of factorization, such as spin-independence of the soft limit. The generalization to QCD is given in Section 2.7, where gluon self-interactions further illustrate some aspects of factorization. We briefly compare our results to SCET in Section 2.8, which contains little more than a repetition of Eqs. (2.3) and (2.4). As an application of the on-shell approach to factorization, we give in Section 2.9 a concise derivation of the Altarelli-Parisi splitting functions in QCD. In particular, due to the factorization formula, we not only derive the splittings functions but show that they apply to any process. Section 2.10 discusses some conclusions and provides a brief outlook.

2.2 Orientation

Our first task is to establish precisely what we mean by factorization, and in what limit we expect it to hold. This section establishes the importance of soft and collinear limits and the notation of lightcone coordinates. It then reviews some aspects of the spinor-helicity formalism, and shows how it can be used to power-count expressions involving polarization vectors.

2.2.1 Power counting momenta

The type of factorization we discuss in this chapter applies to QCD in processes with clearly separated jets of collinear radiation. These jets can be incoming; for example, a proton can be thought of as an incoming collection of collinear radiation. But for simplicity, we focus on processes with outgoing jets only, such as $e^+e^- \to$ jets. Actually, since we will only discuss quarks and gluons, let us write the process as $e^+e^- \to X$, with $\langle X|$ a generic partonic final state.

One can always partition any final state $\langle X|$ into collections $\langle X_i|$, for example with a jet algorithm. For each partition one can sum all the quark and gluon energies into the jet energy Q_i and compute the jet mass m_i from the sum of the parton four-momenta. Then a power counting parameter can be defined as $\lambda_i \equiv m_i/Q_i$. A partition with $\lambda_i = 0$ is massless, thus it can consist of only a single parton, or a set of partons which are exactly collinear to each other. Small but nonzero λ_i mean that the partitions look like collimated collections of particles which are conventionally called jets (we will not need a precise jet definition to show factorization).

What we want to show is that the matrix element for producing any state $\langle X|$ can be computed using a factorized expression when all of the λ_i are small. To get an idea of what this means, consider what kind of final-state partition can produce a small but non-zero λ. For λ to be non-zero, a partition must have at least two partons. Say it has exactly two partons with momenta p^μ and k^μ then the jet mass is

$$m^2 = (p+k)^2 = 2p \cdot k = 4E_p E_k \sin^2 \frac{\theta}{2} \tag{2.5}$$

where θ is the angle between the 3-vectors $\vec{p}$ and $\vec{k}$. Thus, $\lambda = \frac{m}{E_p + E_k} \ll 1$ when either one of energies is small or when the angle between the two is small. More generally,

if there are many particles in the jet, then $\lambda \ll 1$ if and only if the jet contains only particles which are all either soft or close in angle to the same direction (collinear).[3]

To be concrete, let us define the jet momentum as the sum of the momenta of the partons in the partition: $p_J^\mu = \sum_{i \in \text{partition}} p_i^\mu$. Then we can define the light-like four-vectors $n^\mu = (1, \vec{p}_J/|\vec{p}_J|)$ and $\bar{n}^\mu = (1, -\vec{p}_J/|\vec{p}_J|)$. For a jet with a single parton of momentum p^μ, then $E_p n^\mu = p^\mu$ exactly. We can write any four-vector V^μ in light-cone coordinates as

$$V^\mu = \frac{1}{2} V^+ \bar{n}^\mu + \frac{1}{2} V^- n^\mu + V_\perp^\mu \tag{2.6}$$

where $V^+ = n \cdot V$ and $V^- = \bar{n} \cdot V$. Writing $p^\mu = (p^+, p^-, p_\perp^\mu)$ and $k^\mu = (k^+, k^-, k_\perp^\mu)$, and setting the jet energy $Q = E_p + E_k = \frac{1}{2}(p^+ + p^- + k^+ + k^-) = 1$ for simplicity, Eq. (2.5) becomes

$$m^2 = (p+k)^2 = p^+ k^- + p^- k^+ + 2 p_\perp \cdot k_\perp = \lambda^2 \tag{2.7}$$

It follows that for $\lambda \ll 1$, at least one of the momenta must have **collinear scaling**:

$$p^\mu = (p^+, p^-, p_\perp^\mu) \sim (\lambda^2, 1, \lambda) \tag{2.8}$$

and the other can either have collinear scaling or **soft scaling**:

$$k^\mu = (k^+, k^-, k_\perp^\mu) \sim (\lambda^2, \lambda^2, \lambda^2) \tag{2.9}$$

These $\sim$ relations mean that components can be smaller than the expressed power of λ, but not larger (up to perhaps a factor of order one). It may seem that Eq. (2.7)

[3] These soft and collinear regions are of course the same ones which characterize solutions to the Landau equations when external momenta are massless. On the other hand, characterizing the regions through properties of the momenta in the jets, as we have done, avoids any discussion of Feynman diagrams which is more consistent with the on-shell approach.

would be consistent with both k^μ and q^μ scaling like $(\lambda, \lambda, \lambda)$, however such scaling would be inconsistent with our normalization $Q = 1$.[4] We will use the following notation throughout this chapter: $q \parallel p$ means that q is collinear to p, which implies $q \cdot p \sim \lambda^2$, and we will drop the Q when writing the scaling of momenta in terms of λ.

For any number of momenta in a jet, if any two have scaling which is not collinear to that jet direction or soft, the jet mass will be larger than λ. We therefore conclude that if we split the momenta in a state $\langle X|$ into $N + 1$ partitions, all of which have $\lambda_i \ll 1$ and no two have $\lambda \ll 1$ when combined, then N of the partitions must be $\langle X_i|$ which are collinear to some direction n_i^μ and the remaining one must be soft $\langle X_s|$. That is,

$$\langle X| = \langle X_1 X_2 \cdots X_N; X_s| \tag{2.10}$$

We will refer to states of this form as N-jet states. This decomposition does itself not imply factorization; it is just a statement about phase space. The leading order state has one parton in each state, $\langle p_1 p_2 \cdots p_N|$, where p_i are the momenta of the partons in the various jets and there is no soft momentum. States also have helicities, but we suppress helicity indices for simplicity. The general state $\langle X|$ with $\lambda_i \ll 1$ can have additional collinear momenta, which we denote $q_{a_1} \cdots q_{b_1}$ in the first jet, $q_{a_2} \cdots q_{b_2}$ in the second jet, and so on. It can also have particles with soft momenta $k_1 \cdots k_\ell$:

$$\langle X| = \langle p_1 \cdots p_N; q_{a_1} \cdots q_{b_N}; k_1 \cdots k_\ell| \tag{2.11}$$

The generalization to include some incoming and some outgoing particles only amounts to keeping track of appropriate signs.

[4] In the literature $(\lambda, \lambda, \lambda)$ is often called soft scaling, and $(\lambda^2, \lambda^2, \lambda^2)$ is called ultrasoft. We will only be concerned with the latter and will call it simply soft.

What we will show is that the matrix element $\langle X|\mathcal{O}|0\rangle$ of a *hard-scattering operator* $\mathcal{O}$ can be written in a factorized form:

$$\langle X|\mathcal{O}|0\rangle \cong \langle p_1; q_{a_1}\cdots q_{b_1}|\mathcal{O}_1|0\rangle\cdots\langle p_N; q_{a_N}\cdots q_{b_N}|\mathcal{O}_N|0\rangle\langle k_1\cdots k_\ell|\mathcal{O}_s|0\rangle \tag{2.12}$$

at leading order in λ_i for some suitable collinear operators $\mathcal{O}_i$ and soft operator $\mathcal{O}_s$. We assume for simplicity that the hard-scattering operator $\mathcal{O}$ has N fields, one for each collinear direction, with no two fields describing identical particles, and that $\mathcal{O}$ has a non-vanishing matrix element in the leading order state $\langle p_1 p_2\cdots p_N|$. For example, $e^+e^- \to$ dijets is mediated by a combination vector and axial current operators $\mathcal{O}_V = \bar{q}\gamma^\mu q$ and $\mathcal{O}_A = \bar{q}\gamma^\mu\gamma_5 q$. Other examples can be found in [54] or [55].

It is not actually necessary for a matrix element to be expressible in terms of a hard-scattering operator for factorization to hold. As long as the process involves N different directions, the amplitude can factorized at leading power into a sum of expressions of the form on the right-hand-side of Eq. (2.12). We choose to express factorization in the form of Eq. (2.12) in the bulk of this chapter, with $\mathcal{O}$ having N fields each with a unique flavor quantum number, mostly to have cleaner looking equations and to avoid nettlesome combinatoric issues. A demonstration that the factorization we derive applies to more general hard scattering processes, such as those with identical particles, is given in Section 2.5. The only strict requirement for factorization is that no two sectors are collinear. In particular, in cases like forward scattering or Drell-Yan, where incoming partons may be collinear to outgoing spectators, more care is needed to prove factorization [56]. We do not address such cases here.

Regardless of the connection between operator matrix elements and scattering

amplitudes, Eq. (2.12), when made more precise, is a highly nontrivial statement about how Yang-Mills theories simplify. We will therefore eschew any additional discussion of the connection to infrared safe observables and S-matrix elements, focusing instead on perturbative factorization of the given matrix elements.

2.2.2 Spinor helicities and power counting

Matrix elements in theories with spin-1 particles produce expressions involving polarization vectors. For example, they may contain terms like $p \cdot \epsilon$ or $\epsilon_1 \cdot \epsilon_2$. In order to know which of these terms are dominant at small λ, we need to power-count polarizations. These products might vanish for some polarizations, changing which diagrams contribute at the leading power. There are in fact many ways to represent the same physical photon helicity state with polarization vectors, so that the scaling $p \cdot \epsilon$ is not even well-defined given particular states in the Hilbert space. This scaling behavior of expressions involving polarization vectors is easiest to derive if we represent the polarizations in terms of helicity spinors.

In the spinor-helicity formalism, massless left and right handed spinors (i.e. solutions to $\not{p}\, u(p) = 0$) are written as

$$u_L(p)^\alpha = |p\rangle \qquad \text{and} \qquad u_R(p)_{\dot\alpha} = |p] \tag{2.13}$$

where the α and $\dot\alpha$ indices are those of two separate $SU(2)$'s. This way, $SU(2)$-invariant spinor products can be written as

$$\langle pk\rangle = \epsilon^{\alpha\beta}\, |p_\alpha\, |k_\beta = |p_\alpha\, k\rangle^\alpha \qquad \text{and} \qquad [pk] = \epsilon^{\dot\beta\dot\alpha}\, |p]_{\dot\alpha}\, |k]_{\dot\beta} = |p^{\dot\beta}\, k]_{\dot\beta} \tag{2.14}$$

Four-vectors live in the $(\frac{1}{2}, \frac{1}{2})$ representation of the Lorentz group, so they may be

expressed with these indices as well, via

$$p^{\alpha\dot{\alpha}} = \sigma_\mu^{\alpha\dot{\alpha}}\, p^\mu \qquad \text{and} \qquad p^\mu = \frac{1}{2}\bar{\sigma}^\mu_{\dot{\alpha}\alpha}\, p^{\alpha\dot{\alpha}} \tag{2.15}$$

In this representation, masslessness of a four-vector becomes

$$p^2 = \det p^{\alpha\dot{\alpha}} = 0 \tag{2.16}$$

which implies

$$p_{\dot{\alpha}\alpha} = p]\langle p \qquad \text{and} \qquad p^{\alpha\dot{\alpha}} = p\rangle[p \tag{2.17}$$

and

$$2p\cdot k = p_{\dot{\alpha}\alpha}k^{\alpha\dot{\alpha}} = [kp]\langle pk\rangle \tag{2.18}$$

Polarization vectors of a definite helicity are also massless. They can be defined by their normalization: $\epsilon_q^2 = 0$ and $\epsilon_q^*\cdot\epsilon_q = -1$, transversality: $q\cdot\epsilon_q = 0$ and one more condition: $r\cdot\epsilon_q = 0$ for r^μ linearly independent of q^μ. The four-vector r^μ is called the **reference vector**. The above constraints are elegantly encoded with helicity spinors as follows:

$$\epsilon_q^-(r) = \sqrt{2}\,\frac{q\rangle[r}{[qr]} \qquad \text{and} \qquad \epsilon_q^+(r) = \sqrt{2}\,\frac{r\rangle[q}{\langle rq\rangle} \tag{2.19}$$

Thus, for example,

$$\frac{p\cdot\epsilon_q^-}{p\cdot q} = \sqrt{2}\,\frac{[rp]}{[qr][qp]} \tag{2.20}$$

The freedom of choice of reference vector encodes the arbitrariness associated with assigning a specific polarization vector to a given helicity. Consequently, matrix elements that satisfy the Ward identity will be independent of the choice of reference vector.

To see how spinors and spinor products scale with λ, first recall that there is not a unique way to write a massless four-vector in terms of spinors: any little

group transformation $p] \to p]z$ and $\langle p \to \frac{1}{z}\langle p$ for any complex number z leaves $p]\langle p$ unchanged. For real momenta, $|z| = 1$. Since $k^\mu \sim \lambda^2$ for a soft momentum, the associated spinors must scale like $k] \sim \langle k \sim \lambda$. Moreover, soft momenta do not have a specific direction, so, without loss of generality, we can choose the reference vectors for soft-photon polarizations to satisfy $[kr], \langle rk\rangle \sim 1$. The scaling of the soft polarization vectors is then fixed to be $\epsilon_k^\mu \sim 1$.

For collinear momenta, the components of the helicity spinors do not have uniform scaling; nor, therefore, do the polarization vectors. However, since for two collinear four-vectors $2p \cdot q = \langle qp\rangle[pq] \sim \lambda^2$ and since $\langle qp\rangle = [pq]^*$, we conclude that $\langle qp\rangle \sim [pq] \sim \lambda$. Thus we will be able to power count Lorentz-contracted products involving collinear momenta and polarizations.

2.2.3 Wilson lines

Wilson lines play an important role in factorization. They describe the radiation produced by a charged particle moving along a given path in the semi-classical limit. The semi-classical limit applies when the back-reaction of the radiation on the particle can be neglected. In particular, this limit holds when the particle is much more energetic than any of the photons in the radiation, that is, when the photons are all soft. Thus Wilson lines naturally appear in the soft limit of Yang-Mills theory. That they also play a role in collinear limits is less obvious and will be explained in Section 2.4.

An outgoing Wilson line in the n^μ direction is defined by

$$Y_n^\dagger(x) = P\left\{\exp\left[ig\int_0^\infty ds\, n\cdot A(x^\nu + sn^\nu)\, e^{-\varepsilon s}\right]\right\} \tag{2.21}$$

where P denotes path-ordering and $A = A^a T^a$ is the gauge field in the fundamental representation (Wilson lines in other representations are a straightforward generalization). This Wilson line is outgoing because the position where the gauge field $A_\mu(x)$ is evaluated goes from x to ∞ along the n^μ direction. We write $Y_n^\dagger$ for Wilson lines for outgoing particles, and Y_n for outgoing antiparticles (as $\bar{\psi}$ creates outgoing quarks and ψ creates outgoing antiquarks). Explicitly,

$$Y_n(x) = \overline{P}\left\{\exp\left[-ig\int_0^\infty ds\, n\cdot A(x^\nu + sn^\nu)\, e^{-\varepsilon s}\right]\right\} \tag{2.22}$$

where $\bar{P}$ denotes anti-path ordering. We write incoming Wilson lines as

$$\bar{Y}_n(x) = P\left\{\exp\left[ig\int_{-\infty}^0 ds\, n\cdot A(x^\nu + sn^\nu)\, e^{\varepsilon s}\right]\right\} \tag{2.23}$$

$$\bar{Y}_n^\dagger(x) = \overline{P}\left\{\exp\left[-ig\int_{-\infty}^0 ds\, n\cdot A(x^\nu + sn^\nu)\, e^{\varepsilon s}\right]\right\} \tag{2.24}$$

where now the path goes from $-\infty$ to x and the $i\varepsilon$ prescription is switched.

One can have Wilson lines in any representation. For example, an adjoint Wilson line can be written as

$$\mathcal{Y}_n^\dagger(x) = P\left\{\exp\left[ig\int_0^\infty ds\, n\cdot A_\mu^a(x + s\,n)T^a_{\rm adj}\, e^{-\epsilon s}\right]\right\} \tag{2.25}$$

where $(T^a_{\rm adj})^{bc} = if^{bac}$ are the adjoint-representation group generators. A useful relation is that, because

$$(T^c_{\rm adj})^{ab}T^b = [T^a, T^c]\,, \tag{2.26}$$

one can write

$$Y_n^\dagger A_b^\mu T^b\, Y_n = A_a^\mu\, \mathcal{Y}_n^{ab}\, T^b \tag{2.27}$$

In this way, all the relevant Wilson lines in QCD can be expressed in terms of fundamental Wilson lines or their adjoints (which are antifundamental Wilson lines).

Although Wilson lines are non-local, their matrix elements in given external states can be evaluated order by order in perturbation theory. For a state with a single gluon of momentum k^μ and polarization ϵ^μ, we find

$$\langle \epsilon(k)|\, Y_n^\dagger(0)\,|0\rangle = igT^a \int_0^\infty ds\ \langle \epsilon(k)|\, n\cdot A^a(s\,n^\mu)\,|0\rangle\ e^{-\varepsilon s} \tag{2.28}$$

$$= igT^a\, n\cdot\epsilon_k^* \int_0^\infty ds\, e^{is(n\cdot k+i\varepsilon)} \tag{2.29}$$

$$= -gT^a \frac{n\cdot\epsilon_k^*}{n\cdot k+i\varepsilon} \tag{2.30}$$

This is the form of an eikonal vertex, coming from the soft limit of a QCD interaction

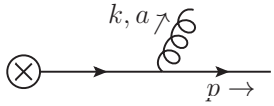

$$= -gT^a \frac{n\cdot\epsilon_k}{n\cdot k+i\varepsilon} \tag{2.31}$$

with the correct $i\epsilon$ prescription (and we have dropped the factor of the amplitude with no emission). For the incoming Wilson line, a similar calculation gives

$$\langle \epsilon(k)|\, \bar{Y}_n\,|0\rangle \ = \ gT^a \frac{n\cdot\epsilon_k}{n\cdot k-i\varepsilon} \ =$$

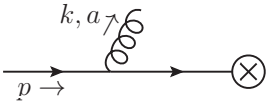

(2.32)

which also has the correct sign and $i\varepsilon$ prescription.

The $e^{\pm\varepsilon s}$ factors in these Wilson lines are required when the Wilson lines are used in time-ordered products to calculate S-matrix elements. This is most clearly seen in perturbation theory, where, as we have shown these $e^{\pm\varepsilon s}$ factors generate the pole displacements for Feynman propagators. The $e^{\pm\varepsilon s}$ factors affect the gauge transformation properties, but only at order ε:

$$Y_n(x) \to e^{i\alpha(x)} Y_n(x) e^{-i\alpha(\infty)} + \mathcal{O}(\varepsilon) \tag{2.33}$$

Thus, for gauge transformations that vanish at infinity[5], $Y_n(x)$ transforms like a

[5]Requiring $\alpha(\infty) = 0$ is not a strong restriction on the class of gauge transformations allowed, since one can always supplement a gauge transformation with a global transformation (with α constant), to set $\alpha(\infty) = 0$. In any case, the factorization formulas we derive are an exact equivalence of matrix elements, at leading power. Their validity does not depend on the concept of gauge invariance.

fundamental in the $\varepsilon \to 0$ limit.

It is perhaps worth noting that similar $\mathcal{O}(\varepsilon)$ corrections are present even in a local quantum field theory. For example, in scalar QCD, the matrix element of the operator $\phi^*\phi$ in a state $\langle \epsilon(q) p_1 p_2|$ containing an outgoing gluon, scalar particle and scalar antiparticle with momenta q, p_1 and p_2 respectively, is

$$\langle \epsilon(q) p_1 p_2|\, \phi^*(0)\phi(0)|0\rangle = -gT^a \left(\frac{p_1 \cdot \epsilon}{p_1 \cdot q + i\varepsilon} - \frac{p_2 \cdot \epsilon}{p_2 \cdot q + i\varepsilon} \right) \tag{2.34}$$

This in fact does not satisfy the Ward identity exactly, but only up to corrections of order ε. Indeed, substituting $\epsilon \to q$, we find

$$\langle q(q) p_1 p_2|\, \phi^*(0)\phi(0)|0\rangle \overset{\epsilon \to q}{=} i\varepsilon g T^a \left(\frac{1}{p_1 \cdot q} - \frac{1}{p_2 \cdot q} \right) + \mathcal{O}(\varepsilon^2) \tag{2.35}$$

which does not vanish exactly. Thus, the danger in violating gauge-invariance at order ε is no worse when using Wilson lines than in a theory with only local operators. In any case, since this chapter is entirely about tree-level matrix elements, the $i\varepsilon$ prescription is irrelevant. Thus, we set $\varepsilon = 0$ from now on.

2.3 Scalar field theory

We begin our exploration of factorization with a simple scalar field theory with Lagrangian

$$\mathcal{L} = \frac{1}{2}\partial_\mu \phi\, \partial^\mu \phi + \frac{g}{3!}\phi^3 \tag{2.36}$$

Since we only work at tree-level, the dimensionality of the coupling g causes no complications. Moreover, all matrix elements are finite so no discussion of regulating divergences is needed.

We consider the matrix elements $\langle X|\mathcal{O}(0)|0\rangle$ of the hard-scattering operator

$$\mathcal{O}(x) = \frac{1}{N!}\phi(x)^N \tag{2.37}$$

in an N-jet state $\langle X| = \langle X_1 \cdots X_N; X_s|$. The normalization of the operator is chosen so that its leading-order matrix element is $\langle p_1 \cdots p_N| \mathcal{O}(0) |0\rangle = 1$. One can add derivatives to the operator with little effect on the following arguments. Indeed, adding derivatives to $\mathcal{O}(x)$ simply produces an overall function of the $P_{X_i} \cdot P_{X_j} \sim Q^2$, where P_{X_i} is the momentum of the $\langle X_i|$ state, that will end up sitting out front of the factorized expressions. Because the complications of adding derivatives to $\mathcal{O}$ are almost entirely notational, we will always ignore derivative insertions in this chapter and describe how to treat scattering much more generally in Section 2.5.

We start by considering only collinear emissions. The diagram with the j-th line emitting a single scalar on top of the leading-order matrix element is:

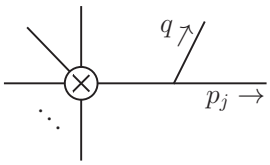

$$= \frac{-g}{2p_j \cdot q} \tag{2.38}$$

where the $\otimes$ indicates an insertion of the operator $\mathcal{O} = \frac{1}{N!}\phi^N$. When q is not collinear to p_j then $q \cdot p_j \sim 1$, whereas, when q is collinear to p_j then $q \cdot p_j \sim \lambda^2 \ll 1$. Therefore, the diagram where the emission comes off the leg to which it is collinear (a **self-collinear emission**) is enhanced by λ^{-2} compared to any of the other diagrams. We can write this as

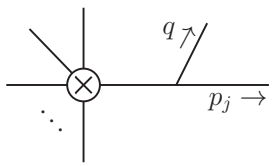

$$\sim \begin{cases} \dfrac{1}{\lambda^2}, & q \parallel p_j \\ 1, & q \not\parallel p_j \end{cases} \tag{2.39}$$

Thus, at leading power, only the diagram with a self-collinear emission is relevant.

Since self-collinear emissions do not change the collinearity of the line from which they are emitted, the above argument can be used inductively to show that for any number of collinear particles, diagrams with all self-collinear emissions are enhanced compared to other diagrams. Diagrammatically, we can write

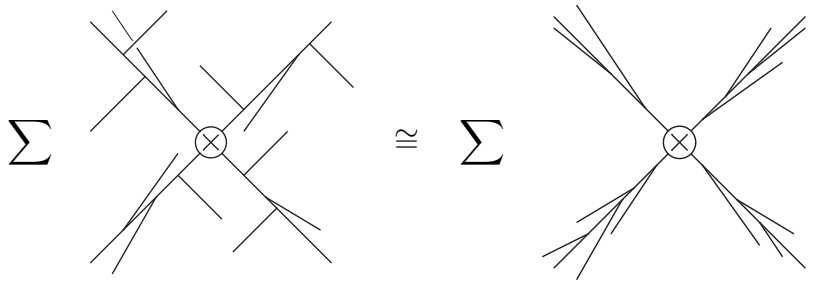

(2.40)

where the sum on the left means the sum of all diagrams consistent with the external state in the matrix element and the sum on the right means only those diagrams with emissions off of a line to which they are themselves collinear. The $\cong$ means that the two sides agree at leading power in λ. The vertex in these diagrams denotes the hard-scattering operator of which we are taking the matrix element and for clarity, only four distinct collinear directions are shown even though we are considering N.

Thus, the matrix element in the scalar case simplifies when all the particles are collinear to one of the N directions. It is given by the product of factors for each sector separately – it factorizes. In terms of matrix elements, Eq. (2.40) can be written as

$$\langle p_1 \cdots p_N; q_{a_1} \cdots q_{b_N}| \, \frac{1}{N!}\phi^N \, |0\rangle \cong \langle p_1; q_{a_1} \cdots q_{b_1}| \, \phi \, |0\rangle \cdots \langle p_N; q_{a_N} \cdots q_{b_N}| \, \phi \, |0\rangle \quad (2.41)$$

where $q_{a_j} \cdots q_{b_j} \parallel p_j$ for each collinear sector, j. Or, more succinctly

$$\langle X_1 \cdots X_N| \, \mathcal{O} \, |0\rangle \cong \langle X_1| \, \phi \, |0\rangle \cdots \langle X_N| \, \phi \, |0\rangle \quad (2.42)$$

This simplification is in fact exactly what one expects from a semi-classical picture: after the hard scattering occurs, collinear particles in each jet can be thought to emit additional scalars, as in a parton shower. There is no interference between emissions from particles moving in different directions.

Next, consider states with soft particles. In Eq. (2.38), if we take $q^\mu \sim \lambda^2$, the soft emission is also enhanced by λ^{-2} irrespective of the direction of the soft radiation. Therefore, unlike the collinear case, no diagrams may be dropped. Furthermore, the Feynman rules do not particularly simplify in the soft limit, so the soft limit of the scalar theory shows no simplifications for the matrix elements under consideration.

In summary, in a scalar field theory, collinear emissions factorize and have a simple semiclassical interpretation. However, since soft emissions do not simplify, the matrix element under consideration does not factorize in scalar field theory at leading power. Except in exceptional cases where soft-emission is not relevant (such as scalar ϕ^3 deep-inelastic scattering [43]), states with soft and collinear momenta are equally relevant to infrared-safe observables at leading power. Thus, since all Feynman diagrams must be evaluated to reproduce the soft limit, collinear factorization by itself is not particularly useful.

2.4 Scalar QED

In scalar field theory, we saw that while self-collinear emissions dominate over collinear emissions from distant legs, leading to an intuitive form of collinear factorization, soft emissions do not simplify in any useful way. As we will see, in gauge theories like scalar QED, there is still collinear factorization, although which diagrams

dominate depends on the gauge. There is also factorization in the soft limit. And, most remarkably, the soft and collinear sectors factorize simultaneously.

We will be considering matrix elements of the gauge-invariant operators $\mathcal{O}$ in the N-jet states discussed in Section 2.2, $\langle X| = \langle X_1 \cdots X_N; X_s|$. The simplest hard-scattering operator in scalar QED, on which we focus, is

$$\mathcal{O}(x) = \frac{1}{(N/2)!} \left[\phi(x)^* \phi(x)\right]^{N/2} \tag{2.43}$$

with N even. Insertions of covariant derivatives in $\mathcal{O}$ correspond to collinear sectors initiated by a photon; we will postpone the discussion of covariant derivatives until Section 2.7 where we discuss QCD and the situation is more interesting. For notational consistency with later results in QCD, we will take the QED coupling constant to be $g = -e$.

As in the previous section, we will start our discussion using states with no soft momenta, $\langle X| = \langle X_1 \cdots X_N|$. This will allow for a clean discussion of the essential ingredients that go into collinear factorization. Subsequently, we discuss states with one particle per collinear sector and many soft particles, $\langle X| = \langle p_1 \cdots p_N; X_s|$ and finally, the simultaneous soft and collinear case, $\langle X| = \langle X_1 \cdots X_N; X_s|$.

2.4.1 Collinear Factorization

Our approach to analyzing the matrix element $\langle X_1 \cdots X_N| \mathcal{O} |0\rangle$ will be to start with the matrix element, $\langle p_1 \cdots p_N| \mathcal{O} |0\rangle$, and to add collinear emissions until the full matrix element is constructed. We start by adding collinear photons only and then discuss adding additional collinear scalars. So let us take the final state of the j-th sector to be $\langle X_j| = \langle p_j, q_{a_j} \cdots q_{b_j}|$ where p_j is a scalar momentum and all the q's are

photon momenta.

In scalar QED, the matrix element for a state with one photon is related to the matrix element for the state with no photons as

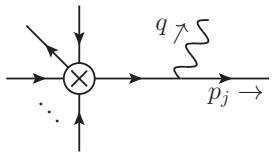

$$= -g\,\frac{p_j \cdot \epsilon_q}{p_j \cdot q + i\varepsilon} \tag{2.44}$$

where the $\otimes$ indicates an insertion of the operator $\mathcal{O} = \frac{1}{(N/2)!}|\phi|^N$ which gives a factor of 1. The 4-point vertex in scalar QED only contributes starting with 2 emissions:

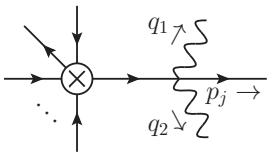

$$= \frac{-2g^2\,\epsilon_{q_1} \cdot \epsilon_{q_2}}{(p_j + q_1 + q_2)^2 + i\varepsilon} \tag{2.45}$$

For collinear emissions, these expressions appear to be enhanced only when the q's are collinear to p_j just like in the scalar theory. However, due to the $p \cdot \epsilon$ and $\epsilon_i \cdot \epsilon_j$ factors in their numerators, the story is not so simple. We need to know how $p \cdot \epsilon$ and $\epsilon_i \cdot \epsilon_j$ scale with λ. For example, for any physical photon helicity, we can choose its associated polarization vector so that $p_j \cdot \epsilon_q = 0$ in which case the first graph would vanish (as would the second for certain helicity choices).

As discussed in Section 2.2.2, expressions involving polarizations are easiest to power-count using helicity spinors. For example, in terms of helicity spinors Eq. (2.44) becomes:

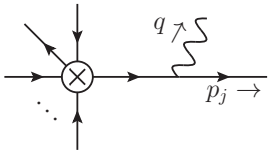

$$= -g\,\frac{p_j \cdot \epsilon_q^-}{p_j \cdot q} = -g\,\sqrt{2}\,\frac{[r p_j]}{[qr][q p_j]} \tag{2.46}$$

where r is the reference vector associated with the polarization vector, ϵ_q^- (the expression with ϵ_q^+ is the complex conjugate). In Section 2.2.2 we showed that the contraction of two spinors corresponding to momenta with collinear scaling scales

like the square-root of the scaling of the contraction of the associated momenta; in equations that is $p_j \cdot q \sim \lambda^2$ implies that $[qp_j], \langle p_j q\rangle \sim \lambda$. Thus, the scaling of a product involving reference-vector spinors $r]$ and $[r$ can be determined once we know in which direction r points.

Let us first choose reference vectors which are *not* collinear to any of the momenta. We call this **generic-r**. In generic-r, $[rp_j] \sim [qr] \sim 1$ and

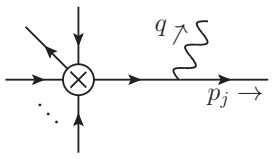

$$= -g\sqrt{2}\,\frac{[rp_j]}{[qr][qp_j]} \sim \frac{1}{[qp_j]} \sim \begin{cases} \dfrac{1}{\lambda}, & q \parallel p_j \\ 1, & q \not\parallel p_j \end{cases} \tag{2.47}$$

Thus, generic-r is similar to ϕ^3 theory (cf. Eq. (2.39)). However, note that the diagrams are less singular: one power of λ cancels due to the scaling of the polarization vectors. In scalar QED there is also a diagram involving the four-point vertex. In generic-r, we find

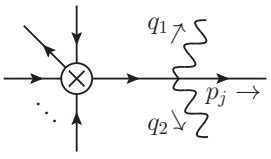

$$\sim \begin{cases} \dfrac{1}{\lambda^2}, & q_1 \parallel q_2 \parallel p_j \\ 1, & q_1 \not\parallel p_j \quad \text{or} \quad q_2 \not\parallel p_j \end{cases} \tag{2.48}$$

This is the same order as two emissions using the 3-point vertex (for soft emissions, as we will see, diagrams involving the 4-point vertex are power suppressed).

By induction, in generic-r, only the diagrams in which all the emissions are self-collinear are relevant at leading power. That is, in generic-r,

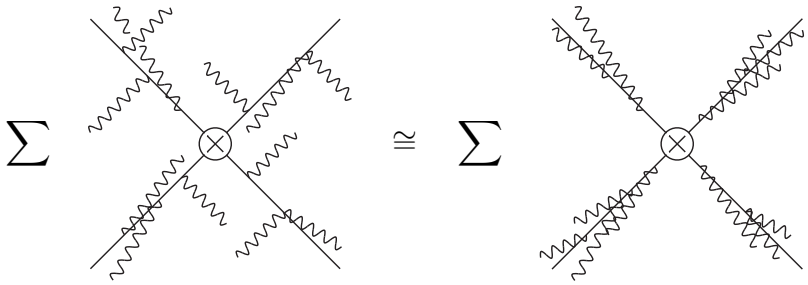

(2.49)

where the sums have the same meaning as in the scalar case: the sum on the left means the sum over all diagrams consistent with the collinear external states, namely all diagrams in $\langle X|\,\mathcal{O}\,|0\rangle$. The sum on the right means only sum over those diagrams for which the emissions in the j direction are from a j-collinear scalar, namely, diagrams for which all emissions are self-collinear.

In terms of matrix elements, Eq. (2.49) can be written as

$$\langle p_1 \cdots p_N; q_{a_1} \cdots q_{b_N}|\,\mathcal{O}\,|0\rangle \cong \langle p_1; q_{a_1} \cdots q_{b_1}|\,\phi^*\,|0\rangle \ldots \langle p_N; q_{a_N} \cdots q_{b_N}|\,\phi\,|0\rangle \tag{2.50}$$

where the collinear photons are labelled such that $q_{a_j}, \cdots, q_{b_j} \parallel p_j$ for each collinear sector, j, and the choice of ϕ versus ϕ^* depends on whether p_i is an outgoing scalar or anti-scalar. This equation is a precise statement of collinear factorization. It is however not gauge-invariant. Indeed, we only showed that it holds for generic-r choices of reference vector.. In fact, the sum of diagrams on the right of Eq. (2.49) does not satisfy the Ward identity and the right-hand side of Eq. (2.50) involves matrix elements of gauge-dependent fields $\phi(x)$.

As a step toward deriving a gauge-invariant form of factorization, consider next a different choice of reference vectors. We previously used generic-r where no reference vectors could be collinear to p_i for all i; to contrast this, we take all of the reference vectors of the j-collinear photons to be *equal* to p_j, namely

$$\textbf{collinear-r}: \qquad r_{a_j}, \cdots, r_{b_j} = p_j \tag{2.51}$$

Then the previously-most-enhanced diagrams will be proportional to

$$\frac{p_j \cdot \epsilon_q^-}{p_j \cdot q} = \sqrt{2}\,\frac{[rp_j]}{[qr][qp_j]}\bigg|_{r=p_j} = 0 \tag{2.52}$$

To see where the leading-power contributions to the matrix element in Eq. (2.50) went, note that the reference vectors for the j-th sector are now themselves enhanced:

$$\epsilon_q^-(r = p_j) = \sqrt{2}\,\frac{q\rangle[r}{[qr]}\bigg|_{r=p_j} = \sqrt{2}\,\frac{q\rangle[p_j}{[qp_j]} \sim \frac{q\rangle[p_j}{\lambda} \tag{2.53}$$

Thus, in collinear-r, the leading-power contributions, those scaling like $\frac{1}{\lambda}$, all come from the non-self-collinear graphs. In diagrams, in collinear-r

$\langle p_1 \cdots p_N; q|\,\mathcal{O}\,|0\rangle$ $=$ $\sum_{i\neq j}$ 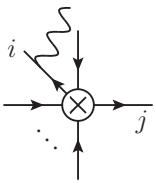

(2.54)

The sum must be the same as the self-collinear graphs which dominate in generic-r, since the sum of all graphs is r-independent. Interpreting this in terms of the dominant diagrams in generic-r or collinear-r, we have found

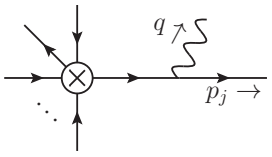

in generic-r $\cong$ $\sum_{i\neq j}$ 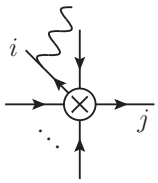

in collinear-r (2.55)

It is informative to check that the sum of graphs in scalar QED is exactly r-independent. The sum of graphs is

$\langle p_1 \cdots p_N; q|\,\mathcal{O}\,|0\rangle$ $=$ 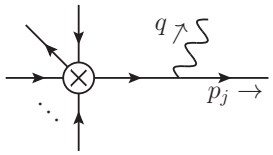

$+$ $\sum_{i\neq j}$ 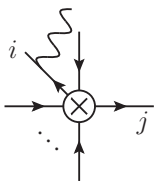

(2.56)

$$= \sum_i (-Q_i g)\frac{p_i \cdot \epsilon_q^-}{p_i \cdot q} \tag{2.57}$$

$$= -g\sqrt{2}\sum_i Q_i \frac{[rp_i]}{[qr][qp_i]} \tag{2.58}$$

where $Q_i = 1$ for a particle or $Q_i = -1$ for an antiparticle (incoming particles would get a relative minus sign). Next, define new massless four-vector t_j^μ. We can use the

Schouten identity to write

$$[rp_i][qt_j] = [qp_i][rt_j] + [t_jp_i][qr] \tag{2.59}$$

This holds for any i, so in particular,

$$\sum_i Q_i \frac{[rp_i]}{[qr][qp_i]} = \sum_i Q_i \frac{[rt_j]}{[qr][qt_j]} + \sum_i Q_i \frac{[t_jp_i]}{[qt_j][qp_i]} \tag{2.60}$$

The first sum has no p_i dependence in the spinor products and vanishes by charge conservation, $\sum_i Q_i = 0$. Thus we have

$$\langle p_1 \cdots p_N; q| \, \mathcal{O} \, |0\rangle = -g\sqrt{2} \sum_i Q_i \frac{[t_jp_i]}{[qt_j][qp_i]} \tag{2.61}$$

which is explicitly r-independent.

Now let us take t_j to point in a direction not collinear to p_j. Then all the spinor products which appear in Eq. (2.61) are $\mathcal{O}(\lambda^0)$ except for $[qp_j] \sim \lambda$. Thus, at leading power, using $Q_j = 1$, we find

$$\langle p_1 \cdots p_N; q| \, \mathcal{O} \, |0\rangle \cong -g\sqrt{2} \frac{[t_jp_j]}{[qt_j][qp_j]} \tag{2.62}$$

Note that t_j can be thought of as an example of a generic-r reference vector. In particular, taking $r = t_j$ in Eq. (2.47) gives exactly Eq. (2.62). In collinear-r, where $r = p_j$, the self-collinear-emission from the p_j line is exactly zero and Eq. (2.62) is produced from the sum of all *other* diagrams. In fact, in collinear-r, Eq. (2.62) can be written as

$$-\, g\, \sqrt{2} \frac{[t_jp_j]}{[qt_j][qp_j]} \overset{p_j=r}{=} -g\, \sqrt{2} \frac{[t_jr]}{[qt_j][qr]} = g\, \frac{t_j \cdot \epsilon_q^-}{t_j \cdot q} \tag{2.63}$$

which is exactly the amplitude coming from a Wilson line in the t_j direction, as in Eq. (2.30), but with opposite sign because Eq. (2.30) involves the conjugated Wilson line.

The above analysis motivates improving Eq. (2.50) by adding Wilson lines in the t_j directions:

$$\langle p_1 \cdots p_N; q_{a_1} \cdots q_{b_N}| \, \mathcal{O} \, |0\rangle \cong \langle p_1; q_{a_1} \cdots q_{b_1}| \, \phi^* W_1 \, |0\rangle \ldots \langle p_N; q_{a_N} \cdots q_{b_N}| \, W_N^\dagger \phi_N \, |0\rangle \tag{2.64}$$

where the outgoing Abelian Wilson line is

$$W_j(x) = \exp\left(- ig \int_0^\infty ds \, t_j \cdot A(x^\mu + s \, t_j^\mu) \, e^{-\varepsilon s} \right) \tag{2.65}$$

To check Eq. (2.64), we evaluate one of the terms on the right-hand-side with one emission. This emission can come out of ϕ or out of W_j, giving

$$\langle p_j; q| \, \phi^* W_j \, |0\rangle = -g\sqrt{2} \frac{[r p_j]}{[qr][q p_j]} - g\sqrt{2} \frac{[t_j r]}{[q t_j][qr]} \tag{2.66}$$

Using the Shouten identity this simplifies to

$$\langle p_j; q| \, \phi^* W_j \, |0\rangle = -g\sqrt{2} \frac{[t_j p_j]}{[q t_j][q p_j]} \tag{2.67}$$

Thus the factorized expression is r-independent and agrees with Eq. (2.62), which is the full matrix element at leading power.

More generally, the factorized expression will be r-independent for any number of emissions since the operators $\phi^* W_j$ in the matrix elements are gauge invariant. Moreover, since the Wilson line contributions to the matrix element are of the form $\frac{[t_j r]}{[q t_j][qr]}$ which scale like λ^0 in generic-r, they can be set to 1 in generic-r. Thus Eq. (2.64) reduces to Eq. (2.50) which we have already shown agrees with full scalar QED at leading power in generic-r. Since Eq. (2.64) is reference-vector independent and agrees with full scalar QED for a specific reference-vector choice, it must agree for all reference vectors. Hence, we have proven the factorization formula in Eq. (2.64).

In summary, we have shown that matrix elements of the gauge-invariant operator, $\mathcal{O} = \frac{1}{(N/2)!}|\phi|^N$, in states with N collinear sectors, each composed of a collinear scalar and many collinear photons, factorize into N separately-gauge-invariant matrix elements as in Eq. (2.64). We can write collinear factorization succinctly as

$$\langle X_1 \cdots X_N | \, \mathcal{O} \, |0\rangle \cong \langle X_1 | \, \phi^* W_1 \, |0\rangle \cdots \langle X_N | \, W_N^\dagger \phi \, |0\rangle \tag{2.68}$$

This expression holds for any choice of polarization vectors. In fact, it holds for any hard-scattering operator $\mathcal{O}$ even with additional derivatives in it or for scattering mediated by operators with different numbers of fields. The effect of considering more general scattering is to simply multiply Eq. (2.68) by an overall function, $H(P_1, \ldots, P_N)$, where P_i is the total momentum of the i-th sector, as discussed in Section 2.5.

In proving the above factorization of collinear sectors, we used states of one charged scalar and an arbitrary number of photons collinear to each direction. This was done for simplicity; the factorization holds for more general states, $|X_j\rangle$, of an arbitrary number of j-collinear scalars and photons that carry the quantum numbers of a single scalar. The splitting of a photon into particle-anti-particle pair is reference vector independent and therefore only enhanced for self-collinear emissions and splittings. Thus, the diagrammatic factorization of Eq. (2.49) becomes (in generic-r)

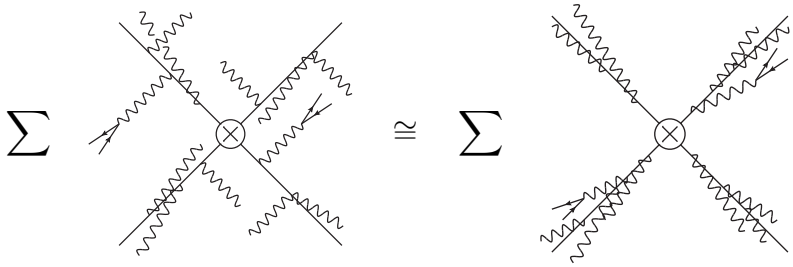

(2.69)

and the rest follows exactly as above.

2.4.2 Soft Factorization

In this subsection we will ignore any collinear dynamics by considering states with only one collinear momentum in each sector. We discuss the simultaneous factorization of the soft and collinear sectors in Section 2.4.3. In terms of matrix elements, we will consider the simplified problem of factorizing the soft emissions in

$$\langle p_1 \cdots p_N; X_s | \, \mathcal{O} \, |0\rangle \tag{2.70}$$

from the hard-scattering matrix element $\langle p_1 \cdots p_N | \, \mathcal{O} \, |0\rangle = 1$. As a further initial simplification, we will consider $\langle X_s |$ to consist of soft photons only. Any soft scalars in $\langle X_s |$ must couple to collinear lines through a virtual-soft photon, so we can deal with soft scalars once we have understood how soft photons decouple.

A convenient feature of the soft limit is that we do not need to worry about polarization-vector subtleties since soft emissions are not associated with a specific direction. Indeed, as observed in Section 2.2.2, we can just use $k \sim \lambda^2$ and $\epsilon \sim 1$. Alternatively, we can choose generic-r for all of the soft polarizations; we will see that our final result is gauge-invariant and hence independent of this choice.

Now, consider the addition of soft emissions to the hard-scattering matrix element. For one emission, the graph is

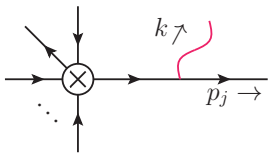

$$= -g \, \frac{p_j \cdot \epsilon_k}{p_j \cdot k + i\varepsilon} \sim \frac{g}{\lambda^2} \tag{2.71}$$

where soft photons are colored red and have long wavelengths. In scalar QED there

are also diagrams with a 4-point vertex:

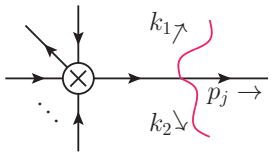

$$= \frac{-g^2\,\epsilon_{k_1}\cdot\epsilon_{k_2}}{p\cdot(k_1+k_2)+i\varepsilon} \sim \frac{g^2}{\lambda^2} \tag{2.72}$$

We see that when considering soft emissions, diagrams involving the four-point vertex (which scale like λ^{-2}) are subleading compared to diagrams involving two emissions from three-point vertices (which scale like λ^{-4}).

Next, consider the sum of the most-enhanced soft emissions off of a single collinear line. For ℓ soft emissions off of a scalar with momentum $p_j^\mu = E_j n_j^\mu$, we can use $p_j + k_i \cong p_j$ to write the matrix element as

$\sum_{\text{perms}}$ 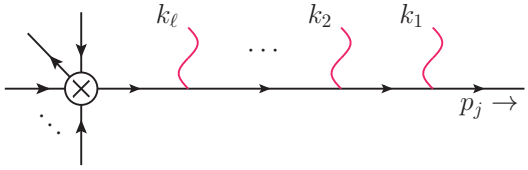

$$\cong \sum_{\text{perms}} (-g)^\ell \frac{p_j\cdot\epsilon_1}{p_j\cdot k_1}\frac{p_j\cdot\epsilon_2}{p_j\cdot(k_1+k_2)}\cdots\frac{p_j\cdot\epsilon_\ell}{p_j\cdot\sum_{i=1}^{\ell}k_i} \tag{2.73}$$

where the sum on "perms" means to sum over all permutations of the soft photons. Note that each term is independent of the energy of the scalar, E_j and only depends on its direction n_j^μ. After some algebra (known as the eikonal identity), this reduces to

$\sum_{\text{perms}}$ 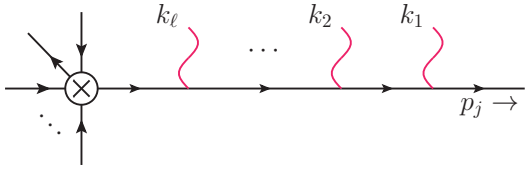

$$\cong (-g)^\ell \frac{n_j\cdot\epsilon_1}{n_j\cdot k_1}\frac{n_j\cdot\epsilon_2}{n_j\cdot k_2}\cdots\frac{n_j\cdot\epsilon_\ell}{n_j\cdot k_\ell} \tag{2.74}$$

This form of the amplitude indicates that in the soft limit, the separate soft emissions are totally uncorrelated in scalar QED. Moreover, each factor can immediately be seen to be reproducible as the matrix element of a Wilson line, as in Eq. (2.30). In the

Abelian case, the Wilson line is

$$Y_j^\dagger(x) = \exp\left(ig\int_0^\infty ds\, n_j \cdot A(x^\mu + s\, n_j^\mu)\, e^{-\varepsilon s}\right) \tag{2.75}$$

and the result is

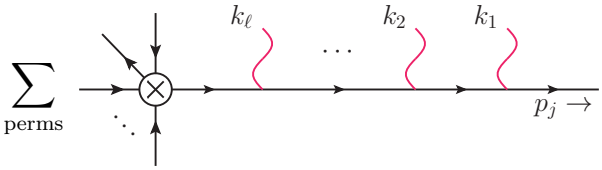

$$\cong \langle k_1 \cdots k_\ell |\, Y_j^\dagger(0)\, |0\rangle \tag{2.76}$$

Although the delightfully simple form in Eq. (2.74) is particular to Abelian gauge theories (it is indicative of Abelian exponentiation [57]), that multiple soft emissions can be written in terms of matrix elements of Wilson lines, as in Eq. (2.76) is also true in the non-Abelian case, as we discussion in Section 2.7.

The generalization of Eq. (2.76) to soft emissions off of multiple lines simply requires the inclusion of multiple Wilson lines on the right-hand-side. In terms of operator matrix elements, the general result is

$$\langle p_1 \cdots p_N; k_1 \cdots k_\ell |\, \mathcal{O}\, |0\rangle \;\cong\; \langle p_1 \cdots p_N |\, \mathcal{O}\, |0\rangle\, \langle k_1 \cdots k_\ell |\, Y_1^\dagger \cdots Y_N\, |0\rangle \tag{2.77}$$

We will now prove this using only Eq. (2.76) and a straightforward enumeration of the diagrams associated with the contractions on the two sides. Because our proof only uses Eq. (2.76) we will be able to recycle it for soft-collinear factorization, spinor QED and QCD below.

First, note that both sides of Eq. (2.77), in the soft limit, consist of a sum of terms with different numbers of $\frac{n_i\cdot\epsilon_k}{n_i\cdot k}$ factors for each i. On the left-hand side, each factor comes from the contraction of a photon with the i-th scalar and on the right-hand side, from a contraction of a photon with the i-th Wilson line. Thus, let

us define the set of integers $\{\ell_i\}$ corresponding to a particular partitioning of the number of photons connecting to each direction. That is, ℓ_1 photons connect to the first scalar, ℓ_2 to the second, and so on. It is then clear that Eq. (2.77) should hold for each set $\{\ell_i\}$ separately.

For each Feynman diagram, it is easy to read off what $\{\ell_i\}$ is. Let $\mathcal{D}_{\{\ell_i\}}$ be some diagram with ℓ_i photons attached to the i-th leg. For example, we might take

$\mathcal{D}_{1,2,2,1,3} \equiv$ 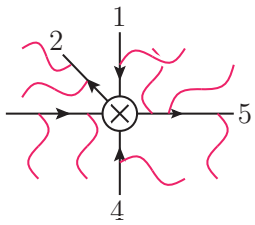

(2.78)

If we choose a fiducial diagram $\mathcal{D}_{\{\ell_i\}}$ for each possible set of integers $\{\ell_i\}$ satisfying $0 \leq \ell_i \leq \ell$ and $\sum_i \ell_i = \ell$, then we can write the matrix element as

$$\langle p_1 \cdots p_N; k_1 \cdots k_\ell | \, \mathcal{O} \, |0\rangle = \sum_{\{\ell_i\}} \sum_{\substack{\text{perms of} \\ \{k\} \hookrightarrow \{\ell_i\}}} \sum_{\substack{\text{perms} \\ \text{on } p_1}} \cdots \sum_{\substack{\text{perms} \\ \text{on } p_N}} \mathcal{P}\big[\mathcal{D}_{\{\ell_i\}}\big] \tag{2.79}$$

The first sum is over the partitionings $\{\ell_i\}$. The second sum, denoted "perms of $\{k\} \hookrightarrow \{\ell_i\}$", is over the permutations of which ℓ_i photons, $k_1^i \cdots k_{\ell_i}^i$, connect to which leg, for each i. The "perms on p_j" changes the ordering by which the photons connect to the j-th line, keeping $\{\ell_i\}$ and $\{k\} \hookrightarrow \{\ell_i\}$ fixed. Finally, $\mathcal{P}[\mathcal{D}_{\{\ell_i\}}]$ means apply the product of all these permutations to the fiducial diagram for the given $\{\ell_i\}$.

Now, let us evaluate these sums. For the "perms of p_N" sum, we are to hold the emissions off of legs 1 through $N-1$ fixed and sum only over permutations of the photons attached to the N leg. This rest-of-the-diagram provides an overall multiplicative factor to Eq. (2.76) which has no effect on the correspondence between

the soft photons attached to leg N and the Wilson line, Y_N. Thus we have

$$\sum_{\substack{\text{perms}\\ \text{of } p_N}} \mathcal{P}\big[\mathcal{D}_{\ell_1,\ldots,\ell_{N-1},\ell_N}\big] = \langle k_1^N \cdots k_{\ell_N}^N |\, Y_N \,|0\rangle \;\; \mathcal{D}_{\ell_1,\ldots,\ell_{N-1},0} \tag{2.80}$$

Similarly, we can now proceed to the evaluation of the "perms of p_{N-1}" sum to produce a matrix element of the $N-1$ Wilson line. We can continue in this way until there are no lines left and we have only $\mathcal{D}_{0,\ldots,0} = \langle p_1 \cdots p_N |\, \mathcal{O} \,|0\rangle$. Thus Eq. (2.79) becomes

$$\langle p_1 \cdots p_N; k_1 \cdots k_\ell |\, \mathcal{O} \,|0\rangle \cong \langle p_1 \cdots p_N |\, \mathcal{O} \,|0\rangle \sum_{\{\ell_i\}} \sum_{\substack{\text{perms of}\\ \{k\}\hookrightarrow\{\ell_i\}}} \prod_{i=1}^{N} \langle k_1^i \cdots k_{\ell_i}^i |\, Y_i^\dagger \text{ or } Y_i \,|0\rangle \tag{2.81}$$

where "$Y_i^\dagger$ or Y_i" means $Y_i^\dagger$ if p_i is a particle or Y_i if p_i is an anti-particle.

The last step is simply to note that $\sum_{\{\ell_i\}} \sum_{\{k\}\hookrightarrow\{\ell_i\}}$ exactly coincides with the sum of contractions of the composite operator $Y_1^\dagger \cdots Y_N$ with the photons in the external state $\langle k_1 \cdots k_\ell|$. This should not come as a surprise since these sums came from the contractions of the Lagrangian insertions with the same external state on the left-hand side of Eq. (2.79). Hence, Eq. (2.81) reduces to Eq. (2.77) which was our desired result.

Now that we have understood how soft photons decouple from collinear lines, we can immediately generalize Eq. (2.77) to include soft scalar-anti-scalar pairs in the state $\langle X_s|$ which leads to

$$\langle p_1 \cdots p_N; X_s |\, \mathcal{O} \,|0\rangle \cong \langle p_1 \cdots p_N |\, \mathcal{O} \,|0\rangle \;\; \langle X_s |\, Y_1^\dagger \cdots Y_N \,|0\rangle \tag{2.82}$$

This generalization is immediate because soft scalars must couple through a soft photon which is approximately on-shell and we have shown that the latter couples to collinear lines via the soft Wilson lines, Y_j. Therefore, if we simply let

$\langle X_s| Y_1^\dagger \cdots Y_N |0\rangle$ evolve under the full scalar QED Lagrangian, we can describe soft scalar production by an emission from a soft Wilson line, followed by a splitting from the Lagrangian. A similar story holds for pair creation from a collinear photon and was discussed at the end of Section 2.4.1.

The bright side of the heavy notation that we introduced in this section is that every equation after Eq. (2.76) only relied on how fields are contracted with states in quantum field theory. Therefore, as long as Eq. (2.76) continues to hold, the above proof will work for path-ordered Wilson lines in QCD as well as with any modification to $\mathcal{D}_{0,\ldots,0}$. The former will be used in Section 2.7 to show soft factorization in QCD and the latter will be used in the next section to show soft-collinear factorization in scalar QED

2.4.3 Simultaneous Soft-Collinear Factorization

We now tackle the full problem of factorizing matrix elements of the form

$$\langle X_1 \cdots X_N; X_s| \mathcal{O} |0\rangle \tag{2.83}$$

where $\langle X_j|$ is a state of many collinear particles, $\langle X_s|$ is a state of many soft particles, and $\mathcal{O} = \frac{1}{(N/2)!}|\phi|^N$ is the hard-scattering operator. As above, since soft scalars must come from pair creation initiated by a soft photon, when discussing how the soft sector decouples from the collinear sectors, we only need to worry about soft photons. We therefore assume $\langle X_s|$ just contains soft photons.

Soft coherence

One way to understand why soft-collinear factorization holds is to think of it in terms of coherence [27, 58]. In a classical theory, the electromagnetic field far away from a set of charged particles is only sensitive to the net charge at leading order in the multipole expansion. In the same way, soft radiation is only sensitive to the net charge of a set of particles all collinear to the same direction. For example, if there are two particles with charges Q_1 and Q_2 and momenta p_1 and p_2 with $p_1 \parallel p_2 \parallel n$, then the two diagrams for emitting a soft photon of momentum k and polarization ϵ add as follows:

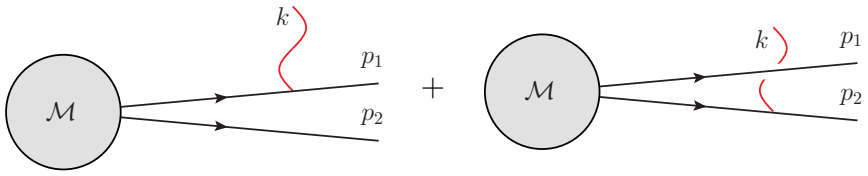

$$= \left(Q_1 \frac{p_1 \cdot \epsilon}{p_1 \cdot k} + Q_2 \frac{p_2 \cdot \epsilon}{p_2 \cdot k} \right) \times \mathcal{M} \;\cong\; (Q_1 + Q_2) \frac{n \cdot \epsilon}{n \cdot k} \times \mathcal{M} \tag{2.84}$$

This amplitude is the same as one where the soft photon was emitted from a single line in the n direction with charge $Q_1 + Q_2$. That is the general idea, at least.

Unfortunately, Eq. (2.84) does not hold generally. The problem is that $\mathcal{M}$ could depend on k differently in the two diagrams, in which case we would not be able to simply take $k \to 0$ because $k \cdot p_1$ and $k \cdot p_2$ are the same size as $p_1 \cdot p_2$, namely $\mathcal{O}(\lambda^2)$. In other words, we must worry about diagrams that "tangle" the soft and collinear emissions. For example, with one soft and one collinear photon, there are

three diagrams in scalar QED which connect these photons to the same leg:

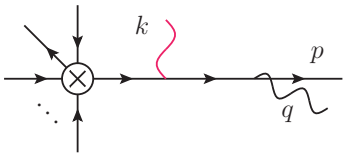

$$= \frac{-g\,(p+q)\cdot\epsilon_k}{p\cdot q+(p+q)\cdot k}\,\frac{-g\,p\cdot\epsilon_q}{p\cdot q} \sim \frac{-g\,(p+q)\cdot\epsilon_k}{\lambda^2+\lambda^2}\,\frac{-g\,p\cdot\epsilon_q}{\lambda^2}$$

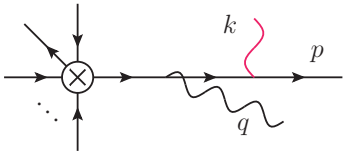

$$= \frac{-g\,(p+k)\cdot\epsilon_q}{p\cdot q+(p+q)\cdot k}\,\frac{-g\,p\cdot\epsilon_k}{p\cdot k} \sim \frac{-g\,p\cdot\epsilon_q}{\lambda^2+\lambda^2}\,\frac{-g\,p\cdot\epsilon_k}{\lambda^2} \tag{2.85}$$

and

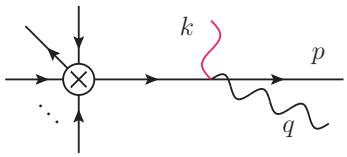

$$= \frac{-g^2\,\epsilon_k\cdot\epsilon_q}{p\cdot q+(p+q)\cdot k} \sim \frac{-g^2\,\epsilon_k\cdot\epsilon_q}{\lambda^2+\lambda^2}$$

Here, the soft photons are colored red and are drawn with broader wiggles than the collinear photons. The naive soft coherence argument of Eq. (2.84) would imply that only the second diagram should contribute, but clearly the first diagram is the same order in the power-counting.

Of course, coherence does actually hold, and it is not too hard to simplify these amplitudes to see it directly. With spinor-helicity methods, we can prove some useful and non-obvious identities, such as

$$\epsilon_q^+\cdot\epsilon_k^+ = \frac{p\cdot\epsilon_q^+\,q\cdot\epsilon_k^+}{p\cdot q}+\frac{k\cdot\epsilon_q^+\,p\cdot\epsilon_k^+}{p\cdot k}-\frac{p\cdot\epsilon_q^+\,p\cdot\epsilon_k^+ q\cdot k}{p\cdot q\,p\cdot k} \tag{2.86}$$

$$\epsilon_q^+\cdot\epsilon_k^- = \frac{p\cdot\epsilon_q^+\,q\cdot\epsilon_k^-}{p\cdot q}+\frac{k\cdot\epsilon_q^+\,p\cdot\epsilon_k^-}{p\cdot k}-\frac{p\cdot\epsilon_q^+\,p\cdot\epsilon_k^- q\cdot k}{p\cdot q\,p\cdot k}-\underbrace{\frac{\langle qp\rangle[kp]}{[pq]\langle pk\rangle}}_{=1} \tag{2.87}$$

where both of these equations hold for any reference vector choices and any four-momentum p, and the last term is 1 if the momenta are real. The other possible helicity choices can be found be conjugating the above equations. Now we can simplify

the tangled diagrams of Eq. (2.85) as follows:

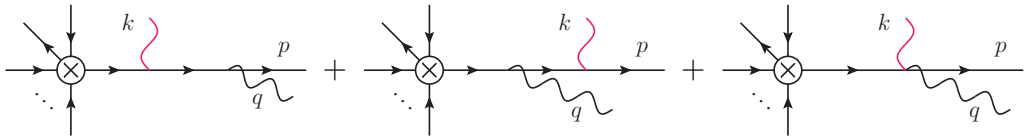

$$= \frac{(-g)^2}{p\cdot q + (p+q)\cdot k}\left[(p+q)\cdot\epsilon_k\,\frac{p\cdot\epsilon_q}{p\cdot q} + (p+k)\cdot\epsilon_q\,\frac{p\cdot\epsilon_k}{p\cdot k} - \epsilon_k\cdot\epsilon_q\right] \tag{2.89}$$

$$= \begin{cases} (-g)\dfrac{p\cdot\epsilon_q^{\pm}}{p\cdot q}\,(-g)\dfrac{p\cdot\epsilon_k^{\pm}}{p\cdot k} & \text{for } \pm\pm \text{ polarizations} \\ (-g)\dfrac{p\cdot\epsilon_q^{\pm}}{p\cdot q}\,(-g)\dfrac{p\cdot\epsilon_k^{\mp}}{p\cdot k} + \dfrac{(-g)^2}{p\cdot q + (p+q)\cdot k} & \text{for } \pm\mp \text{ polarizations} \end{cases} \tag{2.90}$$

where this equality is completely general; it holds for any reference vector choice for either photon as well as any on-shell four momenta, p, q, k.

Eq. (2.90) says that the sum of the three tangled diagrams reduces to an eikonal form plus a term that is polarization vector independent. Since the leading power diagrams for one soft and one collinear emission scale like g^2/λ^3, the extra term in Eq. (2.90) is a power correction. Thus, at leading power the sum of the tangled graphs reduces to the eikonal form, which is simply the product of the separate amplitudes for soft and collinear emissions. In particular, the soft photon factorizes off as expected, and is only sensitive to the net charge of the scalar, independent of whether there are collinear photons nearby.

Although it is surely possible, it would certainly be cumbersome to evaluate matrix elements explicitly for an arbitrary number of soft and collinear emissions in scalar QED. Moreover, analyzing the diagrams directly in scalar QED would also not easily generalize to an analysis for QCD. Fortunately, soft-collinear factorization can be derived much more simply by exploiting reference-vector independence, which generalizes easily to more-complicated gauge theories.

General soft-collinear factorization

We begin with a lemma:

Lemma. *Two expressions that are independent of the choice of reference vectors, r_i, and that agree at leading power for particular r_i, must agree at leading power for any r_i.*

This lemma is the trivial statement that two constant functions that agree somewhere, agree everywhere. It is nevertheless extremely powerful. Since the matrix elements in full gauge theories and factorized expressions in terms of Wilson lines are both r_i-independent, this lemma reduces the problem of proving factorization to working with particular choices of r_i.

Consider first states $\langle p_1 \cdots X_j \cdots p_n; X_s|$ with an arbitrary number of soft photons, but where all of the collinear photons are collinear to the same direction n_j^μ. Let r_s denote the reference vector for the soft photons and r_c denote the reference vector for the collinear photons. First choose generic-r for the collinear photons so that the relevant diagrams at leading power have only self-collinear emissions. Now, since the soft momenta $\{k\}$ are not collinear to p_j, choosing $r_s = p_j$ does not make their polarization vectors, ϵ_k, enhanced.[6] With these choices, the diagrams which contribute at leading power have the collinear photons coming off *only* the j-th scalar

[6]The region of phase-space for which k is both collinear to p and soft is not interesting at tree-level. At tree-level, one is free to choose whether to call this photon soft or collinear; it will factorize either way. At loop-level, the soft-collinear region is more subtle [59].

and the soft photons coming off of *all but* the j-th scalar:

$$\langle p_1 \cdots X_j \cdots p_N; X_s | \, \mathcal{O} \, |0\rangle \overset{\substack{r_s = p_j \\ \text{gen}-r_c}}{\cong} \sum_{\text{coll: only } j} \sum_{\text{soft: no } j}$$

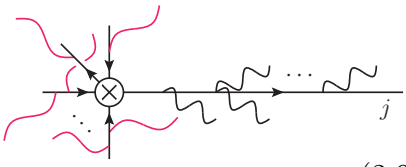

(2.91)

Since no diagram in this set has soft and collinear photons connected to the same line, we can use the separate arguments for soft and collinear factorization to show that these diagrams factorize. That is, writing the sum over soft emissions as in Eq. (2.79), using Eq. (2.80) and then recombining the leftover sums, we have

$$\langle p_1 \cdots X_j \cdots p_N; X_s | \, \mathcal{O} \, |0\rangle \overset{\substack{r_s = p_j \\ \text{gen}-r_c}}{\cong} \langle p_1 \cdots X_j \cdots p_N | \, \mathcal{O} \, |0\rangle \times \langle X_s | \, Y_1^\dagger \cdots Y_{j-1} Y_{j+1} \cdots Y_N \, |0\rangle \tag{2.92}$$

Now, since we are assuming $r_s = p_j$, any matrix element of Y_j with soft photons is power suppressed: $\langle X_s | \, Y_j \, |0\rangle \sim 0$. Therefore, we can add Y_j to the right-hand side of Eq. (2.92) without changing it at leading power. Thus, we have

$$\langle p_1 \cdots X_j \cdots p_N; X_s | \, \mathcal{O} \, |0\rangle \cong \langle p_1 \cdots X_j \cdots p_N | \, \mathcal{O} \, |0\rangle \, \langle X_s | \, Y_1^\dagger \cdots Y_N \, |0\rangle \tag{2.93}$$

Although we have only shown that this holds when r_c is generic and $r_s = p_j$, by the lemma, since both sides are reference-vector independent, it must hold for any reference vectors.

There is not a diagram-by-diagram correspondence in Eq. (2.93). However, it is possible to identify sets of diagrams whose sums agree at leading power. We will continue to work in generic-r for the collinear photons, so that all the diagrams which contribute at leading power to Eq. (2.93) have the collinear photons connected to leg j. Then, the particular sets of diagrams we need in order to prove soft-collinear

factorization are the equivalent of Eq. (2.76), namely, diagrams where all the soft momenta connect to the j line:

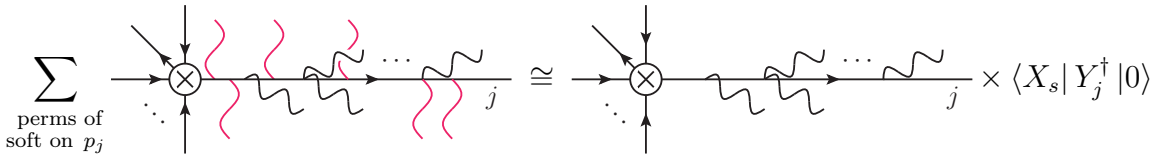

(2.94)

Here, the sum is over permutations where the soft photons connect, holding the topology of the collinear photons fixed but arbitrary. This diagrammatic relation is the key to soft-collinear factorization: it says that soft photons can be simply stripped off of Feynman diagrams, like leaves off a sprig of thyme.

We will prove Eq. (2.94) by induction on the number of soft photons. For zero soft-photons, the equation is trivially satisfied. So let us assume Eq. (2.94) holds for any number of soft photons less than n. Now, consider the diagrams which contribute to the left-hand side of Eq. (2.93) with n photons and let $\mathcal{D}_{\{\ell_i\}}$ be a fiducial diagram in that sum with ℓ_i soft photons on the i-th collinear line and $\sum_i \ell_i = n$. Note that, here $\mathcal{D}_{\{\ell_i\}}$ has a fixed topology of self-collinear emissions in the j-th sector as well as all of the soft photons. Now, as in Eq. (2.79), write the sum of diagrams in Eq. (2.93) as:

$$\langle p_1 \cdots X_j \cdots p_N; X_s| \mathcal{O} |0\rangle = \sum_{\substack{\text{perms of} \\ \text{coll.}}} \sum_{\{\ell_i\}} \sum_{\substack{\text{perms of} \\ \{k\}\hookrightarrow\{\ell_i\}}} \sum_{\substack{\text{perms} \\ \text{on } p_j}} \cdots \sum_{\substack{\text{perms} \\ \text{on } p_N}} \mathcal{P}\big[\mathcal{D}_{\{\ell_i\}}\big] \tag{2.95}$$

For simplicity, we sum over the permutations of attachments to the j-th line last. The sums with $i \neq j$ can be performed using Eq. (2.80), which holds even with collinear emissions on the j leg. The last sum to do is over the "perms on p_j" of $\mathcal{D}_{0,\ldots,\ell_j,\ldots,0}$. If

$\ell_j < n$, we can perform this sum using the induction hypothesis:

$$\sum_{\substack{\text{perms}\\ \text{of } p_j}} \mathcal{P}\left[\mathcal{D}_{0,\ldots,\ell_j,\ldots,0}\right] \cong \mathcal{D}_{0,\ldots,0}\ \langle k_1^j \cdots k_{\ell_j}^j |\, Y_j^\dagger\, |0\rangle \quad \text{for} \quad \ell_j < n \tag{2.96}$$

The only sum we cannot perform is the one when all n photons attach to leg j. So let us add and subtract $\sum_{\text{perms of coll.}} \mathcal{D}_{0,\ldots,0} \langle k_1 \cdots k_n |\, Y_j^\dagger\, |0\rangle$ to Eq. (2.96). When we add it, we have a sum of terms with matrix elements of soft Wilson lines just like Eq. (2.81). These Wilson lines can then combine into a single composite operator. We thus have

$$\begin{aligned}\langle p_1 \cdots X_j \cdots p_N; X_s |\, \mathcal{O}\, |0\rangle \cong \langle p_1 \cdots X_j \cdots p_N |\, \mathcal{O}\, |0\rangle \, \langle X_s |\, Y_1^\dagger \cdots Y_N\, |0\rangle \\ + \sum_{\substack{\text{perms of}\\ \text{coll.}}} \left[\sum_{\substack{\text{perms}\\ \text{on } p_j}} \mathcal{D}_{0,\ldots,n,\ldots,0} \;-\; \mathcal{D}_{0,\ldots,0}\, \langle k_1 \cdots k_n |\, Y_j^\dagger\, |0\rangle \right]\end{aligned} \tag{2.97}$$

Since the first line holds on its own, by Eq. (2.93), the second line must vanish. Moreover, since nothing we have said depended on summing over the collinear permutations, the term in square brackets vanishes on its own. This proves Eq. (2.94).

With Eq. (2.94) proven, we find ourselves in exactly the position we were in Section 2.4.2 with Eq. (2.94) taking the place of Eq. (2.76) and $\mathcal{D}_{0,\ldots,0}$ a specific diagram in $\langle X_1 \cdots X_N |\, \mathcal{O}\, |0\rangle$ instead of being $\langle p_1 \cdots p_N |\, \mathcal{O}\, |0\rangle$. Since the arguments of Section 2.4.2 did not depend on $\mathcal{D}_{0,\ldots,0}$, we can prove that $\langle X_s |\, Y_1^\dagger \cdots Y_N\, |0\rangle$ factors off of each possible collinear diagram in $\langle X_1 \cdots X_N |\, \mathcal{O}\, |0\rangle$ exactly as it was done for $\langle p_1 \cdots p_N |\, \mathcal{O}\, |0\rangle$. Hence,

$$\langle X_1 \cdots X_N; X_s |\, \mathcal{O}\, |0\rangle \overset{\text{gen}-r_c}{\cong} \langle X_1 \cdots X_N |\, \mathcal{O}\, |0\rangle \, \langle X_s |\, Y_1 \cdots Y_N^\dagger\, |0\rangle \tag{2.98}$$

Now, since both sides of this equation are r-independent, we can drop the restriction that the collinear photons are in generic-r, by the lemma.

Finally, since the soft emissions are factorized off, we can now factorize the collinear sectors as in Eq. (2.68) and use the same argument as before to allow for soft scalars in $\langle X_s|$, giving the final form for factorization in scalar QED:

$$\boxed{\langle X_1 \cdots X_N; X_s | \, \mathcal{O} \, |0\rangle \cong \langle X_1 | \, \phi^* W_1 \, |0\rangle \ldots \langle X_N | \, W_N^\dagger \phi \, |0\rangle \, \langle X_s | \, Y_1^\dagger \cdots Y_N \, |0\rangle} \tag{2.99}$$

Let us review the ingredients that went into this derivation. First, we used separate soft and collinear factorization. We also used various facts about which classes of diagrams could contribute with certain reference-vector choices, and of course reference-vector independence. We did not use any results specific to scalar QED or even to Abelian gauge theories; the identical arguments may be used in any gauge theory to prove soft-collinear factorization.

2.4.4 The position-space picture

Before moving on to theories more complicated than scalar QED, it is worth revisiting the physical picture behind factorization since it is identical in spinor QED or QCD. Although matrix elements are rarely computed in position space, position space is where our physical intuition lies. Since collinear fields have transverse momenta that scale like $p_\perp \sim \lambda Q$, the associated radiation field has a characteristic transverse size of $x_\perp \sim (\lambda Q)^{-1}$. In contrast, since soft momenta scale like $k \sim \lambda^2 Q$ in all components, the soft radiation field varies over scales $x \sim (\lambda Q)^{-2}$. In particular, since soft photons have wavelengths which are a factor of λ^{-1} larger than the

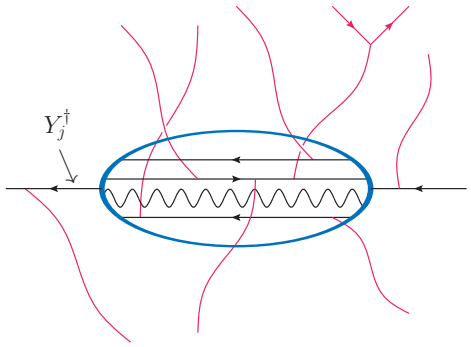

Figure 2.1: The physical picture of soft photons emitted by a classical source, $Y_j^\dagger$. The blue oval represents magnification that shows the substructure of the collinear sector which is invisible to the soft photons.

width of the collinear sector (the jet), they cannot resolve the jet's substructure, only its net charge. This is shown pictorially in Figure 2.1.

Outside of the jets, the soft particles interact, and split into scalars on time scales $\delta t \sim (\lambda\, Q)^{-2}$. None of these additional soft particles can probe the jet's substructure either. That is why the soft Lagrangian is a totally decoupled from the collinear Lagrangian – soft photons only see the jet as a classical source of radiation in the direction n^μ, which is what the Wilson line encodes. In fact, if one changes to radial coordinates, so the jets become parallel lines extending form $\tau = \pm\infty$ [53], one can literally think of the jets as parallel wires whose moving charges only leave a collective imprint on the exterior magnetic field.

The position-space picture of collinear factorization is similar to the soft case just described. Due to the scaling of the momenta of collinear particles, collinear radiation is confined into a set of cones. The radiation in the j-th cone (call it the j-cone) cannot resolve any of the dynamics outside of that cone; it can only see radiation that is emitted into it. In particular, an individual collinear sector is insensitive to

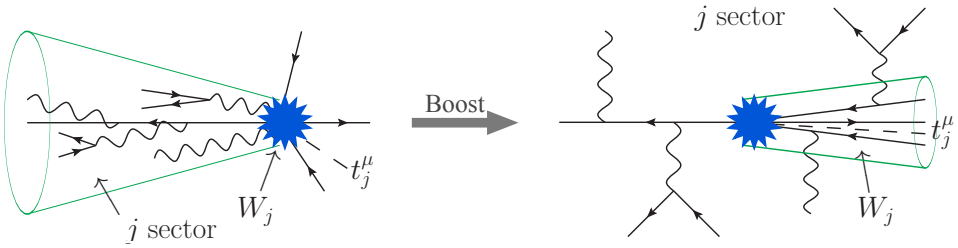

Figure 2.2: The physical picture of collinear photons emitted by classical source, W_j. The picture on the left is in the frame of the hard scattering and that on the right is in the frame where each component of the j-collinear momenta are the same size, λ.

the direction of travel of the charges outside of its cone, just as the soft photons could not resolve the substructure in a collinear sector. Therefore, all the charges outside of the cone can be deformed into the same direction, say t_j^μ, in which case the charges add exactly as in Eq. (2.84). This is why an individual collinear sector sees the Wilson line, W_j; a classical source of radiation traveling in the t_j direction with opposite charge to that in the cone.

We can make this story even closer to that of the soft by boosting in the j-th direction with a gamma factor of λ^{-1}. Then the j-cone becomes the whole space except a cone in the opposite direction which contains all of the radiation that was originally outside of the j-cone. Call this new cone the $\bar{j}$-cone. Now, all of the charges that were originally outside of the j-cone are in the $\bar{j}$-cone and act as a single classical source for radiation into the j-sector (which now fills almost the whole space, just as the soft sector did). The freedom of choice of the direction of the Wilson line, t_j, comes from the fact that any direction outside of the j-cone gets boosted into the $\bar{j}$-cone. This picture is shown in Figure 2.2.

2.5 Factorization for general S-matrix elements

So far we have considered factorization for processes which can be written at leading-order as matrix elements of local hard-scattering operators $\mathcal{O}(x)$ composed of N fields. Factorization in the form on the right-hand-side of Eq. (2.99) actually holds more generally, for any process involving N distinct directions, whether or not we represent the hard scattering as the matrix element of a local operator with N fields. The generalization is perhaps easiest to see through an example.

Consider the scattering $\gamma\gamma \to \phi\phi^\star$ in scalar QED. At tree-level, there are 3-diagrams giving

$$i\mathcal{M} = \quad + \quad + \tag{2.100}$$

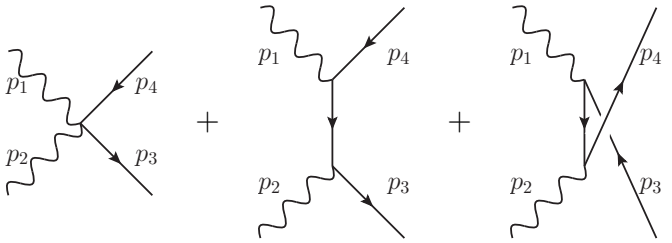

$$= 2ie^2 \left[(\epsilon_1 \cdot \epsilon_2) - \frac{(p_4 \cdot \epsilon_1)(p_3 \cdot \epsilon_2)}{p_4 \cdot p_1} - \frac{(p_3 \cdot \epsilon_1)(p_4 \cdot \epsilon_2)}{p_3 \cdot p_1} \right] \tag{2.101}$$

There is not an easy way to write this amplitude as the matrix element of a gauge-invariant local operator $\mathcal{O}$ with two scalar and two photon fields. The difficulty is that because the photons are identical, operators like $\frac{1}{p_1 \cdot p_3} p_3^\mu p_4^\nu D_\mu \phi D_\nu \phi^\star$ give contractions with both photons. Factorization nevertheless holds for this process. In fact, as we will see, factorization holds for each diagram separately, as if it represents an independent hard process.

To begin, consider the most enhanced graphs when soft photons or photons collinear to p_3 or p_4 are added to the t-channel diagram. In generic-r, the only way to get a collinear enhancement is to have self-collinear emissions. Then, the only way

to get a soft enhancement is by emission off of the 3 or 4 line because they are almost on shell. Thus, at leading power the t-channel part of the matrix element is given by a sum of graphs of the form

$$\langle X_3 X_4; X_s | \epsilon_1(p_1)\epsilon_2(p_2)\rangle \Big|_{t\text{-channel}} \cong \sum$$

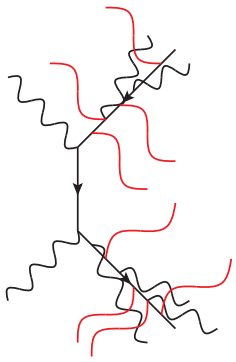

(2.102)

Using the key soft-collinear factorization equation, Eq. (2.94), we can strip the soft photons off of these graphs giving a factor of $\langle X_s|\, Y_3^\dagger Y_4\,|0\rangle$ multiplying the same graphs with no soft photons. Then, we use reference-vector independence and collinear factorization, as in Eq. (2.68), to write the collinear sectors as matrix elements of Wilson lines $\langle X_3|\, \phi^\star W_3\,|0\rangle$ and $\langle X_4|\, W_4^\dagger \phi\,|0\rangle$. The u-channel and 4-point diagram factorize in the same way. We thus have

$$\begin{aligned}\langle X_3 X_4; X_s | \epsilon_1(p_1)\epsilon_2(p_2)\rangle \cong -2i &\left[g^{\mu\nu} - \frac{P_4^\mu P_3^\nu}{P_4\cdot P_1} - \frac{P_3^\mu P_4^\nu}{P_3\cdot P_1}\right] \\ &\times \langle 0|\, \bar W_1^\dagger D_\mu \bar W_1\,|\epsilon_1(p_1)\rangle\, \langle 0|\, \bar W_2^\dagger D_\nu \bar W_2\,|\epsilon_2(p_2)\rangle \\ &\times \langle X_3|\, \phi^\star W_3\,|0\rangle\, \langle X_4|\, W_4^\dagger \phi\,|0\rangle\, \langle X_s|\, Y_3^\dagger Y_4\,|0\rangle \end{aligned} \quad (2.103)$$

where P_3 and P_4 are the total momenta of the states $\langle X_3|$ and $\langle X_4|$. In QED, we could have written ieA_μ instead of $\bar W^\dagger D_\mu \bar W$ but we write the matrix element this way so that the matching coefficient only has dependence on momenta, independent of the spins. In QCD, similar factorized forms will arise with $\bar W^\dagger D_\mu \bar W$ reproducing matrix elements with multiple collinear partons in a gluon jet.

The result is that the S-matrix elements for this scattering process in scalar QED factorize. The factorization worked simply because soft and collinear emissions cannot couple to off-shell particles in Feynman diagrams at leading power (in generic-r). The same arguments apply to other scattering processes and to more complicated gauge theories like QCD. Thus, factorization holds for any hard scattering process with independent collinear sectors, irrespective of whether or not that process is written as the matrix element of a local operator.

2.6 Spinor QED

In the previous section, soft-collinear factorization was proven (at tree-level) in scalar QED. We now discuss how things change with spinors instead of scalars, and in the next section, go from QED to QCD.

Consider the following gauge-invariant hard-scattering operator in QED with N flavors:

$$\mathcal{O} = \bar{\psi}_1 \cdots \psi_N \tag{2.104}$$

We introduce the flavor indices on the fields only to simplify the contractions of the fields with states – one can easily drop the subscripts. We are interested in factorizing matrix elements of this operator in states comprising collinear and soft momenta, namely

$$\langle X_1 \cdots X_N; X_s | \, \mathcal{O} \, |0\rangle \tag{2.105}$$

Here we assume the flavor of the i-th jet matches the i-th field, for simplicity. We continue to ignore collinear sectors initiated by a photon, which means that we do

not consider covariant derivatives in the hard-scattering operator and the states $\langle X_j|$ have the flavor quantum numbers of a single fermion. Operators with derivatives or γ-matrices in the operator can easily be added, with the following proof hardly changing. Collinear sectors initiated by a gauge boson will be treated in the QCD section where they are more interesting.

In this section we will show that the addition of spin does not affect the results found in scalar QED. It does, however, require a little more notation. At leading order, when $\langle X| = \langle p_1 \cdots p_N|$, the matrix element is not 1 but rather

$$\langle p_1 \cdots p_N| \mathcal{O} |0\rangle = \bar{u}_1(p_1) \cdots v_N(p_N) \tag{2.106}$$

where $u_i(p_i)$ or $v_i(p_i)$ are the particle or antiparticle spinor states contracted according to the fields in $\mathcal{O}$. A useful shorthand will be to pool everything that each spinor is contracted with into one object we denote H^j. Thus,

$$\langle p_1 \cdots p_N| \mathcal{O} |0\rangle = \bar{u}_1 H^1 = \cdots = H^N v_N \tag{2.107}$$

That is, H^j is just the hard-scattering matrix element with the j-th spinor stripped off. In spinor-helicity notation

$$\langle p_1 \cdots p_N| \mathcal{O} |0\rangle = [p_1 H^1] = \langle p_2 H^2 \rangle \cdots = [H^N p_N] \tag{2.108}$$

with the bracket type depending on the helicity of the spinors, not whether it is particle or antiparticle. Here we have used the freedom of little group scaling to choose the spinor helicity for the momentum p_j to be exactly the spinor in the state $\langle p_j|$.

2.6.1 Collinear Factorization

We start by considering only collinear photons; extra collinear spinors will come from insertions of the Lagrangian as in scalar QED and soft photons will be treated below. The derivation of collinear factorization is essentially the same as for scalar QED because in generic-r exactly the same diagrams are enhanced. To see this, note that for a single collinear emission off of a massless spinor in QED, the leading order matrix element becomes

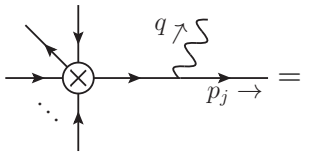

$$= \frac{-g\,\bar{u}_j \not{\epsilon}_q (\not{p}_j + \not{q})}{2p_j \cdot q}\, H^j = \frac{-g\, p_j \cdot \epsilon_q}{p_j \cdot q}\, \bar{u}_j H^j - \frac{g\,\bar{u}_j \not{\epsilon}_q \not{q}}{2p_j \cdot q}\, H^j \tag{2.109}$$

where the Dirac equation $\bar{u}_j \not{p}_j = 0$ has been used. The first term is very similar to the scalar-QED result and follows the same story as the before: in generic-r it only contributes at leading power when q is collinear to p_j, whereas for the collinear-r choice ($r = p_j$ for all photons collinear to p_j), the polarization vector itself is enhanced as in Eq. (2.53) and all *but* the self-collinear emissions contribute.

The final term in Eq. (2.109) is new. Since all the other (old) terms satisfy the Ward identity, this term must satisfy the Ward identity by itself, which is easy to check:

$$\frac{g\bar{u}(p_j) \not{\epsilon}_q \not{q}}{2p_j \cdot q}\, H^j \overset{\epsilon_q \to q}{=} \frac{g\bar{u}(p_j) \not{q} \not{q}}{2p_j \cdot q}\, H^j = \frac{g\bar{u}(p_j) q^2}{2p_j \cdot q}\, H^j = 0 \tag{2.110}$$

Thus this term, by itself, is reference-vector independent, which is also easy to check with helicity spinors:

$$\frac{g\bar{u}(p_j) \not{\epsilon}_q \not{q}}{2p_j \cdot q} H^j = \sqrt{2} g \frac{[p_j q]\langle r q\rangle [q H^j]}{\langle q r\rangle [p_j q] \langle q p_j\rangle} = \sqrt{2} g \frac{[q H^j]}{\langle p_j q\rangle} \tag{2.111}$$

So, independently of the reference-vector choice, the new term will only contribute at leading power when $q \parallel p_j$, that is, for self-collinear emissions. Such emissions will

come from a field emitting a photon through a Lagrangian interaction (as opposed to from a Wilson line), just as they do in the unfactorized expression.

Thus, we have exactly the same diagrammatic factorization as in Eq. (2.49) and by the same gauge-symmetry arguments, we get the same result as Eq. (2.68), namely

$$\langle X_1 \cdots X_m | \, \bar{\psi}_1 \cdots \psi_m \, |0\rangle \cong \langle X_1 | \, \bar{\psi}_1 W_1 \, |0\rangle \ldots \langle X_m | \, W_m^\dagger \psi_m \, |0\rangle \tag{2.112}$$

The right-hand side of this equation reproduces Eq. (2.109) for one emission. More generally, terms like $\frac{\not{\epsilon}_q \not{q}}{p_j \cdot q}$ will always come from Lagrangian emissions, while the the eikonal terms, $\frac{p_j \cdot \epsilon_q}{p_j \cdot q}$, either come from the Lagrangian (in generic-r) or the Wilson lines (in collinear-r).

2.6.2 Soft and soft-collinear factorization

The addition of spin has no affect on the factorization of soft emissions because soft emissions cannot flip the spin of non-soft particles. For example, in the soft limit of QED

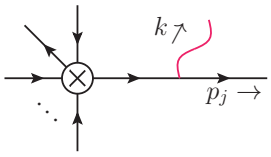

$$= \frac{-g\bar{u}_j \not{\epsilon}_k (\not{p}_j + \not{k})}{2p_j \cdot k} H^j \cong -g \frac{p_j \cdot \epsilon_k}{p_j \cdot k} \, \bar{u}_j H^j \tag{2.113}$$

This vertex is identical to the scalar QED result in Eq. (2.71). Since the soft limit is spin independent, soft factorization is identical in QED and scalar QED.

More generally, a useful fact is that the soft limit of the matrix element for a photon interacting with a particle of any spin or mass has the same eikonal form. The physical reason is simply that an arbitrarily soft photon does not have enough energy to flip the helicity of a particle. A proof proceeds as follows: let $\zeta_s^\alpha(p)$ be the

wavefunction for a particle of mass m and helicity s that interacts with a gauge boson through a current J^μ. For example, for spin 1, $\zeta_s^\alpha(p) = \epsilon_h^\mu(p)$ are the polarization vectors and for spin $\frac{1}{2}$, $\zeta_s^\alpha(p) = u_s^i(p)$ are the Dirac spinors. By unitarity, we can always write the two-point function for this particle as a sum of dyads:

$$G^{\alpha\beta}(x,y) = \int d^4p\, e^{ip(x-y)}\, \frac{i\sum_s \zeta_s^\alpha(p)\zeta_s^\beta(p)^\dagger}{p^2 - m^2 + i\varepsilon} \tag{2.114}$$

The key ingredient for the proof of spin independence is that the vertex for the emission of a soft gauge boson from an on-shell ζ particle is of the form [60]:

$$\langle p, s'|\, J^\mu(0)\, |p, s\rangle = \zeta_s^\alpha(p)^\dagger\, \Gamma^\mu_{\alpha\beta}\, \zeta_{s'}^\beta(p) = 2\, p^\mu\, \delta_{ss'} \tag{2.115}$$

The last equality is the statement of helicity conservation. Combining Eqs. (2.114) and (2.115), we get

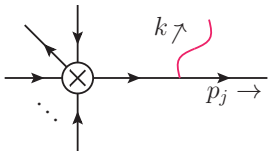

$$\begin{aligned} &\cong ig\, \epsilon_{k\,\mu}\, \bar{u}_s(p_j) \cdot \Gamma^\mu \cdot \frac{i\sum_{s'} u_{s'}(p_j)\bar{u}_{s'}(p_j)}{(p_j+k)^2 - m^2} H^j \\ &= ig\, \epsilon_{k\,\mu}\, 2p_j^\mu\, \frac{i\sum_{s'} \delta_{ss'}\bar{u}_{s'}(p_j)}{2p_j\cdot k} H^j \\ &= -g\, \frac{p_j\cdot\epsilon_k}{p_j\cdot k}\, \bar{u}_s(p_j) H^j \end{aligned} \tag{2.116}$$

Thus, the eikonal form of the soft interaction holds for any mass and spin. For non-Abelian gauge bosons this expression just gets multiplied by a generator matrix. Although this proof may seem pedantic for QED where the eikonal form can be derived much more directly, the spin-independence of the soft limit is very useful more generally. For example, it is actually quite cumbersome to show the eikonal form for a soft gluon emitted from a collinear gluon in QCD. Thus, Eq. (2.115) will be put to pragmatic use in the next section.

Since soft factorization is identical in spinor QED as in scalar QED, the derivation of soft-collinear factorization from Section 2.4.3 goes through unchanged. Therefore, in QED the same soft-collinear factorization formula as in Eq. (2.99) holds, with the replacement $\phi \to \psi$:

$$\boxed{\langle X_1 \cdots X_N; X_s | \, \mathcal{O} \, |0\rangle \cong \langle X_1 | \, \bar{\psi}_1 W_1 \, |0\rangle \ldots \langle X_N | \, W_N^\dagger \psi_N \, |0\rangle \, \langle X_s | \, Y_1^\dagger \cdots Y_N \, |0\rangle} \tag{2.117}$$

2.7 QCD

We are now ready to tackle the final details relevant for factorization in QCD. We wish to factorize matrix elements of a gauge-invariant hard-scattering operator of the form

$$\mathcal{O}^\mu = \bar{\psi}_1 \cdots \bar{\psi}_{m-1} (D^\mu) \psi_{m+1} \cdots \psi_N \tag{2.118}$$

with $N-1$ spinors and one covariant derivative. Here, as in the spinor QED section, the subscripts on the spinor fields are flavor indices added only to simplify the combinatorics. Color indices are suppressed to avoid clutter (cf. Eq. (2.125) below). Removing the flavor indices or considering more than a single covariant derivative requires us to keep track of tedious combinatoric factors and contractions among different spinors which dirty the expressions in our factorization proof but do not change the results in any substantial way. Such cases are best dealt with in a similar fashion to that described in Section 2.5. The covariant derivative D^μ in the operator is an easy way to give the operator non-zero matrix elements in a state with a gluon

in a particular direction. We consider matrix elements of this operator between the vacuum and the N-jet final state $\langle X| = \langle X_1 \cdots X_N; X_s|$, with each state $\langle X_j|$ either a quark jet, with the flavor of a single quark species, or the gluon jet which we place in $\langle X_m|$. The matrix element of this operator in the simplest such state, with $N-1$ spinors and one gluon is,

$$\langle p_1 \cdots p_m, a \cdots p_N| \, \mathcal{O}^\mu \, |0\rangle = \bar{u}_1(p_1) \cdots (-igT^a)\epsilon^\mu(p_m) \cdots v_N(p_N) \tag{2.119}$$

$$\equiv \bar{u}_1(p_1) H_1^\mu = \cdots = \epsilon^\mu(p_m) H_m \tag{2.120}$$

as in Eq. (2.106) or Eq. (2.107). We are considering the simplest possible operator, $\mathcal{O}$, for clarity. Operators with nontrivial Dirac structure and insertions of partial derivatives change nothing but the form of the above H_i's.

2.7.1 Collinear Factorization

For gluons emitted off of a quark line, collinear factorization follows immediately from the generic-r choice of reference vectors. In generic-r only self-collinear emissions are enhanced. That is,

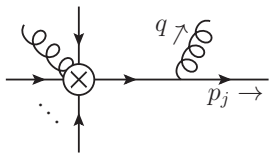

$$\overset{\text{gen. } r}{\sim} \bar{u}_j(g\lambda^{-1})H_j^\mu \tag{2.121}$$

while

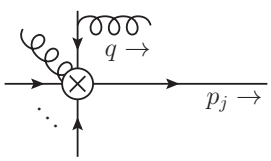

$$\overset{\text{gen. } r}{\sim} \bar{u}_j(g\lambda^{0})H_j^\mu \tag{2.122}$$

Although the momentum going into the hard vertex depends on $q + p_j$, this induces no additional enhancement.

For a gluon jet, collinear emissions follow the same pattern. In generic-r, self-collinear emissions

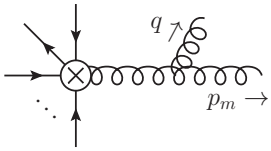

$$\overset{\text{gen. } r}{\sim} \frac{g}{\lambda}\epsilon^\mu H_m \qquad \text{and}$$

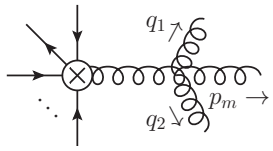

$$\overset{\text{gen. } r}{\sim} \left(\frac{g}{\lambda}\right)^2 \epsilon^\mu H_m \tag{2.123}$$

dominate over emissions off of other legs

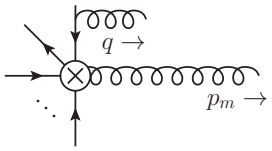

$$\overset{\text{gen. } r}{\sim} g\lambda^0\epsilon^\mu H_m \tag{2.124}$$

Thus, only self-collinear emissions are relevant at leading power, for either quark or gluon jets.

Collinear factorization in generic-r is therefore identical in QCD and QED. We can write the result as

$$\langle X_1 \cdots X_N | \, \mathcal{O}^\mu \, |0\rangle \overset{\text{gen. } r}{\cong} \langle X_1 | \, \bar{\psi}_1^{l_1} \, |0\rangle \cdots \langle X_m | \, (D^\mu)^{l_{m-1} l_{m+1}} \, |0\rangle \ldots \langle X_N | \, \psi_N^{l_N} \, |0\rangle \tag{2.125}$$

Here, we have displayed the fundamental color indices $l_1 \cdots l_N$ explicitly. These indices are all contracted since the original operator $\mathcal{O}$ was gauge invariant. The notation $(D^\mu)_{ij} \equiv \delta_{ij}\partial^\mu - igT^a_{ij}A^{a\mu}$ is the usual covariant derivative in the fundamental representation.

The reference-vector independent leading-power result is the generalization of Eq. (2.64):

$$\langle X_1 \cdots X_N | \, \mathcal{O}^\mu \, |0\rangle \cong$$
$$\langle X_1 | \, \bar{\psi}_1^{l_1} W_1^{l_1 h_1} \, |0\rangle \cdots \langle X_m | \, W_m^{\dagger\, h_{m-1} l_{m-1}} (D^\mu)^{l_{m-1} l_{m+1}} W_m^{l_{m+1} h_{m+1}} \, |0\rangle \ldots \langle X_N | \, W_N^{\dagger\, h_N l_N} \psi_N^{l_N} \, |0\rangle \tag{2.126}$$

where now the W are non-Abelian path-ordered Wilson lines and the new h_i color indices are summed over. One might be concerned that because the product $W^{\dagger\, hl}\psi^l$ carries a color index, h, it is not gauge invariant. However, the h index affects the transformation properties at $x = \infty$ which are trivial.

Finally, to make contact with our expectations from the physical intuition that a gluon jet should see a collinear Wilson line in the adjoint representation coming from the rest of the hard scattering process, we can use Eq. (2.27), $W_n^\dagger A_b^\mu T^b\, W_n = A_a^\mu\, \mathcal{W}_n^{ab}\, T^b$. So, it is indeed the case that the radiation from the rest of the event into a jet initiated by a gluon, A_a, in the collinear limit appears as if coming from a classical source of the form of a Wilson line in the adjoint representation, $\mathcal{W}^{ab}$.

2.7.2 Soft Factorization

The factorization of soft gluons off of the hard scattering matrix element is only different from the scalar-QED case in that we cannot use the eikonal identity as in Eq. (2.74) because the generator matrices do not commute. However, this changes nothing since the Wilson line is path ordered and exactly makes up for this:

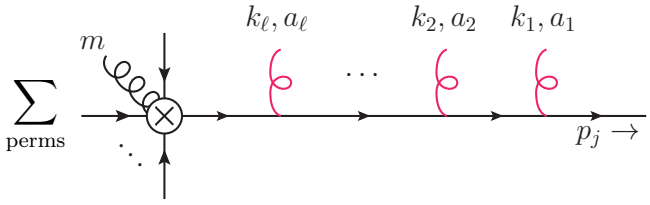

$$= \bar{u}(p_j)\left(\sum_{\text{perms}} (-g)^\ell \frac{n_j\cdot\epsilon_1}{n_j\cdot k_1} T^{a_1} \frac{n_j\cdot\epsilon_2}{n_j\cdot(k_1+k_2)} T^{a_2}\cdots \frac{n_j\cdot\epsilon_\ell}{n_j\cdot\sum_{i=1}^{\ell} k_i} T^{a_\ell}\right) H_j^\mu \tag{2.127}$$

$$= \bar{u}(p_j)\,\langle k_1\cdots k_\ell|\, Y_j^\dagger(0)\,|0\rangle\, H_j^\mu$$

Similarly, we can use general soft gauge-boson vertex of Eq. (2.115) as was done in Eq. (2.116) to show that

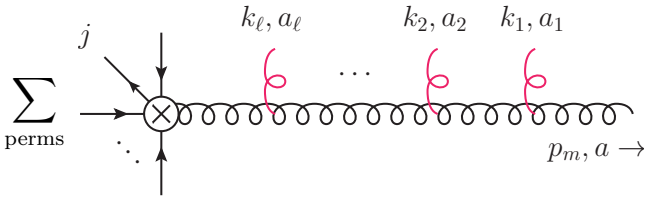

$$= \left(\sum_{\text{perms}} (-g)^\ell \frac{n_m \cdot \epsilon_1}{n_m \cdot k_1} T^{a_1}_{\text{adj}} \frac{n_m \cdot \epsilon_2}{n_m \cdot (k_1 + k_2)} T^{a_2}_{\text{adj}} \cdots \frac{n_m \cdot \epsilon_\ell}{n_m \cdot \sum_{i=1}^{\ell} k_i} T^{a_\ell}_{\text{adj}} \right) \epsilon^\mu_{p_m} H_m \tag{2.128}$$

$$= \langle k_1 \cdots k_\ell | \left(\mathcal{Y}^\dagger_m(0) \right)^{ab} |0\rangle \ \epsilon^\mu_{p_m} H^b_m$$

where $\mathcal{Y}_i$ is the usual soft Wilson but in the adjoint representation and in the last line we wrote the adjoint color indices explicitly.

Eq. (2.127) and (2.128) are the QCD equivalents of Eq. (2.76), which as mentioned in Section 2.4.2 is all we need to show, since all of the arguments in that section were completely general. Thus, using the arguments of Section 2.4.2, we arrive at the QCD equivalent of Eq. (2.82), namely

$$\begin{aligned} &\langle p_1 \cdots p_N; k_1 \cdots k_\ell | \, \bar{\psi}_1^{l_1} \cdots (D^\mu)^{l_{m-1} l_{m+1}} \cdots \psi_N^{l_N} |0\rangle \\ &\qquad = \langle p_1 \cdots p_N | \, \bar{\psi}_1^{l_1} \cdots (D^\mu)^{l_{m-1} l_{m+1}} \cdots \psi_N^{l_N} |0\rangle \\ &\qquad \times \langle k_1 \cdots k_\ell | \, Y_1^{\dagger \, l_1 h_1} \cdots Y_m^{h_{m-1} l_{m-1}} Y_m^{\dagger \, l_{m+1} h_{m+1}} \cdots Y_N^{h_N l_N} |0\rangle \end{aligned} \tag{2.129}$$

Note that one does not have to go through all of the arguments of Section 2.4.2 to figure out the contractions of indices in the equation above. For example, Eq. (2.127) shows that a collinear quark field, $\bar{\psi}^h$ should become $\bar{\psi}^l Y^{\dagger lh}$. Also, one does not need to worry about how the derivative in D^μ acts on the soft Wilson line because it is power suppressed.

We can now do the usual replacement $\langle k_1 \cdots k_\ell| \to \langle X_s|$, allowing $\langle X_s|$ to contain soft quarks, because any soft quarks must come soft-gluon splitting at leading power.

2.7.3 Soft-Collinear Factorization

The simultaneous soft and collinear factorization in QCD parallels that of scalar QED completely; the only difference being the more complicated non-Abelian charges of QCD. For example, the soft coherence of Eq. (2.84) is the same. Imagine taking $k \to 0$ naively as in Eq. (2.84) where we ignore k in any internal lines. Then taking $\mathcal{M} = 1$, $P = p + q_1 + q_2$ and the collinear-gluon three-point vertex to be $-iV_3^{\rho\alpha\beta} f^{ebc}$, we have:

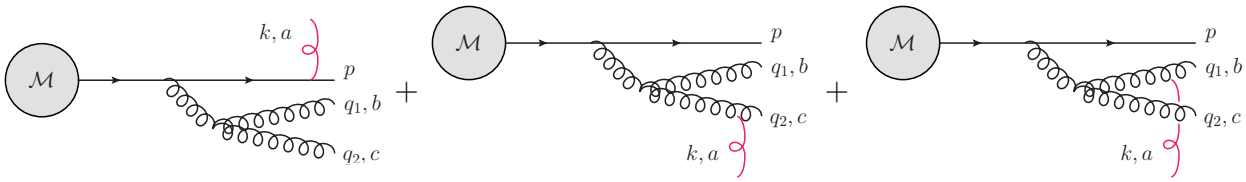

$$
\begin{aligned}
&= \bar{u}_p \frac{g\gamma_\rho}{(q_1+q_2)^2} \frac{\not{P}}{P^2} V_3^{\rho\alpha\beta} \left[t^a t^e f^{ebc} \frac{-g\, p\cdot\epsilon_k}{p\cdot k} - t^e f^{ebc'} \frac{g\, q_2\cdot\epsilon_k (T^a_{\text{adj}})_{cc'}}{q_2\cdot k} - t^e f^{eb'c} \frac{g\, q_1\cdot\epsilon_k (T^a_{\text{adj}})_{bb'}}{q_1\cdot k} \right] \\
&= \bar{u}_p \frac{g\gamma_\rho}{(q_1+q_2)^2} \frac{\not{P}}{P^2} V_3^{\rho\alpha\beta} \left[t^e t^a f^{ebc} + i t^d \big(f^{aed} f^{bce} + f^{bed} f^{cae} + f^{ced} f^{abe} \big) \right] \frac{-g\, n\cdot\epsilon_k}{n\cdot k} \\
&= \bar{u}_p \frac{g\gamma_\rho\, t^e}{(q_1+q_2)^2} \frac{i\not{P}}{P^2} \big(-iV_3^{\rho\alpha\beta} f^{ebc} \big) \frac{-g\, n\cdot\epsilon_k\, t^a}{n\cdot k}
\end{aligned}
\tag{2.130}
$$

To get the second line we used the general soft vertex of Section 2.6.2 and to get the last equation we used the Jacobi identity. The last line shows that the soft gluon only sees the total charge of the collinear sector.

However, as in Eq. (2.84), this only works if we assume the soft gluon momentum k is much softer than all the other momenta, which is too strong of a restriction. In fact k, can be of the same order as the $p \cdot q_i \sim \mathcal{O}(\lambda^2)$. Hence, we again have to worry

about the tangled diagrams, which means we must also consider:

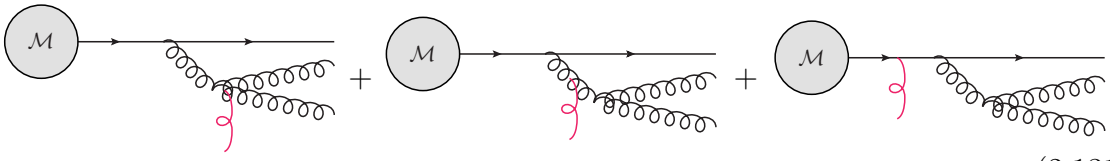

(2.131)

Indeed, summing these three diagrams with those in Eq. (2.130) would give the eikonal form for the soft emission, but we want to prove soft-collinear factorization more generally.

Luckily we have already done so! Section 2.4.3 used nothing about scalar QED; it only used that soft factorization and collinear factorization had been shown on their own. We have already shown both collinear and soft factorization separately in sections 2.7.1 and 2.7.2, so all we need to do is go through Section 2.4.3 step by step to get a general proof for QCD.

The only extra detail of QCD is the color indices which we already know how to contract from Eq. (2.129). Therefore, we can simply write down Eq. (2.98) for QCD as:

$$\begin{aligned}\langle X_1 \cdots X_N; X_s |\, \bar{\psi}_1^{l_1} \cdots (D^\mu)^{l_{m-1} l_{m+1}} \cdots \psi_N^{l_N} \,|0\rangle \\ = \langle X_1 \cdots X_N |\, \bar{\psi}_1^{l_1} \cdots (D^\mu)^{l_{m-1} l_{m+1}} \cdots \psi_N^{l_N} \,|0\rangle \\ \times \langle X_s |\, Y_1^{\dagger\, l_1 h_1} \cdots Y_m^{h_{m-1} l_{m-1}} Y_m^{\dagger\, l_{m+1} h_{m+1}} \cdots Y_N^{h_N l_N} \,|0\rangle \end{aligned} \tag{2.132}$$

Now that the soft gluons are factorized, we use Section 2.7.1 (generic-r and reference-vector independence), in particular Eq. (2.126), to get the general soft-collinear fac-

torization in QCD:

$$\begin{aligned}
&\langle X_1 \cdots X_N; X_s | \, \bar{\psi}_1^{l_1} \cdots (D^\mu)^{l_{m-1} l_{m+1}} \cdots \psi_N^{l_N} \, |0\rangle \\
&\quad = \langle X_1 | \, (\bar{\psi}_1 W_1)^{l_1} \, |0\rangle \cdots \langle X_m | \, (W_m^\dagger D^\mu W_m)^{l_{m-1} l_{m+1}} \, |0\rangle \ldots \langle X_N | \, (W_N^\dagger \psi_N)^{l_N} \, |0\rangle \\
&\qquad\qquad \times \langle X_s | \, Y_1^{\dagger \, l_1 h_1} \cdots Y_m^{h_{m-1} l_{m-1}} Y_m^{\dagger \, l_{m+1} h_{m+1}} \cdots Y_N^{h_N l_N} \, |0\rangle
\end{aligned} \tag{2.133}$$

Note that the l_j index on each of the collinear matrix elements and on each soft Wilson line transforms at infinity, so each term in this equation is separately gauge invariant.

Eq. (2.133) is our final result and has been proven at tree-level for arbitrary collinear states $\langle X_j|$ either initiated by a quark or a gluon and an arbitrary soft state $\langle X_s|$. It is the statement that, when considering the scattering of energetic massless particles interacting with gauge bosons, the form of soft and collinear emissions simplifies tremendously. Hard-scattered particles see only a collinear Wilson line with charge opposite their own in place of all possible collinear gauge-boson emissions from the rest of the scattering. Furthermore, they emit soft gauge bosons in the form of a classical source moving in their direction of travel with their charge.

2.8 SCET

To touch base with SCET, in particular the formulation in [51], we note that each matrix element on the right-hand side of Eq. (2.133) can be computed with a

separate copy of the QCD Lagrangian. We can formalize this by writing an effective Lagrangian which is the sum of $N+1$ copies of the QCD Lagrangian:

$$\mathcal{L}_{\text{eff}} = \mathcal{L}_{\text{soft}} + \sum_{j=1}^{N} \mathcal{L}_j \tag{2.134}$$

Then we assign separate quantum numbers j or s to the particles in X_j and X_s associated with their sector, with the fields in the Lagrangians $\mathcal{L}_j$ or $\mathcal{L}_{\text{soft}}$ being only able to create or destroy particles with the appropriate quantum number. Once this is done, we can simply combine all the matrix elements together to write

$$\begin{aligned}
&\langle X_1 \cdots X_m; X_s | \, \bar{\psi}_1 \cdots D^\mu \cdots \psi_N \, |0\rangle \\
&= \langle X_1 \cdots X_m; X_s | \, \big(\bar{\psi}_1 \, W_1 \, Y_1^\dagger\big) \cdots \big(Y_m \, W_m^\dagger \, D^\mu \, W_m \, Y_m^\dagger\big) \cdots \big(Y_N \, W_N^\dagger \, \psi_N\big) \, |0\rangle_{\mathcal{L}_{\text{eff}}}
\end{aligned} \tag{2.135}$$

In this way both sides are matrix elements of an operator with a Lagrangian. In this form, the agreement can be pursued beyond tree-level with corrections absorbed into a finite Wilson coefficient on the right-hand side.

This formulation of SCET is most similar to the Luke/Freedman formulation [51], which partly inspired the current work, but even simpler since we do not attempt to make the agreement palatable to the inclusion of power corrections. More explicitly, the Luke/Freedman formulation has fields in the operators evaluated at different positions, such as $x_{\bar{n}} \equiv (n \cdot x, 0, \vec{x}_\perp)$, as in the multipole formulation of SCET [49, 50]. The simple way to see why soft and collinear fields interact only at $x_{\bar{n}}$ is that these positions are within the jet cone, which is where the soft and collinear radiation can overlap. However, as long as the Lagrangian is defined to contain decoupled sectors, changing the location at which the fields are evaluated in this way only affects subleading powers.

Both the Luke/Freedman and the multipole formulation of SCET differ somewhat from label SCET [46–48]. In label SCET, fields are all evaluated at the same point, but the interactions are not those of full QCD. Instead there are an intricate set of SCET Feynman rules, derived by integrating out large components of spinors, as is done in heavy quark effective theory, and then removing certain interactions through field redefinitions. For soft interactions, these rules are the eikonal Feynman rules. For collinear sectors, the rules are equivalent to QCD in light-cone gauge [49]. It has already been observed that label SCET, after a field redefinition which decouples the soft from the collinear interactions in the Lagrangian, is equivalent to having multiple copies of QCD [61].

We will not attempt to explain, justify or defend any formulation of SCET in this thesis. As far as anyone can tell, all the formulations are equivalent at leading power. The point of this section is merely to reiterate the observation of [51] that factorization can be phrased in terms of QCD fields and a Lagrangian which contains multiple independent copies of QCD. Indeed, the point of this chapter is essentially to give a transparent proof of the observations made in [51], using on-shell methods.

2.9 Application: the QCD Splitting Functions

As an application of the factorized expressions that we have derived, we will compute the tree-level splitting functions in QCD. Perhaps the simplest way to compute unpolarized splitting functions is following Altarelli and Parisi [62] by squaring the relevant three-point vertex and summing over spins. For this sum, they use the

replacement

$$\sum_{\text{pols}} \epsilon_q^{*\nu} \epsilon_q^{\mu} \to \begin{cases} \delta^{ij} - \frac{q^i q^j}{q^2} & i,j > 0 \\ 0 & \text{otherwise} \end{cases} \tag{2.136}$$

It is important to use this replacement, and not the simpler $\sum_{\text{pols}} \epsilon^{*\nu}\epsilon^{\mu} \to -g^{\mu\nu}$, since the simpler replacement assumes the Ward identity is satisfied, which is not the case for a single emission off of a single leg of a matrix element. The replacement in Eq. (2.136) is equivalent to a sum over polarization vectors with reference vector choice $r^\mu = (1,0,0,-1)$. Instead, if one chooses the reference vector to be in the direction of the quark that splits, one would find a different answer for the splitting functions: zero.

In the on-shell language we have been advocating, the correct cross section to evaluate is $|\langle p;q|\,\bar{\psi}\,W_t\,|0\rangle|^2$. In this case, summing over polarizations will be independent of reference vector, even if $r \sim p$. Of course, the usual calculation using physical polarizations produces the right answer since in this case the contributions from the Wilson line are power suppressed. It is nevertheless illustrative (and easy) to see the computation performed using spinor helicity methods. Moreover, since we have already shown that $|\langle p;q|\,\bar{\psi}\,W_t\,|0\rangle|^2$ factorizes off from any matrix element when q becomes collinear to p this approach automatically also proves the universality of splitting functions. The connection between the splitting functions and collinear factorization in effective field theory was also observed in [63, 64].

2.9.1 Quark-gluon splitting function

We have shown that for a generic process with a collinear sector initiated by a quark, the matrix element factorizes into $\langle X_j|\,\bar{\psi}\,W_j\,|0\rangle$ times a matrix element that has no collinear radiation in the n_j direction. Here, W_j points in some direction t^μ not collinear to n_j. Therefore, the quark-gluon splitting amplitude is given by:

$\langle p;q,a|\,\bar{\psi}\,W_j\,|0\rangle\;=$ 

(2.137)

times the rest of the amplitude, $\mathcal{M}(p+q)$, which carries a color and spinor index. That is,

$$\mathcal{M}_{\text{split}} = \bar{u}(p)\left[\frac{t\cdot\epsilon(q)}{t\cdot q} - \frac{p\cdot\epsilon(q)}{p\cdot q} - \frac{\not{\epsilon}(q)\not{q}}{2p\cdot q}\right] g\,T^a\mathcal{M}(P) \tag{2.138}$$

where $P = p+q$. The nice thing about this expression is that, because it satisfies the Ward identity, we can choose any reference vector for $\epsilon^\mu(q)$. Moreover, since we have proven collinear factorization for any hard-scattering operator, we know that this expression is the universal collinear-splitting amplitude.

Instead of doing the calculation in generic-r, like in Eq. (2.136), we use collinear-r. Thus we take $r = p$. Then,

$$\epsilon_q^- = \sqrt{2}\,\frac{p]\langle q}{[qp]} \qquad \text{and} \qquad \epsilon_q^+ = \sqrt{2}\,\frac{q]\langle p}{\langle pq\rangle} \tag{2.139}$$

both of which satisfy

$$p\cdot\epsilon(q) = 0 \tag{2.140}$$

Let us also take the spinor to be right-handed, namely $\bar{u}(p) = [p$. Then for ϵ^- we find

$$\mathcal{M}_{\text{split}}^{R,-} = \sqrt{2}\,g\frac{[tp]}{[tq][qp]}[p\,T^a\mathcal{M} = \sqrt{2}\,\frac{g}{[qp]}\frac{z}{\sqrt{1-z}}\,[P\,T^a\mathcal{M} \tag{2.141}$$

and for ϵ^+ we find

$$\mathcal{M}^{R,+}_{\text{split}} = \sqrt{2}\, g \left(\frac{\langle pt \rangle}{\langle qt \rangle \langle pq \rangle} [p - \frac{1}{\langle qp \rangle} [q \right) T^a \mathcal{M} = \sqrt{2}\, \frac{g}{\langle pq \rangle} \left(\frac{z}{\sqrt{1-z}} + \sqrt{1-z} \right) [P\, T^a \mathcal{M} \tag{2.142}$$

where we have used that

$$p^\mu = z\, P^\mu \qquad \text{and} \qquad q^\mu = (1-z)\, P^\mu \tag{2.143}$$

which implies that

$$[p = \sqrt{z}\, [P, \qquad [q = \sqrt{1-z}\, [P, \qquad \text{etc} \tag{2.144}$$

at leading power.

Using $\mathcal{M}_{\text{split}}$, we can write down the polarized splitting functions:

$$\left|\mathcal{M}^{R,-}_{\text{split}}\right|^2 = \frac{g^2 C_F}{p \cdot q} \frac{z^2}{1-z} \left|\mathcal{M}_{\text{orig}}\right|^2 \quad \text{and} \quad \left|\mathcal{M}^{R,+}_{\text{split}}\right|^2 = \frac{g^2 C_F}{p \cdot q} \frac{1}{1-z} \left|\mathcal{M}_{\text{orig}}\right|^2 \tag{2.145}$$

where $\left|\mathcal{M}_{\text{orig}}\right|^2 = \left|[P\mathcal{M}(P)\right|^2$ is the original amplitude without collinear splitting. By parity invariance, we must also have

$$\left|\mathcal{M}^{L,-}_{\text{split}}\right|^2 = \frac{g^2 C_F}{p \cdot q} \frac{1}{1-z} \left|\mathcal{M}_{\text{orig}}\right|^2 \quad \text{and} \quad \left|\mathcal{M}^{L,+}_{\text{split}}\right|^2 = \frac{g^2 C_F}{p \cdot q} \frac{z^2}{1-z} \left|\mathcal{M}_{\text{orig}}\right|^2 \tag{2.146}$$

The unpolarized splitting function is given by the sum of the two:

$$\left|\mathcal{M}^{\text{unpol}}_{\text{split}}\right|^2 = \frac{g^2 C_F}{p \cdot q} \frac{1+z^2}{1-z} \left|\mathcal{M}_{\text{orig}}\right|^2 \tag{2.147}$$

which is the familiar result.

2.9.2 Gluon-gluon splitting function

Next, consider the gluon splitting function. In this case, we want to relate the cross section for the emission of two on-shell gluons, of momenta p^μ and q^μ to the

amplitude $\mathcal{M}^{c,\mu}_{\text{orig}}(p+q)$ for producing a single off-shell gluon of momentum $p^\mu + q^\mu$. We have already shown that for the collinear emission of gluons off of gluons, the amplitude in QCD is reproduced by the matrix element $\langle X_j | W_t^\dagger D^\mu W_t | 0 \rangle$ at leading power. Thus, if two n-collinear gluons of color a, b, momenta p, q and polarizations ϵ_p and ϵ_q are omitted, the original amplitude gets modified to

$$\mathcal{M}^{ab}_{\text{split}} = -igf^{abc}\Bigg[\epsilon_p^{*\mu}\frac{t\cdot\epsilon_q^*}{t\cdot q} - \epsilon_q^{*\mu}\frac{t\cdot\epsilon_p^*}{t\cdot p} + \frac{t\cdot\epsilon_p^*}{t\cdot p}\frac{t\cdot\epsilon_q^*}{t\cdot q}\frac{(q-p)^\mu}{2} + \epsilon_p^*\cdot\epsilon_q^*\frac{(p-q)^\mu}{2p\cdot q} - \frac{p\cdot\epsilon_q^*}{p\cdot q}\epsilon_p^{*\mu} + \frac{q\cdot\epsilon_p^*}{q\cdot p}\epsilon_q^{*\mu}\Bigg]\mathcal{M}^{c,\mu}_{\text{orig}}(p+q) \quad (2.148)$$

The first line in Eq. (2.148) comes from the Wilson lines and the second from the usual self-collinear splitting diagram.

Now the original amplitude must satisfy a Ward identity, which holds exactly even if $p+q$ is off-shell. Thus, $(p+q)\cdot\mathcal{M}^c_{\text{orig}} = 0$. Using this constraint, it is easy to check that $\mathcal{M}^{ab}_{\text{split}}$ satisfies the Ward identity exactly for both outgoing gluons (by replacing $\epsilon_p^{*\mu} \to p^\mu$ or $\epsilon_q^{*\mu} \to q^\mu$). Thus we can square the amplitude and sum over all polarizations with the simple replacement $\epsilon^{*\mu}\epsilon^\nu \to -g^{\mu\nu}$, and sum over colors. The most enhanced terms will scale like $|\mathcal{M}_{\text{orig}}|^2\lambda^{-2}$ and we can drop anything subleading. Since $(p+q)\cdot\mathcal{M}^c_{\text{orig}} = 0$ and p and q are collinear, we also have $p\cdot\mathcal{M}_{\text{orig}} \lesssim \lambda$ and $q\cdot\mathcal{M}_{\text{orig}} \lesssim \lambda$. The only terms that remain at leading power are therefore

$$\sum_{\text{pols., cols.}} \left|\mathcal{M}^{ab}_{\text{split}}\right|^2 \cong -\frac{2g^2C_A}{p\cdot q}\left(\mathcal{M}^{c,\mu}_{\text{orig}}\right)^\dagger\mathcal{M}^{c,\nu}_{\text{orig}}\left[g^{\mu\nu}\frac{t\cdot p}{t\cdot q} + g^{\mu\nu}\frac{t\cdot q}{t\cdot p} + \frac{p^\mu q^\nu}{p\cdot q}\right] \quad (2.149)$$

To simplify this expression, it is helpful decompose p^μ and q^μ into a component in the $(p+q)^\mu$ direction which will vanish upon contraction with $\mathcal{M}_{\text{orig}}$ by the Ward identity and a component orthogonal to the $\vec{p}+\vec{q}$ which we call $\vec{p}_\perp$. To keep p^μ and q^μ lightlike, their energies must be shifted slightly. The decomposition can be written

as

$$p^\mu = z(p+q)^\mu + p_\perp^\mu + \delta E\,(1,\vec{0}\,)^\mu \quad \text{and} \quad q^\mu = (1-z)(p+q)^\mu - p_\perp^\mu - \delta E\,(1,\vec{0}\,)^\mu \tag{2.150}$$

where

$$\delta E = \frac{(1-2z)(p+q)^2}{2Q} \sim \lambda^2 \tag{2.151}$$

with $Q = p^0 + q^0$ and $p_T^2 = -p_\perp \cdot p_\perp > 0$ is given by

$$p_T^2 = z(1-z)(p+q)^2 + \delta E^2 \sim \lambda^2 \tag{2.152}$$

At leading power, we can invert this last equation to write $p \cdot q = \frac{p_T^2}{2z(1-z)} + \mathcal{O}(\lambda^4)$.

Now we can simplify Eq. (2.149). Since t is not collinear to p or q, we have

$$\frac{t \cdot p}{t \cdot q} \cong \frac{z}{1-z} \tag{2.153}$$

Next, we observe that the $p^\mu q^\nu$ term in Eq. (2.149) can be written as $-p_\perp^\mu p_\perp^\nu$ at leading power because the Ward identity kills the $(p+q)^\mu$ terms. Thus,

$$\sum_{\text{pols., cols.}} \left|\mathcal{M}^{ab}_{\text{split}}\right|^2 \cong -\frac{2g^2 C_A}{p \cdot q} \big(\mathcal{M}^{c,\mu}_{\text{orig}}\big)^\dagger \mathcal{M}^{c,\nu}_{\text{orig}} \left[g^{\mu\nu} \left(\frac{z}{1-z} + \frac{1-z}{z} \right) - 2z(1-z) \frac{p_\perp^\mu p_\perp^\nu}{p_T^2} \right] \tag{2.154}$$

which agrees with the polarized splitting function (cf. $\hat{P}_{gg}^{\mu\nu}$ in [27]). For the unpolarized splitting we discard spin correlations, by performing an average over azimuthal angle. This amounts to replacing in Eq. (2.149)

$$p^\mu q^\nu \to -p_\perp^\mu p_\perp^\nu \to -\frac{1}{2}\, p_T^2\, \delta_\perp^{\mu\nu} \to \frac{1}{2}\, p_T^2\, g^{\mu\nu} \tag{2.155}$$

where each step is valid at leading power and the first and last arrows exploit the Ward identity on $\mathcal{M}_{\text{orig}}$.

Inserting Eqs. (2.152), (2.153) and (2.155) into Eq. (2.149) we then find

$$\sum_{\text{pols., cols.}} \left|\mathcal{M}^{ab}_{\text{split}}\right|^2 \cong \frac{2g^2 C_A}{p\cdot q}\left[\frac{z}{1-z}+\frac{1-z}{z}+z(1-z)\right]\times \sum_{\text{pols., cols.}} \left|\epsilon^*_\rho \mathcal{M}^{c,\rho}_{\text{orig}}\right|^2 \quad (2.156)$$

where the last factor is exactly the probability without splitting of the completely general process. The rest is the gluon-gluon splitting function in QCD.

In summary, we have shown that the quark-gluon and gluon-gluon splitting functions are universal and reference-vector independent.

2.10 Conclusions

The main result of this chapter is a proof at tree-level of factorization for matrix elements of operators in QCD. We show that matrix elements of operators with N fields in states whose momentum is either collinear to one of N directions or soft can be written in a factorized form as

$$\langle X_1\cdots X_N; X_s|\,\bar\psi\cdots\psi\,|0\rangle \cong \langle X_1|\,\bar\psi W_1\,|0\rangle\cdots\langle X_N|\,W_N^\dagger\psi\,|0\rangle\,\langle X_s|\,Y_1^\dagger\cdots Y_N\,|0\rangle \quad (2.157)$$

where $\cong$ means the two sides are equivalent at leading power in an expansion parameter λ determined by the scaling of the momenta in the state $\langle X_1\cdots X_N; X_s|$. This equation with explicit color indices and gluon jets included is given in Eq.(2.133). In this equation both sides contain matrix elements of operators in QCD. That is, these are not effective field theory fields, although the connection to Soft-Collinear Effective Theory becomes trivial once this form is written down (see Section 2.8).

In order to prove Eq. (2.157) using only the scaling of momenta and not assigning scaling behavior to unphysical fields, we made critical use of the spinor-helicity for-

malism. Spinor-helicity methods let us assign scaling behavior to polarization vectors based on their momenta and the choice of an arbitrary reference vector. Crucially, the reference vector can be chosen differently for different gluons. By showing elements of factorization for certain reference vector choices and then showing reference-vector independence of the factorized result, the final factorization formula followed.

Although choosing reference vectors sounds similar to choosing a gauge, the two are vastly different. Gauge choices are made for unphysical fields which can create and destroy any gluon state. Thus one cannot assign different gauges to different sectors without chopping up the gauge field in some way, as in the effective field theory approach, or by attempting to formulate an incredibly nonlocal gauge condition. The spinor-helicity approach gets around awkward gauge conditions by choosing a reference-vector basis for the states directly, with the fields remaining in Feynman gauge (or whatever gauge one wants).

We have proven Eq. (2.157) and its generalizations only at tree level. However, the equivalence probably holds to all orders in perturbation theory. The only modification should be that the right-hand side must be multiplied by a finite hard function $C(P_i)$ depending on the jet directions and energies but independent of λ. One can easily envision an all-orders proof which builds on the tree-level result, which contains all the infrared-singular real-emission graphs, and unitarity to relate the real-emission and virtual graphs. Indeed, unitarity constraints are efficiently encoded with on-shell methods like those we have employed here at tree-level. Pursuing this direction could conceivably lead to rigorous proofs of factorization for a wide variety of processes.

On a more practical side, a clean formulation of factorization, as in Eq. (2.157),

may lead to new calculations in perturbative QCD. For example, a similar formula has already lead to one of the first studies of a jet-shape observable in SCET at subleading power [52]. Although so far, no results new to perturbative QCD have been obtained this way, it is easy to imagine that subleading power factorization may eventually play a role in collider physics, as it has in heavy quark physics.

Chapter 3

All-orders factorization for e^+e^- annihilation

3.1 Introduction

Factorization is at the heart of any quantitative prediction using quantum chromodynamics (QCD). Probably the most familiar type of factorization, which we call *hard factorization*, justifies the use of fixed-order perturbation theory for sufficiently inclusive quantities. It lets us use perturbative calculations involving partons (quarks and gluons) to make precise predictions for experimentally measurable quantities involving color-neutral hadrons. The intuition for hard factorization is that scattering has a component which freezes in at short distances and can only incoherently influence the long-distance components. For many observables, the long-distance physics can be integrated over with essentially unit probability. Somewhat less intuitive, but also logical after a little thought, is the factorization of infrared-sensitive physics

into soft and collinear components. This *soft-collinear factorization* can be anticipated classically, since very-long distances modes (soft physics) can only probe the net (color) charge of a collection of particles traveling in nearly the same direction. Conversely, energetic collinear particles cannot have their momentum changed much by low-energy soft modes. Although the physical picture of hard-soft-collinear factorization is simple, rigorously establishing exactly what it implies about scattering amplitudes in gauge theories is not.

Factorization has a long history, with an eclectic variety of approaches yielding a nuanced picture of when and where factorization should hold, and in what form. In this chapter, we eschew two serious complications: 1) we ignore non-perturbative effects associated with strong-coupling, discussing only power corrections associated with the kinematics of massless partons rather than corrections of order $\Lambda_{\rm QCD}/Q$ and 2) we avoid configurations where final-state particles are collinear to initial state particles. Even within this limited scope, although much is known, a precise formulation of factorization in terms of QCD matrix elements has been lacking. It is the goal of this chapter to provide such a formulation and proof.

As we will review and rederive, the essence of factorization is revealed by studying the infrared (IR) structure of gauge theories. An obvious necessary condition for an IR divergence is that some propagators blow up. Sufficient conditions are quite a bit more complicated. First, the poles associated with on-shell momenta must be *pinched*, so that one cannot just integrate over them [45, 65]. Second, the numerator structure of integrands, which is gauge-dependent, can make an integral more or less divergent than the propagator denominators alone imply. In certain gauges, such as

lightcone gauge, the possible virtual momenta contributing to the IR singularities – the so-called *pinch surface* – turns out to be remarkably simple: all virtual momenta q^μ must either be exactly proportional to one of the external momenta $q^\mu = \alpha p_i^\mu$ with $\alpha \geq 0$ or exactly vanish, $q^\mu = 0$. A picture of such a surface is often drawn as a reduced diagram with hard, jet and soft regions [41, 42, 66], similar for example to Eq. (3.148) below.

Unfortunately, understanding the singular pinch surface, that is, the topology of exactly zero momentum or exactly collinear lines, does not immediately translate to a precise statement of hard factorization or soft-collinear factorization. Indeed, descending from the pinch surface to a statement about finite amplitudes requires a whole new set of justifications. For example, one must relate the unphysical power-counting of a pinch surface of finite phase-space volume to the physical power-counting of external momenta. In particular, infrared divergences associated with the soft pinch surface (where $k^\mu = 0$) depend on whether that surface is approached from a likelike (the soft region) or spacelike (the Glauber region) direction. Other subtleties include avoiding double-counting in the soft-collinear region (the *zero bin*), restricting the phase space for real and virtual integrations in the soft function without reintroducing dependence on the hard scale, and introducing Wilson lines to restore gauge invariance without spoiling the leading-power factorization. Despite these challenges, factorization has been proven at the amplitude and amplitude-squared level in a number of contexts [67–69]. Factorization formulas for cross-sections of certain observables have been presented [15, 16, 35, 70–74] allowing for resummation of large logarithms associated with the pinch surface.

In deep-inelastic lepton-hadron scattering (DIS), the pinch surface is particularly simple. In this case, factorization has been understood since the 1970s and has been used to compute phenomenologically important quantities, namely the DGLAP splitting functions [62, 75–77]. These splitting functions describe the leading-power behavior of certain amplitudes when an additional collinear parton is added; they also provide kernels for the renormalization group (RG) evolution of parton distribution functions (PDFs). In DIS, the splitting functions and PDF evolution can be rigorously defined through an operator product expansion (OPE) [78, 79], which has led to their computation at 2 loops [80, 81] and 3 loops [82]. The OPE for DIS is possible because it involves the matrix element of two currents whose analytic structure in the complex plane is particularly simple. That the same splitting functions apply for PDF evolution in some other process, for example the Drell-Yan process, can occasionally be shown by direct calculation [83]. However, to show universality of the PDFs more generally requires a general proof of hard-collinear factorization. Subtleties associated with proton-proton scattering, where initial state partons can be collinear to final state particles, complicate factorization [44, 47, 56]. Needless to say, showing that the same PDFs apply to any scattering process (if indeed they do) is an extremely important open question, beyond the scope of this thesis.

An alternative, more pragmatic, approach skips both the pinch surface and the OPE and simply computes the diagrams relevant for factorization directly, usually in dimensionally regularized perturbation theory. Following this approach, universality of collinear splittings was shown at 1-loop by Bern and Chalmers in 1995 [84] by studying collinear limits of 5-point amplitudes in QCD. Hard-collinear factorization

can be written heuristically as

$$\mathcal{M}_n \overset{p_1 \| \cdots \| p_m}{\cong} \mathbf{Sp}(p_1, \ldots, p_m) \cdot \mathcal{M}_{n-m} \tag{3.1}$$

with $\mathcal{M}_n$ an n-external-particle matrix-element, $p_1^\mu \cdots p_m^\mu$ the external momenta which become collinear, and $\cong$ indicating the two sides agree at leading power. The important point in this formula is that the splitting function $\mathbf{Sp}(p_1, \ldots, p_m)$ has no dependence on any of the non-collinear momenta in the process. Formulas like Eq. (3.1) and the explicit formulas for $\mathbf{Sp}(p_1, \ldots, p_m)$ in d dimensions are important for precision calculations in QCD. We will give more-precise operator definitions of the objects in this equation in Section 3.12.1. In 1999, Kosower proved Eq. (3.1) at leading color (large N_c) to all orders in perturbation theory [85]. The factorization of IR (soft and collinear) tree-level amplitudes to all orders was shown in [27]. Ref. [56] has discussed difficulties with Eq. (3.1) when initial and final states are collinear. Avoiding such situations, we will show that Eq. (3.1) holds to all orders in QCD, at finite N_c. Indeed, hard-collinear factorization is a corollary of the more general hard-soft-collinear factorization formula we prove in this chapter.

The factorization of soft emissions from generic matrix elements is also believed to satsify a formula similar to Eq. (3.1). For example, in the limit that a single soft gluon of momentum q^μ becomes soft, tree-level amplitudes factorize as [86]

$$\mathcal{M}_n \overset{q \text{ soft}}{\cong} \epsilon_\mu(q)\, \mathbf{J}_a^\mu \cdot \mathcal{M}_{n-1} \tag{3.2}$$

The soft current $\mathbf{J}_a^\mu$ is an operator acting in color space. In 2000, Catani and Grazzini proved this formula at 1-loop, with an explicit computation of $\mathbf{J}_a^\mu$, and conjectured that the formula holds to all orders [87]. In 2013, the soft current was computed at

2-loops in [88,89]. These calculations were all done in dimensional regularization and have applications in perturbative QCD, such as to the N^{3}LO Higgs-boson inclusive cross-section. As with Eq. (3.1), our general factorization formula contains the hard-soft factorization embodied in Eq. (3.2) as a special case. We prove this equation to all orders and provide regulator-independent and gauge-invariant operator definitions of the objects involved in Section 3.12.2.

Remarkably, a factorization theorem valid at leading power to all orders in α_s is not strictly required for resummation to all orders in α_s of certain leading or next-to-leading logarithms. For example, by combining $\mathcal{O}(\alpha_s)$ collinear splitting functions, $\mathcal{O}(\alpha_s)$ soft-coherence effects, and $\mathcal{O}(\alpha_s^2)$ Sudakov effects (associated with the overlapping soft-collinear region), Catani, Marchesini and Webber derived a powerful coherent-branching algorithm [90]. Coherent branching is the backbone of the Monte Carlo event generator approach to QCD. It has also been used for resummation of many observables at the next-to-leading logarithmic level [7, 90–92]. A related observation is that QCD simplifies dramatically in the limit that gluons are strongly ordered in energy [86, 93, 94], particularly at large N_c. This approximation has led to the resummation of certain leading logarithms, such as non-global ones [95, 96] which no other method has yet tamed.

A relatively recent approach to factorization is provided by Soft-Collinear Effective Theory (SCET) [46, 47, 49, 50]. The idea behind SCET is to hypothesize which IR modes contribute to QCD scattering processes and to write fields in QCD as sums of fields with soft or collinear quantum numbers corresponding to the hypothesized modes. Different components are assigned different scaling behavior and the QCD

Lagrangian is expanded to leading power (or beyond). The resulting effective theory has Feynman rules which are significantly more complicated than those of QCD. These rules simplify somewhat after a field redefinition which moves the soft-collinear interactions from the Lagrangian into the operators. Proofs using the effective Lagrangian are then carried out under the assumption that the only modes necessary for the proof are those in the effective theory. Therefore, proofs of factorization in SCET must be interpreted with some care. An advantage of the SCET approach is that with operator definitions of the various objects, the hard-soft-collinear decoupling is completely transparent and resummation of large logarithms can be done through the renormalization group. This has lead to precise predictions of jet observables at colliders [6, 8, 9, 17, 18, 23, 25]. Another advantage is that the power counting makes it straightforward, in principle, to go beyond leading power if desired. On the other hand, the derivation of SCET has been done in a gauge in which the physics is quite unintuitive, for example with polarization vectors which are longitudinally polarized at leading power (see [3]). SCET removes the soft-collinear double counting by simply not summing over the zero-momentum bin in the discrete sum over labels. A somewhat simpler formulation of SCET was presented recently by Freedman and Luke in [51] and connects more directly to the current work, as discussed in Section 3.13.

In this chapter, we present and prove a factorization formula for amplitudes in gauge theories, building upon insights from many of the approaches discussed above. All of the interesting features of this formula can be seen in the simpler case of factorization for matrix elements of the operator $\mathcal{O} = \frac{1}{(N/2)!}|\phi|^N$ in scalar QED.

There, our formula reads

$$\boxed{\langle X|\,\mathcal{O}\,|0\rangle \;\cong\; \mathcal{C}(S_{ij})\,\frac{\langle X_1|\,\phi^\star W_1\,|0\rangle}{\langle 0|\,Y_1^\dagger W_1\,|0\rangle}\,\cdots\,\frac{\langle X_N|\,W_N^\dagger\phi\,|0\rangle}{\langle 0|\,W_N^\dagger Y_N\,|0\rangle}\;\langle X_s|\,Y_1^\dagger\cdots Y_N\,|0\rangle} \tag{3.3}$$

This formula applies to final states $\langle X|$ which can be partitioned into N regions of phase space such that the total momentum P_j^μ in each region has an invariant mass which is small compared to its energy. More explicitly, we demand $P_j^2 < \lambda^2 (P_j^0)^2$, where $P_j^0 = E_j$ is the energy of the jet, for some number $\lambda \ll 1$ which is used as a power-counting parameter. For such states, the momentum q^μ of any particle has to be either collinear to one of N lightlike directions, n_j^μ, meaning $n_j \cdot q < \lambda^2 q^0$, or soft, meaning $q^0 < \lambda^2 P_j^0$. Thus we can write for the final state $\langle X| = \langle X_1 \cdots X_N; X_s|$, where all the particles with momentum collinear to n_j are contained in the *jet* state $\langle X_j|$ and the particles that are soft are in $\langle X_s|$. This explains the states in Eq. (3.3). The Wilson coefficient $\mathcal{C}(S_{ij})$ is a function *only* of the Lorentz-invariant combinations $S_{ij} \equiv (P_i + P_j)^2 \cong 2P_i \cdot P_j$ of jet momenta P_j^μ in each direction; it does not depend at all on the distribution of energy within the jet or on the soft momenta and, therefore, it does not depend on λ. The objects Y_j are Wilson lines going from the origin to infinity in the directions of the jets, and the W_j are Wilson lines in directions t_j^μ only restricted not to point in a direction close to that of the corresponding jet. We give more precise definitions of the Wilson lines in Section 3.2. The symbol $\cong$ in Eq. (3.3) indicates that any IR-regulated amplitude or IR-safe observable computed with the two sides will agree at leading power in λ.

Eq. (3.3) implies hard-collinear factorization (Eq. (3.1)) and hard-soft factorization (Eq. (3.2)) as special cases. For example, if a two-body final state $\langle X|$ is modified by adding a soft photon of momentum q^μ, then one can calculate the effect

of this extra emission by taking the ratio of the right-hand side of Eq. (3.3) with and without the emission. Most of the terms drop out of the product, leaving

$$\mathbf{J}_a^\mu = \frac{\langle \epsilon^\mu(p); a | \, Y_1^\dagger Y_2 \, | 0 \rangle}{\langle 0 | \, Y_1^\dagger Y_2 \, | 0 \rangle} = g_s T^a \left(\frac{p_2^\mu}{p_2 \cdot q} - \frac{p_1^\mu}{p_1 \cdot q} \right) + \mathcal{O}(g_s^3) \tag{3.4}$$

We will give general operator definitions for the splitting amplitude, $\mathbf{Sp}(p_1, \cdots p_N)$, and the soft current, $\mathbf{J}$, and discuss their universality in Section 3.12 after we present the generalization of Eq. (3.3) to QCD in Section 3.11 (see Eq. (3.207)). Beyond providing an all-orders proof of Eq. (3.3), as well as an operator definition and proof of universality of $\mathbf{Sp}$ and $\mathbf{J}$, we hope that our general method of proof will itself be useful in future discussions of formal questions on the structure of perturbative amplitudes. We also hope that our approach to factorization, and the ensuing discussion of SCET in Section 3.13, will help bridge the gap between the traditional factorization methods in the QCD literature and those of SCET, as well as provide further insight into the formulation of SCET by Freedman and Luke in [51].

Eq. (3.3) was derived at tree-level in Ch. 2 and in the paper by the author and collaborators [3]. At tree-level, the Wilson coefficient and the vacuum matrix elements in the denominators of Eq. (3.3) are all 1 and the factorization formula reduces to

$$\langle X | \, \mathcal{O} \, | 0 \rangle \overset{\text{tree}}{\cong} \langle X_1 | \, \phi^\star W_1 \, | 0 \rangle \cdots \langle X_N | \, W_N^\dagger \phi \, | 0 \rangle \, \langle X_s | \, Y_1^\dagger \cdots Y_N \, | 0 \rangle \tag{3.5}$$

in agreement with the formula from [3], given in Ch. 2 in Eq. (2.99).

There are two differences between Eqs. (3.3) and (3.5), both of which represent important physical effects. First, the nontrivial Wilson coefficient in the all-loop formula enables the factorized expression to reproduce hard-virtual corrections. Using Eq. (3.3), one can isolate the Wilson coefficient using a trivial soft sector $\langle X_s | = \langle 0 |$

and collinear sectors with a single particle in each $\langle X_j| = \langle p_j|$. Then $\lambda = 0$ exactly, and

$$\mathcal{C}(s_{ij}) = \frac{\langle p_1 \cdots p_N | \, \mathcal{O} \, | 0 \rangle}{\frac{\langle p_1 | \, \phi^\star W_1 \, | 0 \rangle}{\langle 0 | \, Y_1^\dagger W_1 \, | 0 \rangle} \cdots \frac{\langle p_N | \, W_N^\dagger \phi \, | 0 \rangle}{\langle 0 | \, W_N^\dagger Y_N \, | 0 \rangle} \, \langle 0 | \, Y_1^\dagger \cdots Y_N \, | 0 \rangle} \tag{3.6}$$

This is a statement of purely-virtual factorization. Note that, since $\lambda = 0$ exactly, this is an equality, not just a leading-power equivalence. The nontrivial content in this definition is that the right-hand side is IR finite, which we shall prove. Moreover, we shall prove that the Wilson coefficient is independent of the states $\langle X_1 \cdots X_N; X_s|$, so that Eq. (3.6) unambiguously specifies $\mathcal{C}(s_{ij})$ at leading power.

The second difference between tree-level factorization and all-orders factorization is the denominators in Eq. (3.3). These represent a type of zero-bin subtraction for loops. Recall that for external states which are both soft and collinear, one is free to put them in $\langle X_s|$ or $\langle X_j|$ — the factorization formula holds with either choice. However, since all integrals are taken over $\mathbb{R}^{1,3}$, the soft-collinear region of loop momenta is included in both the soft and collinear matrix elements in the factorized formula, thus their overlap must be removed. The term *zero bin* stems from effective theory language, where one (formally) chops up phase space into a discrete sum over soft and collinear sectors. The zero bin is the soft-collinear overlap sector in the sum, which must be subtracted not to double count [59]. The equivalence between the zero-bin subtraction in SCET and dividing by a matrix element of Wilson lines has been shown in [97].[1]

Besides the salient differences between the tree-level and all-orders factorization

[1]Conveniently (or misleadingly) when dimensional regularization is used to control both the UV and IR divergences, the vacuum matrix elements of Wilson lines are all scaleless and identically vanish. Thus, the zero-bin subtraction is easy to miss, as it was in many early SCET papers.

formulas, there is an important conceptual subtlety: starting at 1-loop, both sides of Eq. (3.3) are IR divergent. Declaring two infinite quantities equivalent at leading power is not as absurd as it first sounds. With an IR regulator it is, of course, perfectly well defined. Conceptually, one could interpret the leading power equivalence $\cong$ in this equation as meaning that whenever an IR-safe observable is computed by integrating over an appropriate collection of final states $\langle X|$, the two sides of Eq. (3.3) produce the same cross section at leading power in λ. For example, a typical IR-safe jet observable is $\tau = \frac{1}{Q^2}(\sum_i m_i^2 + QE_{\text{out}})$: the sum over the jet masses and the out-of-jet energy. Then $\frac{d\sigma}{d\tau}$ will agree when computed with either side of Eq. (3.3) up to corrections subleading in τ. With this in mind, one can still work at the amplitude level without an explicit IR regulator.

To be clear, we do not require or expect the IR divergences on the two sides of Eq. (3.3) to exactly agree. Indeed, as soon as real-virtual diagrams contribute, the IR divergences will not exactly agree. To see this note that the real-emission graphs computed with Eq. (3.3) only agree at leading power and so an IR-divergent virtual graph with a subleading real emission tacked on will show up on the left-hand side of Eq. (3.3) but not on the right-hand side. This implies that the IR divergences can only precisely agree when $\lambda = 0$ (no emissions), as in Eq. (3.6).[2] However, subleading-power IR-divergences will contribute at subleading power to observables, so the disagreement of subleading-power IR-singularities does not invalidate the leading-power equivalence in Eq. (3.3).

Regarding the power counting, our factorization theorem will be proven at lead-

[2]One can of course add subleading-power operators to the right-hand side of Eq. (3.3) so that subleading IR divergences cancel. To get all the IR divergences to cancel, one would need an infinite number of operators and the factorized expression would be identical to the full theory.

ing power in λ, a small parameter that only depends on the external momentum in the state $\langle X|$. We do not count powers of anything except the external momentum in the matrix element under consideration. When we discuss scaling of virtual momenta near IR sensitive regions, we will talk about scaling with κ (see Section 3.2), but only to motivate dropping certain loop amplitudes completely. Our proof actually holds at leading power in $N+1$ separate power counting parameters, λ_c^i and λ_s, one for each collinear sector and another for the soft. It will be clear that our proof does not require $\lambda_c^i = \lambda_s$, and we can therefore derive the factorization theorem (at simultaneous leading power in all small parameters) for different types of soft and collinear momentum scalings. As we discuss in Section 3.13 this implies that our factorization formula unifies what are considered to be two separate effective field theories in the literature, namely SCET_I and SCET_II.

This chapter attempts to give some intuition for the factorization formula rather than simply a proof. We therefore take our time with the presentation, including many examples. Section 3.2 establishes some of our notation and reviews some basic concepts. Sections 3.3 and 3.4 give examples. Although the proof does not rely on these two example sections, the special cases considered illustrate many of the issues which come up in the proof and are useful for making some of the abstractions more concrete. Section 3.5 outlines the proof but has no results. The proof begins in earnest in Section 3.6. In this section we explain how Feynman diagrams can be written as sums of colored diagrams with red lines engendering soft-sensitivity and blue lines soft-insensitive. This section would be quite short if not for the examples we include. Section 3.7 proves a set of lemmas which establish the physical-gauge

reduced-diagram picture manifesting hard factorization. The difference between our reduced diagrams and reduced diagrams in the literature (see for example [41, 42, 66]) is that our diagrams correspond to specific functions of finite-external momenta computed through loop integrals over all of $\mathbb{R}^{1,3}$, while the traditional reduced diagrams describe only the pinch surface where all virtual momenta are either exactly zero or exactly proportional to an external momentum. To prove soft-collinear factorization, we introduce a special gauge we call *factorization gauge* in Section 3.8. The soft-collinear decoupling proof is given in Section 3.9. The rest of the chapter discusses the generalization to QCD, some special cases, the QCD splitting functions and soft currents, the connection to SCET, and a brief look forward.

3.2 Preliminaries

To begin, we establish in this section some of the basic features of amplitudes we will exploit for factorization. We first review the importance of soft and collinear momenta. We then discuss how soft and collinear regions of virtual momenta can be separated without chopping up the loop momenta into sectors.

Let us begin with some terminology. We will distinguish **soft divergences** from **collinear divergences**, both of which are defined in Section 3.2.2. We refer to **IR divergences** as either soft or collinear. We use λ to power-count external momenta, as discussed in Section 3.2.1. We use κ to power-count loop momenta. The notation $p \parallel q$ is used to denote when two momenta, either real or virtual, are nearly collinear according to the appropriate power counting. The notation $p \propto q$ is reserved for when two momenta are exactly collinear, that is, when they are **proportional** to each other.

Following [3], the symbol $\cong$ indicates that two expressions agree at leading power in the limit of external particles becoming soft or collinear in an amplitude. That is, it refers power counting in λ, not κ. More precisely

$$A \cong B \quad \Longleftrightarrow \quad \frac{A}{B} = 1 + \mathcal{O}(\lambda) \tag{3.7}$$

We also define

$$A \;\cong_{\text{IR}}\; B \quad \Longleftrightarrow \quad \frac{A}{B} = \mathcal{O}(\lambda^0) \tag{3.8}$$

This less restrictive IR-equivalence will be used in Section 3.9 to avoid keeping track of modifications of the hard-amplitude along the steps of soft-collinear factorization.

We are often interested not only in whether a loop is IR divergent, but whether it would be IR divergent if two external particles were proportional, or if an external momentum were exactly zero. If this happens we say the loop is **IR sensitive**. An IR-sensitive loop is IR divergent when $\lambda = 0$ (though it need not be for $\lambda > 0$). IR sensitivity is discussed more in Section 3.2.2 with an example given in Section 3.4.2.

3.2.1 Power counting for external momenta

A key observation which makes factorization important is that soft and collinear momenta dominate cross sections. At tree level, this is easy to see. Consider a process with outgoing final-state momenta p_i^μ of zero mass. At tree level, each intermediate momentum k^μ must be a linear combination of external momenta p_i^μ: $k^\mu = p_1^\mu + \cdots + p_n^\mu$. Thus $k^2 = \sum_{i,j} p_i \cdot p_j$. Since each $p_i \cdot p_j$ is positive definite, k^2 can only vanish if p_i^μ is exactly proportional to p_j^μ for each i and j in the sum, or if a p_i^μ has zero energy. The dominant regions of phase space where the propagators are large are,

therefore, the regions where momenta are collinear: $p_i \parallel p_j$, or soft: $E_i \ll Q$, with Q the center-of-mass energy. This is discussed extensively in [3].

We, therefore, focus on final states $\langle X|$ partitioned into collinear sectors $\langle X_1| \cdots \langle X_N|$ and a single soft sector $\langle X_s|$. Let m_i and E_i be the invariant mass and energy of the net momentum $P_i^\mu = \sum_{\text{sector } i} p_j^\mu$ in each sector, and define $\lambda_i = m_i/E_i$ for the collinear sectors and $\lambda_s = E_s/Q$ for the soft sector. We assume $\lambda_i \ll 1$ for every sector, so that the contribution of the state $\langle X| = \langle X_1| \cdots \langle X_N| \langle X_s|$ to a cross section will scale like inverse powers of all λ_i. It is for these states that hard-soft-collinear factorization holds.

3.2.2 Power counting for virtual momenta

The soft and collinear regions of phase space are also important because they lead to IR divergences in loops. IR divergences come from virtual-particle momenta going on-shell. Let us call **loop momenta** those being integrated over. That is, denoting the loop momenta as k_i^μ, the loop measure is $\prod_i \dfrac{d^4k_i}{(2\pi)^4}$. Any **virtual momentum** l^μ in a Feynman diagram is a linear combination of loop momenta and external momenta: $l^\mu(k_i, p_i)$. Thus, for a virtual propagator to blow up, the virtual momentum must go on-shell, which makes the loop momentum either soft or collinear to one of the jet directions. Since we associate infrared divergences with virtual lines, it is convenient to route the momenta so that the virtual momentum in question is one of the loop momenta, k^μ. We say a given diagram has a **soft divergence** associated with k^μ if it is still divergent when each component of k^μ is restricted to be smaller than some arbitrarily small scale, $\kappa^2 Q$, for any $\kappa > 0$. A **collinear divergence** re-

quires the specification of a finite, non-zero lightlike momentum, p^μ; the singularity is then present in any integration region containing p^μ. We take **infrared divergence** to mean either soft or collinear.

A shortcut to determining whether a given integral is IR divergent is through its scaling behavior, which can be understood in lightcone coordinates. Given two distinct lightlike directions n_a^μ and n_b^μ, we can uniquely decompose any 4-vector k^μ as

$$k^\mu = k_b\, n_a^\mu + k_a\, n_b^\mu + k_\perp^\mu \tag{3.9}$$

with $k_\perp^\mu$ defined by this equation and

$$k_a = \frac{n_a \cdot k}{n_a \cdot n_b}, \qquad k_b = \frac{n_b \cdot k}{n_a \cdot n_b} \tag{3.10}$$

We can then consider rescaling the components by factors of $0 < \kappa < 1$ raised to various powers

$$k^\mu \to \kappa^b k_b\, n_a^\mu + \kappa^a k_a\, n_b^\mu + \kappa^c k_\perp^\mu \quad \text{with} \quad a, b \geq 0,\ a + b > 0,\ c > 0 \tag{3.11}$$

We require $a, b \geq 0$, $c > 0$ and $a + b > 0$, so that as $\kappa \to 0$ these rescalings zoom in on a possibly singular region. For example, $a, b, c > 0$ scales $k^\mu \to 0$ (the soft region), whereas $b = 0$ and $a, c > 0$ scales $k^\mu \to k_b\, n_a^\mu$ (the a-collinear region). We say an integral is **power-counting finite** if, including the measure, it scales like κ to a positive power under a given rescaling of this form.

The purpose of these rescalings is that they are related to whether or not a diagram is infrared divergent:

Conjecture. (**Power-Counting Finiteness Conjecture**) *A Feynman integral is infrared finite if and only if it scales as a positive power of κ under all possible rescalings in Eq.* (3.11).

That an infrared-finite Feynman integral scales as a positive power of κ for any rescaling is easy to prove: a convergent integral must have a convergent Riemann sum. The converse, that scaling implies infrared finiteness, is also quite logical. We are certainly not aware of any counterexamples. Nor do we know of a rigorous proof. This conjecture is assumed to hold in practically every factorization proof, and we assume it too. For a discussion of a slightly stronger version of this conjecture, see page 428 of [98].

A convenient simplification is that it is not necessary to consider all possible values of $a, b, c \geq 0$. In determining the leading power of κ with a given scaling, all that matters is which terms can be dropped with respect to which other terms – any scaling that drops the same terms gives the same integrand with the same singularities. Between two power-counting regions that allow two different terms to be dropped lies a boundary where both terms must be kept. Because more terms must be kept on the boundary, if a boundary region is power-counting finite then the regions it bounds must also be power-counting finite. This simplifies the types of power-counting we need to consider.

In a given Feynman loop diagram, we always have one propagator whose denominator is k^2 (by our choice of momentum routing). Under the rescaling in Eq. (3.11),

$$k^2 = 2n_a \cdot n_b k_a k_b + k_\perp^2 \to \kappa^{a+b}\, 2n_a \cdot n_b k_a k_b + \kappa^{2c}\, k_\perp^2 \tag{3.12}$$

So, if $a + b > 2c$, we may drop $k_a k_b$ in place of $k_\perp^2$, and if $a + b < 2c$, $k_\perp^2$ can be dropped with respect to $k_a k_b$. We might also have denominators $(k - p_a)^2$ for some p_a^μ. If p_a^μ is not lightlike, then $(k - p_a)^2 \sim p_a^2 \sim \kappa^0$. A more relevant case is when p_a^μ

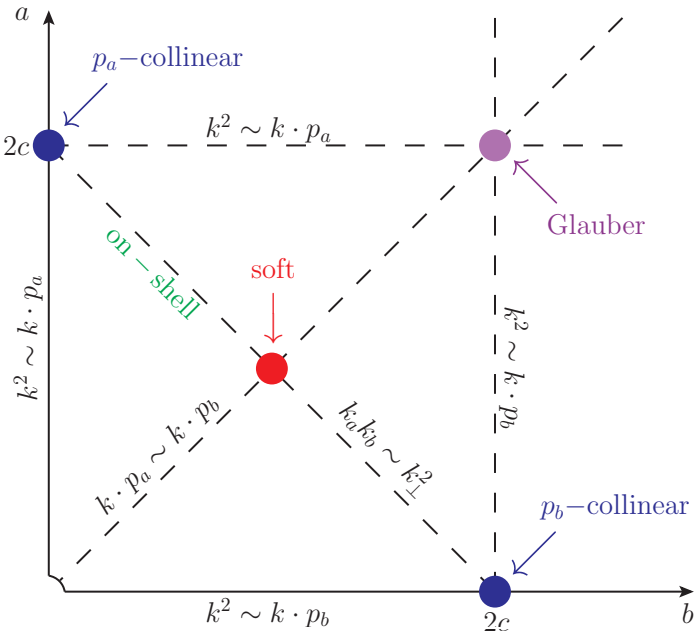

Figure 3.1: Scalings, $k \sim (\kappa^b, \kappa^a, \kappa^c)$, that could give power-counting IR divergences.

is lightlike. Then it makes sense to choose one of our basis vectors n_a^μ to point along p_a^μ. In this case, a term $k \cdot p_a \to \kappa^a \, k \cdot p_a$ may appear in a denominator. Similarly, $k \cdot p_b \to \kappa^b \, k \cdot p_b$ may appear. Thus there are four relevant scaling behaviors:

$$k_a k_b \sim \kappa^{a+b}, \quad k_\perp^2 \sim \kappa^{2c}, \quad k \cdot p_a \sim \kappa^a \quad k \cdot p_b \sim \kappa^b \tag{3.13}$$

In expanding for small κ, all we do is drop some of these when they are smaller than others. If an integral is power-counting finite when two terms are of comparable size, it is necessarily power-counting finite when one of them is dropped. So we can restrict our considerations to scalings where two (or more) of these terms are comparable.

There are six regions where two of the scalings in Eq. (3.13) are equal. These form the lines in Figure 3.1. For example, one of the diagonal lines has $a + b = 2c$ so that $k_a k_b \sim k_\perp^2$ and $k^2 \to \kappa^{2c} \, k^2$. This scaling is special as it keeps on-shell momenta on-shell. In particular, this line shows the only relevant scalings for external momenta.

Exponents	Conditions	Momenta scaling	Name
$(a,b,c)=(0,0,0)$:	$k_a k_b \sim k_\perp^2 \sim k\cdot p_a \sim k\cdot p_b$	$k^\mu \sim (1,1,1)$	hard
$(a,b,c)=(2,0,1)$:	$k_a k_b \sim k_\perp^2 \sim k\cdot p_a$	$k^\mu \sim (1,\kappa^2,\kappa)$	p_a-collinear
$(a,b,c)=(0,2,1)$:	$k_a k_b \sim k_\perp^2 \sim k\cdot p_b$	$k^\mu \sim (\kappa^2,1,\kappa)$	p_b-collinear
$(a,b,c)=(2,2,2)$:	$(k_a k_b \sim k_\perp^2)$ & $(k\cdot p_a \sim k\cdot p_b)$	$k^\mu \sim (\kappa^2,\kappa^2,\kappa^2)$	soft
$(a,b,c)=(2,2,1)$:	$k_\perp^2 \sim k\cdot p_a \sim k\cdot p_b$	$k^\mu \sim (\kappa^2,\kappa^2,\kappa)$	Glauber

Table 3.1: Scalings relevant for factorization.

The scalings where two lines intersect are the four solid dots. If an integral is infrared finite at all of these points, it is automatically infrared finite under any scaling. The points in the corners come from three scalings being equal and the center point, at $a=b=c$ has $k\cdot p_a \sim k\cdot p_b$ and $k_a k_b \sim k_\perp^2$. The most overlapping region, where all four scalings are equal requires $a=b=c=0$. This is hard scaling which does not tell us about infrared divergences since it does not zoom in on a possibly singular region. The point at the origin in Figure 3.1, where $a=b=0$ but $c\neq 0$ also cannot produce infrared divergences since for $\kappa=0$, k^μ is offshell. We are also free to choose one of a,b,c arbitrarily if it is not zero; for example, we can set $c=1$ by replacing κ by $\kappa'=\kappa^{1/c}$.

Thus, we can restrict the discussion to the scalings listed in Table 3.1. Of these, hard scaling does not produce infrared divergences. Soft and collinear scaling both imply $k^2\to\kappa^2 k^2$. In particular, timelike, spacelike and lightlike momenta stay timelike, spacelike and lightlike, respectively. Glauber scaling, on the other hand, turns timelike and lightlike momenta into spacelike momenta as $\kappa\to 0$, preserving

only the spacelike nature.

The set of scalings we need to consider is even smaller for the processes that have no collinear directions in the initial state. When there are only final state particles, for example in a decay, we know the infrared divergences must cancel among real and virtual corrections at each order in α_s. The reason infrared finiteness can be proven in this case is because, by unitarity, a decay is the imaginary part of a $1 \to 1$ total cross section whose analytic structure is particularly simple. Not only does infrared finiteness hold, but there is a one-to-one correspondence between the momenta producing infrared divergences in real emission contributions and the virtual contributions. This is easiest to see using old-fashioned perturbation theory (see Chapter 13 of [98]). In a real emission graph with only final state particles, all the virtual lines without loop momenta flowing through them are timelike. As we take $\lambda \to 0$ these timelike momenta approach the lightcone from within, and give rise to soft and collinear real-emission phase-space singularities. Because these phase-space divergences come from timelike momenta becoming lightlike, there cannot be any phase-space singularities with Glauber scaling, which as $\kappa \to 0$ makes timelike momenta spacelike. Then, by infrared finiteness of the total decay rate, there cannot be Glauber singularities in loop integrals either. We conclude that, when considering only final-state collinear directions, only soft and collinear scalings can possibly produce infrared divergences.

When there are collinear particles in the initial state, we expect that unitarity-based arguments should still hold, even if they have not yet been rigorously proven. The complication is that with collinear particles in the initial state, the virtual mo-

menta in real-emission graphs can be spacelike. In particular, a virtual particle with momentum $k = p^\mu - p'^\mu$ connecting an initial state particle of momenta p^μ to a final state particle of momentum p'^μ can be spacelike and have Glauber scaling if p^μ is collinear to p'^μ. Thus Glauber scaling is important for forward scattering. In this chapter, we will only have final state collinear directions, so we can ignore Glauber scaling. A technical pinch-analysis proof of the irrelevance of Glauber scaling for decay processes can be found in Chapter 5 of [99].

We conclude that we only need to consider soft scaling, and collinear scaling in each relevant direction. If upon $k^\mu \to \kappa^2 k^\mu$, an integral scales like κ to a positive power, the integral is not soft divergent. If it scales like κ^0 (it cannot scale like κ to a negative power, see [42] or Lemma 2), there might be a soft divergence. Collinear divergences are determined by rescaling k^μ as

$$k^\mu \to \frac{n_b \cdot k}{n_a \cdot n_b}\, n_a^\mu + \kappa^2 \frac{n_b \cdot k}{n_a \cdot n_b}\, n_b^\mu + \kappa\, k_\perp^\mu \tag{3.14}$$

If the integral scales like κ to a non-positive power, there is a potential collinear divergence. Otherwise, the integral is collinear finite in the n_a^μ direction.

In practice, Eq. (3.14) implies that to find a collinear divergence associated with the direction p^μ of an external momentum, we rescale

$$\begin{aligned} d^4k &\to \kappa^4\, d^4k \\ k^2 &\to \kappa^2\, k^2 \\ k \cdot p &\to \kappa^2\, k \cdot p \end{aligned} \tag{3.15}$$

If q is another loop momenta, then the scaling depends on whether q is being consider

collinear to p or not:

$$k \cdot q \;\to k \cdot q \times \begin{cases} \kappa^2, & q \parallel p \\ 1, & q \not\parallel p \end{cases} \tag{3.16}$$

For collinear-sensitive power counting (see below), the same scaling rules apply (depending on whether $q \parallel p$ or not) if q is a sum of external momenta.

As an example, consider the 1-loop scalar integral:

$$I = \int \frac{d^4k}{(2\pi)^4} \frac{1}{\big(k^2 + i\varepsilon\big)\big((p_1+k)^2 + i\varepsilon\big)\big((p_2+k)^2 + i\varepsilon\big)} \tag{3.17}$$

with $p_1^2 = p_2^2 = 0$. In the soft limit,

$$\begin{aligned} \frac{d^4k}{k^2(p_1+k)^2(p_2+k)^2} &\xrightarrow{k \text{ soft}} \frac{\kappa^8 d^4k}{\kappa^4 k^2(\kappa^2 2p_1\cdot k + \kappa^4 k^2)(\kappa^2 2p_2\cdot k + \kappa^4 k^2)} \\ &= \frac{d^4k}{k^2(2p_1\cdot k)(2p_2\cdot k)}\kappa^0 + \mathcal{O}(\kappa^2) \end{aligned} \tag{3.18}$$

Thus there is a potential logarithmic soft divergence in this integral. In the limit where $k \parallel p_1$, we choose $n_a^\mu = p_1^\mu$. Then

$$\begin{aligned} \frac{d^4k}{k^2(p_1+k)^2(p_2+k)^2} &\xrightarrow{k \parallel p_1} \frac{\kappa^4 d^4k}{\kappa^2 k^2(\kappa^2 2p_1\cdot k + \kappa^2 k^2)(2p_2\cdot k + \kappa^2 k^2)} \\ &= \frac{d^4k}{k^2(p_1+k)^2\, 2p_2\cdot k}\kappa^0 + \mathcal{O}(\kappa^2) \end{aligned} \tag{3.19}$$

Thus, there is a potential collinear divergence in the p_1^μ direction. By the symmetry of the integral, there is a potential collinear divergence in the p_2^μ direction as well.

In some cases, an integral does not have a divergence associated with a specific power counting despite the integrand scaling like κ^0 (for example, the Glauber scaling in decay processes). Indeed, one can often deform the integration contour away from the singularity. If this deformation cannot be done, the singularity is said to be

pinched. While there is a close connection between our approach and the results of a pinch analysis, we can conveniently avoid the discussion of contour deformation all together. Although we will use strongly that some diagrams with on-shell internal lines are not soft sensitive, we will not directly use the Landau equations [45] or their interpretation by Coleman and Norton [65] in our proof. Instead, we will show that two expressions agree at leading power in λ, including both infrared divergent and infrared finite contributions. The connection between infared divergences and the leading power in λ is through the notion of infrared sensitivity which we discuss next.

3.2.3 Infrared sensitivity

We are often interested not in actually divergent integrals, but in integrals which would be divergent if $\lambda = 0$. That is, they would scale like κ to a non-positive power if two external collinear particles were exactly proportional, or if a soft external particle had exactly zero momenta. We generalize the concept of an IR divergence to encompass such situations by saying that a loop is **IR sensitive** if it is IR divergent when $\lambda = 0$. Of course, a loop that is IR divergent (for any λ) is also IR sensitive. For a loop to be infinite at $\lambda = 0$ but finite for $\lambda \neq 0$, we know λ must be acting like an IR regulator. For example,

$$\int_0^1 d\kappa \frac{1}{\kappa + \lambda} = \ln \frac{\lambda + 1}{\lambda} \cong -\ln \lambda \tag{3.20}$$

The equivalent in a real diagram with $p \parallel q$ might be $\ln \lambda = \ln \frac{(p+q)^2}{Q^2}$.

When computing probabilities of IR-safe physical observables we square the amplitude and integrate over phase space of the external particles. The integration over phase space encloses the region where $\lambda = 0$; in fact, it is this region that cancels the

IR divergences in virtual loops. Thus, to preserve IR finiteness of physical observables, we must treat loops that are IR divergent when $\lambda = 0$ the same as we do loops that are IR divergent for any λ. Therefore, IR sensitivity is the appropriate concept to use when discussing loops and emissions together, rather than IR divergence.

When power counting IR-sensitive loops, instead of setting $\lambda = 0$ and counting powers of κ, we can simply count powers of κ and λ together. By power counting λ and κ as of the same order, we ensure that all the terms are kept that are necessary for the cancellation of IR divergences between real and virtual particles at leading power of a physical IR-safe observable.

For the power counting, we only count *powers*. This means that we treat $\ln\lambda$ as being the same order as λ^0. Therefore, a logarithmically divergent integral can be of the same order as a finite integral. Examples are given in Section 3.4.2, where we see that we must treat

$$\frac{1}{\lambda} \;\cong\; \frac{\ln\lambda}{\lambda} \;\cong\; \frac{\text{log divergent}}{\lambda} \tag{3.21}$$

The point is that power-suppression really requires an extra power of λ. This is consistent with the leading power of an IR-safe cumulant reproducing both the constant term and the terms which are powers of logarithms:

$$R(\alpha_s, \lambda) = f(\alpha_s) + f_1(\alpha_s)\ln\lambda + f_2(\alpha_s)\ln^2\lambda + \cdots \tag{3.22}$$

In a perturbative fixed-order or resummed calculation, certain terms in this expansion are reproduced, but the leading power factorization formula is *capable* of reproducing every term in such an expansion.

3.2.4 Lightcone gauge

Traditionally, lightcone gauge has been particularly useful for studying soft-collinear factorization. In lightcone gauge, the gluon Feynman propagator is

$$D_F^{ab;\mu\nu}(k) = \delta^{ab}\,\frac{i\Pi^{\mu\nu}(k)}{k^2+i\varepsilon} \tag{3.23}$$

with

$$\Pi^{\mu\nu}(k) = -g^{\mu\nu} + \frac{r^\mu k^\nu + r^\nu k^\mu}{r\cdot k} \tag{3.24}$$

where r^μ is lightlike and its overall scale does not matter. The propagator numerator, $\Pi^{\mu\nu}(k)$, satisfies

$$r_\mu \Pi^{\mu\nu}(k) = 0 \tag{3.25}$$

and

$$k_\mu \Pi^{\mu\nu}(k) = \frac{k^2}{r\cdot k} r^\nu \tag{3.26}$$

which vanishes as $k^2 \to 0$.

Eq. (3.26) produces a crucial feature of lightcone gauge: if $k \propto p$ where p^μ is some lightlike direction, then $p_\mu \Pi^{\mu\nu}(k) = 0$. In particular, near a collinear singularity, a numerator $p\cdot\Pi(k)$ gives a suppression factor of κ. To be more explicit, we will often find numerator structures from virtual gluons of the form $p\cdot\Pi(k)\cdot q$ for some momenta p and q. To study the limit when $k \parallel p$, we use Eq. (3.14) with $n^\mu = p^\mu$ and r^μ generic. Then

$$\begin{aligned} p\cdot\Pi(k)\cdot q &= -p\cdot q + \frac{r\cdot p\, k\cdot q + r\cdot q\, k\cdot p}{r\cdot k} \\ &\to -p\cdot q + \frac{p\cdot q\, r\cdot k + \kappa^2 p\cdot k\, r\cdot q + \kappa r\cdot p\, k_\perp\cdot q + \kappa^2 r\cdot q\, k\cdot p}{r\cdot k} \\ &= \kappa\left[\frac{r\cdot p\, k_\perp\cdot q}{r\cdot k} + 2\kappa\frac{p\cdot k\, r\cdot q}{r\cdot k}\right] \end{aligned} \tag{3.27}$$

This extra factor of κ strongly restricts the type of diagrams which are collinear sensitive in lightcone gauge; it makes many graphs finite (or collinear insensitive) which would be divergent if the numerator structure scaled like κ^0.

Lightcone gauges are sometimes called *physical gauges*, as the ghosts decouple and the propagator numerator is a sum over physical polarizations when the gluon goes on-shell:

$$\Pi^{\mu\nu}(k) = -g^{\mu\nu} + \frac{r^\mu k^\nu + r^\nu k^\mu}{r\cdot k} \quad \stackrel{k^2=0}{\longrightarrow} \quad \sum_{h=\pm} \epsilon_h^\mu(k;r)\,\epsilon_h^{\nu\,*}(k;r) \tag{3.28}$$

Recall that the basis of gluon polarizations $\epsilon_\pm^\mu(k;r)$ is uniquely specified by a reference vector r^μ to which the polarizations are orthogonal, and that the polarizations satisfy $r_\mu\epsilon_\pm^\mu(k;r) = k_\mu\epsilon_\pm^\mu(k;r) = 0$. The factor of κ coming from the numerator of the lightcone gauge propagator in Eq. (3.27) is similar to the extra factor of λ suppression of collinear-emission diagrams in generic-r compared to say, their scalar field theory counterparts [3]. That is, $p\cdot\Pi(k) \sim \kappa$ when $k \parallel p$ can be thought of, via Eq. (3.28), as a consequence of the transversality of the polarization vectors, which implies that $p\cdot\epsilon(q) \sim \lambda$ when $p \parallel q$.

In [3], the freedom to choose reference vectors for the gluon polarizations was used extensively to prove factorization at tree level. There, it was shown that two important choices of r were

$$\textbf{generic-}r: \qquad r \not\parallel p_j \quad \text{for any } j \tag{3.29}$$

and

$$\textbf{collinear-}r: \qquad r \parallel p_j \quad \text{for some } j \tag{3.30}$$

For example, choosing collinear-r for the polarizations of the soft gluons and generic-r

for the polarizations of the collinear gluons simplified the disentangling of soft and collinear radiation.

For loops, we can of course choose r generic (not parallel to any p_j), which we call a **generic-lightcone gauge**, or we can choose $r \parallel p_j$ for some p_j, which we call **collinear-lightcone gauge**. To prove factorization at loop level, however, it will be helpful to be able to choose lightcone gauges for the soft-virtual gluons and collinear-virtual gluons separately. We introduce a gauge called **factorization gauge** in Section 3.8 which provides this flexibility. We will refer to either lightcone gauge with generic choice of r or factorization gauge with generic choice of r_c as **physical gauges**. This is not quite a standard usage since 1) all lightcone gauges are usually considered physical and 2) ghosts do not completely decouple in factorization gauge (see Section 3.8.2). Since our definition is morally equivalent to the usual definition, we do not feel a new term is needed.

3.2.5 Wilson Lines

Wilson lines describe the radiation produced by a charged particle moving along a given path in the semi-classical limit. The semi-classical limit applies when the back reaction of the radiation on the particle can be neglected, so that the particle behaves like a source of charge. In particular, this limit holds when the particle is much more energetic than any of the radiation, that is, when the radiation is soft. The physical picture of how Wilson lines arise in the soft and collinear limits of Yang-Mills theories is discussed in [3].

We define a soft Wilson line in the n_j^μ by

$$Y_j^\dagger(x) = P\left\{\exp\left[ig\int_0^\infty ds\, n_j\cdot A(x^\nu + sn_j^\nu)\, e^{-\varepsilon s}\right]\right\} \tag{3.31}$$

where P denotes path-ordering and $A_\mu = A_\mu^a T^a$ is the gauge field in the fundamental representation (Wilson lines in other representations are a straightforward generalization). This Wilson line is outgoing because the position where the gauge field $A_\mu(x)$ is evaluated goes from x to ∞ along the n_j^μ direction. We write $Y_j^\dagger$ for Wilson lines for outgoing particles, and Y_j for outgoing antiparticles (as $\bar\psi$ creates outgoing quarks and ψ creates outgoing antiquarks). Explicitly,

$$Y_j(x) = \overline{P}\left\{\exp\left[-ig\int_0^\infty ds\, n_j\cdot A(x^\nu + sn_j^\nu)\, e^{-\varepsilon s}\right]\right\} \tag{3.32}$$

where $\overline{P}$ denotes anti-path ordering. We will not bother to discuss incoming Wilson lines in this chapter; they are defined in Ch. 2.

Wilson lines can be in any representation. For example, an adjoint Wilson line can be written as

$$\mathcal{Y}_j^\dagger(x) = P\left\{\exp\left[ig\int_0^\infty ds\, n_j\cdot A_\mu^a(x + s\, n_j)T^a_{\rm adj}\, e^{-\epsilon s}\right]\right\} \tag{3.33}$$

where $(T^a_{\rm adj})^{bc} = if^{bac}$ are the adjoint-representation group generators. Since

$$(T^c_{\rm adj})^{ab}T^b = [T^a, T^c]\,, \tag{3.34}$$

fundamental and adjoint Wilson lines are related as

$$Y_j^\dagger T^a\, Y_j = \mathcal{Y}_j^{ab}\, T^b \tag{3.35}$$

This identity is occasionally useful to write all of the Wilson lines for QCD in terms of fundamental and antifundamental Wilson lines.

From a practical perspective, the most important facts about Wilson lines for this chapter are their Feynman rules and their gauge-transformation properties. Their Feynman rules are exactly the eikonal rules, coming from the soft limit of a QCD interaction:

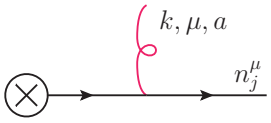

$$\overset{k\to\text{soft}}{=} -gT^a \frac{n_j^\mu}{n_j \cdot k + i\varepsilon} = \langle k, \mu; a| \, Y_j^\dagger \, |0\rangle \tag{3.36}$$

with the correct $i\epsilon$ prescription. Here $\langle k, \mu; a| \, Y_j^\dagger \, |0\rangle$ means the off-shell matrix element for a gluon with polarization $\epsilon^\mu(k)$ and color a with the polarization vector stripped off. That $Y_n^\dagger$ gives the eikonal Feynman rules persist at any order [3]. The $e^{\pm\varepsilon s}$ factors in the Wilson lines are required to produce the correct $i\varepsilon$ prescription for the Feynman rules (see [3]).

We denote collinear Wilson lines as $W_j^\dagger$. They are mathematically identical to soft Wilson lines but the path is different. While soft Wilson lines point in the direction of the particle they represent, collinear Wilson lines point in some other direction t_j^μ:

$$W_j^\dagger(x) = P\left\{\exp\left[ig\int_0^\infty ds\, t_j \cdot A(x^\nu + s t_j^\nu)\, e^{-\varepsilon s}\right]\right\} \tag{3.37}$$

We always take t_j^μ to *not* be collinear to n_j^μ, that is, $t_j \not\parallel n_j$. As discussed in [3] and as we will see here, while soft Wilson lines account for the soft radiation of a particle, collinear Wilson lines account for the collinear radiation from all the *other* particles.

3.3 Example 1: one-loop Wilson coefficient

The general proof of factorization will be presented starting in Section 3.5. To understand this proof, we first provide two examples. For the first example, in this

section we discuss factorization for $\langle p_1, p_2|\, \phi^\star \phi\, |0\rangle$ at 1-loop order. This is perhaps the simplest 1-loop amplitude for which factorization holds. What we will show here at 1-loop order is that

$$\langle p_1, p_2|\, \phi^\star \phi\, |0\rangle = \mathcal{C}(s_{12})\, \frac{\langle p_1|\, \phi^\star W_1\, |0\rangle}{\langle 0|\, Y_1^\dagger W_1\, |0\rangle}\, \frac{\langle p_2|\, W_2^\dagger \phi\, |0\rangle}{\langle 0|\, W_2^\dagger Y_2\, |0\rangle}\, \langle 0|\, Y_1^\dagger Y_2\, |0\rangle \tag{3.38}$$

where $s_{12} = (p_1 + p_2)^2$. Note that Eq. (3.38) is an exact equality, not a leading power equivalence, because there are no particles collinear to each other and no soft particles, so $\lambda = 0$. It is also somewhat trivial: it is just a definition of $\mathcal{C}(s_{12})$. The nontrivial part is showing that $\mathcal{C}(s_{12})$ is IR finite. The next example, in Section 3.4, discusses what happens when one of the sectors has two collinear particles and provides a nontrivial check on the universality of $\mathcal{C}(s_{12})$.

3.3.1 Overview of graphs

There are five graphs contributing to the left-hand side of Eq. (3.38) at 1-loop order. Four of them involve only one leg

$G_a^{(11)} =$ 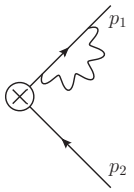

, $G_b^{(11)} =$ 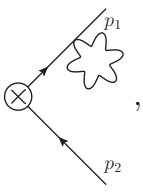

, $G_a^{(22)} =$ 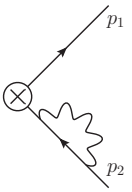

, $G_b^{(22)} =$ 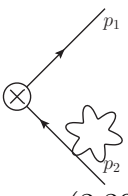

(3.39)

and the final diagram connects both legs.

$G^{(12)} =$ 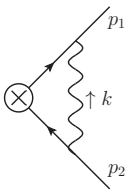

(3.40)

For the right-hand side of Eq. (3.38), there are a number of graphs involving emissions from the collinear Wilson lines W_i. Recall from Eq. (3.37) that the Wilson

lines are defined with a certain direction t_i^μ. For simplicity, let us choose $t_1 = t_2 = r$ to be some random direction not collinear to either p_1 or p_2. Then, if we work in a generic-lightcone gauge with the same reference vector, r^μ, all of the graphs involving W_i precisely vanish. The remaining non-vanishing diagrams are

$$\langle p_1|\phi^\star|0\rangle \;=\; \text{ 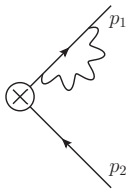 } \;+\; \text{ 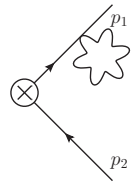 } \;=\; G_a^{(11)} + G_b^{(11)} \tag{3.41}$$

and

$$\langle p_2|\phi|0\rangle \;=\; \text{ 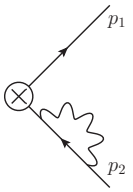 } \;+\; \text{ 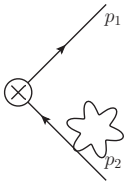 } \;=\; G_a^{(22)} + G_b^{(22)} \tag{3.42}$$

and those involving soft Wilson lines Y_i. The diagrams in Eqs. (3.41) and (3.42) precisely agree with those in Eq. (3.39). Let us denote the diagrams coming from soft Wilson lines with the subscript *soft-sens.* So the remaining terms are

$$\begin{aligned}\mathcal{C}(s_{12})\,\frac{\langle 0|\,Y_1^\dagger Y_2\,|0\rangle}{\langle 0|\,Y_1^\dagger\,|0\rangle\,\langle 0|\,Y_2\,|0\rangle} &= \mathcal{C}(s_{12})\,\frac{1 + G^{(11)}_{\text{soft-sens.}} + G^{(22)}_{\text{soft-sens.}} + G^{(12)}_{\text{soft-sens.}}}{(1 + G^{(11)}_{\text{soft-sens.}})(1 + G^{(22)}_{\text{soft-sens.}})} + \mathcal{O}(\alpha^2) \\ &= \mathcal{C}(s_{12})\,[1 + G^{(12)}_{\text{soft-sens.}} + \mathcal{O}(\alpha^2)]\end{aligned} \tag{3.43}$$

where $G^{(ij)}_{\text{soft-sens.}}$ is the graph found by contracting Y_i with Y_j. Note that the Feynman rules from the soft Wilson line are eikonal, so there are no 4-point vertices, and therefore, no G_b-type graphs. Solving for $\mathcal{C}(s_{12})$ we find

$$\mathcal{C}(s_{12}) = 1 + G^{(12)}_{\text{not-soft-sens.}} + \mathcal{O}(\alpha^2) \tag{3.44}$$

where

$$G^{(12)}_{\text{not-soft-sens.}} \equiv G^{(12)} - G^{(12)}_{\text{soft-sens.}} \tag{3.45}$$

Thus, to verify Eq. (3.38) at 1-loop order all we need to show is that $G^{(12)}_{\text{not-soft-sens.}}$ is IR finite.

3.3.2 IR finiteness

The graph of interest is

$G^{(12)} =$ 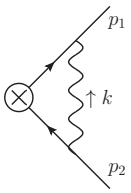

$= -g^2 \int \frac{d^4k}{(2\pi)^4} \frac{(2p_1-k)^\alpha}{(p_1-k)^2+i\varepsilon} \frac{i\Pi_{\alpha\beta}(k)}{k^2+i\varepsilon} \frac{(2p_2+k)^\beta}{(p_2+k)^2+i\varepsilon}$ (3.46)

where $\Pi^{\mu\nu}$ is given in Eq. (3.24) in lightcone gauge. The soft graph, from the matrix element of Wilson lines is

$$G^{(12)}_{\text{soft-sens.}} = \int \frac{d^4k}{(2\pi)^4} \frac{-ig^2\, p_1\cdot\Pi(k)\cdot p_2}{\big(-p_1\cdot k+i\varepsilon\big)\big(k^2+i\varepsilon\big)\big(p_2\cdot k+i\varepsilon\big)} \tag{3.47}$$

Note that Eq. (3.47) can be obtained from Eq. (3.46) with the eikonal approximation. More precisely, we can use the identity

$$\frac{1}{(p+k)^2+i\varepsilon} = \frac{1}{2p\cdot k+i\varepsilon}\left(1-\frac{k^2}{(p+k)^2+i\varepsilon}\right) \tag{3.48}$$

which holds at $p^2=0$. This identity lets us replace propagators in the full graph with a sum of eikonal propagators, plus a correction proportional to k^2. It is similar to the Grammar-Yennie decomposition [100] used in many factorization proofs in QCD [41, 43, 66]. Since the original graph was logarithmically divergent in the soft limit ($k\to 0$), the k^2 factors will make the remainder soft finite. That is $G^{(12)}_{\text{not-soft-sens.}} = G^{(12)} - G^{(12)}_{\text{soft-sens.}}$ is soft finite.

To see collinear finiteness, we will show that in a generic-lightcone gauge, both $G^{(12)}$ and $G^{(12)}_{\text{soft-sens.}}$ are separately collinear finite. Consider the case $k^\mu \parallel p_1^\mu$. Then

under collinear rescaling $k^2 \to \kappa^2 k^2$ and $k \cdot p_1 \to \kappa^2 k \cdot p_1$. If we ignore the numerator in Eq. (3.46), the diagram would scale like κ^0 and be logarithmically divergent. For the scaling of the numerator, we note that we are exactly in the situation where Eq. (3.27) applies. That is,

$$p_1 \cdot \Pi(k) \cdot p_2 = \kappa \frac{r \cdot p_1 k_\perp \cdot p_2}{r \cdot k} + \mathcal{O}(\kappa^2) \tag{3.49}$$

for a generic choice of lightcone gauge reference vector r^μ. This extra factor of κ makes the $G^{(12)}$ convergent when $k \parallel p_1$. A similar analysis for $k \parallel p_2$ shows that $G^{(12)}$ is completely collinear finite. The same argument shows that $G^{(12)}_{\text{soft-sens.}}$ is collinear finite, and therefore $G^{(12)}_{\text{not-soft-sens.}}$ has no IR singularities and Eq. (3.38) is verified at 1-loop order.

For the IR-finite contribution from $G^{(12)}_{\text{not-soft-sens.}}$, which contributes to the Wilson coefficient, we introduce the diagrammatic notation

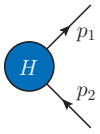

$$= 1 + G^{(12)}_{\text{not-soft-sens.}} + \mathcal{O}(\alpha^2) \tag{3.50}$$

This is a type of reduced diagram we call **hard**. A hard diagram is IR finite, but relevant at leading power.

3.3.3 Explicit result and $\mathbf{t}_j^\mu$-independence

To calculate the Wilson coefficient, rather than scalar QED, we consider the more phenomenologically relevant case of a vector current decaying to a $q\bar{q}$ pair, where $\mathcal{O} = \bar{\psi}\gamma^\mu\psi$. For this case, the factorization formula states

$$\langle p_1; p_2| \, \bar{\psi}\gamma^\mu\psi \, |0\rangle \cong \mathcal{C}(s_{12}) \, \gamma^\mu_{\alpha\beta} \frac{\langle p_1| \, \bar{\psi} W_1 \, |0\rangle^\alpha}{\langle 0| \, Y_1^\dagger W_1 \, |0\rangle} \frac{\langle p_2| \, W_2^\dagger \psi \, |0\rangle^\beta}{\langle 0| \, W_2^\dagger Y_2 \, |0\rangle} \, \langle 0| \, Y_1^\dagger Y_2 \, |0\rangle \tag{3.51}$$

where α and β are Dirac spin indices. To calculate the Wilson coefficient, it is easiest to use Feynman gauge rather than lightcone gauge, where all of the Wilson-line self-interactions vanish. In pure dimensional regularization, all of the diagrams from the factorized expression are scaleless and exactly vanish. The Wilson coefficient is therefore given by $G^{(12)}$ with the $\frac{1}{\varepsilon}$ and $\frac{1}{\varepsilon^2}$ terms dropped (the UV divergences are removed with $\overline{\text{MS}}$ counterterms and the IR cancel in the matching). The Wilson coefficient then comes out to [8, 63, 64, 101]

$$\mathcal{C}(s_{12}) = 1 - \frac{\alpha}{4\pi}\left(8 - \frac{\pi^2}{6} + \ln^2\frac{-\mu^2}{s_{12}} + 3\ln\frac{-\mu^2}{s_{12}}\right) + \mathcal{O}(\alpha^2) \tag{3.52}$$

The Wilson coefficient result is independent of both the IR regulator and the collinear Wilson line directions t_1^μ and t_2^μ.

To see the t_1^μ and t_2^μ independence more nontrivially and the importance of the zero-bin subtraction, one must use an IR regulator other the dimensional regularization. Following [59] on the zero-bin subtraction in SCET (where more details are given) we consider adding an off-shellness regulator. The differences between our approach and SCET are that 1) we use an operator definition of the zero-bin subtraction; 2) we do not have separate soft and collinear modes: all interactions are those in full QCD; and 3) we allow for the collinear Wilson lines to point in arbitrary directions, t_j^μ. These differences are all minor, and the results can essentially be drawn from Eqs. (65)-(70) of [59] with small modifications.

We can decompose any momentum into lightcone coordinates using the directions in the soft and collinear Wilson lines, n_1^μ and t_1^μ:

$$p^\mu = \frac{p\cdot t_1}{n_1\cdot t_1} n_1^\mu + \frac{p\cdot n_1}{n_1\cdot t_1} t_1^\mu + p_\perp^\mu \tag{3.53}$$

The off-shellness regulator keeps $n_1{\cdot}p_1 > 0$ even if $p_1 \propto n_1$ as in the external state. Thus

$$p_1^2 = \frac{2}{n_1{\cdot}\,t_1}(n_1{\cdot}p_1)(t_1{\cdot}p_1) > 0 \tag{3.54}$$

We could also have decomposed with respect to n_2^μ and t_2^μ. If we perform the calculation in $4-2\varepsilon$ dimensions, ε will regulate the UV and soft divergences, with the collinear divergences cut off by the off-shellness.

First, consider the self-energy graphs on the external legs. These are trivially identical on both sides of Eq.(3.51) (with any regulator) thus they can be ignored in the matching. Although this is also true in label SCET, it is not trivially true, since the Feynman rules for collinear fields are different from full theory fields.

For the remaining graphs, we present only the double-logarithmic terms for simplicity, since these manifest all the interesting cancellation. On the left-hand side of Eq. (3.51), the only full-theory graph needed is

$G^{(12)} =$ 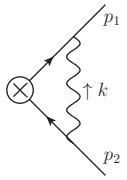

$\overset{\text{DL}}{=} -\bar{v}\gamma^\mu u\, C_F \dfrac{\alpha_s}{2\pi} \ln\dfrac{p_1^2}{s_{12}} \ln\dfrac{p_2^2}{s_{12}}$ (3.55)

where $\overset{\text{DL}}{=}$ means equal at double-logarithmic order.

The graphs needed in the factorized expression are the soft Wilson line graph:

$$\langle 0|\, Y_1 Y_2^\dagger \,|0\rangle \overset{\text{DL}}{=} -C_F \frac{\alpha_s}{4\pi}\left\{ \frac{2}{\varepsilon_{\text{UV}}^2} + \frac{2}{\varepsilon_{\text{UV}}} \ln\frac{-\mu^2\, s_{12}}{p_1^2 p_2^2} + \ln^2\frac{-\mu^2\, s_{12}}{p_2^2\, p_1^2} \right\} \tag{3.56}$$

the collinear graphs, without the leg corrections:

$$\langle p_1|\,\bar{\psi}W_1\,|0\rangle \overset{\text{DL}}{=} -\bar{u}\,C_F\frac{\alpha_s}{4\pi}\left\{-\frac{2}{\varepsilon_{\text{UV}}\varepsilon_{\text{IR}}}-\frac{2}{\varepsilon_{\text{IR}}}\ln\frac{\mu^2}{-p_1^2}-\ln^2\frac{\mu^2}{-p_1^2}+\left(\frac{2}{\varepsilon_{\text{IR}}}-\frac{2}{\varepsilon_{\text{UV}}}\right)\ln\frac{\mu}{t_1{\cdot}p_1}\right\} \tag{3.57}$$

$$\langle p_2|\,W_2^\dagger\psi\,|0\rangle \overset{\text{DL}}{=} -C_F\frac{\alpha_s}{4\pi}\left\{-\frac{2}{\varepsilon_{\text{UV}}\varepsilon_{\text{IR}}}-\frac{2}{\varepsilon_{\text{IR}}}\ln\frac{\mu^2}{-p_2^2}-\ln^2\frac{\mu^2}{-p_2^2}+\left(\frac{2}{\varepsilon_{\text{IR}}}-\frac{2}{\varepsilon_{\text{UV}}}\right)\ln\frac{\mu}{t_2{\cdot}p_2}\right\}v \tag{3.58}$$

and the zero-bin subtractions:

$$\widehat{Z}_1=\frac{1}{N_c}\text{tr}\,\langle 0|\,Y_1^\dagger W_1\,|0\rangle \overset{\text{DL}}{=} C_F\frac{\alpha_s}{4\pi}\left(\frac{2}{\varepsilon_{\text{IR}}}-\frac{2}{\varepsilon_{\text{UV}}}\right)\left(\frac{1}{\varepsilon_{\text{UV}}}+\ln\frac{\mu^2}{-p_1^2}-\ln\frac{\mu}{t_1{\cdot}p_1}\right) \tag{3.59}$$

$$\widehat{Z}_2=\frac{1}{N_c}\text{tr}\,\langle 0|\,W_2^\dagger Y_2\,|0\rangle \overset{\text{DL}}{=} C_F\frac{\alpha_s}{4\pi}\left(\frac{2}{\varepsilon_{\text{IR}}}-\frac{2}{\varepsilon_{\text{UV}}}\right)\left(\frac{1}{\varepsilon_{\text{UV}}}+\ln\frac{\mu^2}{-p_2^2}-\ln\frac{\mu}{t_2{\cdot}p_2}\right) \tag{3.60}$$

This notation and normalization for the zero bin subtraction will be explained in Sections 3.11 and 3.13. Note that the appearance of the hard scales $t_1{\cdot}p_1$ and $t_2{\cdot}p_2$ is illusory — using Eq. (3.54), one can express $\widehat{Z}_1$ and $\widehat{Z}_2$ in terms of the off-shellnesses $n_1{\cdot}p_1$ and $n_2{\cdot}p_2$ alone.

Therefore,

$$\frac{\langle p_1|\,\bar{\psi}W_1\,|0\rangle}{\widehat{Z}_1} \overset{\text{DL}}{=} -\bar{u}\,C_F\frac{\alpha_s}{4\pi}\left\{-\frac{2}{\varepsilon_{\text{UV}}^2}-\frac{2}{\varepsilon_{\text{UV}}}\ln\frac{\mu^2}{-p_1^2}-\ln^2\frac{\mu^2}{-p_1^2}\right\} \tag{3.61}$$

$$\frac{\langle p_2|\,W_2^\dagger\psi\,|0\rangle}{\widehat{Z}_2} \overset{\text{DL}}{=} -C_F\frac{\alpha_s}{4\pi}\left\{-\frac{2}{\varepsilon_{\text{UV}}^2}-\frac{2}{\varepsilon_{\text{UV}}}\ln\frac{\mu^2}{-p_2^2}-\ln^2\frac{\mu^2}{-p_2^2}\right\}v \tag{3.62}$$

These equations show that each collinear sector is independent of the Wilson-line directions, t_j^μ, and is only p_j-collinear sensitive as evidenced by the cancellation of the ε_{IR} poles.

Putting everything together up to 1-loop we find:

$$\gamma^\mu_{\alpha\beta}\frac{\langle p_1|\, W_1\bar{\psi}\,|0\rangle^\alpha}{\widehat{Z}_1}\frac{\langle p_2|\, W_2^\dagger\psi\,|0\rangle^\beta}{\widehat{Z}_2}\,\langle 0|\, Y_1^\dagger Y_2\,|0\rangle$$
$$\overset{\text{DL}}{=} -\bar{v}\gamma^\mu u\, C_F\frac{\alpha_s}{4\pi}\left\{-\frac{2}{\varepsilon_{\text{UV}}^2}-\frac{2}{\varepsilon_{\text{UV}}}\ln\frac{\mu^2}{-s_{12}}+\ln^2\frac{\mu^2}{-s_{12}}+2\ln\frac{-p_2^2}{\mu^2}\ln\frac{-p_1^2}{\mu^2}\right\} \quad (3.63)$$

Comparing to the full-QCD matrix element shown in Eq. (3.55), we see that, to double-logarithmic order, the IR-divergences in the full theory and factorized expression exactly agree.

3.4 Example 2: two collinear particles

As the next illustrative example, we consider a state with two particles in one jet. That is we consider $\langle p_1, q; p_2|\, \phi^\star\phi\,|0\rangle$, for which the factorization formula reads

$$\langle p_1, q; p_2|\, \phi^\star\phi\,|0\rangle \;\cong\; \mathcal{C}(S_{12})\,\frac{\langle p_1, q|\, \phi^\star W_1\,|0\rangle}{\langle 0|\, Y_1^\dagger W_1\,|0\rangle}\,\frac{\langle p_2|\, W_2^\dagger\phi\,|0\rangle}{\langle 0|\, W_2^\dagger Y_2\,|0\rangle}\,\langle 0|\, Y_1^\dagger Y_2\,|0\rangle \quad (3.64)$$

where $P_1^\mu = p_1^\mu + q^\mu$, $P_2^\mu = p_2^\mu$ and $S_{12} \cong (P_1+P_2)^2 \equiv Q^2$. In this case, the two sides are not equal, but equal at leading power in λ, where $\lambda = P_1^2/Q^2$. We also must show that the Wilson coefficient $\mathcal{C}(S_{12})$ is the same function computed with minimal collinear sectors, as in the previous section. This example will illustrate the role played by real-emission and IR-sensitive graphs in factorization.

3.4.1 Overview of graphs

In this example, since we have an external photon, we must choose a reference vector for its polarization. It is natural to choose the same generic-r reference vector as in the lightcone-gauge photon propagator. So $r_\mu\epsilon^\mu(q) = q_\mu\epsilon^\mu(q) = 0$. These

constraints define the polarization vectors that are consistent with generic-lightcone gauge completely:

$$\epsilon^-(q;r) = \sqrt{2}\,\frac{q\rangle[r}{[qr]} \qquad \text{and} \qquad \epsilon^+(q;r) = \sqrt{2}\,\frac{r\rangle[q}{\langle rq\rangle} \tag{3.65}$$

where we use the spinor-helicity formalism to ease the discussion of the dependence on the reference vector, r, of amplitudes. Our conventions for the spinor-helicity formalism are given in [3], however, we will not need any details of the spinor-helicity formalism in this chapter as everything we need concerning polarization vectors will be taken from [3]. We also choose $t_1 = t_2 = r$ for the collinear Wilson lines to decouple them completely. Thus we can set $W_1 = W_2 = 1$ in this example.

As in the previous example, many graphs contribute to both the left-hand side and right-hand side of Eq. (3.64). In particular, all graphs involving one leg only in the full theory matrix element, such as

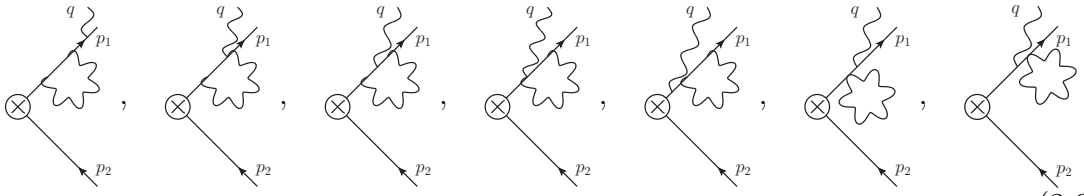

(3.66)

contribute to the right-hand side through $\langle p_1, q|\,\phi^\star\,|0\rangle$. Also trivially-factorizing cross terms, such as

$$\langle p_1, q|\,\phi^\star\,|0\rangle_{\text{tree}}\,\langle p_2|\,\phi\,|0\rangle_{\text{1-loop}} \;=\; \tag{3.67}$$

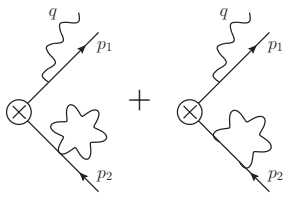

contribute identically on both sides of Eq. (3.64).

The remaining graphs from the left-hand side of Eq. (3.64) either have a loop

connecting the two legs and the emission coming off either the p_1 leg:

$$G^{(12),a} \equiv \quad , \qquad G^{(12),b} \equiv \quad , \qquad G^{(12),c} \equiv \qquad (3.68)$$

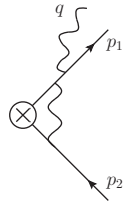

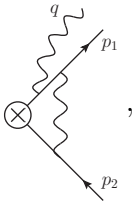

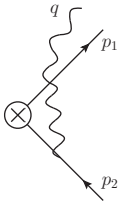

or they have the emission coming off of the p_2 leg with the loop anywhere:

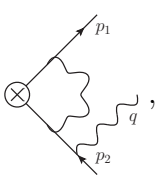

, 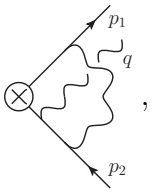

, 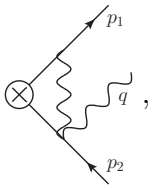

, 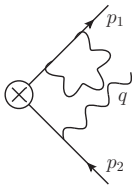

, ... (3.69)

With generic reference vectors, the twelve graphs in Eq. (3.69) are power suppressed compared to the graphs where the emission comes off of the p_1 leg. Indeed, graphs which contribute at leading power must have a factor of $\frac{1}{q\cdot p_1} \sim \lambda^{-2}$, as does $G^{(12),a}$. The graphs with the emission coming from the p_2 leg have instead $\frac{1}{q\cdot p_2} \sim \lambda^0$ factors which are subleading power. The fact that non-self-collinear emissions are power suppressed in generic-lightcone gauge was discussed elaborately in [3]. This result holds at loop level as well, simply because in generic-lightcone gauge a non-self-collinear emission can never have an enhanced propagator. We will come back to the general discussion in the next section and focus, for now, on the 1-loop example at hand. The result is that we do not need to consider the graphs in Eq. (3.69) at leading power.

Note that the power suppression in λ holds whether or not the graphs are IR finite. Although power counting something infinite may seem bizarre, one should keep in mind that the IR divergences in loops are always ultimately canceled by phase-space integrals in computing IR-safe observables. Thus, power-suppressed IR

divergences translate to power-suppressed finite contributions, which is why we can drop them.

The remaining graphs contributing to the right-hand side of Eq. (3.64) come from the tree-level real emission multiplied by the Wilson coefficient and soft-Wilson-line terms at 1-loop order:

$$\langle p_1, q|\,\phi^\star\,|0\rangle_{\text{tree}} \times \left\{ \mathcal{C}(S_{12})\,\frac{\langle 0|\,Y_1^\dagger Y_2\,|0\rangle}{\langle 0|\,Y_1^\dagger\,|0\rangle\,\langle 0|\,Y_2\,|0\rangle} \overset{\text{1-loop}}{=} \langle 0|\,\overbrace{Y_1^\dagger Y_2}\,|0\rangle + G^{(12)}_{\text{not-soft-sens.}} \right\} \tag{3.70}$$

where $G^{(12)}_{\text{not-soft-sens.}}$, defined in Eq. (3.45), comes from the calculation of the 1-loop Wilson coefficient in the previous section.

What we will now show is that the $\langle 0|\,\overbrace{Y_1^\dagger Y_2}\,|0\rangle$ term in Eq. (3.70) reproduces the sum of the soft limits of $G^{(12),a}$ or $G^{(12),b}$ at leading power, the $G^{(12)}_{\text{not-soft-sens.}}$ term reproduces the non-soft part of $G^{(12),a}$ at leading power, and both $G^{(12),c}$ and the non-soft part of $G^{(12),b}$ are power suppressed, hence proving Eq. (3.64) at 1-loop order.

3.4.2 The graph $G^{(12),a}$

Writing out the Feynman rules, we find

$$G^{(12),a} = \; g\,\frac{p_1\cdot\epsilon}{p_1\cdot q} \times ig^2 \int \frac{d^4k}{(2\pi)^4}\,\frac{(2p_1+2q-k)\cdot\Pi(k)\cdot(2p_2+k)}{k^2\,(p_2+k)^2\,(p_1+q-k)^2} \tag{3.71}$$

As in the previous example, we will write this graph as

$$G^{(12),a} = G^{(12),a}_{\text{soft-sens.}} + G^{(12),a}_{\text{not-soft-sens.}} \tag{3.72}$$

where the soft-sensitive part is found by dropping terms which are subleading in κ after the rescaling $k^\mu \to \kappa^2 k^\mu$. We draw the soft limit with the soft photon colored

red and with a long wavelength. That is,

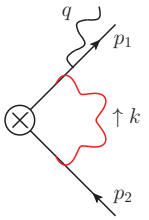

$$= G^{(12),a}_{\text{soft-sens.}} = g\,\frac{p_1\cdot\epsilon}{p_1\cdot q}\times\int\frac{d^4k}{(2\pi)^4}\,\frac{2ig^2\,(p_1+q)\cdot\Pi(k)\cdot p_2}{k^2\,(p_2\cdot k+i\varepsilon)\,\big((p_1+q)^2-2(p_1+q)\cdot k+i\varepsilon\big)} \tag{3.73}$$

This graph is not IR divergent, but it is IR sensitive. Because $(p_1+q)^2\sim\lambda^2$, in taking the soft limit, we did not drop $2(p_1+q)\cdot k$ in favor of $(p_1+q)^2$. Doing so would have assumed a certain order of limits, essentially $\kappa\ll\lambda$, which would lead to inconsistent results. More precisely, if we were to integrate over the phase space of q to produce an IR-safe cross section, the region where $q\cdot p_1\approx 0$ must be treated independently of the region of $k^\mu\approx 0$ in the loop integral. That is, the only way for the order of integration of the loop and phase-space integrals to not matter is if we keep both terms.

Now, since we keep $(p_1+q)^2>0$ the loop integral is not soft-divergent. This is clear from counting powers of κ as $k^\mu\to\kappa^2k^\mu$, which gives $G^{(12),a}_{\text{soft-sens.}}\to\kappa G^{(12),a}_{\text{soft-sens.}}$. However, if $(p_1+q)^2=0$, the loop scales like κ^0 and is logarithmically soft divergent. Thus, for $(p_1+q)^2\sim\lambda^2$ with λ small, λ acts like an IR cutoff. We, therefore, have that

$$G^{(12),a}_{\text{soft-sens.}}\;\sim\;g\,\frac{p_1\cdot\epsilon}{p_1\cdot q}\,g^2\ln\lambda \tag{3.74}$$

This singular-λ dependence must be reproduced by the factorized expression, as the Wilson coefficient is λ independent. On the other hand, the non-soft part of the loop, $G^{(12),a}_{\text{not-soft-sens.}}=G^{(12),a}-G^{(12),a}_{\text{soft-sens.}}$ is free of soft divergences, even at $\lambda=0$ (except for the prefactor, of course). This follows from the eikonal substitution in Eq. (3.48)

which adds additional powers of k^2 to the non-soft part.

Both the soft and non-soft parts of the loop are also collinear finite in generic-lightcone gauge. This holds for the exact same reason that $G^{(12)}_{\text{not-soft-sens.}}$ was collinear-finite in the previous section: in generic–lightcone gauge, the numerator of $G^{(12),a}$ is suppressed when k becomes collinear to p_1 or p_2 as in Eq. (3.26) and Eq. (3.27). Thus, $G^{(12),a}$ is collinear-finite (even when $(p_1+q)^2=0$), implying that $G^{(12),a}_{\text{not-soft-sens.}}$ is IR-insensitive (collinear and soft insensitive) since $G^{(12),a}_{\text{not-soft-sens.}}$ has the soft sensitivity subtracted off.

Because the loop integral in $G^{(12),a}_{\text{not-soft-sens.}}$ is IR-finite even when $(p_1+q)^2=0$, we can expand it in powers of λ in the integrand, and only keep the leading term. The leading term in this expansion corresponds to treating $P_1^\mu = p_1^\mu + q^\mu$ as being lightlike. Performing this expansion on $G^{(12),a}$ and $G^{(12),a}_{\text{soft-sens.}}$ shows that they reduce to the integrals in $G^{(12)}$ and $G^{(12)}_{\text{soft-sens.}}$, respectively, from the previous section. Since both loops are the same, so is their difference, $G^{(12),a}_{\text{not-soft-sens.}}$. That is,

$$G^{(12),a}_{\text{not-soft-sens.}}\big(P_1,p_2\big) \;\cong\; -g\,\frac{p_1\cdot\epsilon}{p_1\cdot q}\times G^{(12)}_{\text{not-soft-sens.}}\big(P_1,p_2\big) \overset{\text{1-loop}}{\cong}$$

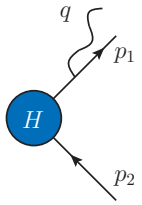

(3.75)

where $G^{(12)}_{\text{not-soft-sens.}}(p_1,p_2)$ was the IR-finite and λ-independent 1-loop contribution to the Wilson coefficient found in the previous section.

Therefore, the graph $G^{(12),a}_{\text{not-soft-sens.}}$ from the left-hand side of Eq. (3.64) is reproduced by the factorized expression in last term in brackets in Eq. (3.70).

3.4.3 The graph $G^{(12),b}$

We now analyze the second diagram that seems to break collinear factorization in Eq. (3.68), namely

$$G^{(12),b} = 2ig^3 \int \frac{d^4k}{(2\pi)^4} \frac{(2p_1 - k)\cdot\Pi(k)\cdot(2p_2 + k)\,(p_1 - k)\cdot\epsilon}{k^2(p_2 + k)^2(p_1 - k)^2(p_1 + q - k)^2} \tag{3.76}$$

The soft limit of this graph, again keeping the IR-sensitive parts, is

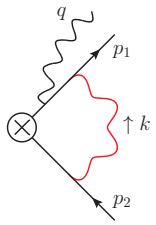

$$\equiv G^{(12),b}_{\text{soft-sens.}} = -2g\,p_1\cdot\epsilon \int \frac{d^4k}{(2\pi)^4} \frac{ig^2\; p_1\cdot\Pi(k)\cdot p_2}{k^2\,p_2\cdot k\,p_1\cdot k\left((p_1+q)^2 - 2(p_1+q)\cdot k\right)} \tag{3.77}$$

This graph is soft divergent, scaling as κ^0 even with $(p_1 + q)^2 \neq 0$, thus it must be reproduced in the factorized expression.

Next, we will show that $G^{(12),b}_{\text{not-soft-sens.}}$ is collinear sensitive, but power suppressed compared to $G^{(12),a}_{\text{not-soft-sens.}}$. First, to see that $G^{(12),b}$ is collinear finite at finite $(p_1+q)^2$, we note that for $(p_1 + q)^2$ positive and fixed, the $(p_1 + q - k)^2$ propagator cannot go on-shell when other propagators do, so the loop is not more singular than $G^{(12),a}$. As with $G^{(12),a}$, it would be collinear divergent for $k \parallel p_1$ or $k \parallel p_2$ but for the fact that the numerator vanishes by Eq. (3.26) and Eq. (3.27) which causes the integral to be collinear finite for $(p_1 + q)^2 \neq 0$.

Now, if $(p_1 + q)^2 = 0$, then the integral would be p_1-collinear divergent (though it remains p_2-collinear finite). This can be seen by taking $p_1 \propto q$ in which case k^μ scales like

$$k^\mu \sim \kappa^0\, p_1^\mu + \kappa^2\, p_2^\mu + \kappa\, k_\perp^\mu \tag{3.78}$$

and so $G^{(12),b}$ in Eq. (3.76) scales like

$$G^{(12),b} \sim \int d^4k\kappa^4 \, \frac{\kappa\,\kappa}{\kappa^2\,\kappa^0\,\kappa^2\,\kappa^2} \sim \kappa^0 \tag{3.79}$$

where we used that $d^4k \sim \kappa^4$, $(2p_1 - k)\cdot\Pi(k)\cdot(2p_2 + k) \sim \kappa$, $k\cdot\epsilon \sim \kappa$, and $(p_2 + k)^2 \sim \kappa$. We thus see that $G^{(12),b}$ is logarithmically p_1-collinear divergent. We have made all of these arguments for $G^{(12),b}$, but they apply also to $G^{(12),b}_{\text{soft-sens.}}$ and hence to $G^{(12),b}_{\text{not-soft-sens.}}$. Then, given that $G^{(12),b}_{\text{not-soft-sens.}}$ is completely IR-finite when $(p_1+q)^2 \neq 0$ but logarithmically p_1-collinear divergent when $(p_1+q)^2 = 0$, we must have that it scales like

$$G^{(12),b}_{\text{not-soft-sens.}} \sim g^3 \ln\left[(p_1+q)^2\right] \sim g^3 \ln\lambda \tag{3.80}$$

for small λ. This is power suppressed compared to say Eq. (3.75) which scales like λ^{-1}. Thus, we can drop $G^{(12),b}_{\text{not-soft-sens.}}$ at leading power.

3.4.4 The graph $G^{(12),c}$

Finally, we have the graph with the scalar-QED 4-point vertex

$G^{(12),c} \equiv$ 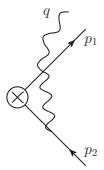

$= -2ig^3 \int \frac{d^4k}{(2\pi)^4} \frac{\epsilon\cdot\Pi(k)\cdot(2p_2+k)}{k^2(p_2+k)^2(p_1+q-k)^2}$ (3.81)

We will show that this graph is completely power suppressed.

To see if there are soft divergences, we look at the soft limit of $G^{(12),c}$. First, note that if $(p_1+q)^2 \neq 0$ then $G^{(12),c}$ would be finite in the soft limit, as can be seen by counting powers of the soft momentum in the integrand which gives d^4k/k^3. On the other hand, for $(p_1+q)^2 = 0$, the integrand of $G^{(12),c}$ becomes d^4k/k^4 signaling a

logarithmic divergence. Thus, we must have that, in the soft region of the integral,

$$G^{(12),c} \overset{\text{soft}}{\sim} g^3 \ln(p_1+q)^2 \sim g^3 \ln\lambda^2 \ll \frac{g^3}{\lambda} \tag{3.82}$$

Hence, in the soft limit, $G^{(12),c}$ is power suppressed.

We have seen that $G^{(12),c}$ is power suppressed in the soft limit. Next, we will now show that the same is true for the collinear limits of the integral, meaning that the entire graph $G^{(12),c}$ is a power correction in our factorization formula. We start by showing that $G^{(12),c}$ is p_2-collinear finite in generic-lightcone gauge. This holds for the same reason as for the other collinear-finite graphs: were it not for the numerator, $G^{(12),c}$ would be logarithmically p_2-collinear divergent. However, when k becomes collinear to p_2, $\Pi(k)$ becomes the polarization sum of photons in the p_2 direction which is transverse to p_2. Hence $\Pi(k)\cdot(2p_2+k)\to 0$ when $k \parallel p_2$. These are the words that describe Eq. (3.26) and Eq. (3.27). Hence, $G^{(12),c}$ is p_2-collinear finite.

$G^{(12),c}$ is also p_1-collinear finite, but only when $(p_1+q)^2 \neq 0$. This can be seen by power counting the denominator, as k becomes collinear to p_1. For $(p_1+q)^2=0$, the denominator of $G^{(12),c}$ causes it to be logarithmically divergent, but in this case the numerator does not vanish as $k \parallel p_1$ since $\Pi(k)$ is not transverse to ϵ. That is,

$$\epsilon^\mu \Pi_{\mu\nu}(k) \;=\; -\epsilon_\nu + \frac{k\cdot\epsilon\, r_\nu}{r\cdot k} \;\longrightarrow\; -\epsilon_\nu \qquad \text{for } k \parallel p_1 \parallel q \tag{3.83}$$

where we used that $r\cdot\epsilon = 0$. Thus, when $k \parallel p_1$ the numerator of $G^{(12),c}$ looks like $p_2\cdot\epsilon$ which does not vanish. Since $G^{(12),c}$ is collinear finite for $(p_1+q)^2\neq 0$ and has a logarithmic divergence for $k \parallel p_1$ when $(p_1+q)^2=0$, we conclude that in the $k \parallel p_1$ region of the integral

$$G^{(12),c} \overset{p_1\text{-coll}}{\sim} g^3 \ln(p_1+q)^2 \sim g^3 \ln\lambda^2 \ll \frac{g^3}{\lambda} \tag{3.84}$$

Thus, the entire integral in $G^{(12),c}$ is power suppressed compared to the leading-power matrix element, $\dfrac{p_1 \cdot \epsilon}{p_1 \cdot q} \sim \lambda^{-1}$.

3.4.5 Putting it together

We have shown that most of the contributions to Eq. (3.64) agree identically on both sides. The ones that do not are $G^{(12),a}$, $G^{(12),b}$ and $G^{(12),c}$ in Eq. (3.68) for the left hand side and Eq. (3.70) for the right-hand side. Of these, $G^{(12),c}$ is power suppressed, as is the non-soft part of $G^{(12),b}$. Thus the nontrivial leading-power diagrams are

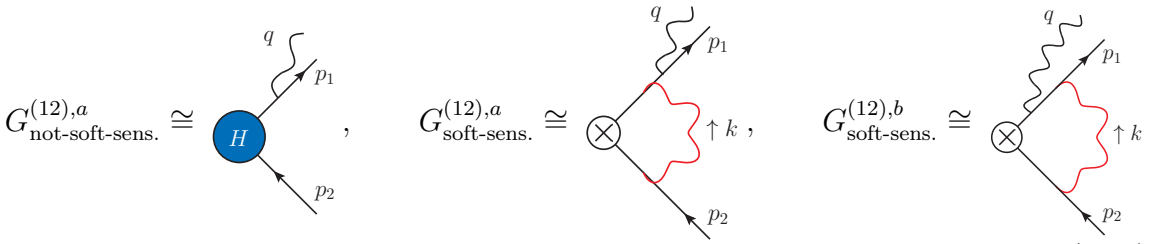

(3.85)

We also showed that $G^{(12),a}_{\text{not-soft-sens.}}$ reproduces the contribution from the Wilson coefficient in Eq. (3.70). Thus what remains is to show that the contribution connecting the two soft Wilson lines in the factorized expression agrees with $G^{(12),a}_{\text{soft-sens.}} + G^{(12),b}_{\text{soft-sens.}}$ at leading power. We do this by direct calculation.

Let us define a lightlike directions $n_i^\mu = (1, \vec{n}_i)$, such that $p_i^\mu = \frac{1}{2}\bar{n}_i \cdot p_i \, n_i^\mu$, then

$$
\begin{aligned}
G^{(12),a}_{\text{soft-sens.}} + G^{(12),b}_{\text{soft-sens.}} &= \int \frac{d^4k}{(2\pi)^4} \, \frac{2ig^3 \, p_1 \cdot \epsilon}{k^2 \, p_2 \cdot k \left((p_1+q)^2 - 2(p_1+q)\cdot k\right)} \\
&\qquad \times \left[\frac{(p_1+q)\cdot \Pi(k) \cdot p_2}{p_1 \cdot q} - \frac{p_1 \cdot \Pi(k) \cdot p_2}{p_1 \cdot k} \right] \\
&\cong \int \frac{d^4k}{(2\pi)^4} \, \frac{\frac{1}{2}ig^3 \, n_1 \cdot \Pi(k) \cdot p_2 \; p_1 \cdot \epsilon}{k^2 \, p_2 \cdot k \left(p_1 \cdot q - (p_1+q)\cdot k\right)} \left[\frac{\bar{n}_1 \cdot (p_1+q)}{p_1 \cdot q} \frac{\frac{1}{2}\bar{n}_1 \cdot p_1 \, n_1 \cdot k}{p_1 \cdot k} - \frac{\bar{n}_1 \cdot p_1}{p_1 \cdot k} \frac{p_1 \cdot q}{p_1 \cdot q} \right] \\
&\cong \int \frac{d^4k}{(2\pi)^4} \, \frac{ig^3 \, p_1 \cdot \Pi(k) \cdot p_2 \; p_1 \cdot \epsilon}{k^2 \, p_2 \cdot k \left(p_1 \cdot q - (p_1+q)\cdot k\right)} \left[\frac{(p_1+q)\cdot k}{p_1 \cdot q \, p_1 \cdot k} - \frac{p_1 \cdot q}{p_1 \cdot q \, p_1 \cdot k} \right] \\
&= -g \frac{p_1 \cdot \epsilon}{p_1 \cdot q} \times ig^2 \int \frac{d^4k}{(2\pi)^4} \, \frac{n_1 \cdot \Pi(k) \cdot n_2}{k^2 \, n_1 \cdot k \, n_2 \cdot k}
\end{aligned}
\tag{3.86}
$$

The first term is the tree-level term in $\langle p_1, q| \, \phi^\star \, |0\rangle$ and the second term is the loop integral, $\langle 0| \, \overbrace{Y_1^\dagger Y_2} \, |0\rangle$, where the photon propagates between the Wilson lines. This is exactly equal to the rest of the factorized expression by Eq. (3.70).

This completes the check that the sum of the 1-loop diagrams on both sides of Eq. (3.64) agree at leading power and that the Wilson coefficients are the same and IR insensitive.

3.5 Outline of all-orders proof

In the previous two sections, we checked special cases of the factorization formula at 1-loop order by matching diagrams. This approach is not sustainable for an all-orders proof. Moreover, even when two diagrams are identical on both sides, dropping them from consideration somewhat obscures the physics of factorization. For example, the loops in Eq. (3.66) have both soft and non-soft parts, but it was easier not to separate them when matching them loop-for-loop with those in $\langle p_1, q| \, \phi^\star \, |0\rangle \, \langle p_2| \, \phi \, |0\rangle$. If we had separated the soft and non-soft parts, we would have found that the sum of the

non-soft parts of the graphs in Eq. (3.66) is exactly $\langle p_1, q| \phi^\star |0\rangle \,/\, \langle 0| Y_1^\dagger |0\rangle$ and the soft parts are exactly $\langle p_1, q| \phi^\star |0\rangle_{\text{tree}} \langle 0| \overline{Y_1^\dagger Y_2} |0\rangle$, where the contraction indicates the the photon connects only to $Y_1^\dagger$. Both these approaches are equivalent, but in the latter we see that all of the soft physics is contained in $\langle 0| Y_1^\dagger Y_2 |0\rangle$; $\langle p_1, q| \phi^\star |0\rangle \,/\, \langle 0| Y_1^\dagger |0\rangle$ is soft-inensitive.

Proving soft-collinear factorization in general, will involve 4 steps

1. Write each diagram contributing to the matrix element in the full theory as a sum of colored diagrams where each virtual gluon can either contribute to a soft singularity, in which case we call it soft sensitive (and draw it with a long-wavelength red line), or it cannot, in which case we call it soft insensitive (and draw it with a blue line).

2. Drop diagrams which cannot contribute at leading power and identify finite diagrams. Doing this in physical gauges lets us write the full-theory matrix element as the sum of colored diagrams with a restricted topology in the following way

$$\langle X_1 \cdots X_N; X_s| \mathcal{O} |0\rangle \overset{\text{physical gauges}}{\cong} \sum_{\text{diagrams}}$$

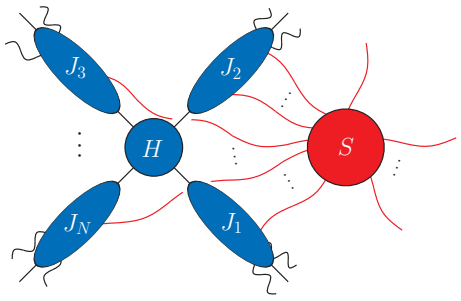

(3.87)

We call the toplogy indicated on the right-hand side the **reduced diagram**. It has the following properties:

- Each colored diagram in the sum corresponds to a precise Feynman inte-

gral, with loop momenta integrated over all of $\mathbb{R}^{1,3}$. Note that our reduced diagrams are different from those used in [41, 42, 66], which are pictures representing the pinch surface, not computable functions.

- The "jet" amplitudes, labeled J_j are soft insensitive and collinear sensitive only in their own, p_j directions. That is, there are no p_j-collinear sensitivities in the J_i jet amplitudes for $i \neq j$.
- All soft sensitivity comes from virtual gluons in (or connecting to) the "soft" amplitude.
- The blue ball in the center is called the "hard" amplitude. It is infrared insensitive (IR finite for any λ, and hence, independent of λ at leading power). It only depends on the net collinear momenta coming in from each direction and no soft particles or red lines connect to it. This property will establish that the Wilson coefficient in the factorization theorem is independent of the external state, as is expected in an operator product expansion.

3. Examine factorization gauge, which gives the flexibility needed for an efficient proof of soft-collinear decoupling. Although ghosts do not decouple completely, we show that they do not contribute new IR sensitivities and do not affect the reduced diagram in Eq. (3.87).

4. Using factorization gauge, show that the soft gluons can be disentangled from the non-soft gluons. This step follows quite naturally from the proof of tree-level disentangling in [3]. In the process, show that the factorized reduced diagrams

are exactly reproduced by gauge-invariant matrix elements in the factorization formula.

As with the 1-loop examples above, we will prove these steps in a more-or-less gauge-theory independent way, using QCD and scalar QED for examples. In this approach, technical details specific to QCD, such as color structures, become mostly notational. These are discussed in Section 3.11.

3.6 Step 1: Coloring (separating soft sensitivities)

The first step is to separate the soft-sensitive physics from that which is soft-insensitive. As in the examples, we define soft-sensitive to mean either that a loop has a power-counting soft-divergence or that it would have one for kinematic configurations corresponding to $\lambda = 0$.

Soft sensitivity is a property that each virtual particle may have. We want to write each Feynman diagram as the sum of what we call **colored diagrams** where the color of each virtual line in a colored diagram indicates if it is soft sensitive or not. We have already seen examples of this separation at 1-loop: in Section 3.3 the soft-sensitive version of the graph $G^{(12)}$ in Eq. (3.46) was explicitly given as $G^{(12)}_{\text{soft-sens.}}$ in Eq. (3.47), and it was shown that the not-soft-singular part, $G^{(12)}_{\text{not-soft-sens.}} = G^{(12)} - G^{(12)}_{\text{soft-sens.}}$, was soft finite. The same was done with $G^{(12)a,b}$ in Section 3.4.

Beyond 1-loop, it is not possible to split each diagram into one soft-sensitive and one soft-insensitive piece, since all of the loops are tangled up in a generic graph. More generally, we would like to expand in each virtual momenta. The only complication is that all the virtual momenta are not independent and so the expansion has to be

done iteratively. These iterations can be done algorithmically, starting from the most soft-sensitive graphs, as we now explain. Section 3.6.1 gives the algorithm, which is perhaps easiest to understand through the examples in Sections 3.6.2, 3.6.3 and 3.6.4.

3.6.1 Decomposition into colored diagrams

Consider sets $\Omega = \{\ell_1^\mu, \ell_2^\mu, \ldots\}$ of virtual momenta in a particular Feynman diagram G which can all go to $\ell_i^\mu = 0$ simultaneously. For a given set Ω, we can expand the integrand to leading order around $\ell_i^\mu = 0$ for all the $\ell_i^\mu \in \Omega$ simultaneously. We want to do this very carefully, dropping only terms which *must* be small when $\ell_i^\mu = 0$. For example, if p^μ is an external collinear momentum, then we can drop l_i^2 compared to $l_i \cdot p$. We do not want to drop l_i^μ compared to any external soft momentum, or to any other virtual momentum ℓ_k^μ which go soft simultaneously with ℓ_i^μ. We also drop $l_i \cdot p_j$ compared to $(p_1 + p_2)^2$ for two collinear momenta p_1^μ and p_2^μ if and only if p_1^μ and p_2^μ are in different collinear sectors. If they are in the same sector then we allow that $(p_1 + p_2)^2 \sim \lambda^2$ can be arbitrarily small.

Let us call the leading term in the expansion according to this procedure the **soft limit** of the set Ω in G and denote it by $G_{\mathcal{S}(\Omega)}$. The soft limit defined in this way allows us to see if a set Ω is soft-sensitive simply by looking at the scaling of $G_{\mathcal{S}(\Omega)}$ (or equivalently of G) under $\ell_i^\mu \to \kappa^2 \ell_i^\mu$ for all $\ell_i^\mu \in \Omega$. By not dropping soft momenta compared to terms which could possibly vanish for certain external momenta, we are effectively taking the leading power of κ at $\lambda = 0$. Taking the soft limit in this way implies that

$$\lim_{\Omega \to \text{soft}} G \;=\; \lim_{\Omega \to \text{soft}} G_{\mathcal{S}(\Omega)} \tag{3.88}$$

so that $G - G_{\mathcal{S}(\Omega)}$ is automatically less-singular than G in the limit that all the $\ell_i^\mu \in \Omega$ go soft. The limit in Eq. (3.88) means restricting the integration regions to balls around the point where each momenta in Ω vanish and taking the limit where those balls have vanishing size. The point of taking the soft limit $\mathcal{S}(\Omega)$ is that, since infrared divergences in gauge theories are at most logarithmic (at least in physical gauges, as we will show in the *Log Lemma* (Lemma 2)), the difference $G - G_{\mathcal{S}(\Omega)}$ cannot be soft sensitive in this $\Omega \to$ soft limit.

That all the momenta in a set Ω can go soft together does not imply that G is soft sensitive in this limit. Let $\{\Omega_i\}$ enumerate all the possible sets Ω which *do* have a soft sensitivity in their simultaneous soft limit. Note that which sets are in $\{\Omega_i\}$ is gauge-dependent, and we will be concerned primarily with Ω_i in generic-lightcone gauge. Consider first the largest sets $\{\Omega^i_{\text{max}}\}$, defined as those sets, Ω_i, which are not proper subsets of any other Ω_i's. Now take the soft limit and define

$$G_{\Omega^i_{\text{max}}} \equiv G_{\mathcal{S}(\Omega^i_{\text{max}})} \tag{3.89}$$

Here, $G_{\Omega^i_{\text{max}}}$ refers to a particular integral, for each i, derived form an expansion of the integrand of the original Feynman diagram integral, G. We represent it as a diagram with the same topology as G in which we color all the lines in Ω^i_{max} red and color blue all the lines not in Ω^i_{max}. The blue lines cannot give rise to a soft singularity because we have already taken the maximal soft limit in $G_{\Omega^i_{\text{max}}}$ by construction (this will be shown in Lemma 1 below).

Next, take the sets, $\{\Omega^j_{\text{next}}\}$, defined as being the next largest proper subsets of any of the Ω^i_{max}'s whose simultaneous soft limit engenders a soft sensitivity. Each Ω^j_{next} may be a subset of multiple Ω^i_{max}. Then subtract off from the soft limit of Ω^j_{next}

all of the $G_{\Omega^i_{\rm max}}$ for which it is a subset:

$$G_{\Omega^j_{\rm next}} \equiv \left(G - \sum_{\{i\,;\,\Omega^i_{\rm max} \supsetneq \Omega^j_{\rm next}\}} G_{\Omega^i_{\rm max}} \right)_{\mathcal{S}(\Omega^j_{\rm next})} \tag{3.90}$$

As before, we represent $G_{\Omega^j_{\rm next}}$ as a diagram with the lines in $\Omega^j_{\rm next}$ colored red, and all other lines colored blue to show that they cannot give rise to a soft sensitivity due to the subtraction.

This procedure can be iterated, with subsets of $\Omega^j_{\rm next}$ and so on. In each step, we take subsets, $\Omega^j_{\rm step}$, of the $\Omega^i_{\rm max}$'s of a given size and subtract off G_Ω for every subset, Ω, of the $\Omega^i_{\rm max}$'s for which $\Omega^j_{\rm step}$ is a subset:

$$G_{\Omega^j_{\rm step}} \equiv \left(G - \sum_{\Omega \supsetneq \Omega^j_{\rm step}} G_\Omega \right)_{\mathcal{S}(\Omega^j_{\rm step})} \tag{3.91}$$

Eventually, all of the possible sets of soft-singular lines are exhausted. In particular, in the last step, $\Omega_{\rm last}$ is the empty set. This is a subset of all the other sets, so we have

$$G = G_{\rm last} + \sum_\Omega G_\Omega \tag{3.92}$$

At every stage G_Ω is drawn as the graph G but with the lines in Ω colored red and those not in Ω colored blue. Thus the full graph becomes the sum of colored graphs.

After this procedure, each colored graph represents a particular integral which can have a soft singularity or soft-sensitivity *only* when any of the red lines become soft, but never when any of the blue lines become soft. In other words:

Lemma 1. (**Soft-insensitivity Lemma**) *Soft sensitivities cannot come from the soft region of any set of blue lines.*

Proof. We prove this by induction on the number of blue lines in a colored graph, G_Ω. The first step is to show the result for graphs with the fewest number of blue lines, namely $G_{\Omega_{\max}}$. Indeed, the only way for a line, $\ell_{\text{blue}} \notin \Omega_{\max}$, to be able to give a soft sensitivity in G but not in the simultaneous limit $\Omega_{\max} \cup \ell_{\text{blue}} \to$ soft is if the limit is forbidden by momentum conservation. But then $\lim_{\ell_{\text{blue}} \to \text{soft}} G_{\Omega_{\max}}$ will vanish since the limit where $\Omega_{\max} \to$ soft has already been taken. So the lemma holds for graphs with the least number of blue lines, $G_{\Omega_{\max}}$.

Now, suppose it is true for any colored graph with n or fewer blue lines and consider a colored graph with $n+1$ blue lines, G_Ω. Now consider the most general limit where some subset, ω, of blue lines goes soft. We must show that $\lim_{\omega \to \text{soft}} G_\Omega$ is finite.

By definition

$$G_\Omega = \left(G - \sum_{\Upsilon \supsetneq \Omega} G_\Upsilon \right)_{\mathcal{S}(\Omega)} = G_{\mathcal{S}(\Omega)} - \sum_{\Upsilon \supsetneq \Omega,\, \omega \subseteq \Upsilon} \left(G_\Upsilon \right)_{\mathcal{S}(\Omega)} - \sum_{\Upsilon \supsetneq \Omega,\, \omega \not\subseteq \Upsilon} \left(G_\Upsilon \right)_{\mathcal{S}(\Omega)} \tag{3.93}$$

where the sets Υ are soft-sensitive sets. In the $\omega \to$ soft limit, the last term would involve the soft limit of at least one blue line in a colored graph with n or fewer blue lines which must be finite by the induction hypothesis combined with the fact that

$$\lim_{\omega \to \text{soft}} \left(G_\Upsilon \right)_{\mathcal{S}(\Omega)} = \left(\left(G_\Upsilon \right)_{\mathcal{S}(\Omega)} \right)_{\mathcal{S}(\omega)} = \left(\left(G_\Upsilon \right)_{\mathcal{S}(\Omega \cup \omega)} \right)_{\mathcal{S}(\omega)} \tag{3.94}$$

Therefore, the soft limit we are interested in simplifies to

$$\lim_{\omega \to \text{soft}} G_\Omega = \lim_{\omega \to \text{soft}} \left[G_{\mathcal{S}(\Omega)} - \sum_{\Upsilon \supseteq \Omega \cup \omega} \left(G_\Upsilon \right)_{\mathcal{S}(\Omega)} \right] + \text{finite} \tag{3.95}$$

Now, if $\Omega \cup \omega \not\subseteq \Omega^i_{\max}$ for some i, the term in square brackets in Eq. (3.95) is finite because, in that case, the sum is empty and the soft limit of Ω followed by ω does not

give rise to a soft sensitivity in the first term by momentum conservation (the same argument given in the first-induction step). If Eq. (3.95) is finite, we are done the proof, so assume $\Omega \cup \omega \subseteq \Omega^i_{\max}$ for some i. Consequently, there exists a soft-sensitive set Γ that is the next smallest set containing $\Omega \cup \omega$ for which $\mathcal{S}(\Omega \cup \omega) = \mathcal{S}(\Gamma)$. Therefore, using Eq. (3.94), we have

$$\lim_{\omega \to \text{soft}} G_\Omega = \lim_{\omega \to \text{soft}} \left(G - G_\Gamma - \sum_{\Upsilon \supseteq \Omega \cup \omega,\, \Upsilon \neq \Gamma} G_\Upsilon \right)_{\mathcal{S}(\Gamma)} + \text{finite} \tag{3.96}$$

$$\stackrel{\text{def}}{=} \lim_{\omega \to \text{soft}} \left[G_{\mathcal{S}(\Gamma)} - G_{\mathcal{S}(\Gamma)} + \sum_{\Upsilon \supsetneq \Gamma} \left(G_\Upsilon\right)_{\mathcal{S}(\Gamma)} - \sum_{\Upsilon \supseteq \Omega \cup \omega,\, \Upsilon \neq \Gamma} \left(G_\Upsilon\right)_{\mathcal{S}(\Gamma)} \right] + \text{finite} \tag{3.97}$$

Now we can split the last sum into

$$\sum_{\Upsilon \supseteq \Omega \cup \omega,\, \Upsilon \neq \Gamma} G_\Upsilon = \sum_{\Upsilon \supsetneq \Gamma} G_\Upsilon + \sum_{\Upsilon \supseteq \Omega \cup \omega,\, \Upsilon \not\supseteq \Gamma} G_\Upsilon \tag{3.98}$$

Then, canceling the first four terms we are left with

$$\lim_{\omega \to \text{soft}} G_\Omega = - \lim_{\omega \to \text{soft}} \sum_{\Upsilon \supseteq \Omega \cup \omega,\, \Upsilon \not\supseteq \Gamma} \left(G_\Upsilon\right)_{\mathcal{S}(\Gamma)} + \text{finite} \tag{3.99}$$

Finally, either $\Gamma = \Omega \cup \omega$ in which case the above sum is empty and $\lim_{\omega \to \text{soft}} G_\Omega$ is finite, or the $\omega \to$ soft limit forces other lines in $\Gamma \setminus (\Omega \cup \omega)$ to go soft along with those in ω. The latter case means that for every term in the above sum, $\lim_{\omega \to \text{soft}} G_\Upsilon$ involves taking a blue line soft which gives a finite result by the induction hypothesis. Thus, $\lim_{\omega \to \text{soft}} G_\Omega$ is always finite. □

This algorithm may make more sense after a few explicit examples. We have already seen how to separate the soft-sensitive and soft-insensitive parts of graphs at 1-loop order in Sections 3.3 and 3.4, so we move directly to the more complicated 2-loop examples. The first two examples in Sections 3.6.2 and 3.6.3 outline the basics of

the coloring algorithm, having only a single maximal soft-sensitive set. The example in Section 3.6.4 has multiple $\Omega^i_{\max}$'s as well as a discussion about symmetry factors of the colored graphs.

It is also worth pointing out that this separation into red and blue lines is similar to the zero-bin subtraction discussed in [59]. Our blue lines correspond to the propagation of degrees of freedom that can be collinear sensitive but cannot be soft sensitive. This is implemented by recursively subtracting off the soft-sensitive limits from the full-theory graphs. In SCET, collinear fields are defined by summing over discrete labels on momentum space with the label pointing to zero momentum – known as the zero bin – removed. In practice the discrete sum is always turned into an integral and the zero bin is subtracted off. This procedure calls for a soft subtraction for every single collinear line, irrespective of whether or not the line is soft sensitive, but otherwise is similar to our subtraction for the blue lines. Therefore, the SCET-familiar reader could think of our blue lines as a cleaner version of the collinear lines of SCET. In any case, our blue lines are still too complicated to use in practice; by the end, our factorization theorem will be formulated entirely in terms of full-theory Feynman rules with the subtraction procedure implemented by dividing by simple matrix elements of Wilson lines.

In a colored diagram, every line is either soft sensitive (red) or soft insensitive (blue). We sometimes draw soft-insensitive lines as black lines if no expansion is done (for example with external lines). All black lines in the following should technically be drawn blue.

3.6.2 Example one: Tangled 2-loop

Consider the following graph in scalar QED:

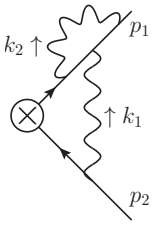

$$\equiv G = \int \frac{(2p_2 + k_1) \cdot \Pi(k_1) \cdot (2p_1 - 2k_2 - k_1)\,(2p_1 - 2k_1 - k_2) \cdot \Pi(k_2) \cdot (2p_1 - k_2)}{k_1^2 (p_2 + k_1)^2 (p_1 - k_1)^2\; k_2^2 (p_1 - k_2)^2 (p_1 - k_1 - k_2)^2} \tag{3.100}$$

where we have dropped constant prefactors and the integration measure, $d^4k_1 d^4k_2$ is left implicit. In Feynman gauge (or other covariant gauges), the gauge-dependent $\Pi(k_i)$ factors count as order 1. Then, this graph has a soft singularity when both photons go soft, or when either one goes soft and the other goes collinear. Note that the virtual scalars can never give rise to a soft sensitivity by helicity conservation, which can easily be checked by power counting, say, the $(p_1 - k_2) \to$ soft limit.

Our first step is to write down the soft-singular graph with the most soft lines. This is done by expanding the integrand as if both virtual-photon momenta k_1 and k_2 were soft, giving:

$$G_{\Omega_{\max}} =$$

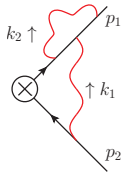

$$= \int \frac{p_2 \cdot \Pi(k_1) \cdot p_1}{k_1^2 p_2 \cdot k_1 (-p_1 \cdot k_1)} \times \frac{p_1 \cdot \Pi(k_2) \cdot p_1}{k_2^2 (-p_1 \cdot k_2)(-p_1 \cdot (k_1 + k_2))} \tag{3.101}$$

Note that we have not dropped either soft momentum with respect to the other. Also, $G_{\Omega_{\max}}$ is clearly soft divergent when both k_1 and k_2 vanish.

Now we would like to write down the part of G that is soft divergent when only one of the photons goes soft (and the other goes collinear). To do this, we expand one of the virtual momentum as if it were soft and leave the other one general. That

is, for k_1 soft we have

$$G_{\Omega^1_{\text{next}}} = \int \frac{p_2 \cdot \Pi(k_1) \cdot (p_1 - k_2)}{k_1^2 p_2 \cdot k_1 (-p_1 \cdot k_1)} \times \frac{(2p_1 - k_2) \cdot \Pi(k_2) \cdot (2p_1 - k_2)}{k_2^2 (p_1 - k_2)^2 (p_1 - k_2)^2} - \left(G_{\Omega_{\text{max}}}\right)_{\mathcal{S}(k_1)} \tag{3.102}$$

With this definition, $G_{\Omega^1_{\text{next}}}$ is clearly finite when k_2 goes soft because we have subtracted that limit off in the form of $\left(G_{\Omega_{\text{max}}}\right)_{\mathcal{S}(k_1)}$. Similarly, we define the k_2-soft-singular graph as

$$G_{\Omega^2_{\text{next}}} = \int \frac{(2p_2 + k_1) \cdot \Pi(k_1) \cdot (2p_1 - k_1)}{k_1^2 (p_2 + k_1)^2 (p_1 - k_1)^2} \times \frac{(p_1 - k_1) \cdot \Pi(k_2) \cdot 2p_1}{k_2^2 (-p_1 \cdot k_2)(p_1 - k_1)^2} - \left(G_{\Omega_{\text{max}}}\right)_{\mathcal{S}(k_2)} \tag{3.103}$$

which is, again, finite in the limit where k_1 goes soft because of the subtraction.

Finally, we have the remainder of the graph, given by

$$G_{\text{last}} = G - G_{\Omega_{\text{max}}} - G_{\Omega^1_{\text{next}}} - G_{\Omega^2_{\text{next}}} \tag{3.104}$$

It is easy to see that G_{last} is finite in any limit $\omega \to$ soft for $\omega \subseteq \{k_1, k_2\}$, for example

$$\lim_{k_1 \to \text{ soft}} G_{\text{last}} = \left(G - G_{\Omega_{\text{max}}}\right)_{\mathcal{S}(k_1)} - \left(G_{\Omega^1_{\text{next}}}\right)_{\mathcal{S}(k_1)} + \text{finite} = G_{\Omega^1_{\text{next}}} - G_{\Omega^1_{\text{next}}} + \text{finite} = \text{finite} \tag{3.105}$$

where we used the definition of $G_{\Omega^1_{\text{next}}}$, that $(G_{\Omega^1_{\text{next}}})_{\mathcal{S}(k_1)} = G_{\Omega^1_{\text{next}}}$ and that $(G_{\Omega^2_{\text{next}}})_{\mathcal{S}(k_1)}$ is finite.

We can now draw these four integrals as separate graphs by denoting which internal lines are taken soft by a longer-wavelength red line and the other lines that are made soft-insensitive by the subtraction are drawn blue. That is,

$G_{\Omega_{\text{max}}} =$ 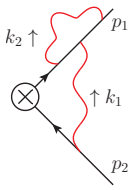

$G_{\Omega^1_{\text{next}}} =$ 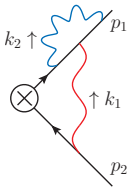

$G_{\Omega^2_{\text{next}}} =$ 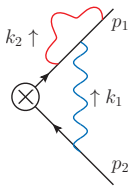

$G_{\text{last}} =$ 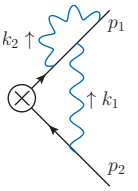

$\left(\begin{matrix}\text{covariant} \\ \text{gauges}\end{matrix}\right)$ (3.106)

and the sum of these four graphs is trivially equal to the original graph, G.

We reiterate that in these modified graphs, only the red, long-wavelength lines can have soft singularities. Each blue line is made soft insensitive by subtracting from the original graph all of the graphs with that line red. In our example, $G_{\Omega_{\max}}$ was subtracted off in Eq. (3.102) and Eq. (3.103) to ensure that the blue line in both G_{Ω_1} and G_{Ω_2} is soft insensitive and all three of $G_{\Omega_{\max}}$, G_{Ω_1} and G_{Ω_2} were subtracted off in Eq. (3.104) in order to make both of the blue lines in G_{last} soft insensitive.

In deriving the decomposition in Eq. (3.106), no scaling of the numerators was used. Thus this decomposition holds in covariant gauges, such as Feynman gauge, where there is no extra numerator suppression. In physical gauges, such as generic-lightcone gauge, the set of colored graphs is different. As will be discussed in detail in Section 3.7 in a physical gauge, there is no singularity when k_2 goes soft and k_1 does not, so Ω_2 is not a possible set with a soft sensitivity. Thus, in a physical gauge, $G_{\Omega_{\max}}$ and G_{Ω_1} are defined as above and $G_{\text{last}} = G - G_{\Omega_{\max}} - G_{\Omega_1}$. So, the colored-graph decomposition of G in a physical gauge is given by the sum of only three graphs:

$G_{\Omega_{\max}} =$ 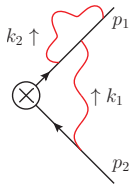

$G_{\Omega^1_{\text{next}}} =$ 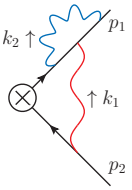

$G_{\text{last}} =$ 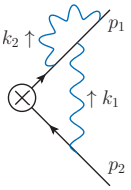

$\begin{pmatrix}\text{physical}\\ \text{gauges}\end{pmatrix}$ (3.107)

3.6.3 Example two: 2 loops, 3 gluons

Consider now a slightly more complicated example, the QCD graph:

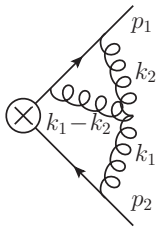

$$\equiv H \tag{3.108}$$

For this graph, when all three gluons go soft, there are 9 powers of soft momenta in the denominator from the propagators, 1 in the numerator from the 3-point vertex, and 8 from the $d^4k_1 d^4k_2$ integration measure. The result is an overall logarithmic divergence (in covariant or physical gauges). This is the soft singularity with the highest number propagators that are simultaneously going soft.

Thus the soft-singular graph with the largest number of soft propagators in it is

$$H_{\Omega_{\max}} = H_{\mathcal{S}(\{k_1,k_2\})} = \tag{3.109}$$

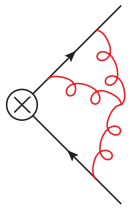

The algebraic expression for $H_{\Omega_{\max}}$ is found by taking the integrand of H and expanding as if k_1 and k_2 were soft but of the same order, as was done in Eq. (3.101).

There are no singularities with only two gluons going soft since momentum conservation will not allow two of the gluons to go soft without the third being soft as well. Thus, the soft-singular configurations with the next largest number of soft internal lines are those with one of the gluons going soft. In covariant gauges there

is a singularity when any of the gluons go soft

$H_{\Omega^1_{\text{next}}} =$ 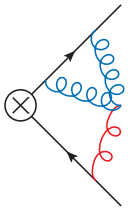 $H_{\Omega^2_{\text{next}}} =$ 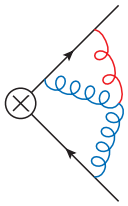 $H_{\Omega^3_{\text{next}}} =$ 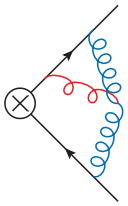 $\begin{pmatrix}\text{covariant}\\ \text{gauges}\end{pmatrix}$ (3.110)

and their algebraic expressions are given by taking the soft limit of one of the gluons and subtracting off $(H_{\Omega_{\text{max}}})_{\mathcal{S}(k_i)}$ to ensure that the other gluons cannot be soft singular. That is

$$H_{\Omega^i_{\text{next}}} = \big(H - H_{\Omega_{\text{max}}}\big)_{\mathcal{S}(k_i)}, \quad i = 1,2 \qquad \text{and} \qquad H_{\Omega^3_{\text{next}}} = \big(H - H_{\Omega_{\text{max}}}\big)_{\mathcal{S}(k_1-k_2)} \tag{3.111}$$

Finally, the soft-insensitive graph is given by

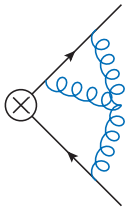 $= H_{\text{last}} = H - H_{\Omega_{\text{max}}} - H_{\Omega^1_{\text{next}}} - H_{\Omega^2_{\text{next}}} - H_{\Omega^3_{\text{next}}}$ $\begin{pmatrix}\text{covariant}\\ \text{gauges}\end{pmatrix}$ (3.112)

Thus we have the decomposition

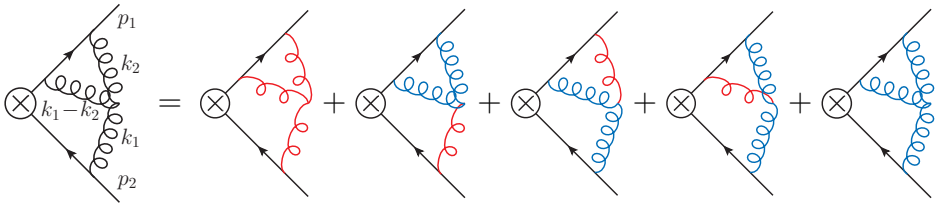

$\begin{pmatrix}\text{covariant}\\ \text{gauges}\end{pmatrix}$ (3.113)

Every graph has its soft sensitivities manifest, since none of the blue lines admit a soft sensitivity by construction.

We will see in Section 3.7 that in physical gauges Ω^2_{next} and Ω^3_{next} are soft insensitive. Thus, $H_{\Omega_{\text{max}}}$ and $H_{\Omega^1_{\text{next}}}$ are defined as above, but $H_{\Omega^2_{\text{next}}}$ and $H_{\Omega^3_{\text{next}}}$ do not

exist, thereby modifying the definition of H_{last} to $H_{\text{last}} = H - H_{\Omega_{\max}} - H_{\Omega^1_{\text{next}}}$. The colored diagram expansion in physical gauges is then:

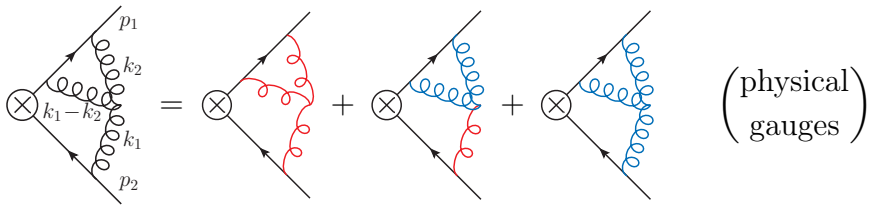

(3.114)

3.6.4 Example three: soft-gluon decoherence

For our final example, we consider a graph that does not have a unique maximal set of soft lines that contribute to a soft sensitivity:

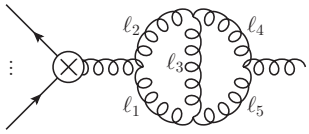

$\equiv I$ (3.115)

Due to momentum conservation, there is no way for all the gluons to go soft in the loops; at least a single continuous line of non-soft momentum must flow through the graph. This means that there are multiple maximally soft-sensitive sets of different sizes.

First we define the soft graphs with the maximal sets of soft-sensitive lines:

$I_{\Omega^1_{\max}} =$ 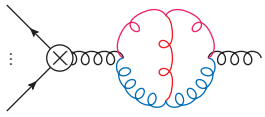 $= I_{\mathcal{S}(\{\ell_2,\ell_3,\ell_4\})}$ (3.116)

$I_{\Omega^2_{\max}} =$ 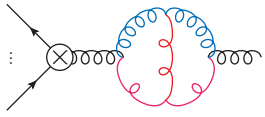 $= I_{\mathcal{S}(\{\ell_1,\ell_3,\ell_5\})}$ (3.117)

$I_{\Omega^3_{\max}} =$ 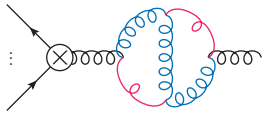 $= I_{\mathcal{S}(\{\ell_1,\ell_4\})}$ (3.118)

$I_{\Omega^4_{\max}} =$ 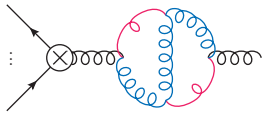 $= I_{\mathcal{S}(\{\ell_2,\ell_5\})}$ (3.119)

The algebraic expressions for these graphs are found by taking the soft limit of the relevant virtual momenta in I. Note that although no subtraction is performed, none of the blue lines can give rise to soft sensitivities due to momentum conservation. Although $I_{\Omega^1_{\max}} = I_{\Omega^2_{\max}}$ and $I_{\Omega^3_{\max}} = I_{\Omega^4_{\max}}$, these graphs are generated by expanding in different non-overlapping regions of the virtual momentum phase space in the original integral, I. Thus they correspond to separate colored graphs. This separation foreshadows the separation of QCD gluons into soft (red) and collinear (blue) gluons in the factorized expression.

Now, take the next largest subsets that admit a soft sensitivity, Ω^j_{next}, and define the corresponding colored graph via the subtraction procedure. In every case, the sets $\Omega^j_{\text{next}} = \{\ell_j\}$ have a single soft line:

$$I_{\Omega^j_{\text{next}}} = \left(I - \sum_{i\,;\,\ell_j \in \Omega^i_{\max}} I_{\Omega^i_{\max}} \right)_{\mathcal{S}(\ell_j)} \tag{3.120}$$

and define the last graph as

$$I_{\text{last}} = I - \sum_{j=1}^{5} I_{\Omega^j_{\text{next}}} - \sum_{i=1}^{4} I_{\Omega^i_{\max}} \tag{3.121}$$

We draw these graphs by coloring every line that has a soft limit taken red and the other lines blue:

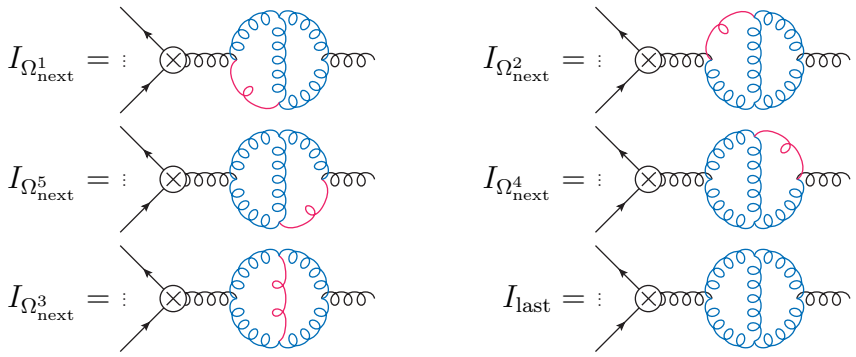

(3.122)

(3.123)

(3.124)

The blue lines either have a soft subtraction or are soft finite by momentum conservation.

It is easy to check that no blue lines can give rise to a soft sensitivity. To be explicit, we check that this is the case for I_{last} in the limit where ℓ_1 goes soft. First note that only $I_{\Omega^1_{\text{next}}}$, $I_{\Omega^2_{\text{max}}}$ and $I_{\Omega^3_{\text{max}}}$ can have a soft singularity in the $\ell_1 \to 0$ limit because only these graphs have a red ℓ_1-line. Thus,

$$\begin{aligned}\lim_{\ell_1\to 0} I_{\text{last}} &= \lim_{\ell_1\to 0}\left[I - I_{\Omega^1_{\text{next}}} - I_{\Omega^2_{\text{max}}} - I_{\Omega^3_{\text{max}}}\right] + \text{finite} \\ &= I_{\mathcal{S}(\ell_1)} - \left(I - I_{\Omega^2_{\text{max}}} - I_{\Omega^3_{\text{max}}}\right)_{\mathcal{S}(\ell_1)} - \left(I_{\Omega^2_{\text{max}}}\right)_{\mathcal{S}(\ell_1)} - \left(I_{\Omega^3_{\text{max}}}\right)_{\mathcal{S}(\ell_1)} + \text{finite} \\ &= \text{finite}\end{aligned}$$

Finally, note that all of the colored graphs in the decomposition of I are equal to another colored graph except for $I_{\Omega^3_{\text{next}}}$ and I_{last}. That is,

$$I = \sum_{i=1}^{4} I_{\Omega^i_{\text{max}}} + \sum_{j=1}^{5} I_{\Omega^j_{\text{next}}} + I_{\text{last}}$$

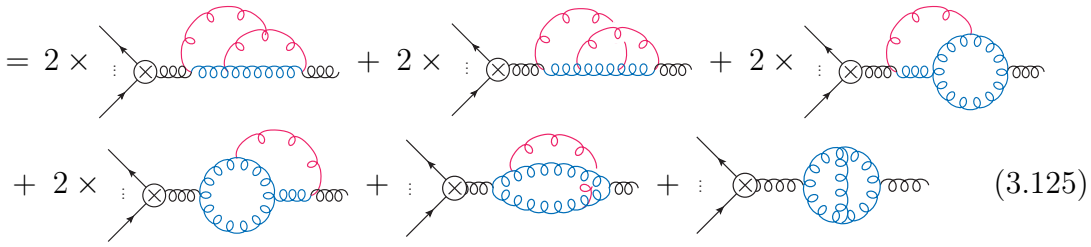

(3.125)

In the graphs that are doubled, the coloring breaks the $\mathbb{Z}_2$ symmetry of the original graph, I. Because of this symmetry I gets a symmetry factor of $1/2$. In the graphs where the coloring breaks the symmetry, the factors of 2 directly cancel this factor of $1/2$. In the graphs where the coloring preserves the symmetry, no factor of 2 results and the original symmetry factor of I is preserved. Thus, the final integrals have exactly the symmetry factor corresponding to the symmetries of the colored graphs.

It is easy to see that this happens quite generally, as expected in an effective theory where the red and blue lines are distinguishable particles.

3.7 Step 2: Reduced diagrams

At this point, we have a procedure for writing any Feynman graph as a sum of graphs each of which has all its lines marked as either soft-sensitive (red) or soft-insensitive (blue). As discussed in some of the examples, the coloring is gauge-dependent. The coloring also does not indicate if a graph is collinear-sensitive. In this section we prove a set of lemmas that determine which graphs can be soft or collinear sensitive. The lemmas in Section 3.7.1 are very general. They apply to QCD Feynman diagrams, independent of the coloring. Conclusions about collinear sensitivity, for example, apply equally well to soft-sensitive and soft-insensitive lines. The lemmas in Sections 3.7.2 and 3.7.3 are more specific to the colored diagrams. Taken together, the lemmas imply a simplified reduced-diagram structure which encapsulates hard factorization and facilitates soft-collinear factorization.

Our reduced diagrams are very similar to the reduced diagrams describing the pinch surfaces [41,42,66]. Indeed, our reduced diagrams include the singular momenta defining this surface ($k^\mu = 0$ or $k^\mu = \alpha p^\mu$ for some external p^μ), but also have a precise expression as integrals (with singular and nonsingular parts) derived from the full Feynman diagrams as described in the previous section.

Recall that we define **physical gauges** as either lightcone gauge, with a generic choice of reference vector, or factorization gauge (see Section 3.8) with generic r_c. Our physical gauges also have generic reference vectors for the polarizations of external

collinear particles. In the literature, *physical gauges* often refers more generally to any gauge whose propagator-numerator corresponds to a sum over physical polarizations, including axial gauges. We will not need to consider such a generality.

To be clear, although we do not say so explicitly in the formulation of each lemma, all the lemmas in this section are only proven to hold in physical gauges. Most of them in fact do not hold in Feynman gauge, which plays no role in our proof.

3.7.1 Finding the IR sensitivities

We now discuss how to locate the IR sensitivities in graphs. IR sensitivity is a delicate thing. One IR-insensitive line can contaminate a whole subdiagram, removing its IR sensitivity. This fact formalized in the *Zombie Lemma* (Lemma 5). However, Lemma 5 requires the proof of the *Log Lemma* (Lemma 2), which states that IR sensitivities in graphs are at most logarithmic. Other facts that will be necessary to determine where IR sensitivities lie in QCD graphs are also proven in the process of showing Lemma 2.

Our first step is to prove that in physical gauges, IR sensitivities are at most logarithmic:

Lemma 2. (**Log Lemma**) *According to the power counting discussed in Section 3.2, in physical gauges any Feynman diagram in QCD (or any other renormalizable theory with only gauge interactions) scales at worst like κ^a with $a \geq 0$. Thus IR divergences are at most logarithmic.*

This fact has been known for decades [42]. We reproduce the proof here for completeness and to facilitate the proofs of Lemmas 4 through 9.

Although we will not discuss covariant gauges much, it is also known that in Feynman gauge, individual diagrams can have divergences more severe than logarithmic [43]. These power divergences provide an obstruction to using reduced diagrams for a transparent picture of hard factorization. Of course, the power divergences cancel in a gauge-invariant sum over diagrams, but this cancellation is of little use in a diagram-by-diagram analysis. Lightcone gauge with non-generic choices of reference vectors also do not lead to the same simple reduced-diagram picture.

The two lemmas that will be proven during the proof of Lemma 2 are:

Lemma 3. (**Collinear Lemma**) *Consider two lines of a given diagram. If the lines cannot become collinear due to momentum conservation or if they give rise to a κ suppression when they do become collinear, then a virtual particle connecting between them cannot be collinear sensitive.*

Lemma 4. (**4-point Lemma**) *There are no diagrams with soft-sensitive gluons attaching to soft-insensitive lines through a 4-point vertex.*

Proof of Lemmas 2, 3 and 4. We will focus on proving the Log Lemma (Lemma 2), and mention the other two lemmas as they come up.

Before getting into the proof, we will need to establish the form of the various vertices in the theory in the limit where all of the particles involved are soft or collinear. First, as discussed in [3], the 3-point vertex involving a soft gauge boson has the following limiting behavior:

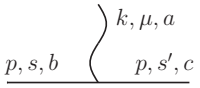

$$\cong \; -i2g_s\, T^a_{bc}\, \delta_{ss'}\, p^\mu, \qquad \text{for } k \text{ soft and } p \text{ on-shell and not soft} \tag{3.126}$$

where a, b and c are color indices and s and s' are helicities (the wave functions of the non-soft particles are included). This result holds if the non-soft lines represent particles of any spin [60], in particular, these lines can be gluons. Similarly, the all-collinear vertex with at least one gauge boson is proportional to the momentum flowing through the vertex, by Lorentz invariance:

$$\propto\ p^\mu \propto q^\mu, \qquad \text{for } p \parallel q \tag{3.127}$$

Again, this is true irrespective of the spin of the particles in the straight lines and only when the lines are on-shell.

Now for the proof; we prove the Log Lemma (Lemma 2) by induction on the number of loops. Tree-level diagrams trivially scale like κ^0, so Lemma 2 holds for $n = 0$. Then suppose it holds for $n - 1$ loops and consider adding another loop. We will consider all possible ways to add a loop using 3- and 4-point vertices.

For massless particles, propagators blow up when virtual lines are either soft or collinear. Let us begin with the soft case. According to the power-counting rules in Section 3.2, when the new line goes soft the measure associated with a soft line power counts as $d^4k \sim \kappa^8$ and the denominator of the propagator of the soft line counts as $k^2 \sim \kappa^4$. If the soft line connects via 3-point vertices to two lines of momentum p_1^μ and p_2^μ, then the new loop adds two more propagators with denominators $(p_i \pm k)^2$ for $i = 1, 2$. If p_i^μ is off-shell, this scales like κ^0; if p_i^μ is on-shell and not soft, it scales like $p_i \cdot k \sim \kappa^2$; and if p_i^μ is soft it scales like κ^4. The numerator of the propagators, combined with the 3-point vertices, power count the same as $p_i + k$. If p_i^μ is not soft, then $p_i + k \sim \kappa^0$; if p_i^μ is soft, then $p_i + k \sim \kappa^2$. Thus when p_i^μ is off-shell, the numerator and denominator combine to κ^0; if p_i^μ is on-shell but not-soft, they

combine to $\kappa^0/\kappa^2 \sim \kappa^{-2}$ and if p_i^μ is soft, they combine to $\kappa^2/\kappa^4 \sim \kappa^{-2}$. The worst scaling is therefore when p_i^μ is on-shell, and then,

$$\frac{p_i + k}{(p_i + k)^2} \sim \kappa^{-2} \qquad \text{for} \quad p_i^2 = 0 \quad \text{(either soft or not-soft)} \tag{3.128}$$

Thus, adding a soft loop with 3-point vertices only gives an enhancement if both lines it connects to are on-shell, in which case, the new loop power counts as

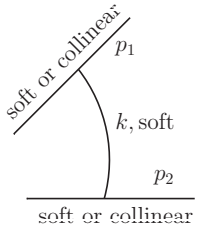

$$: \qquad d^4k \, \frac{1}{k^2} \, \frac{p_1 + k}{(p_1 + k)^2} \, \frac{p_2 + k}{(p_2 - k)^2} \;\sim\; \kappa^8 \, \frac{1}{\kappa^4} \, \frac{1}{\kappa^2} \, \frac{1}{\kappa^2} \;\sim\; \kappa^0 \tag{3.129}$$

on top of the original loop's power counting.

To be more precise, the lines with momenta p_1 and p_2 which connect to the soft momenta k and go on-shell do not have to *directly* connect to k. Even if there are some loops in the graph, as long as there are lines which go on-shell and connect to k there will still be an enhancement. We can simply think of these loops as producing a composite vertex:

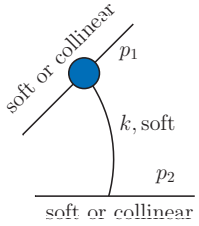

$$: \qquad d^4k \, \frac{1}{k^2} \, \frac{p_1 + k}{(p_1 + k)^2} \, \frac{p_2 + k}{(p_2 - k)^2} \;\sim\; \kappa^8 \, \frac{1}{\kappa^4} \, \frac{1}{\kappa^2} \, \frac{1}{\kappa^2} \;\sim\; \kappa^0 \tag{3.130}$$

Since there are no extra complications with such composite vertices, we will leave the composite case implicit in this proof.

Next suppose the new loop with the soft momentum connects via at least one 4-point vertex. This happens by the new gluon connecting to a 3-point vertex in the $n-1$ loop graph. Again, the only way to get an enhancement is if the lines it

connects to are on-shell. Due to the 4-point vertex, the additional loop adds only two propagators rather than three. The new propagator denominators are k^2 and $(p_i + k)^2$. The $n-1$-loop graph had a 3-point vertex, with either all three momenta collinear or one of them soft. Using Eq. (3.126) and Eq. (3.127), we see that the original 3-point vertex gave a contribution to the numerator of the graph of the form:

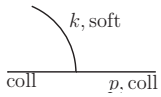

$$\propto\ p_\mu \Pi^{\mu\nu}(k) \sim \kappa^0 \qquad \text{or} \qquad \propto\ p_\mu \Pi^{\mu\nu}(q) \sim \kappa,\ \text{for } p \parallel q \tag{3.131}$$

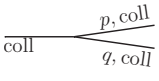

Whereas, when we add the loop with the 4-point vertex, this becomes

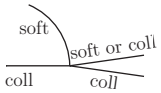

$$\propto\ g^{\mu\nu} g^{\rho\sigma} \sim \kappa^0 \tag{3.132}$$

Thus, there is a possible additional κ^{-1} from killing the numerator suppression if the original graph had an all-collinear 3-point vertex. So, connecting a soft loop to a collinear line via a 4-point vertex adds a loop that power counts either as

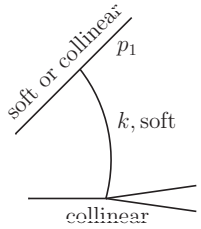

$$: \qquad d^4k\, \frac{1}{k^2}\, \frac{p_1 + k}{(p_1 + k)^2}\, \kappa^{-1}\ \sim\ \kappa^8\, \frac{1}{\kappa^4}\, \frac{1}{\kappa^2}\, \kappa^{-1}\ \sim\ \kappa \tag{3.133}$$

or as

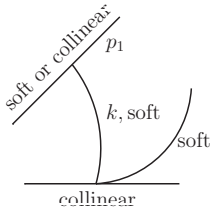

$$: \qquad d^4k\, \frac{1}{k^2}\, \frac{p_1 + k}{(p_1 + k)^2}\ \sim\ \kappa^8\, \frac{1}{\kappa^4}\, \frac{1}{\kappa^2}\ \sim\ \kappa^2 \tag{3.134}$$

In both cases, the new graph scales like a higher power of κ than the graph it modified. By the same argument, adding a soft loop that connects to a collinear line on each end via a 4-point vertex will be (even more) IR finite. By the induction hypothesis, the rest of the graph scales at worst like κ^0, so any time we add a 4-point vertex with

both soft and collinear momentum flowing through it, we get a $\kappa^{\geq 1}$ scaling. Thus, we see that there cannot be a soft sensitivity when a soft gluon attaches to non-soft gluons through a 4-point vertex. This proves the *4-point Lemma* (Lemma 4).

When *all* the relevant lines go soft, the 4-point vertices *can* contribute at leading-power. To see this, consider the case where the soft loop connects to all-soft lines through a 4-point vertex and assume for now that the other end connects via a 3-point vertex. This case is just like the previous discussion in that the new loop adds only two new propagators of the form k^{-2} and $(p_i + k)^{-2}$ and kills some of the suppression coming from the original 3-point vertex that became a 4-point vertex. However, in the all-soft case, the 3-point vertex suppression is a power of the soft momenta, which goes like κ^2 instead of κ from the collinear case, so the new loop power counts as

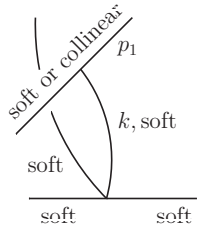

$$: \qquad d^4k \, \frac{1}{k^2} \, \frac{p_1 + k}{(p_1 + k)^2} \, \kappa^{-2} \;\sim\; \kappa^8 \, \frac{1}{\kappa^4} \, \frac{1}{\kappa^2} \, \kappa^{-2} \;\sim\; \kappa^0 \tag{3.135}$$

Similarly, if the new soft loop connects to all-soft lines via a 4-point vertex on both ends, we only add one propagator, but we kill two κ^2-suppressed numerators, giving

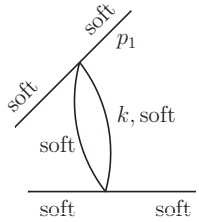

$$: \qquad d^4k \, \frac{1}{k^2} \, \kappa^{-2} \, \kappa^{-2} \;\sim\; \kappa^8 \, \frac{1}{\kappa^4} \, \kappa^{-2} \, \kappa^{-2} \;\sim\; \kappa^0 \tag{3.136}$$

Thus 4-point vertices involving all soft lines must be included. We have now exhausted all possible ways of adding a loop that can go soft and we have found that they all add a power counting of κ^a for $a \geq 0$ to the original graph. This proves the Log Lemma as far as soft-scaling alone is concerned.

Now consider adding a line that can have a collinear sensitivity. As in the soft case, there are a number of ways that this can take place and we will systematically consider each possibility. For the diagram to possibly be IR divergent the momentum in the line must be going collinear to the momenta of the lines it connects to on at least one end. Let us suppose first that it is not also collinear to the line it connects to on the other end. Adding a line like this introduces two new on-shell propagators if it connects to the line to which it is collinear with a 3-point vertex, and only a single on-shell propagator if it connects with a 4-point vertex. In the first case, the all-collinear 3-point vertex will be proportional to the momentum flowing through it, as in Eq. (3.127), and this will give a suppression when contracted with any of the propagators (or external polarization vectors) it connects to. This is because, in physical gauges, the propagator numerators are equal to the polarization-vector sum when the momentum in a propagator goes on-shell. Thus, $p_\mu \Pi^{\mu\nu}(q) \sim \kappa$ for $p \parallel q$ and we have

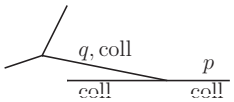

$$: \qquad d^4q \, \frac{1}{q^2} \, \frac{1}{(p+q)^2} \, p_\mu \Pi^{\mu\nu}(q) \;\sim\; \kappa^4 \, \frac{1}{\kappa^2} \, \frac{1}{\kappa^2} \, \kappa \;\sim\; \kappa \tag{3.137}$$

If the all-collinear vertex is a 4-point vertex, then we only get one new collinear propagator. However, going from an all-collinear 3-point vertex to a 4-point vertex kills the suppression that we just discussed, so we have

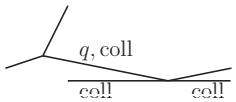

$$: \qquad d^4q \, \frac{1}{q^2} \, \kappa^{-1} \;\sim\; \kappa^4 \, \frac{1}{\kappa^2} \, \kappa^{-1} \;\sim\; \kappa \tag{3.138}$$

Finally, if the 4-point vertex has a soft line connecting to it, it will give a finite loop due to Eq. (3.133). We conclude that unless the new line is collinear to the momenta on both ends, and in particular that all the relevant lines are on-shell, the new diagram will have additional κ suppression compared to the $n-1$ loop graph.

Combining Eq. (3.137) and Eq. (3.138), we conclude that whenever a particle travels between two lines that could not originally go collinear, or that is κ-suppressed if they do become collinear, the resulting loop is κ-suppressed, and therefore, collinear insensitive. This proves the *Collinear Lemma* (Lemma 3).

It remains to show that when the momenta are all on-shell, the overall scaling is at worst κ^0. We have shown this already for soft singularities. So consider the remaining case when the new line goes collinear to all of the lines to which it connects. If both vertices are 3-point, we get three collinear propagators and two κ-suppressed products in the numerator:

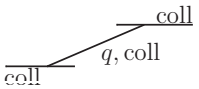

$$: \qquad d^4q\,\frac{1}{q^2}\,\frac{1}{(p+q)^2}\,\frac{1}{p^2}\,p_\mu\Pi^{\mu\nu}(q)p_\nu \;\sim\; \kappa^4\,\frac{1}{\kappa^2}\,\frac{1}{\kappa^2}\,\frac{1}{\kappa^2}\,\kappa\,\kappa \;\sim\; \kappa^0 \tag{3.139}$$

If only one of the vertices is a 3-point vertex, then adding the loop adds two propagators, one κ-suppressed product in the numerator due to the all-collinear 3-point vertex, and one κ enhancement due to the removal of one of the original all-collinear 3-point vertices. Thus, graphs with one 3-point and one 4-point vertex power count as:

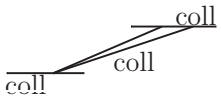

$$: \qquad d^4q\,\frac{1}{q^2}\,\frac{1}{(p+q)^2}\,p_\mu\Pi^{\mu\nu}(q)\,\kappa^{-1} \;\sim\; \kappa^4\,\frac{1}{\kappa^2}\,\frac{1}{\kappa^2}\,\kappa\,\kappa^{-1} \;\sim\; \kappa^0 \tag{3.140}$$

Finally, if the added loop connects on both ends to all-collinear 4-point vertices, then only one collinear propagator is added, but two 3-point vertices are removed causing two additional κ^{-1} enhancements:

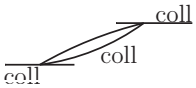

$$: \qquad d^4q\,\frac{1}{q^2}\,\kappa^{-1}\,\kappa^{-1} \;\sim\; \kappa^4\,\frac{1}{\kappa^2}\,\kappa^{-1}\,\kappa^{-1} \;\sim\; \kappa^0 \tag{3.141}$$

So, all possible additional loops that involve all-collinear vertices power count as κ^0 and are logarithmically collinear singular.

We have shown that any possible addition of a loop power counts as κ^a for $a \geq 0$. Therefore, by induction, every graph in physical gauges power counts like κ^a for $a \geq 0$ and is at most logarithmically divergent. This proves Lemma 2. □

Now, let us define the term **subdiagram** to mean a part of a larger diagram that could be cut out with an arbitrarily shaped (possibly 3D) cookie cutter. A subdiagram is considered as a function of the generic (not necessarily on-shell) momenta of the lines that the cookie cutter cut. These lines are considered to be external lines of the subdiagram, though they may have been internal in the original graph. Internal lines in a subdiagram are the complement of external lines.

With this definition, we can now make a useful observation about how IR-insensitive lines scale with κ to establish how IR-insensitive graphs can *infect* any line they come in contact with, making it also IR insensitive. This observation is encapsulated by the following lemma:

Lemma 5. (**Zombie Lemma**) *Consider adding a new internal line L to a subdiagram with no IR-sensitive lines. If at least one end of L attaches to an internal line of the original subdiagram, then L is IR insensitive.*

Proof. Since no line in the subdiagram is IR sensitive, in any soft or collinear limit the subdiagram scales like κ^a for some $a > 0$. First, consider whether the line L can have a soft sensitivity. When L becomes soft, it produces a loop that scales like κ^0 at most. However, this only happens if the lines it connects to are on-shell (or it produces an on-shell line elsewhere in the subdiagram). By assumption, one of these

lines is an internal line from the original subdiagram, so there is a corresponding κ^a suppression from the rest of the subdiagram. Thus, overall the subdiagram is still soft insensitive and so is the line L. That L cannot be collinear sensitive follows directly from the *Collinear Lemma* (Lemma 3). Thus L is IR insensitive and the Lemma is proven. □

3.7.2 IR insensitivity of the hard amplitude

Two immediate consequences of the above lemmas completely characterize the hard amplitude:

Lemma 6. (**Hard-Blue Lemma**) *Any all-blue 1PI subdiagram containing the hard-scattering vertex is IR insensitive.*

Proof. Any 1PI subdiagram that contains the hard-scattering vertex must have momenta from two different collinear sectors piping through it. Consequently, there must be a line L that connects between two lines that cannot simultaneously become collinear by momentum conservation. The *Collinear Lemma* (Lemma 3) then implies that L is not collinear sensitive. Since L is blue (by hypothesis), it is soft insensitive as well, and hence IR-insensitive. Now, starting with the 1-loop graph containing L, we can build up the rest of the 1PI subdiagram by adding new lines (inserting vacuum loops in the middle of L is allowed). Whenever a new line connects to L, or to the network of lines previously connected to L, it is IR-insensitive by the *Zombie Lemma* (Lemma 5). Alternatively, a new line might connect to external lines of the subdiagram. If it connects two in the same sector, the graph cannot be 1PI. If it connects two in different sectors, the new line is IR-insensitive for the same reason L

is, and we can replace L by this new line to continue our argument. Thus every line in the 1PI subdiagram is IR-insensitive, as was to be shown. □

Lemma 7. (**Hard-Red Lemma**) *Red lines cannot connect to internal lines of an all-blue 1PI subdiagram containing the hard-scattering vertex.*

Proof. Any all-blue 1PI subdiagram containing the hard vertex is IR-insensitive by the *Hard-Blue Lemma* (Lemma 6). Any line connecting to an internal line of this subdiagram must also be IR-insensitive, by the *Zombie Lemma* (Lemma 5). Since red lines are soft sensitive, by definition, these lines cannot be red. □

These two lemmas explain why some colored graphs are absent in physical gauges. For example, as discussed in Section 3.6.3, the diagrams

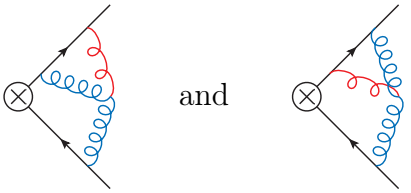

(3.142)

are IR (in particular, soft) insensitive in generic-lightcone gauge and therefore, absent from the colored-graph decomposition. The diagrams

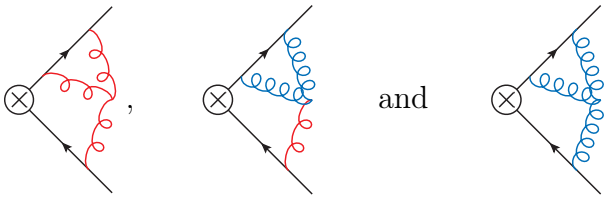

(3.143)

are present because the first two are IR divergent and the third is the IR-finite "last" graph in the decomposition. Note that the second diagram in Eq. (3.143) does not satisfy the hypothesis of the *Hard-Blue Lemma* (Lemma 6) because without the red line, it is not a 1PI graph containing the hard vertex.

3.7.3 Power-suppressed colored graphs

So far, we have only characterized where the IR sensitivities are. Some diagrams, despite being IR sensitive contribute only at subleading power and can be dropped from a leading-power factorization theorem. We have already seen an example of subleading diagrams in Section 3.4. There, in particular in Eq. (3.75) and Eq. (3.80), we found that for $q \parallel p_1$,

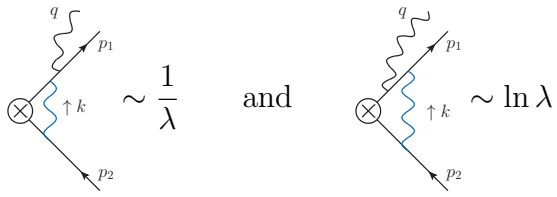

$$\sim \frac{1}{\lambda} \quad \text{and} \quad \sim \ln \lambda \tag{3.144}$$

In this example, the soft-insensitive loop in the first graph is IR-finite, so the λ^{-1} comes from the tree-level splitting on external leg. In the second graph, the loop is tangled with the emission. At $\lambda = 0$, the graph would be divergent, but for $\lambda > 0$ it is not. Thus the graph scales like $\ln \lambda \ll \lambda^{-1}$. The second graph is therefore subleading compared to the first and can be dropped. In a sense, the IR-insensitive loop *eats* the enhancement of the real emission. This is to be contrasted with IR-sensitive loops which do not eat emissions. For example,

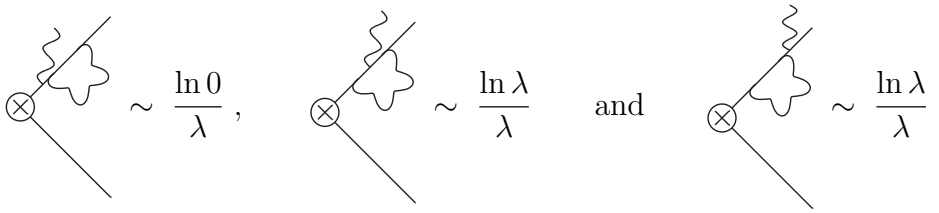

$$\sim \frac{\ln 0}{\lambda}\,, \qquad \sim \frac{\ln \lambda}{\lambda} \quad \text{and} \quad \sim \frac{\ln \lambda}{\lambda} \tag{3.145}$$

In each case, the graphs are divergent without the emission. In particular, the loop in the second graph cannot eat the emission.

The generalization of this example is embodied in the following lemma:

Lemma 8. (**Loop-emission Lemma**) *Any diagram with an IR-insensitive 1PI*

subdiagram that has a real emission attached to an internal leg is power suppressed compared to a corresponding diagram where the emission comes off of an external leg.

Proof. An IR-insensitive subdiagram that is 1PI has at least one overall power of suppression when approaching the soft and collinear limits. That is, it scales like κ^a for some $a > 0$. Suppose some line in the loop has momenta $q+k$ in it, where q is the external momenta and k is the loop momenta. Adding an external collinear emission connecting inside the loop gives an additional propagator with momentum $p+q+k$ with p the new external momenta. Since $(p+q)^2 \sim \lambda^2$, when k goes collinear to q, this propagator scales like

$$\frac{1}{(p+q)^2 + 2(p+q)\cdot k + \kappa^2} \sim \frac{1}{\lambda^2 + \kappa^2} \tag{3.146}$$

In physical gauges, the vertex contracted with the polarization gives $(p+2q+2k)\cdot\epsilon \sim \lambda + \kappa$ when all of these momenta are collinear. The net effect is therefore $\dfrac{\kappa+\lambda}{\kappa^2+\lambda^2}$. So if of n emissions, m are inside the loop the diagram scales like

$$\frac{1}{\lambda^{n-m}} \int d\kappa\, \kappa^{a-1} \left(\frac{\lambda+\kappa}{\lambda^2+\kappa^2}\right)^m \sim \begin{cases} \dfrac{\ln\lambda}{\lambda^{n-a}}, & m \geq a \\ \dfrac{1}{\lambda^{n-m}}, & m < a \end{cases} \ll \frac{1}{\lambda^n} \tag{3.147}$$

Thus the diagrams with any number of collinear emissions coming from within the loop are power suppressed compared to the diagram with $m = 0$, where all the emissions are outside the loop.

Soft emissions are similar. Adding a soft emission to an IR-insensitive subdiagram gives $(\lambda^2+\kappa^2)^{-1}$ for the propagator, as before but now $(p+k+q)\cdot\epsilon \sim 1$ since although k and q are soft, p is not. Thus each new emission from within the loop

gives $(\lambda^2 + \kappa^2)^{-1}$ compared to λ^{-2} from outside the loop, and becomes suppressed upon integration as above.

Thus, for either soft or collinear emissions, emissions coming out of an IR-finite loop (or an IR-finite, 1PI subdiagram) are power suppressed and can be dropped at leading power. □

A final lemma finishes the required ingredients for the advertised reduced diagram picture:

Lemma 9. (**Self-Collinear Lemma**) *Graphs where a collinear gluon is emitted from a leg to which it cannot be collinear near an IR sensitivity are power suppressed compared to graphs where the gluon can be collinear to the leg it is emitted from near an IR sensitivity.*

Proof. This lemma was proven for tree-level graphs in [3], using that self-collinear emissions have an enhanced propagator compared to non-self-collinear ones. The subdiagram to which a collinear emission is connected must be IR sensitive, by the previous Lemma (Lemma 8), and therefore, cannot connect to 1PI subdiagram containing the hard vertex with only blue lines, by the *Hard-Blue Lemma* (Lemma 6). Thus the subdiagram to which the emission is connected can only contain external momenta associated with a single collinear sector before the emission is added. Thus, near an IR sensitivity all of the propagators in the subdiagram are either soft or collinear to the same direction and the lemma follows from the same reason it did at tree level. □

That completes the lemmas. As a reminder, all of these lemmas hold in physical

gauges, as defined at the beginning of this section, and are generally violated in Feynman or other covariant gauges.

3.7.4 General reduced diagram

With these lemmas we have all of the rules required to *reduce* the most general graphs that contribute to N-jet-like scattering in a physical gauge. We first expand the various loop momenta and soft external momenta in their soft limit to write a diagram as a sum of colored diagrams with soft-sensitive virtual particles and soft-insensitive ones. The lemmas guide the coloring, by indicating where the soft sensitivities can be, they indicate which red or blue lines can have associated collinear sensitivities, and which colored diagrams are power suppressed (even if IR sensitive) compared to other diagrams with the same external states at the same order in perturbation theory.

To draw the physical-gauge reduced diagram, first note that the *Hard-Blue Lemma* (Lemma 6) tells us that each diagram has an IR-insensitive core, given by the largest-possible 1PI subdiagram containing the hard vertex which has only blue lines. By the *Loop-emission Lemma* (Lemma 8), no real emissions can come out of this core. Thus the hard core connects to the rest of the diagram only through a single line in each sector.

Now let us temporarily ignore red lines. Then there are only collinear singularities. By the *Collinear Lemma* (Lemma 3), it is impossible for any IR-sensitive graph to involve external momenta from two different collinear sectors. Thus, outside of the IR-insensitive core, the only collinear-sensitive subdiagrams are self-energy-type

corrections to each sector. No blue lines go between sectors, or they would remove the IR sensitivity, by Lemma 6, and should have been included in the core. Moreover, all collinear emissions come from self-collinear sectors, by the *Self-Collinear Lemma* (Lemma 9). Now add the red lines back in. These lines can connect anywhere, except to the IR-insensitive core by Lemma 7.

We have therefore shown that any colored diagram can be drawn as

$$\langle X_1 \cdots X_N; X_s | \, \mathcal{O} \, |0\rangle \overset{\text{physical gauges}}{\cong} \sum_{\text{diagrams}}$$

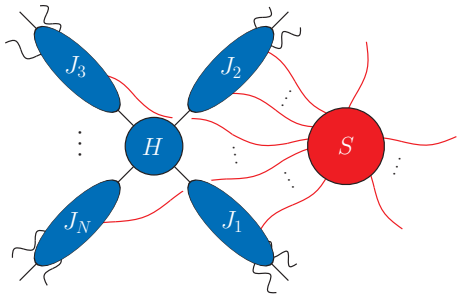

(3.148)

This reduced diagram has all the properties claimed in Section 3.5. We call the sum over soft-insensitive (blue) 1PI subdiagrams involving the hard vertex the **hard amplitude** and the sum of all soft-insensitive (blue) corrections to each external leg the **jet amplitude**. All of the soft-sensitive (red) lines are in the **soft amplitude**, which is not necessarily connected. Note that these are amplitudes, in contrast to the common use of hard jet and soft functions to refer to squares of the amplitudes. This reduced diagram displays hard factorization. We have not yet shown how the jet and soft amplitudes can be disentangled which requires soft-collinear factorization.

In generic lightcone gauge, where there are no ghosts, every line in or exiting S is soft sensitive and is colored red. Because all the lines entering S are soft-sensitive, no momenta within S can be dropped with respect to any other momenta. Thus,

there is no expansion done by the coloring algorithm applied to S and the loops within S are given by the full-QCD Feynman rules. The lines leaving S connecting to the J_j blobs have been expanded, and have eikonal interactions with the J_j blob. As we will see in the next section, in factorization gauge, there are ghosts in the S blob. Ghosts are always IR-insensitive, thus they should be colored blue. Since the ghosts are blue without any expansion, the S blob still contains all the unmodified loops of full QCD. In summary, in any physical gauge, the S amplitude connects to the rest of the diagram through soft-sensitive (red) lines with eikonal interactions and all the internal loops of S are the same as in full QCD.

Before moving on to soft-collinear factorization, we pause to discuss the physically rich structure of the reduced diagram in Eq. (3.148). The hard factorization displayed here is a consequence of the geometrical property that the jet and soft subdiagrams attach to the hard subdiagram by a single line. Moreover, near the IR sensitivities in the loops, this line is almost on-shell and carries the net momentum of the jet. The hard subdiagram is therefore a completely independent process that depends only on a single net momentum and the overall quantum numbers for each collinear sector. Since the hard subdiagram has a smooth $\lambda \to 0$ limit, it is completely insensitive to corrections of order λ; namely, it is completely insensitive to the distribution of collinear momenta among the external states $\langle X_1 \cdots X_N; X_s|$.

The IR-finiteness of the hard amplitude arises because, in physical gauges, there are additional suppression factors from numerators in regions where the virtual particles go on-shell. Since the hard amplitude is IR-insensitive, all the dynamics it encapsulates takes place at short-distance. Only distances of order $(\Delta x)_H = (P_i \cdot P_j)^{-1/2}$

are relevant. Since the hard diagram communicates with the rest of the process only through the single lines which are off-shell by of order λ, these interactions take place at distances $(\Delta x)_J \sim \lambda^{-1}(\Delta x)_H$ away from the hard core. The subsequent non-soft (i.e. collinear) interactions take place around $(\Delta x)_J$, but in different directions. These collinear particles can then only communicate with each other through the exchange of long-wavelength modes, at distances of order $(\Delta x)_S = \lambda^{-2}(\Delta x)_H$. The single particle in each sector coming out of the hard vertex corresponds to the single partons in hard matrix elements which can be calculated first and then either showered through a Monte Carlo event generator or convolved against analytic jet and soft functions in an inclusive calculation.

It is important to note that the intuitive picture drawn in Eq. (3.148) is only valid in physical gauges, such as generic-lightcone gauge. In Feynman gauge or non-generic-lightcone gauges with enhanced polarization vectors Eq. (3.148) is totally destroyed and the factorization becomes completely opaque [43]. Although this seems like an esoteric point, these unphysical gauges are often used in discussions of factorization, such as in the original formulation of SCET [46, 47]. For more discussion of this point see [3].

3.8 Step 3: Factorization Gauge

We saw in the previous section that generic-lightcone gauge limits the types of diagrams which can contribute at leading power. Let us temporarily imagine restricting the region of integration of the loop momenta so that the soft-sensitive lines are forced to be soft and the soft-insensitive lines are forced to be collinear to

some direction (instead of integrating them over $\mathbb{R}^{1,3}$ like we should). Then each reduced diagram would just be some integrals over soft and collinear particles with the same topologies as discussed in [3], and it seems like the same proof of soft-collinear decoupling would apply nearly unchanged. However, [3] made heavy use of the freedom to choose different reference vectors for different external particles. In particular, a different reference vector r_j^μ is chosen for each distinct collinear sector as well as another, r_s^μ, for the soft sector. For this to work at loop level, we need to be able to choose the reference vector for a lightcone-gauge propagator to depend on the direction that the virtual gluon is going. We call a gauge with this flexibility **factorization gauge**. Factorization gauge is critical to our proof and will be useful even when the virtual phase space is unrestricted over $\mathbb{R}^{1,3}$.

This section introduces factorization gauge. In factorization gauge, ghosts do not completely decouple, as they do in lightcone gauge. However, we will show that ghosts do not give rise to additional IR sensitivities. The next section will use factorization gauge to rigorously prove soft-collinear factorization, following essentially the same procedure as in [3].

3.8.1 Definition

We would like to be able to choose a different lightcone-gauge reference vector for each sector in the reduced diagram, which is the loop-level equivalent of choosing different reference vectors for the polarizations of each sector which was done in [3]. That is, we would like to choose a gauge such that the numerator of the gluon

propagator is given by:

$$\Pi^{\mu\nu}(k) = -g^{\mu\nu} + \frac{r^\mu(k)k^\nu + r^\nu(k)k^\mu}{r(k)\cdot k} \tag{3.149}$$

with

$$r^\mu(k) = \begin{cases} r_s^\mu\,, & k \text{ soft} \\ r_j^\mu\,, & k \parallel p_j \\ r_h^\mu\,, & \text{otherwise} \end{cases} \tag{3.150}$$

We assume r_s^μ, r_j^μ and r_h^μ to be lightlike and take r_s^μ and r_j^μ as the reference vectors for polarizations of soft and collinear external gluons. Given that for loop momenta k being soft or collinear is equivalent to $-k$ being the same, we will further define

$$r^\mu(k) = r^\mu(-k) \tag{3.151}$$

so we only need to specify r^μ for positive-energy momenta. In practice, we will only use two different reference vectors: $r_j^\mu = r_c^\mu$ for all j and $r_h^\mu = r_s^\mu$. Although our arguments will only use the freedom to choose r_c and r_s separately, we define factorization gauge with the full $N+2$ different reference-vector choices since this is consistent with our freedom to choose the reference vectors for the external gluons separately. [3]

To be concrete, we can make Eq. (3.150) precise by chopping up phase space. For example, we can draw a Euclidean ball of size $\lambda^2 Q$ around $k = 0$ for the soft region, draw cones of angle λ around each jet region, and let everything else count as hard. The precise partitioning will not matter for the proof of factorization.

Note that both soft-sensitive and soft-insensitive gluons have unrestricted momenta. For example, soft-sensitive (red) lines can be collinear or hard in which case

[3] Lightcone gauges with different (constant) reference vectors for different sectors have appeared in the SCET literature [102].

their propagator has r_j or r_h. Factorization gauge does not assign a different reference vector to different lines in the reduced diagram (which would not be gauge-invariant). The assignment of reference vector is based only on the gluons' momentum, which is a legitimate gauge choice.

To implement this gauge choice into the Lagrangian, we can use the following non-local gauge fixing term:

$$\mathcal{L}_{\text{g-f}}(x) = -\frac{1}{2\xi}\Big(r^\mu (i\partial)\, A^a_\mu(x)\Big)^2 \tag{3.152}$$

and then take $\xi \to \infty$. This gives a Faddeev-Popov determinant of

$$\det\Big(\frac{1}{g} r(i\partial)\cdot D^{\text{adj}}\Big) = \int \mathcal{D}c\,\mathcal{D}\bar{c}\,\exp\Big(-i\int d^4x\,\bar{c}^a\,\big(r(i\partial)\cdot D^{ab}\big)\,c^b\Big) \tag{3.153}$$

Therefore, the ghosts couple to gluons via

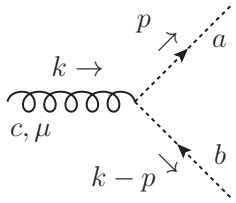

$$\propto\; g\, f^{abc}\, r^\mu(p) \tag{3.154}$$

Thus, the vertex Feynman rule depends on $r^\mu(p)$ with p^μ the momentum of the ghost.

The gluon propagator is

$$= \quad \frac{i\,\delta^{ab}}{k^2 + i\varepsilon}\,\Pi^{\mu\nu}(k) \tag{3.155}$$

with $\Pi^{\mu\nu}(k)$ given in Eq. (3.149) which satisfies (for lightlike r^μ)

$$r_\mu(k)\,\Pi^{\mu\nu}(k) = 0 \tag{3.156}$$

Recall that in lightcone gauge (where r^μ is constant), although the ghost-gluon vertex is still proportional to r^μ, any graph where a ghost couples to a virtual gluon is zero,

due to Eq. (3.156). If r^μ is also the reference vector of the external polarizations, then the ghosts completely decouple diagram-by-diagram (for a different choice of external reference vector, individual diagrams with ghosts may not vanish but their sum must due to the Ward identity, which guarantees reference-vector independence). In factorization gauge, when a gluon of momentum k couples to a ghost of momentum p, where $r(k) \neq r(p)$, the vertex will not be orthogonal to the gluon propagator or polarization. Thus, ghosts do not completely decouple in factorization gauge. Nevertheless, ghosts play a very small role in factorization, as we now show.

3.8.2 Ghosts Decoupling

Although ghosts do not completely decouple, we will now show that ghosts cannot give rise to IR sensitivities. In particular, this means that ghost lines can never be red and can only contribute IR-insensitive loops internal to the hard, jet and soft blobs of Eq. (3.148).

The fact that ghost loops do not give rise to IR sensitivities can be anticipated using unitarity. Independent of the gauge choice, we are always free to choose different reference vectors for the polarizations of external gluons in different IR sectors (as was extensively used in [3]). By unitarity, these on-shell soft and collinear gluons should be in one-to-one correspondence with cuts of loops near IR singularities. We then expect that in a gauge consistent with choosing different reference vectors for different IR sectors (i.e. factorization gauge) ghosts should not exist in IR-sensitive loops, since the ghosts cannot exist as external particles.

Ghosts cannot be part of IR-sensitive loops because near the IR-sensitive re-

gions of integration, factorization gauge looks like a regular lightcone gauge in which ghosts decouple. That is, because the sum of soft momenta is soft and the sum of collinear momenta (to a single direction) is collinear, the all-soft and all-collinear ghost-ghost-gluon vertices vanish when contracted with the gluon propagator or external polarization exactly as they do in lightcone gauge. Therefore, ghosts will only modify the internal structure of the hard, jet and soft blobs by adding to them IR-insensitive loops.

What other types of vertices can give rise to IR sensitivities? Momentum conservation rules out the possibility of vertices with off-shell and two collinear momenta or off-shell and a soft and collinear momentum. The *Collinear Lemma* (Lemma 3) says that a vertex with an off-shell momentum and two-hard on-shell momenta that are not collinear to each other cannot give rise to an IR sensitivity. So, we only need to consider ghost loops with singularities where the vertices in the loop have mixed-on-shell momenta. There are then two possibilities

1. Collinear ghost/soft ghost/collinear gluon, such as in

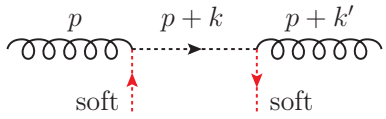

(3.157)

   where p is a collinear and k and k' are soft. Or

2. Collinear ghost/collinear ghost/soft gluon,

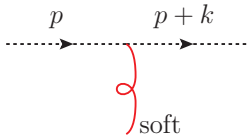

(3.158)

   with p collinear and k soft.

In situations of the first type, one of the vertices is proportional to $r^\mu(k'-k)$ and the other vertex to $r^\mu(p+k)$. The $r^\mu(k'-k)$ is not orthogonal to the collinear-gluon propagator, $\Pi^{\mu\nu}(p)$, because k and k' are soft, so this vertex will not vanish. However, these non-vanishing vertices are always accompanied with the other vertex which is proportional to $r^\mu(p+k)$ which is equal to $r^\mu(p)$ since $p \parallel p+k$, and $r^\mu(p)$ is orthogonal to $\Pi^{\mu\nu}(p)$. Hence graphs with segments like in Eq. (3.157) always vanish near the singularity. A vertex of the second type, Eq. (3.158) does not automatically vanish on its own, since $r^\mu(p) \not\equiv r^\mu(k)$. However, since there are no external ghosts, a ghost with a collinear momentum can only give rise to an IR sensitivity if it came from a gluon with collinear momentum. Thus there must be a vertex of the first type somewhere in the graph making the graph vanish in the IR sensitive region of the ghost.

That being said, we are not arguing that the soft gluon in Eq. (3.158) cannot give rise to a soft sensitivity irrespective of the ghost momentum; we are only showing that the ghost lines themselves cannot give rise to IR sensitivities when they go on-shell. For example, we could have the following soft-sensitive graphs:

$G_1 \;=$ 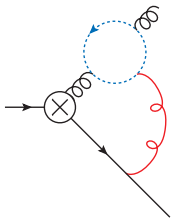 , $\qquad G_2 \;=$ 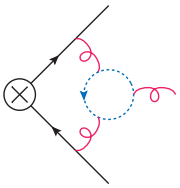 (3.159)

In both cases, the integrand vanishes when the red-gluon(s) go soft and the ghost goes soft or collinear. However, when the ghost is off-shell, the red gluon(s) can go soft giving rise to a soft sensitivity of the same form as from the corresponding graphs where the ghost loop is contracted to a point.

The most important point that we use from this section is that ghost lines cannot be soft sensitive (red). Since we can treat ghosts as blue lines, any 1PI-blue subdiagrams that contain the hard vertex are IR insensitive by the *Hard-Blue Lemma* (Lemma 6), irrespective of whether or not they contain ghosts. Furthermore, the *Loop-emission Lemma* (Lemma 8) tells us that such subdiagrams do not have external emissions connecting to them. Hence, the reduced-diagram picture in Eq. (3.148) is unchanged in factorization gauge, except for the fact that now the hard, jet and soft amplitudes may contain IR-insensitive ghost loops.

3.9 Step 4: Soft-collinear factorization

The all-orders proof of soft-collinear factorization can now be built upon the skeleton of the tree-level proof from [3]. This is made possible by factorization gauge, in particular, our ability to choose a different reference vector for (real and virtual) soft momenta, r_s, and for (real and virtual) collinear momenta, r_j. We will choose all of the r_j's to be a particular generic direction r_c not collinear to any of the collinear sectors; we call this the generic-r_c choice. For the soft reference vector we will go back and forth between choosing r_s in a particular collinear direction and r_s generic, building up elements of soft-collinear factorization as we go. We take $r_h = r_s$ for simplicity.

Before getting started, it is worth noting how coloring works in matrix elements involving Wilson lines. One should color these diagrams just as with diagrams involving only local fields. Since emissions from Wilson lines already have eikonal vertices, they are exactly equal to their leading expansion in the soft-limit. Thus, in matrix

elements involving only Wilson lines, such as $\langle 0| Y_j^\dagger W_j |0\rangle$, all the lines are red. These lines interact with each other through an S blob just like in Eq. (3.148). In matrix elements involving Wilson lines and fields, on the other hand, such as $\langle 0| \phi^\star W_j |0\rangle$, there can be both blue and red lines. As discussed in the previous section, in factorization gauge, the S blob can also have blue lines if there are ghosts just like in the non-Wilson line matrix elements.

Although we use scalar QED notation, operators in QCD look similar, with extra gauge and spin indices floating around. As far as hard-soft-collinear factorization is concerned, the differences between scalar QED and QCD are almost entirely notational. Thus we postpone the presentation of QCD matrix elements until Section 3.11.

3.9.1 Soft and collinear factorization separately

To begin, consider diagrams which only have red lines connecting to bare collinear sectors and call them $G_{\text{pure red}}$. Recall that diagrams with red lines are derived from full theory diagrams by expanding to leading order around the limit where the momenta in all the red lines are small. This expansion is the same as the eikonal expansion. Equivalently we can expand by taking all the non-soft lines infinitely hard. This infinite-hard limit removes the dynamics from the non-soft lines, making them appear is classical sources which can be represented with Wilson lines. Thus, the sum

of graphs of the form $G_{\text{pure red}}$ give matrix elements of Wilson lines:

$$\sum G_{\text{pure red}} \equiv$$ 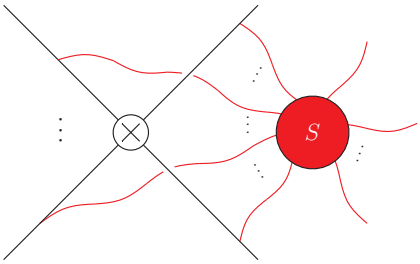 $$= \langle X_s | Y_1^\dagger \cdots Y_N | 0 \rangle \qquad (3.160)$$

where the sum over all possible diagrams of this topology is implicit. This equality holds in any gauge.

It is not hard to prove Eq. (3.160) directly. The Wilson lines $Y_j^\dagger$ exactly give the eikonal Feynman rules, so doing the contraction-combinatorics just like in [3], we see that the sum of the red lines connecting to the collinear ones is the same as the if the red lines connected to the soft Wilson lines. Since the S blob gives all-possible QCD interactions (including ghosts in factorization gauge), we exactly get the matrix element of Wilson lines in Eq. (3.160) to all-loop order.

For Eq. (3.160) to work the symmetry factors in the original uncolored loops must turn into the symmetry factors of the red loops. This is not hard to check. As discussed in Section 3.6.4, for every symmetry of an uncolored graph that is broken by the coloring, there are exactly as many different-but-equivalent soft sensitivities. So the symmetry factors work out correctly.

Pure collinear factorization is harder to discuss using colored diagrams. While diagrams with the maximal number of red lines are reproduced from a simple gauge-invariant Wilson line structure, diagrams with the maximal number of blue lines do not have any special simplifying property. Indeed, the Feynman rules for blue lines are a mess since they are given by differences between full QCD Feynman rules and eikonal Feynman rules. Moreover, graphs with all red lines are just as collinear

sensitive as graphs with all blue lines.

Instead, it is perhaps useful to consider the following rather trivial diagrammatic identity, forgetting about the coloring altogether:

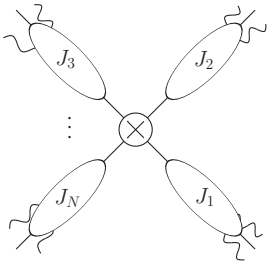

$$= \langle X_1 | \, \phi^\star \, | 0 \rangle \cdots \langle X_N | \, \phi \, | 0 \rangle \tag{3.161}$$

where, again, a sum over diagrams of the topology shown is implicit. In this equation, the right hand side is simply the sum over all graphs in scalar QCD with only self-energy corrections to each collinear sector. We saw such a structure emerge from the reduced diagram picture. Recall from the *Hard-Blue Lemma* (Lemma 6) that when a gluon connects between two different collinear sectors, there is no collinear sensitivity associated with it. Thus the diagrams on the right give the maximally collinear sensitive contributions to an amplitude at each order in perturbation theory in physical gauges.

3.9.2 Soft-collinear factorization with a single collinear sector

We have seen that the sum of all graphs with the only red lines connecting to naked collinear sectors is reproduced by a matrix element of Wilson lines, as in Eq. (3.160), and that the self-energy type corrections to a single collinear sector are given by matrix elements of fields, as in Eq. (3.161). To prove soft-collinear factorization, the next step, as in [3], is to factorize amplitudes containing both soft sensitivity and collinear sensitivity in one direction.

Let us define $G_{J_j \otimes S}$ as the sum of all colored diagrams that, when the red lines are removed, have collinear sensitivity to the j direction and no collinear sensitivity to any other direction. These are diagrams with any type of red or blue self-energy corrections to the j-leg, any number of blue lines in the hard vertex, and any number of red lines connecting the j-sector to other sectors. These diagrams all have the form

$G_{J_j \otimes S} =$ 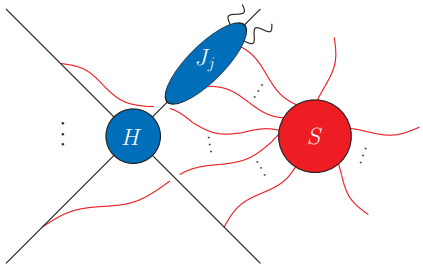

(3.162)

That $G_{J_j \otimes S}$ is a sum of such diagrams is left implicit. The J_j blob means all possible soft-insensitive loops (only blue lines) consistent with the external emissions in $\langle X_j|$ and the S blob means all-possible graphs with only red lines (soft-sensitive lines or soft external lines) coming out. Note that the restriction that J_j have only blue lines is only a convention. It does not restrict the relevant subdiagrams, since any red self-energy contributions are simply absorbed into S. The S blob does not have to be 1PI, planar or even connected.

It is not hard to write down an operator definition of $G_{J_j \otimes S}$. As long is r_c is generic

$$\langle X_j; X_s|\, Y_1^\dagger \cdots \phi^\star \cdots Y_N\, |0\rangle \overset{\substack{\text{any } r_s \\ \text{gen. } r_c}}{\cong} G_{J_j \otimes S} \tag{3.163}$$

There is an implicit choice of H in this equation. The Y_i Wilson lines for $i \neq j$ provide the eikonal interactions between the red lines and the $i \neq j$ collinear sectors. The $\phi_j^\star$ allows for any possible self-energy type graphs in the j sector. Although the left-hand side is gauge-invariant, in unphysical gauges (such as Feynman gauge

or factorization gauge with a non-generic $r_c \parallel p_j$), there will be collinear-sensitive diagrams with gluons going between different Wilson lines, or between a Wilson line and the j sector. The *Hard-Blue Lemma* (Lemma 6), which guarantees that such lines are only soft-sensitive, critically uses that a physical gauge was chosen in the collinear sensitive region.

Now we will show that in factorization gauge with $r_h = r_s = p_j$ there are no soft-sensitive graphs in $G_{J_j \otimes S}$ with lines connecting the S blob to the J_j blob. This is the loop-level version of the tree-level result that when $r_s = p_j$ any graph with soft external lines connecting to the p_j-collinear sector is power suppressed. At tree level, the decoupling happens because the eikonal vertex gives a factor of $p_j \cdot \epsilon(r_s)$ which is power suppressed when $r_s \cong p_j$. At loop level, we need to show that all the relevant graphs have a similar structure and are therefore similarly power suppressed.

Although there is no restriction that red lines have soft momenta – in general, red lines are integrated over all of $\mathbb{R}^{1,3}$ – there is a restriction that red lines do have to be soft sensitive. Their soft sensitivity is inherent in the coloring, as discussed in Section 3.6. Thus, consider the soft-sensitive region of a subdiagram with red gluon emerging from the jet blob. It looks like

$$S^\mu(k; \{p_j\}, r_s, r_c, r_h) \;=\; \vdots \quad \otimes \quad J_j \quad k, \mu \tag{3.164}$$

where all the indices are suppressed except the Lorentz index on the soft line. Here, S^μ is a function of the momentum k, the external-collinear momentum $\{p_j\}$ and the reference vectors associated with our gauge choice; that is, we imagine having done all of the loops in the collinear blob, J_j. We now state a simple Lemma pertaining to

which Lorentz structures can carry the μ index in S^μ:

Lemma 10. (**Soft-Attachment Lemma**) *When $r_s = r_h$, the soft sensitivity can only come from the term in $S^\mu(k;\{p_j\},r_s,r_j,r_h)$ proportional to p_j^μ.*

Proof. The first step is to show that $S^\mu(k;\{p_j\},r_s,r_j,r_h)$ has no term proportional to r_j^μ at leading power. The only way to get an r_j^μ term in S^μ is from the soft line connecting to a line that goes collinear to the j-jet direction. However then, the leading power soft vertex is eikonal, namely, proportional to p_j^μ instead of r_j^μ as discussed in Eq. (3.126) (as discussed in Section 3.8.2, the soft gluon cannot connect to a collinear ghost). So any terms proportional to r_j^μ are κ suppressed near the collinear sensitivity. Then, when the collinear region is integrated over, the κ-suppressed integrals give a finite value proportional to the volume of the collinear region, namely, λ to some positive power. Thus r_j^μ terms are power suppressed in loops and trees alike.

Now, since the r_j^μ term is power suppressed, we are left with $r_s^\mu = r_h^\mu$, k^μ and p_j^μ. However, when the red line is contracted with a soft propagator or a soft external polarization, any term proportional to r_s^μ vanishes exactly and any term proportional to k^μ will be suppressed in κ. So these terms cannot contribute to a soft sensitivity in the red line. This proves the lemma. □

Therefore, if we make the non-generic choice: $r_s = r_h = p_j$, which we call **collinear $\mathbf{r}_s$**, there will be no soft sensitivities connecting to the j-collinear sector. We state this as a lemma:

Lemma 11. (**Collinear-$\mathbf{r_s}$ Lemma**) *There are no soft-sensitive (red) lines connecting to the j-collinear sector in factorization gauge in collinear-r_s ($r_s^\mu = r_h^\mu = p_j^\mu$).*

Proof. The result is easy to see for a single soft line by Lemma 10, since when $r_s = p_j$ any soft propagator or external polarization vector will be orthogonal to p_j^μ. Now suppose we have many lines connecting to the j-collinear sector. Working our way inwards towards the hard vertex, the outermost line must be soft-insensitive by the argument for a single line, since it does not depend on the momentum of the other potentially-soft lines. If the outermost-red line connects to a different collinear sector, then by the *Hard-Blue Lemma* (Lemma 6) the rest of the lines must be blue and IR insensitive or, if any of the other lines are external-soft emissions, the whole graph is power-suppressed by *Loop-emission Lemma* (Lemma 8). So the lemma is proved in this case. On the other hand, if the outermost line connects back to the j-collinear sector, because it is soft insensitive, it will just contribute to the blue-collinear blob and we can start the argument over again starting from the next-outermost line. In this way, we see that no soft-sensitive (red) lines can connect to the j-collinear sector in collinear-r_s. □

For the rest of this chapter we will take all of the collinear-reference vectors, $\{r_j\}$, to be the same generic direction, r_c, that is not collinear to any of the collinear sectors. Furthermore, we will always take $r_h = r_s$. Neither of these choices is necessary, but they simplify the discussion. We have shown that if one chooses $r_s = p_j$ there are actually no red lines connecting to the J_j blob in Eq. (3.162). This means that no expansion was done to the integrals in the the J_j blob and therefore the J_j blob is exactly the same as in the full theory. Thus the set of relevant colored graphs contributing to $G_{J_j \otimes S}$ is somewhat different in generic-lightcone gauge from

factorization gauge with $r_s = p_j$:

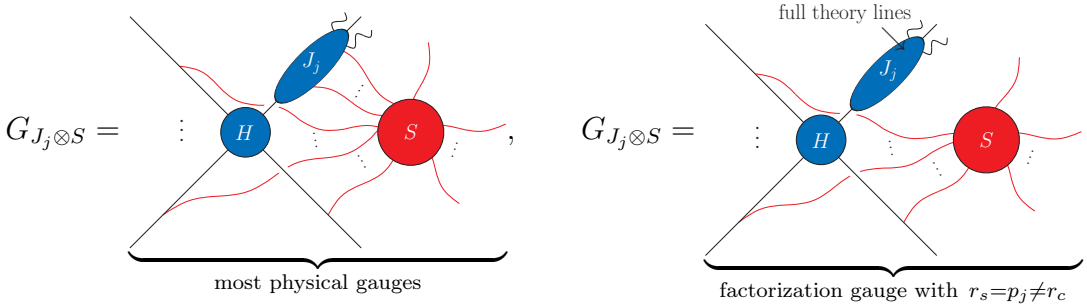

(3.165)

In most physical gauges, there are blue self-energy bubbles in the J_j blob, red self-energy bubbles attaching to the J_j blob, as well as red lines leaving this blob and connecting to the other legs and to external-soft emissions. However, in factorization gauge with $r_s^\mu = p_j^\mu$, the J_j blob is unmodified from full QCD and no red lines connect to it. The H, J and S blobs are all different in the two cases.

Now, since there are no soft-sensitive lines connecting to the J_i blob when $r_s = p_j$, the amplitude from summing all the relevant graphs is closely related to the amplitude from a product of Wilson lines, as in Section 3.9.1. More precisely,

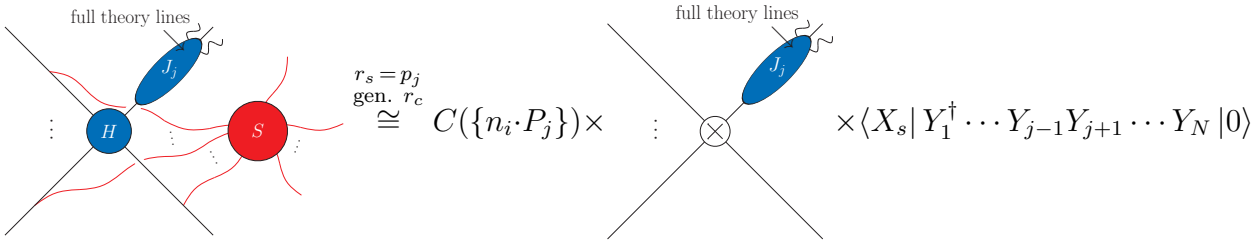

(3.166)

where P_j^μ is the net collinear momentum in the j sector, n_i^μ is the lightlike direction of the i sector and $\mathcal{C}(\{n_i \cdot P_j\})$ is an IR-finite function of $n_i \cdot P_j$ for $i \neq j$.

A subtle point is that $\mathcal{C}(\{n_i \cdot P_j\})$ does not have to equal the sum of the graphs in the hard amplitude $H(P_j, k_i)$ evaluated at $k_i^\mu = 0$ for all the soft loop momenta. To see where the difference comes from, recall that the H blob is IR insensitive, so it

is finite when any of the momentum from the red lines goes soft. Thus, we can write

$$\int_{\{k_i\}} H(P_j,k_i)\,S(k_i,n_i) = H(P_j,0)\int_{\{k_i\}} S(k_i,n_i) + \int_{\{k_i\}} \big(H(P_j,k_i)-H(P_j,0)\big)\,S(k_i,n_i) \tag{3.167}$$

This allows us to extract the loops over the soft-sensitive red lines, $S(k_i,n_i)$, from the soft-insensitive loops, $H(P_j,k_i)$. Since the soft-sensitive loops are at most logarithmically divergent by the *Log Lemma* (Lemma 2), the second term is finite because $H(P_j,k_i)-H(P_j,0)$ vanishes when the $k_i\to 0$. Thus, we can pull out an overall IR-insensitive power series, $\mathcal{C}(\{n_i\cdot P_j\})$, times the pure-eikonal loops which are identically given by the matrix element of Wilson lines shown in Eq. (3.166). Now, the second term on the right-hand side of Eq. (3.167) could either be power-suppressed (for example, if the $k_i\to 0$ limit in question is tangled with a soft emission by Lemma 8), or it could be some IR-finite integral multiplying a lower-order IR-sensitive contribution from the soft Wilson-line matrix element. Thus, $\mathcal{C}(\{n_i\cdot P_j\})$ is not equal to $H(P_j,0)$ in general. Instead, it is some IR insensitive power series in the perturbative coupling that starts at 1. Despite the difference, $\mathcal{C}(\{n_i\cdot P_j\})$, like $H(P_j,0)$, only depends on the net momenta in each collinear sector. The difference is from the subtraction terms on the right-hand side of Eq. (3.167) which is subleading power when tangled with external emissions, by Lemma 8.

Now, combining Eq. (3.163), Eq. (3.165) and Eq. (3.166), and that, since the J_j blob contains no red lines it is simply all the corrections to the j-sector in full QCD, we have

$$\langle X_j;X_s|\,Y_1^\dagger\cdots\phi^\star\cdots Y_N\,|0\rangle \overset{\substack{r_s=p_j\\ \text{gen. } r_c}}{\cong} \mathcal{C}(\{n_i\cdot P_j\})\,\langle X_j|\,\phi^\star\,|0\rangle\,\langle X_s|\,Y_1^\dagger\cdots Y_{j-1}Y_{j+1}\cdots Y_N\,|0\rangle \tag{3.168}$$

In other words, $r_s = p_j$ lets us disentangle a field from the product of Wilson lines.

3.9.3 Bootstrapping in $Y_j^\dagger$ and W_j

At this point, following [3], we want to insert $Y_j^\dagger$ into $Y_1^\dagger \cdots Y_{j-1} Y_{j+1} \cdots Y_N$ in Eq. (3.168) to make it gauge invariant. Recall that at tree-level choosing $r_s = p_j$ for the external soft particles forces $Y_j^\dagger$ to contribute only power-suppressed terms. When loops are involved, it is not quite that simple, since the red lines are not restricted to be soft. Indeed, self-contractions in $Y_j^\dagger$ (self-energy graphs on the j-leg) are collinear sensitive, since in the collinear-sensitive region the gluon propagator has the collinear reference vector r_c instead of r_s. Thus it is true at tree-level but not at loop-level that inserting $Y_j^\dagger$ only gives a power-suppressed modification in collinear-r_s.

When $r_s = p_j$, contractions of $Y_j^\dagger$ with the other Y_i's are soft insensitive by the *Collinear-r_s Lemma* (Lemma 11) and must be blue. Then, by the *Hard-Blue Lemma* (Lemma 6), we know that any contractions of $Y_j^\dagger$ with the other Y_i's are IR insensitive in physical gauges, as are any 1PI subdiagrams containing such contractions. So when $r_s = p_j$, the *only* new IR sensitivities that arise from adding in the $Y_j^\dagger$ are the collinear sensitivities in new self-energy type corrections to the p_j sector, namely from purely self-contractions of the $Y_j^\dagger$ operator. The sum of the purely self-contractions of $Y_j^\dagger$ is trivially given by $\langle 0 | Y_j^\dagger | 0 \rangle$. Therefore, if we not only add the $Y_j^\dagger$ into the product of $Y_1^\dagger \cdots Y_{j-1} Y_{j+1} \cdots Y_N$ but also divide by $\langle 0 | Y_j^\dagger | 0 \rangle$, the new collinear-sensitive contributions from $Y_j^\dagger$ will be completely removed, and this addition does not change the IR sensitivities.

The net effect of adding $Y_j^\dagger$ to the product of Wilson lines and dividing by

$\langle 0|\, Y_j^\dagger\, |0\rangle$ is not nothing. There are graphs from this modification with gluons going between $Y_j^\dagger$ and one of the other legs. These contributions are soft insensitive (in factorization gauge with $r_s = r_p$) and collinear insensitive (since they connect different legs, by Lemma 6), thus they are IR insensitive. Using the same procedure as outlined in Eq. (3.167), we can absorb the IR-insensitive difference into a modification of the Wilson coefficient, which means that Eq. (3.168) becomes

$$\langle X_j; X_s|\; Y_1^\dagger \cdots \phi^\star \cdots Y_N\, |0\rangle \overset{\substack{r_s = p_j \\ \text{gen. } r_c}}{\cong} \mathcal{C}'(\{n_i{\cdot}P_j\})\; \langle X_j|\, \phi^\star\, |0\rangle\; \frac{\langle X_s|\, Y_1^\dagger \cdots Y_N\, |0\rangle}{\langle 0|\, Y_j^\dagger\, |0\rangle} \tag{3.169}$$

for some new IR-insensitive function $\mathcal{C}'(\{n_i \cdot P_j\})$.

This is the second time we find two objects with the same leading-power IR sensitivities differing by an IR-insensitive set of loops. Rather than modifying the Wilson coefficient, $\mathcal{C}(\{n_i{\cdot}P_j\})$, in each step for the IR-insensitive part, let us introduce the symbol $\cong_{\text{IR}}$ to mean that the IR-sensitivities on both sides agree at leading power. For example, with this notation, Eq. (3.169) becomes:

$$\langle X_j; X_s|\; Y_1^\dagger \cdots \phi^\star \cdots Y_N\, |0\rangle \overset{\substack{r_s = p_j \\ \text{gen. } r_c}}{\cong_{\text{IR}}} \langle X_j|\, \phi^\star\, |0\rangle\; \frac{\langle X_s|\, Y_1^\dagger \cdots Y_N\, |0\rangle}{\langle 0|\, Y_j^\dagger\, |0\rangle} \tag{3.170}$$

An $\cong_{\text{IR}}$ equivalence implies that a $\cong$ equivalence holds if some IR finite Wilson coefficient, $\mathcal{C}(\{P_i \cdot P_j\})$, is multiplied on one side. That is

$$A \;\cong_{\text{IR}}\; B \quad\Longleftrightarrow\quad \frac{A}{B} \cong \mathcal{C}(S_{ij}) \tag{3.171}$$

for some IR-insensitive function $\mathcal{C}(S_{ij})$, where $S_{ij} = (P_i + P_j)^2$.

Next, we show that collinear Wilson lines can be added without changing the IR structure. Recall that collinear Wilson lines W_j have the same definition as soft

Wilson lines Y_j, but while the Y_j point along the jet direction p_j, the W_j lines point in some direction t_j which is only restricted not to be collinear to p_j. In lightcone gauge, if we choose $t_j = r$, then W_j simply decouples since the gluons all have $t_\mu^j \, \Pi^{\mu\nu}(k) = 0$ for any k and $W_j = 1$ effectively. In factorization gauge with $r_s = p_j$ and t_j and r_c generic, the Wilson lines do not decouple completely. However, it is still true that

$$\frac{\langle X_j | \, \phi^\star W_j \, | 0 \rangle}{\langle 0 | \, Y_j^\dagger W_j \, | 0 \rangle} \overset{\substack{r_s = p_j \\ \text{gen. } r_c}}{\cong_{\text{IR}}} \frac{\langle X_j | \, \phi^\star \, | 0 \rangle}{\langle 0 | \, Y_j^\dagger \, | 0 \rangle} \tag{3.172}$$

This is true for exactly the same reason that we could bootstrap $Y_j^\dagger$ into Eq. (3.169): when $r_s = p_j$, any lines connecting to $\phi^\star$ and $Y_j^\dagger$ are blue by Lemma 11. This means, by Lemma 6, that the only new IR sensitivities introduced on the left-hand side of Eq. (3.172) are those coming from purely self contractions of W_j which cancel in the ratio, proving Eq. (3.172).

Now, since no red lines can connect to $\phi^\star$ or to $Y_j^\dagger$ when $r_s = p_j$, the right-hand side of Eq. (3.172) must be soft insensitive. This implies that the left-hand side is soft insensitive too. Since the left-hand side is gauge invariant, it is soft insensitive in any gauge. In other words, $\langle X_j | \, \phi^\star W_j \, | 0 \rangle \, / \, \langle 0 | \, Y_j^\dagger W_j \, | 0 \rangle$ contains only blue lines. Moreover, these all-blue-line graphs cannot come from $\langle 0 | \, Y_j^\dagger W_j \, | 0 \rangle$ or $\langle X_j | \, W_j \, | 0 \rangle$ since these matrix elements, involving Wilson lines only, always have red lines attaching to the Wilson lines (with an arbitrary S blob connecting them). Thus the blue lines can come from $\langle X_j | \, \phi^\star \, | 0 \rangle$ or from contractions between W_j and $\phi^\star$. However, blue contractions between W_j and $\phi^\star$ are IR insensitive by the *Hard-Blue Lemma* (Lemma 6). Therefore, we have

$$\frac{\langle X_j | \, \phi^\star W_j \, | 0 \rangle}{\langle 0 | \, Y_j^\dagger W_j \, | 0 \rangle} \overset{\text{gen. } r_c}{\cong_{\text{IR}}} \langle X_j | \, \phi^\star \, | 0 \rangle \Big|_{\text{blue only}} = \otimes \; \boxed{J_j} \; = \text{soft insensitive} \tag{3.173}$$

where the J_j blob has only blue lines. We use this result below to strip the red lines off of a general matrix element.

Let us pause briefly to give an interpretation of $\langle 0|\, Y_j^\dagger W_j\, |0\rangle$. Note that $\langle X_j|\, \phi^\star W_j\, |0\rangle$ has both collinear and soft sensitivities, but $\langle X_j|\, \phi^\star W_j\, |0\rangle \,/\, \langle 0|\, Y_j^\dagger W_j\, |0\rangle$ has only blue lines so it is soft-insensitive. Thus $\langle 0|\, Y_j^\dagger W_j\, |0\rangle$ is subtracting off the contribution which is both soft and collinear sensitive. Dividing by it implements the subtraction procedure known as the zero-bin subtraction in SCET. We will discuss this further in Section 3.13 where we contrast our matrix-element definition with that used in the SCET literature.

Returning to Eq. (3.172), if we combine it with Eq. (3.170), we find

$$\langle X_j; X_s|\, Y_1^\dagger \cdots \phi^\star \cdots Y_N\, |0\rangle \;\cong_{\text{IR}}\; \frac{\langle X_j|\, \phi^\star W_j\, |0\rangle}{\langle 0|\, Y_j^\dagger W_j\, |0\rangle} \times \langle X_s|\, Y_1^\dagger \cdots Y_N\, |0\rangle \tag{3.174}$$

Although we only showed this IR-equivalence in collinear r_s ($r_s = r_h = p_j$, generic r_c) since both sides of this equation are gauge invariant, it must hold for any choice of r_s or r_c and more generally in any gauge (including Feynman gauge). Thus, Eq. (3.174) is not restricted to a particular gauge.

Note that Eq. (3.174) holds for any number of soft Wilson lines. As a special case, when there are two sectors:

$$\langle X_j; X_s|\, \phi^\star\, Y_i\, |0\rangle \;\cong_{\text{IR}}\; \frac{\langle X_j|\, \phi^\star W_j\, |0\rangle}{\langle 0|\, Y_j^\dagger W_j\, |0\rangle} \times \langle X_s|\, Y_j^\dagger\, Y_i\, |0\rangle \tag{3.175}$$

which holds for any i and j.

3.9.4 Sprig of thyme

Eq. (3.174) (or more simply, Eq. (3.175)) establishes soft-collinear factorization for a single non-minimal collinear sector. When multiple sectors are non-minimal, we clearly cannot choose $r_s = p_j$ for all j simultaneously to repeat the above derivation. However, since Eq. (3.174) is gauge-independent, this is not necessary, as we will see.

When r_s^μ is not collinear to p_j^μ, Eq. (3.174) still holds, since it is gauge invariant. For generic choices of r_s, there are soft-sensitive diagrams with red lines connecting to the J_j blob contributing to Eq. (3.174). Although there is no diagram-by-diagram correspondence in Eq. (3.174), the sum of diagrams with a J_j blob and a fixed number n of red lines attaching to it do correspond. In fact, as we will now show,

$$\sum_{\text{perms on } j} \quad \overset{\text{gen. } r_c}{\underset{\text{IR}}{\cong}} \quad \frac{\langle X_j |\, \phi^\star W_j \,| 0\rangle}{\langle 0 |\, Y_j^\dagger W_j \,| 0\rangle} \times Y_j^\dagger \Big|_{n \text{ red}} \tag{3.176}$$

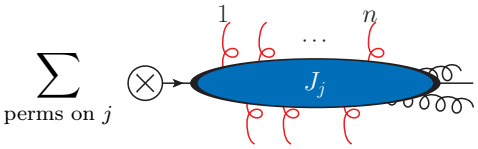

On the left-hand side, the usual J_j blob is defined to have only blue (soft-insensitive) lines and to have all such lines summed over and their integrals evaluated. We are considering diagrams which have n generically off-shell red lines attaching to this J_j blob. In a full diagram the red lines can be closed into a loop, contracted with polarizations for external soft particles, or connect to a J blob in another sector (not shown); we simply slice them close to their attachment to the J_j blob and treat them as off-shell. The $\sum_{\text{perms on } j}$ means the sum over permutations of all possible ways of connecting the red lines to J_j blob on the left-hand side. The right side has these same red lines now connecting to a $Y_j^\dagger$ Wilson line; the $Y_j^\dagger$ on the right-hand side is meant to be taken at the same order as the number of red lines on the left, as indicated by the $|_n$.

Eq. (3.176) is the loop-level equivalent of the tree-level Eq. (94) in [3]. It shows that red lines can be stripped off of arbitrarily complicated jet amplitudes, like leaves off a sprig of thyme, independent of where those red lines connect in the rest of the diagram.

Proof of Eq. (3.176) (**Sprig-of-Thyme**) . We will prove Eq. (3.176) by induction on the number of red lines n leaving the J_j blob. The key, as in [3], is to cancel all diagrams which contribute to both sides of Eq. (3.176) but have fewer than n red lines attaching to the J_j blob using Eq. (3.175) and the induction hypothesis. The remaining diagrams will have all n red lines connecting to the J_j blob so that Eq. (3.176) follows from Eq. (3.175).To avoid the notational quagmire of an algebraic induction proof as was done in Ch. 2, in this chapter we take a diagrammatic approach.

To begin note that both sides of Eq. (3.175) can be decomposed into colored diagrams. We will thus consider all of the blue diagrams in Eq. (3.175) with a fixed number of red lines emerging from the J_j blob.

n=0: With no red lines coming out of $Y_j^\dagger$, this Wilson line is simply 1 and Eq. (3.176) follows from Eq. (3.173) exactly:

$$\overset{\text{gen. } r_c}{\cong_{\text{IR}}} \quad \frac{\langle X_j |\, \phi^\star W_j \,| 0\rangle}{\langle 0 |\, Y_j^\dagger W_j \,| 0\rangle} \tag{3.177}$$

n=1: Consider Eq. (3.175) with one red end attached anywhere. Since there is only one red end attached, the red line must be part of $\langle X_s| = \langle k|$. Then the left-hand side of Eq. (3.175), at this order, is given by

$$\langle X_j; k |\, \phi^\star\, Y_i \,| 0\rangle \Big|_{1 \text{ red}} \overset{\text{gen. } r_c}{\cong_{\text{IR}}} \sum_{\text{perms on } j}$$

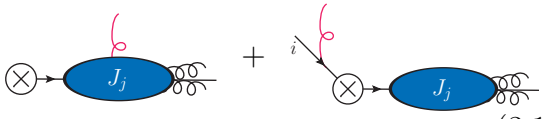

(3.178)

On the right-hand side of Eq. (3.175) the red line can only come from one of the Wilson lines in $\langle k|\, Y_j^\dagger Y_i\, |0\rangle$ (since the other factor is all blue), so

$$\left(\frac{\langle X_j|\, \phi^\star W_j\, |0\rangle}{\langle 0|\, Y_j^\dagger W_j\, |0\rangle}\, \langle X_s|\, Y_j^\dagger Y_i\, |0\rangle\right)\Big|_{1\text{ red}} = \frac{\langle X_j|\, \phi^\star W_j\, |0\rangle}{\langle 0|\, Y_j^\dagger W_j\, |0\rangle}\left(\langle k|\, Y_j^\dagger\, |0\rangle\Big|_{1\text{ red}} + \langle k|\, Y_i\, |0\rangle\Big|_{1\text{ red}}\right) \tag{3.179}$$

By Eq. (3.175), Eqs (3.178) and (3.179) are equal. By Eq. (3.177), the second term on the right-hand sides of Eqs (3.178) and (3.179) are separately equal. This leaves

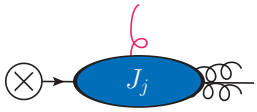

$$\overset{\text{gen. } r_c}{\underset{\text{IR}}{\cong}} \frac{\langle X_j|\, \phi_j^\star W_j\, |0\rangle}{\langle 0|\, Y_j^\dagger W_j\, |0\rangle} \times \langle k|\, Y_j^\dagger\, |0\rangle\Big|_{1\text{ red}} \tag{3.180}$$

We can now strip off the polarization vector (the contraction with the external state) because the vertex Feynman rule is the same for a red line in a loop connecting to another sector or for a real-emission, as discussed in Eq. (3.126) and also in the *Soft-Attachment Lemma* (Lemma 10). Thus, Eq. (3.180) establishes Eq. (3.176) for $n = 1$.

n=2: At $n = 2$, if the red lines are all external, Eq. (3.175), gives

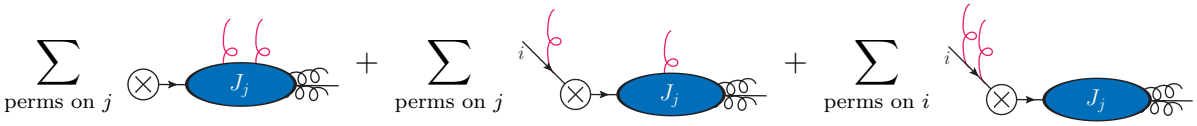

$$\overset{\text{gen. } r_c}{\underset{\text{IR}}{\cong}} \frac{\langle X_j|\, \phi_j^\star W_j\, |0\rangle}{\langle 0|\, Y_j^\dagger W_j\, |0\rangle}\left(\langle k_1, k_2|\, Y_j^\dagger Y_i\, |0\rangle\right)\Big|_{2\text{ red}} \tag{3.181}$$

Using Eq. (3.177), the $\sum_{\text{perms on } i}$ terms cancel term-by-term with the $\mathcal{O}(g^2)$ contractions of the external states with the Y_i Wilson line. The middle term cancels with the $\mathcal{O}(g)$ contractions of the external states with the Y_i and $Y_j^\dagger$ operators using the previous induction step, Eq. (3.180). We are left with

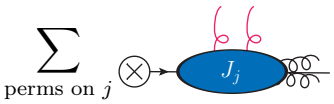

$$\overset{\text{gen. } r_c}{\underset{\text{IR}}{\cong}} \frac{\langle X_j|\, \phi^\star W_j\, |0\rangle}{\langle 0|\, Y_j^\dagger W_j\, |0\rangle} \times \langle k_1, k_2|\, Y_j^\dagger\, |0\rangle\Big|_{2\text{ red}} \tag{3.182}$$

This and the previous case are almost identical to the tree-level proof since there are as many external emissions as orders, n. That is, there are no red loops and we simply cancel off emissions off of the $i \neq j$ sector term-by-term using the previous induction hypotheses.

If the red lines are in a loop, then all cases where the red lines do not both come off the j line still cancel by the previous induction steps (which already have the polarization vectors stripped off). Thus, after canceling these terms off in Eq. (3.175), we are left with:

$$\sum_{\text{perms on } j} \quad \overset{\text{gen. } r_c}{\underset{\text{IR}}{\cong}} \quad \frac{\langle X_j |\, \phi^\star W_j \,| 0\rangle}{\langle 0 |\, Y_j^\dagger W_j \,| 0\rangle} \langle 0 |\, \overset{\sqcap}{Y_j^\dagger} \,| 0\rangle \Big|_{2 \text{ red}} \tag{3.183}$$

The indicated contraction is superfluous, since $\langle 0 |\, Y_j^\dagger \,| 0\rangle$ only has red lines and we are restricting it to only 2 red vertices. The combination of Eq. (3.182) and Eq. (3.183) mean that Eq. (3.176) holds for $n = 2$.

Arbitrary n: It should now be clear how the induction step works: at every step, all of the diagrams in Eq. (3.175) cancel except those with all of the red lines on the jth sector. That is, using all of the previous induction steps, this cancellation occurs between all of the contractions of the Wilson lines except those that only involve $Y_j^\dagger$. After canceling the terms off, we are left with the result for any n. Hence, Eq. (3.176) is proved.

□

3.9.5 Final steps

Eq. (3.176) implies that we can strip red lines off sector-by-sector of the general reduced-diagram in Eq. (3.148):

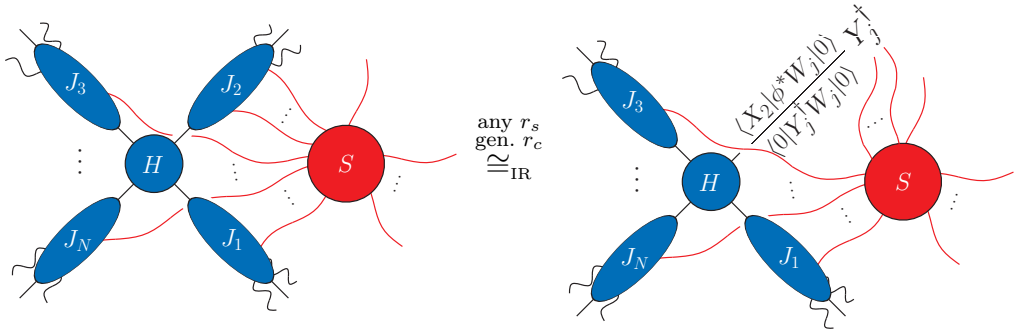

(3.184)

Once the red lines are stripped off of every collinear sector, they connect from the soft Wilson lines, through the S blob, to the external emissions. The S blob gives all possible interactions with the full QCD Lagrangian Feynman rules, so the red lines are exactly described by the matrix element $\langle X_s|\, Y_1^\dagger \cdots Y_N\,|0\rangle$ in QCD. Thus,

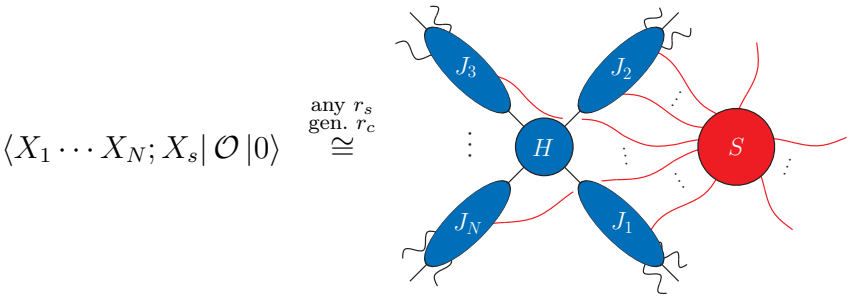

$$\overset{\substack{\text{any } r_s \\ \text{gen. } r_c \\ \cong_{\text{IR}}}}{} \underbrace{\frac{\langle X_1|\,\phi^\star W_1\,|0\rangle}{\langle 0|\,Y_1^\dagger W_1\,|0\rangle}}_{\text{blue only, } J_1} \cdots \underbrace{\frac{\langle X_N|\,W_N^\dagger \phi\,|0\rangle}{\langle 0|\,W_N^\dagger Y_N\,|0\rangle}}_{\text{blue only, } J_N} \times \underbrace{\langle X_s|\,Y_1^\dagger \cdots Y_N\,|0\rangle}_{\text{red only, } S} \tag{3.185}$$

The braces describe which parts of the reduced diagram the indicated quantities reproduce, in physical gauges. Since both sides are gauge invariant, this factorization formula holds in any gauge, even covariant ones.

This completes the proof of hard-soft-collinear factorization. To clean things up, we can drop the $\cong_{\text{IR}}$ sign in favor of the leading-power equality, $\cong$, by adding in the Wilson coefficient. At every stage that we have dropped IR-insensitive loops, they have not contained external emissions by Lemma 8, so the Wilson coefficient is still independent of the states, $\langle X_j|$ and $\langle X_s|$, and only depends on the net momentum in each collinear sector (using the procedure of Eq. (3.167)). Therefore, we have our final factorization formula:

$$\boxed{\langle X_1 \cdots X_N; X_s | \, \mathcal{O} \, |0\rangle \;\cong\; C(S_{ij}) \, \frac{\langle X_1 | \, \phi^\star W_1 \, |0\rangle}{\langle 0 | \, Y_1^\dagger W_1 \, |0\rangle} \, \cdots \, \frac{\langle X_N | \, W_N^\dagger \phi \, |0\rangle}{\langle 0 | \, W_N^\dagger Y_N \, |0\rangle} \, \langle X_s | \, Y_1^\dagger \cdots Y_N \, |0\rangle}$$
(3.186)

3.10 General scattering amplitudes

So far, we have discussed factorization for matrix elements of local operators. None of the arguments given to derive the structure of the reduced diagram in Eq. (3.148) actually require the scattering to be mediated by a single operator. In calculating a general scattering matrix element, any line that cannot go on-shell cannot be IR sensitive. Thus off-shell lines can be included in the hard amplitude of the reduced diagram and absorbed into the Wilson coefficient.

For example, we have already shown that matrix elements for the operator $|\phi|^2$ between the vacuum and final states $\langle X_3 X_4; X_s|$ factorize as

$$\langle X_3 X_4; X_s | \, \phi^\star \phi \, |0\rangle \cong \mathcal{C}_{|\phi|^2}(S_{34}) \, \frac{\langle X_3 | \, \phi^\star W_3 \, |0\rangle}{\langle 0 | \, Y_3^\dagger W_3 \, |0\rangle} \, \frac{\langle X_4 | \, W_4^\dagger \phi \, |0\rangle}{\langle 0 | \, W_4^\dagger Y_4 \, |0\rangle} \, \langle X_s | \, Y_3^\dagger Y_4 \, |0\rangle \quad (3.187)$$

where $S_{34} = (P_3 + P_4)^2$ and $\mathcal{C}_{|\phi|^2}(S_{34}) = 1$ at tree level. Let us compare this to

$\gamma\gamma \to \phi\phi^\star$ in scalar QED. At tree level, three diagrams contribute:

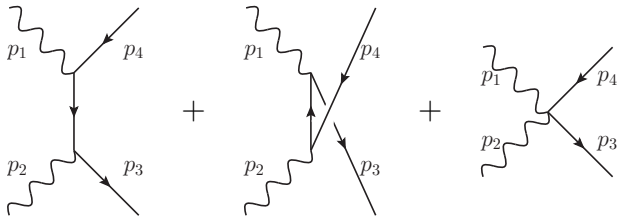

(3.188)

Due to the off-shell lines, this amplitude cannot be written exactly as the matrix element of a local operator. On the other hand, since the lines are off-shell, we can still factorize the amplitude for $\gamma\gamma \to \langle X_3 X_4; X_s|$ as

$$\langle X_3 X_4; X_s|\epsilon^\mu(p_1);\epsilon^\nu(p_2)\rangle \cong \epsilon^1_\mu \epsilon^2_\nu \, \mathcal{C}^{\mu\nu}_{\gamma\gamma\phi\phi^\star}(S_{ij}) \, \frac{\langle X_3|\,\phi^\star W_3\,|0\rangle}{\langle 0|\,Y_3^\dagger W_3\,|0\rangle} \, \frac{\langle X_4|\,W_4^\dagger \phi\,|0\rangle}{\langle 0|\,W_4^\dagger Y_4\,|0\rangle} \, \langle X_s|\,Y_3^\dagger Y_4\,|0\rangle \tag{3.189}$$

with

$$\mathcal{C}^{\mu\nu}_{\gamma\gamma\phi\phi^\star}(s_{ij}) = e^2 \left[\frac{(2p_4^\mu - p_1^\mu)(p_2^\nu - 2p_3^\nu)}{(p_1 - p_4)^2} + \frac{(2p_3^\mu - p_1^\mu)(p_2^\nu - 2p_4^\nu)}{(p_3 - p_1)^2} + 2ig^{\mu\nu} \right] \tag{3.190}$$

at tree level.

At higher orders, the Wilson coefficients $\mathcal{C}_{|\phi|^2}$ and $\mathcal{C}^{\mu\nu}_{\gamma\gamma\phi\phi^\star}$ will get different radiative corrections, but the jet and soft sectors of the factorized processes are identical. The all-orders definitions of the Wilson coefficients are

$$\mathcal{C}_{|\phi|^2}(Q) = \frac{\langle \phi, p_3; \phi^\star, p_4|\,\phi^\star\phi\,|0\rangle}{\dfrac{\langle \phi, p_3|\,\phi^\star W_3\,|0\rangle}{\langle 0|\,Y_3^\dagger W_3\,|0\rangle} \, \dfrac{\langle \phi^\star, p_4|\,W_4^\dagger \phi\,|0\rangle}{\langle 0|\,W_4^\dagger Y_4\,|0\rangle} \, \langle 0|\,Y_3^\dagger Y_4\,|0\rangle} \tag{3.191}$$

and

$$\mathcal{C}_{\gamma\gamma\phi\phi^\star}(Q) = \frac{\langle \phi, p_3; \phi^\star, p_4|\epsilon^\mu(p_1);\epsilon^\nu(p_2)\rangle}{\dfrac{\langle \phi, p_3|\,\phi^\star W_3\,|0\rangle}{\langle 0|\,Y_3^\dagger W_3\,|0\rangle} \, \dfrac{\langle \phi^\star, p_4|\,W_4^\dagger \phi\,|0\rangle}{\langle 0|\,W_4^\dagger Y_4\,|0\rangle} \, \langle 0|\,Y_3^\dagger Y_4\,|0\rangle} \tag{3.192}$$

In either case, the Wilson coefficient only depends on the type of scattering and not on distribution of soft and collinear radiation in the external states $\langle X_3 X_4; X_s|$. Thus,

we see that the factorization arguments given in this chapter apply to any type of scattering process in any gauge theory as long as the external states contain only soft and collinear degrees of freedom.

Factorization holds with identical arguments when there are collinear particles in the initial state, with the only change that the Wilson lines become incoming (see [3]). The situation where particles in the initial state are collinear to particles in the final state are explicitly *excluded* from our formulation. In particular, general hadron-hadron scattering is not described if there are spectator partons with significant energy. The formula does apply to the special case of threshold hadron-hadron scattering, where the partonic center-of-mass is close to the machine energy so the spectator partons are necessarily soft. Expanding around this limit has proved useful in both total-cross-section calculations [103, 104] and jet shape calculations at hadron colliders [16, 17, 23, 71, 105, 106].

3.11 QCD

All of the arguments in the proof of hard-soft-collinear factorization are completely general. They apply to any renormalizable Abelian or non-Abelian gauge theory with any matter content. The change in going from scalar QED to QCD essentially amounts to pinpointing where the color indices go. We will use h_i for fundamental color indices and $a, b, \cdots$ for adjoint indices, with i and j still denoting jet directions.

3.11.1 Jet amplitudes

To add in the color contractions, we trace back through the soft-collinear factorization discussion, replacing scalars with quarks. Eq. (3.173) becomes

$$= \langle X_j | \, \bar{\psi} \, |0\rangle^h \Big|_{\text{blue only}} \tag{3.193}$$

Here the h color index comes from the net color of the state $\langle X_j|$ that exits the jet blob on the left. Now, recall that in factorization gauge with $r_s = p_j$ no soft sensitive lines can attach to the j-collinear sector, which led to Eqs. (3.172) and (3.173). In QCD these equations become

$$\overset{\substack{r_s = p_j \\ \text{gen. } r_c}}{\cong_{\text{IR}}} \langle X_j | \, \bar{\psi} \, |0\rangle^{h'} \left[\frac{1}{\langle 0 | \, Y_j^\dagger \, |0\rangle} \right]^{h'h} \overset{\text{gen. } r_c}{\cong_{\text{IR}}} \langle X_j | \, \bar{\psi} W_j \, |0\rangle^{h'} \left[\frac{1}{\langle 0 | \, Y_j^\dagger W_j \, |0\rangle} \right]^{h'h} \tag{3.194}$$

One can think of W_j as bringing color h' in from infinity to the origin along the t_j direction. Now the vacuum is gauge invariant, so

$$\langle 0 | \, Y_j^\dagger W_j \, |0\rangle^{hh'} = \frac{1}{N_c} \text{tr} \, \langle 0 | \, Y_j^\dagger W_j \, |0\rangle \; \delta^{hh'} \tag{3.195}$$

and therefore

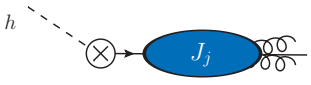

$$\overset{\text{gen. } r_c}{\cong_{\text{IR}}} \; N_c \frac{\langle X_j | \, \bar{\psi} W_j \, |0\rangle^h}{\text{tr} \, \langle 0 | \, Y_j^\dagger W_j \, |0\rangle} \tag{3.196}$$

Similarly, the sprig-of-thyme equation, Eq. (3.176) for a quark jet becomes

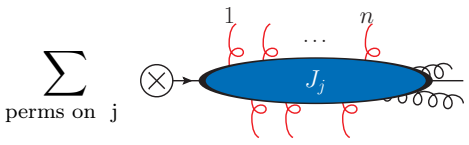

$$\sum_{\text{perms on j}} \overset{\text{gen-}r_c}{\cong_{\text{IR}}} \frac{\langle X_j | \, \bar{\psi} W_j \, |0\rangle^{h'}}{\text{tr} \, \langle 0 | \, Y_j^\dagger W_j \, |0\rangle} \times \left(Y_j^\dagger \right)^{h'h} \Big|_n \tag{3.197}$$

With the N_c factor implicitly absorbed into the Wilson coefficient (by the definition of $\cong_{\text{IR}}$). Pulling n gluons out of the soft Wilson line gives a series of T^a matrices which multiply through to convert h' to h. The color indices on the soft Wilson line

represent a matrix which transforms the color coming out of the hard process due to the soft radiation. It is, of course, highly nontrivial that the color within the jet is manipulated only by $\bar{\psi}$ and W_j and the color of the soft radiation is manipulated only by Y_j, with the two not interacting. It is also true, since the soft radiation only senses the net color charge of the collinear radiation. This follows from our proof because in $r_s = p_j$ the soft radiation comes from everywhere else in the event (which has the opposite color charge as the jet). All of the manipulations we did to prove soft-collinear factorization used only gauge invariance and that in the soft limit, gluon emissions are reproduced by the matrix element of a path-ordered Wilson line (a fact both well-known and proven in [3]).

The sprig-of-thyme for gluon jets is similar, but involves adjoint Wilson lines, $\mathcal{Y}_j$ and $\mathcal{W}_j$ defined in Eq. (3.33). The equivalent of Eq. (3.197) with adjoint vector fields is

$$\sum_{\text{perms on j}} \quad \overset{\text{gen-}r_c}{\underset{\text{IR}}{\cong}} \quad \frac{\langle X_j | A^\mu \mathcal{W}_j | 0 \rangle^b}{\operatorname{tr} \langle 0 | \mathcal{Y}_j^\dagger \mathcal{W}_j | 0 \rangle} \times \left(\mathcal{Y}_j^\dagger\right)^{ba} \Big|_n \tag{3.198}$$

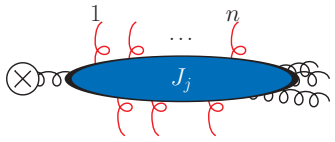

where $\operatorname{tr} \delta^{ab} = d(\text{adj}) = N_c^2 - 1$ is again dropped. Note that adjoint Wilson lines are not themselves Hermetian, despite the fact that the adjoint representation is real. Conjugating a path-ordered Wilson lines reverses the order of the matrices. Thus, the correct relation between an adjoint Wilson line and its conjugate is $(\mathcal{Y}^\dagger)^{ab} = \mathcal{Y}^{ba}$.

Although $A_\mu^c \mathcal{W}_j^{cb}$ is the obvious adjoint-version of $\bar{\psi} W_j$, it is somewhat jarring to see an operator with a raw gauge field instead of covariant derivatives. Of course, since any matrix element of a color-singlet operator will satisfy the Ward identity, any factorized expression containing A_μ^a will also satisfy the Ward identity. It is nevertheless sometimes useful to rewrite the gluon jet function in terms of covariant

derivatives.

If the original operator has A^a_μ in a covariant derivative in the fundamental representation, such as $\mathcal{O} = \bar{\psi}\not{A}\psi$, then A^a_μ will come accompanied by a T^a. Thus there will be a $T^a_{hh'}$ contracted with the a index in (3.198), with h and h' contracted elsewhere in the factorized expression. Now, use $Y_j^\dagger T^a Y_j = \mathcal{Y}_j^{ab} T^b$, as in Eq. (3.35), $(\mathcal{Y}^\dagger)^{ab} = \mathcal{Y}^{ba}$, and $\mathrm{tr}[T^a T^b] = T_F \delta^{ab}$, we find

$$\begin{aligned}
\mathcal{W}_j^{ab}\big(\mathcal{Y}_j^\dagger\big)^{bc} T^c_{hh'} &= \mathcal{W}_j^{ab}\big(Y_j T^b Y_j^\dagger\big)_{hh'} \\
&= T_F^{-1}\mathrm{tr}[T^a T^c]\mathcal{W}_j^{cb}\big(Y_j T^b Y_j^\dagger\big)_{hh'} \\
&= T_F^{-1}\mathrm{tr}[T^a W_j T^b W_j^\dagger]\big(Y_j T^b Y_j^\dagger\big)_{hh'}
\end{aligned} \tag{3.199}$$

Since the Ward identity must be satisfied in any process we consider, replacing $A_\mu \to \partial_\mu$ gives zero. Thus, we can replace $ig_s A^a_\mu \mathrm{tr}[T^a W_j T^b W_j^\dagger] \to \mathrm{tr}[W_j^\dagger D_\mu W_j T^b]$. Therefore, converting the denominator with similar manipulations to those in Eq. (3.199) and absorbing ig_s into the Wilson coefficient, we can write

$$\sum_{\text{perms on j}} \quad \times T^a_{hh'} \overset{\text{gen-}r_c}{\cong}_{\text{IR}} \frac{\mathrm{tr}\,\langle X_j|\, W_j^\dagger D_\mu W_j T^b\,|0\rangle}{\mathrm{tr}\,\langle 0|\, W_j^\dagger (Y_j T^a Y_j^\dagger) W_j T^a\,|0\rangle}\big(Y_j T^b Y_j^\dagger\big)_{hh'}\Big|_n \tag{3.200}$$

Jet amplitudes in this form are occasionally useful since they manifest gauge invariance and only have Wilson lines in the fundamental representation.

3.11.2 Example factorization formulas

To write down the factorization formula in QCD for some process, we simply combine copies of Eqs. (3.197) and (3.200) for each quark or gluon jet direction and contract the loose soft-Wilson lines with the soft-sector final state. For example, a

vector boson decaying to 3 jets can be mediated by a hard-scattering operator of the form

$$\mathcal{O} = \bar{\psi} \not{D} \psi \tag{3.201}$$

The associated factorization formula is, in gluon-jet notation

$$\begin{aligned}
&\langle X_1 X_2 X_3; X_s | \, \bar{\psi} \not{D} \psi \, | 0 \rangle \\
&\cong \mathcal{C}(S_{ij}) \, \gamma^\mu_{\alpha\beta} \, \frac{\langle X_1 | \, \bar{\psi} \, W_1 \, | 0 \rangle^{\alpha \, h_1}}{\mathrm{tr} \, \langle 0 | \, Y_1^\dagger W_1 \, | 0 \rangle} \, \frac{\langle X_j | \, A^\mu \mathcal{W}_j \, | 0 \rangle^a}{\mathrm{tr} \, \langle 0 | \, \mathcal{Y}_j^\dagger \mathcal{W}_j \, | 0 \rangle} \, \frac{\langle X_3 | \, W_3^\dagger \, \psi \, | 0 \rangle^{\beta \, h_3}}{\mathrm{tr} \, \langle 0 | \, W_3^\dagger Y_3 \, | 0 \rangle} \, \langle X_s | \, Y_1^\dagger \mathcal{Y}_2^{\dagger ab} T^b \, Y_3 \, | 0 \rangle^{h_1 h_3}
\end{aligned} \tag{3.202}$$

or, representing the gluons with covariant derivatives,

$$\begin{aligned}
&\langle X_1 X_2 X_3; X_s | \, \bar{\psi} \not{D} \psi \, | 0 \rangle \\
&\quad \cong \mathcal{C}(S_{ij}) \, \gamma^\mu_{\alpha\beta} \, \frac{\langle X_1 | \, \bar{\psi} \, W_1 \, | 0 \rangle^{\alpha \, h_1}}{\mathrm{tr} \, \langle 0 | \, Y_1^\dagger W_1 \, | 0 \rangle} \, \frac{\mathrm{tr} \, \langle X_2 | \, W_2^\dagger D_\mu W_2 T^a \, | 0 \rangle}{\mathrm{tr} \, \langle 0 | \, W_2^\dagger (Y_2 T^b Y_2^\dagger) W_2 T^b \, | 0 \rangle} \, \frac{\langle X_3 | \, W_3^\dagger \, \psi \, | 0 \rangle^{\beta \, h_3}}{\mathrm{tr} \, \langle 0 | \, W_3^\dagger Y_3 \, | 0 \rangle} \\
&\qquad\qquad\qquad\qquad\qquad\qquad \times \langle X_s | \, Y_1^\dagger \, Y_2 T^a Y_2^\dagger \, Y_3 \, | 0 \rangle^{h_1 h_3}
\end{aligned} \tag{3.203}$$

where α and β are Dirac spin indices, a and b are adjoint color indices and h_i are fundamental color indices. To reduce clutter, the N_c and $N_c^2 - 1$ factors from the traces have been absorbed into the Wilson coefficient; to put them back one only needs to divide each zero bin by the dimension of the representation of that sector.

There may be multiple operators contributing to a single hard process. For example, in $ud \to ud$ scattering, there are two relevant hard operators [54]:

$$\mathcal{O}_1 = (\bar{u} T^a \gamma^\mu u)(\bar{d} T^a \gamma^\mu d), \qquad \mathcal{O}_2 = (\bar{u} \gamma^\mu u)(\bar{d} \gamma^\mu d), \tag{3.204}$$

where the parentheses indicate color contractions. For $ud \to ud$ at tree level in QCD, only a single-gluon exchange is relevant and so $\mathcal{O}_2$ is not. At 1-loop and

beyond, both operators are important to correctly reproduce the hard scattering. As in this chapter we have avoided configurations where incoming and outgoing partons can be collinear, the factorization formula has only been shown to hold in threshold kinematical regimes where there is no phase space for hard initial state radiation to end up in the final state [16, 17, 23, 71, 105, 106]. Alternatively, one could think of the factorization formula in this case mediating a decay, like $h \to \bar{u}u\bar{d}d$ rather than a scattering process. Factorization for 4-parton scattering was also studied in [68].

To study $ud \to ud$ near threshold is helpful to have somewhat more general notation. Labeling the hard partons as 1, 2, 3, and 4, the relevant operators are

$$\mathcal{O}_{I\Gamma\Gamma'} = (\bar{q}_4 T_I \gamma_\mu \Gamma q_2)(\bar{q}_3 T_I \gamma^\mu \Gamma' q_1)\,. \tag{3.205}$$

Here, I indexes the color structure ($T_1 = T^a$ or $T_2 = \mathbf{1}$), and Γ and Γ' index the helicity (e.g. $\Gamma = \Gamma' = P_L = P_+ = \frac{1}{2}(1-\gamma_5)$). Helicity and flavor is preserved in QCD, so the helicity of the u fixes the helicity of the $\bar{u}$. There are thus eight relevant operators, since $I = 1, 2$, $\Gamma = \pm$ and $\Gamma' = \pm$. Each set of helicities has a separate factorization, but the color structures can mix.

So the matrix element for a 4 quark-jet decay factorizes as

$$\begin{aligned}
&\mathcal{M}_{\pm\pm} = \mathcal{M}_{\pm\pm}(p_1 + p_2 \to X_3 + X_4 + X_s) \\
&\cong \sum_I \mathcal{C}^I_{\pm\pm}(S_{ij}) \frac{\langle X_4|\,\bar{\psi}_4 W_4\,|0\rangle^{\pm h_4}}{\mathrm{tr}\,\langle 0|\,Y_4^\dagger W_4\,|0\rangle} \frac{\langle p_2|\,\overline{W}_2^\dagger \psi_2\,|0\rangle^{\pm h_2}}{\mathrm{tr}\,\langle 0|\,\overline{W}_2^\dagger \overline{Y}_2\,|0\rangle} \frac{\langle X_3|\,\bar{\psi}_3 W_3\,|0\rangle^{\pm h_3}}{\mathrm{tr}\,\langle 0|\,Y_3^\dagger W_3\,|0\rangle} \frac{\langle p_1|\,\overline{W}_1^\dagger \psi_1\,|0\rangle^{\pm h_1}}{\mathrm{tr}\,\langle 0|\,\overline{W}_1^\dagger \overline{Y}_1\,|0\rangle} \\
&\qquad\qquad \times \langle X_s|\,(Y_4^\dagger T_I \overline{Y}_2)^{h_4 h_2} (Y_3^\dagger T_I \overline{Y}_1)^{h_3 h_1}\,|0\rangle
\end{aligned} \tag{3.206}$$

where $\overline{W}_i$ and $\overline{Y}_i$ are incoming Wilson lines (see [3]). Note that we only write explicitly the color and spin indices of the partons which emerge from the hard scattering.

There are many implicit color and spin indices in the states $\langle X_j|$ and $\langle X_s|$. These colors and spins are important when computing scattering amplitudes, but are usually summed over in computing resummed distributions.

3.11.3 QCD factorization formula

In summary, a general factorization formula in QCD can be written as

$$\begin{aligned}\mathcal{M}_{\{\pm\}} \cong \sum_I \mathcal{C}_{I,\{\pm\}}(S_{ij}) \\ \times \cdots \frac{\langle X_i|\, \bar{\psi}_i W_i \,|0\rangle^{\pm h_i}}{\mathrm{tr}\,\langle 0|\, Y_i^\dagger W_i \,|0\rangle} \cdots \frac{\langle X_j|\, A^\mu \mathcal{W}_j \,|0\rangle^{\pm a_j}}{\mathrm{tr}\,\langle 0|\, \mathcal{Y}_j^\dagger \mathcal{W}_j \,|0\rangle} \cdots \frac{\langle X_k|\, W_k^\dagger \psi_k \,|0\rangle^{\pm h_k}}{\mathrm{tr}\,\langle 0|\, W_k^\dagger Y_k \,|0\rangle} \cdots \\ \times \langle X_s| \cdots (Y_i^\dagger T_I^i)^{h_i l_i} \cdots (\mathcal{Y}_j^\dagger T_I^j)^{l_{j-1} a_j l_{j+1}} \cdots (T_I^k Y_k)^{l_k h_k} \cdots |0\rangle\end{aligned} \tag{3.207}$$

where the $\pm$ indexes the helicities. The l_i indices are contracted within the soft Wilson line matrix element, while the h_i and a_i indices contract with the colors of the jets.

3.12 Splitting functions and soft currents

One application of factorization is that it can provide gauge-invariant and regulator-independent definitions of the collinear-sensitive or soft-sensitive parts of scattering amplitudes. Such definitions may be useful in perturbative QCD calculations if they help simplify or clarify the structure of the infrared divergences. We therefore consider the soft and collinear limits of our formulas separately, deriving definitions of splitting functions and soft currents and thereby proving their universality.

3.12.1 Splitting Functions

Suppose we have a state $\langle X^0| = \langle X_1^0 \cdots X_N^0; X_s^0|$ containing soft and collinear particles and a matrix element $\mathcal{M}_0$ for producing that state. We want to know how $\mathcal{M}_0$ is modified into $\mathcal{M}$ by the addition of extra collinear particles to the j-collinear sector, turning $\langle X_j^0|$ into $\langle X_j|$, while leaving the net momenta in the j sector unmodified at leading power $P_j^\mu \cong P_j^{0\,\mu}$. Let us write the modified matrix element formally as some operator acting on the original matrix element

$$\mathcal{M} = \mathbf{Sp} \cdot \mathcal{M}_0 \tag{3.208}$$

The distribution of the soft radiation in $\langle X_s^0|$ is completely independent of the splitting. The only modification from the addition of collinear particles to $\langle X_j^0|$ is in the matrix element associated with the j-collinear sector.

The factorization formulas for $\mathcal{M}_0$ and $\mathcal{M}$ are almost identical. The relevant parts of the factorization formulas are:

$$\mathcal{M}_0 \cong \frac{\langle X_j^0|\,\bar{\psi}\,W_j\,|0\rangle^{\pm h_j}}{\mathrm{tr}\,\langle 0|\,Y_j^\dagger W_j\,|0\rangle} \cdot \mathcal{M}_{\mathrm{rest}}^{h_j}\,, \qquad \mathcal{M} \cong \frac{\langle X_j|\,\bar{\psi}\,W_j\,|0\rangle^{\pm h_j}}{\mathrm{tr}\,\langle 0|\,Y_j^\dagger W_j\,|0\rangle} \cdot \mathcal{M}_{\mathrm{rest}}^{h_j} \tag{3.209}$$

Now, the spin of each collinear sector, that is, the helicity of the nearly-on-shell particle coming out of the hard vertex, in $\mathcal{M}$ must be the same as in $\mathcal{M}_0$ for the two to be related. So let us fix this helicity $\pm$ and drop the spin indices. Then we can write

$$\mathbf{Sp}(X_j, X_j^0)^{hh'} = \frac{\langle X_j|\,\bar{\psi}\,W_j\,|0\rangle^h}{\langle X_j^0|\,\bar{\psi}\,W_j\,|0\rangle^{h'}} \tag{3.210}$$

The notation here indicates that the splitting functions are operators in color space. Note that the zero-bin subtractions from the denominator of the general factorization formula have dropped out. These denominators are 1 in dimensional regularization,

but here we see that they play no role with any regulator. As we will see, this is also true for soft currents.

To convert Eq. (3.210) into something more practical, let us work out a simple example, following Section 9.1 of [3]. We take $\langle X^0|$ to have a single right-handed antiquark in it with momentum P^μ and color h: $\langle X^0| = \langle \bar{u}_h(P)|$. In terms of spinor helicities, this state is [P and at tree level and

$$\mathcal{M}_0^{hR} \cong [P\mathcal{M}_{\rm rest}^h] \tag{3.211}$$

We take take $\langle X|$ to have a right-handed antiquark of momentum $p^\mu \cong zP^\mu$ and a single gluon with momentum $q^\mu \cong (1-z)P^\mu$ with color a and helicity $\pm$. If the gluon helicity is $-$, the modified amplitude is (see [3])

$$\mathcal{M}^{haR-} = g_s \frac{\sqrt{2}}{[qp]} \frac{z}{\sqrt{1-z}} \, [PT^a_{hh'}\mathcal{M}_{\rm rest}^{h'}] \tag{3.212}$$

Thus the tree-level splitting function for a $-$ helicity gluon is

$$\mathbf{Sp}_{R-}(p,q) = g_s \frac{\sqrt{2}}{[qp]} \frac{z}{\sqrt{1-z}} \mathbf{T}_j \tag{3.213}$$

For a + helicity gluon, the tree-level splitting function is also extractable from [3]:

$$\mathbf{Sp}^{hh'}_{R+}(p,q) = g_s \frac{\sqrt{2}}{\langle pq\rangle} \left(\frac{z}{\sqrt{1-z}} + \sqrt{1-z} \right) T^a_{hh'} \tag{3.214}$$

These splitting functions can be calculated to higher order using Eq. (3.210).

The gluon splitting functions are similar

$$\mathbf{Sp}^{\mathbf{g}}(X_j, X_j^0)^{ab} = \frac{\langle X_j| \, W_j^\dagger A_\mu W_j \, |0\rangle^a}{\langle X_j^0| \, W_j^\dagger A_\mu W_j \, |0\rangle^b} \tag{3.215}$$

The universality of Eq. (3.210) and Eq. (3.215) to all orders for any process is proven by our factorization theorem.

3.12.2 Soft currents

The equivalent of splitting functions for soft radiation are often called soft currents [86]. Extracting their matrix-element definition from the general factorization formula proceeds in the same way as for collinear splittings.

Suppose we have a state $\langle X^0| = \langle X_1^0 \cdots X_N^0; X_s^0|$ containing soft and collinear particles and a matrix element $\mathcal{M}_0$ for producing that state. We want to know how $\mathcal{M}_0$ is modified into $\mathcal{M}$ by the addition of extra soft particles $\langle X_s|$. The modified matrix element can be formally written as

$$\mathcal{M} = \mathbf{J} \cdot \mathcal{M}_0 \tag{3.216}$$

where $\mathbf{J}$ is an operator acting in color space. Isolating the part of the factorization formula involving soft radiation, it follows that

$$\mathbf{J} = \frac{\langle X_s| Y_1^\dagger \cdots \mathbf{T}_I \cdots Y_N |0\rangle}{\langle X_s^0| Y_1^\dagger \cdots \mathbf{T}_I \cdots Y_N |0\rangle} \tag{3.217}$$

Here I indexes the color structures of the relevant operators.

$\mathbf{J}$ has implicit indices which also act on the color of the particles in $\langle X_1 \cdots X_N|$. It is standard to write $\mathbf{J}$ as a function of color-charge operators $\mathbf{T}_j^a$ which act in color space as the SU(3) generator in the representation of net color flowing in direction j. This representation is of course the same as the representation of the Y_j Wilson line. When using color-charge operators, one never needs to perform a color sum, and so there is, trivially, no dependence of $\mathbf{J}$ on the color structure I. That the matrix element for soft emission *only* depends on the net color in each collinear sector, and not how that color is distributed, is a nontrivial consequence of factorization. It was proven to 1-loop by direct computation in [87], and now we have show that it holds

to all orders in g_s, for an arbitrarily complicated collinear sector and any number of hard particles.

In the simplest case, $\langle X_s^0| = \langle 0|$ and $\langle X_s|$ has only one gluon, with momentum q, polarization $\epsilon^\mu(q)$ and color a. Then $\mathbf{J} = \epsilon_\mu \mathbf{J}_a^\mu$. At tree level, $\mathbf{J}$ is:

$$\mathbf{J}^{\mu(0)} = g_s \sum_{j=1}^{m} \mathbf{T}_j \frac{p_j^\mu}{p_j \cdot q} \tag{3.218}$$

where $\mathbf{T}_j$ is the color-charge operator in the j direction. To be more concrete, if there is only a quark and anti-quark jet, then

$$\mathbf{J}^\mu = J^\mu_{ahh'} = \frac{\langle \epsilon^\mu(p); a| \, Y_1^\dagger Y_2 \, |0\rangle^{hh'}}{C_A \mathrm{tr} \, \langle 0| \, Y_1^\dagger Y_2 \, |0\rangle} = g_s T^a_{hh'} \left(\frac{p_1^\mu}{p_1 \cdot q} - \frac{p_2^\mu}{p_2 \cdot q} \right) + \cdots \tag{3.219}$$

The h and h' color indices act on the jets, $\langle X_1| \, \bar{\psi} \, W_1 \, |0\rangle^h \langle X_1| \, W_2^\dagger \psi \, |0\rangle^{h'}$.

In dimensional regularization in $4-2\varepsilon$ dimensions, with outgoing particles only, the 1-loop current is [87]:

$$\mathbf{J}^{\mu(1)} = -\frac{1}{16\pi^2} \frac{1}{\varepsilon^2} \frac{\Gamma^3(1-\varepsilon)\Gamma^2(1+\varepsilon)}{\Gamma(1-2\varepsilon)} \times i f_{abc} \sum_{i \neq j} \mathbf{T}_i^b \mathbf{T}_j^c \left(\frac{p_i^\mu}{p_i \cdot q} - \frac{p_j^\mu}{p_j \cdot q} \right) \left[\frac{-4\pi p_i \cdot p_j}{2(p_i \cdot q)(p_j \cdot q)} \right]^\varepsilon \tag{3.220}$$

In calculating this current, Catani and Grazzini were able to prove that it it is independent of the momenta and color-flow of the process at 1-loop. As noted above, our proof generalizes this observation to all orders. Of course, the factorization formula does not help in actually calculating the soft current in dimensional regularization. The current for one soft gluon emission at 2 loops can be found in [88, 89].

Another familiar result that can be deduced from our all-orders definition of the soft current is that of Abelian exponentiation. Namely, that in an Abelian gauge theory, the soft current is exact at tree level. This follows simply from the fact

that in an Abelian theory, the contraction of a Wilson line with the external state can be pulled out of the rest of the matrix element. Since the Wilson lines are exponentials, pulling out a contraction leaves behind the same Wilson line (just like taking a derivative), so that, to all orders in perturbation theory:

$$J^\mu_{\text{Abelian}} = \frac{\langle q|\, Y_1^\dagger \cdots Y_N\, |0\rangle}{\langle 0|\, Y_1^\dagger \cdots Y_N\, |0\rangle} = \frac{\langle 0|\, Y_1^\dagger \cdots Y_N\, |0\rangle}{\langle 0|\, Y_1^\dagger \cdots Y_N\, |0\rangle} \sum_{j=1}^N \langle q|\, Y_j\, |0\rangle_{\text{tree}} = \sum_{j=1}^N Q_j \frac{n_j^\mu}{n_j \cdot q} \quad (3.221)$$

where Q_j is the QED charge: $Q_j = e$ if it comes from a $Y_j^\dagger$ and $Q_j = -e$ if it comes from a Y_j. Gauge invariance implies that $\sum_{j=1}^N Q_j = 0$.

3.13 Effective Field Theory

In this chapter, our emphasis has been on factorization in QCD at the amplitude level. In our view, working at the amplitude level, rather than at the amplitude-squared level as is often done, makes some elements of factorization more transparent. It also elucidates some aspects of Soft-Collinear Effective Theory (SCET).

Consider Eq. (3.207), which we have proven to leading power in λ. Let us assign particles in each collinear sector $\langle X_j|$ the quantum number $j \in \{1, \ldots, N\}$ and each particle in $\langle X_s|$ the quantum number s. Let us also write an effective Lagrangian that is $N+1$ copies of the QCD Lagrangian

$$\mathcal{L}_{\text{eff}} = \mathcal{L}_{\text{soft}} + \sum_{j=1}^N \mathcal{L}_j \quad (3.222)$$

with fields in each sector only creating and annihilating states with the appropriate quantum numbers. Then we can combine the numerator matrix elements in Eq. (3.207) into a single matrix element in a trivial way.

For example, with two collinear sectors, the factorization formula becomes

$$\langle X_1X_2;X_s|\,\bar\psi\gamma^\mu\psi\,|0\rangle \cong \mathcal{C}_2\,\langle X_1X_2;X_s|\,\frac{\bar\psi_1\,W_1}{\mathrm{tr}\,\langle 0|\,Y_1^\dagger W_1\,|0\rangle/N_c}Y_1^\dagger\gamma^\mu Y_2\frac{W_2^\dagger\,\psi_2}{\mathrm{tr}\,\langle 0|\,W_2^\dagger Y_2\,|0\rangle/N_c}\,|0\rangle_{\mathcal{L}_{\rm eff}} \tag{3.223}$$

if computed with an effective Lagrangian

$$\mathcal{L}_{\rm eff} = \mathcal{L}_{\rm soft} + \mathcal{L}_1 + \mathcal{L}_2 \tag{3.224}$$

The Wilson coefficient $\mathcal{C}_2$ depends only on the net momenta P_1^μ and P_2^μ in each sector, not on the detailed distribution of momenta in $\langle X_1X_2;X_s|$. Since $\mathcal{C}_2$ depends on the hard-scattering operator and not the states, it is a legitimate Wilson coefficient from matching onto an effective field theory.

It is possible to clean up the effective field theory operator a little. Let us define

$$\widehat{Z}_i \equiv \frac{1}{N_c}\mathrm{tr}\,\langle 0|\,W_i^\dagger Y_i\,|0\rangle \tag{3.225}$$

For other color representations, $\widehat{Z}_i$ is defined similarly with the Wilson lines in the appropriate representation and N_c replaced by dimension of the representation. The $\widehat{Z}_i$ factors are both UV and IR divergent. They are, however, independent of λ and any momenta in the process. That is, for given UV and IR regulators, they are power series in α_s. Thus, they can play the role of a kind of field-strength renormalization for jets. Indeed, it is natural to define jet fields as

$$\chi_i \equiv \frac{1}{\widehat{Z}_i}W_i^\dagger\,\psi_i \tag{3.226}$$

These composite fields are gauge invariant (up to a global rotation associated with the net color charge of the jet) and are soft insensitive and collinear sensitive only in the i direction. In terms of the jet fields, Eq. (3.223) becomes simply

$$\bar\psi\gamma^\mu\psi \;\cong\; \mathcal{C}_2\left(\bar\chi_1 Y_1^\dagger\right)\gamma^\mu\left(Y_2\chi_2\right) \tag{3.227}$$

which is a valid leading-power matching equation in an effective theory describing dijet-like states because the Wilson coefficient is IR-insensitive and independent of which external states are used to compute it. Of course, this matching must be done within the régime of validity of the effective theory, which in this case is justified by the factorization theorem that is proved for N-jet-like *final* states.[4]

The effective theory that naturally arises from our factorization formula is very different from the traditional formulation of SCET. Consequently, had we started from the traditional formulation of SCET and derived a factorization formula, it would look very different from the one we have proven. In particular, the Lagrangian and Feynman rules would not be those of full QCD and would not give rise to an all-orders full-QCD definition of the soft current and splitting functions.

Transitioning to the effective field theory language is particularly useful when discussing subleading power corrections in λ. Recent progress has been made toward describing collider-physics observables at subleading power using the formulation of SCET discussed in this section [52].

In [3], the tree-level version of this formulation of SCET (without the vacuum-matrix element denominators) was shown to be equivalent to that discussed by Freedman and Luke [51]. However, with the all-loop factorization theorem in hand we naturally see arise an all-orders matrix-element definition of the zero-bin subtraction (similar to what was shown in [108,109]). In Freedman and Luke's approach to SCET, the zero-bin is subtracted off using an ad-hoc procedure applied on an integral-by-integral basis that essentially comes from mimicking the procedure of the traditional

[4]See [107] for an interesting discussion of how this matching equation can break down when certain initial states are used to perform the matching.

approach to SCET [59]. In the traditional approach, the zero-bin subtraction arises naturally from the SCET Lagrangian. It instructs us to apply a soft subtraction to every single collinear line in each Feynman diagram. This is arguably a more complicated algorithm than dividing by a single gauge-invariant color-coherent vacuum matrix element, as in our factorization formula.

Before moving on, we point out that our factorization formula is derived with fixed external states that come designated as soft or collinear. This was the goal of this chapter. For particles which power-count as soft or collinear, the factorization theorem holds if they are put in either sector. However, to perform phase space integrals in the factorized expression without chopping up phase space, it would be convenient not to place a hard cutoff between sectors. To achieve this, in the language of Section 3.6, the algorithm in Section 3.6.1 would need to be modified to color external-collinear particles blue or red. Then when calculating cross sections, we would be able to integrate the collinear states over their entire phase space, including the soft region. Our expectation is that this would be a simple step using the tools at our disposal, and would give a zero-bin of the form of the eikonal-cross-section subtraction used in the QCD literature (see the discussion in [97,110]). We will come back to this discussion in Ch 4.

Another feature of our approach to factorization is that we did not have to choose the power counting of the soft emissions to be the same as that of the collinear emissions. For example, we could have used a separate λ_s and λ_c:

$$k^\mu \text{ soft} \iff k^\mu \sim \lambda_s^2 Q \qquad \text{and} \qquad q^\mu \parallel p^\mu \iff q\cdot p \sim \lambda_c^2 Q^2,\;\; q^0, p^0 \sim Q \quad (3.228)$$

The factorization theorem holds at leading power in both λ_s and λ_c. In fact, one

could even take a different λ_c in each sector. Taking $\lambda_s = \lambda_c = \lambda$ and transitioning to an effective theory implies the factorization theorem that is appropriate to what is referred to as SCET_I in the literature. If we take instead $\lambda_s^2 = \lambda_c = \lambda$ the factorization theorem still holds. This power-counting is equivalent $k_\text{soft} \sim (\lambda, \lambda, \lambda)$ and $q_\text{coll} \sim (\lambda^2, 1, \lambda)$ in lightcone coordinates, which in the SCET literature is considered to be a different effective field theory, known as SCET_II. The traditional derivation of SCET_II involves rather involved intermediary matching through SCET_I [111]. The factorization theorem presented in this chapter is general enough to unify these two SCETs into a single framework.

3.14 Conclusions

In this chapter we have formulated and proven to all orders in perturbation theory a precise statement of factorization for scattering amplitudes in QCD, given in Eq. (3.207). This formula applies to states with N well-separated jets with any number collinear particles in each jet, $\langle X_j|$ for $j = 1, \ldots, N$, and any amount of soft radiation in any direction, $\langle X_s|$. Suppressing color and spin indices, the formula for quark jets reads:

$$\langle X_1 \cdots X_N; X_s | i \rangle \cong \mathcal{C}(P_i) \frac{\langle X_1 | \bar{\psi} W_1 | 0 \rangle}{\text{tr} \langle 0 | Y_1^\dagger W_1 | 0 \rangle} \cdots \frac{\langle X_N | W_N^\dagger \psi | 0 \rangle}{\text{tr} \langle 0 | W_N^\dagger Y_N | 0 \rangle} \langle X_s | Y_1^\dagger \cdots Y_N | 0 \rangle \tag{3.229}$$

where $|i\rangle$ is, say, some uncolored initial state and $\mathcal{C}(P_i)$ is an IR-finite function depending only on the net momenta in each sector P_i^μ. The symbol $\cong$ means equality at leading power in λ, a physical power counting parameter that constrains only the external momenta in the amplitude. The factorization formula actually holds to lead-

ing power in different power counting parameters λ_s and λ_c^j in each sector. It also holds if there are collinear particles in the initial state, as long as no initial state and final state particles are collinear to each other.

The proof of Eq. (3.229) was broken into two steps, which essentially correspond to hard factorization and soft-collinear factorization. The first step was to determine the structure of the possible graphs that contribute to each type of infrared sensitivity (soft or j-collinear) in the matrix element. The structure of the diagrams relevant at leading power are encoded in the reduced diagram (see Eq. (3.148)), which represents hard factorization in physical gauges. This reduced diagram is similar to reduced diagrams used in the literature to represent the pinch surface. Indeed, our derivation of hard factorization exploits essentially the same observations as these traditional approaches. However, the reduced diagrams traditionally used in the literature are usually defined only for momenta which are exactly $k^\mu = (0, 0, 0, 0)$ or exact proportional to one of the external momenta. In contrast, our reduced diagram represents a precise set of Feynman integrals, defined for all values of external and loop momenta with rules that describe how they are to be calculated. This generalization of the reduced diagram allows for a clean transition to an amplitude-level factorization formula.

The second step in the proof is to factorize the soft-sensitive from the collinear-sensitive contributions to matrix elements. This step builds upon the reduced diagram picture and coloring rules which established hard factorization. The all-orders proof of soft-collinear factorization uses the same logic as was used in [3] for the tree-level proof. In particular, the use of different reference-vector choices used in [3] is critical

also at loop-level. For loops, the reference-vector flexibility must be generalized to momentum-dependent lightcone-gauge reference-vector choices. We call a gauge with this flexibility *factorization gauge*. Within factorization gauge, different choices for the reference vector in the soft region slosh the soft sensitivities around among different colored diagrams within the reduced diagram structure. This lets us see how soft sensitivities factorize from collinear sensitivities for any value of the soft and collinear power-counting parameters, λ_s and λ_c. Once appropriate Wilson lines are added, the final factorization formula is gauge-invariant and applies even in covariant gauges like Feynman gauge.

There are many practical applications of factorization, from the universality of splitting functions and soft currents in QCD [62, 83–85, 87], to regulating infrared divergences in fixed-order calculations [27, 112–115], to the computation of resummed distributions in jet substructure [6, 23–25, 116]. For example, having gauge-invariant and regulator independent definitions for objects which contain universal soft or collinear singularities may be useful as the basis of subtractions for fixed-order calculations in QCD. In many cases, assuming factorization is enough for phenomenological purposes. Having a rigorous proof of factorization of course puts many approximations on firmer footing. But it may also point the way to understanding subtleties of where factorization may break down, such as in the context of forward scattering [44, 56, 61, 107] or non-global logarithms [95, 96, 117–124]. In both of these cases, our expectation is not that the factorization theorem proven in this chapter will immediately resolve the confusions. Instead, we envisage that the physical picture on which the factorization is based, with an intuitive reduced diagram picture and matrix-element zero-bin subtractions, should be a practical scaffold on which to build

a more sophisticated and nuanced picture of factorization in scattering amplitudes.

Chapter 4

Removing phase-space cutoffs

4.1 Introduction

Factorization is at the heart of our ability to use perturbative quantum chromodynamics (QCD) to make theoretical predictions for scattering processes at high-energy particle colliders. It is extremely fortuitous that accurate particle distributions can be computed by convolving universal parton distribution and hadronization models with perturbative calculations of jet formation. While factorization at the non-perturbative level is hard to establish, factorization relevant to the structure and substructure of jets can be understood within perturbation theory. In particular, the radiation patterns in perturbative QCD factorize into hard, collinear and soft contributions. Moreover, subtleties in perturbative factorization (for example, related to non-global logarithms [95, 96, 117, 124–127]) are a limiting factor in many ultra-precise jet-substructure calculations. Thus, there has recently been renewed interest in studying factorization, particularly in the context of Soft-Collinear Effective

Theory (SCET).

A concise formulation of factorization in QCD was proposed and proven in Chs. 2 and 3 which cover the papers by the author and collaborators [3, 4]. These papers build upon decades of insight [42, 48, 51, 60, 65, 69, 128]. Up to color factors, the formula from [4] reads:

$$\langle X_1 \cdots X_N; X_s | \, \mathcal{O} \, | 0 \rangle \;\cong\; \mathcal{C}_{\mathcal{O}}(S_{ij}) \, \frac{\langle X_1 | \, \bar{\psi} W_1 \, | 0 \rangle}{\langle 0 | \, Y_1^\dagger W_1 \, | 0 \rangle} \cdots \frac{\langle X_N | \, W_N^\dagger \psi \, | 0 \rangle}{\langle 0 | \, W_N^\dagger Y_N \, | 0 \rangle} \, \langle X_s | \, Y_1^\dagger \cdots Y_N \, | 0 \rangle \tag{4.1}$$

In this expression, the state $\langle X_1 \cdots X_N; X_s|$ has soft particles, in $\langle X_s|$, and particles collinear to various specified directions, in $\langle X_i|$. The left-hand side is a matrix element in QCD of an operator like $\mathcal{O} = \bar{\psi} \cdots \psi$ in this state. The right hand side is a factorized product of matrix elements, each of which involves only one collinear sector or the soft sector. The symbol $\cong$ indicates that the two sides are identical at leading power. More precisely, if one were to compute some infrared-safe observable dominated by soft or collinear radiation, such as the sum of the jet masses $\tau = \frac{1}{Q^2} \sum m_i^2$, all of the terms in $\frac{d\sigma}{d\tau}$ that are dominant as $\tau \to 0$ will be identical on both sides. More details can be found in Section 4.2 below and in [3] and [4].

The formula in Eq. (4.1) presupposes that the external momenta are designated as soft or collinear. If a particular momentum can be classified as soft or collinear, then the factorized formula will hold whether it is put in $\langle X_s|$ or in the appropriate $\langle X_i|$. For example, we can place all the soft-collinear momenta in the soft sector by designating any particle with energy less than some Λ as soft, and then draw cones of size R around each of the hard directions to distribute particles in the collinear sectors. With such hard cutoffs, one can then square the matrix elements on the right-

hand side of Eq. (4.1) and perform the phase-space integrals over the appropriate measurement function to get a differential distribution. The result will agree at leading power with the the distribution computed using the left-hand side of Eq. (4.1) in the limit $R \to 0$ and $\Lambda \to 0$.

There are two problems with the hard-cutoff prescription for resolving the soft-collinear ambiguity. The first is practical: introducing an extra scale makes the relevant calculations nearly impossible. Moreover, the cutoff dependence may not exactly cancel in the factorized expression and therefore one must either take $R \to 0$ and $\Lambda \to 0$ after the calculation or live with power corrections in these cutoffs. The second is conceptual: the cutoffs violate factorization in the following sense. There will in general be leading-power dependence on the cutoff in the soft and collinear sectors separately (terms like $\frac{1}{\tau} \ln R$, for example) which only cancel when the sectors are combined. Thus the two sectors are not completely separated.

It would be great if we could simply perform phase-space integrals over each sector separately including all momenta. This is not as crazy as it sounds. We know that including very energetic virtual momenta in the soft or collinear sectors causes no problem, since the modification can always be compensated for in the matching coefficient ($\mathcal{C}_{\mathcal{O}}(S_{ij})$ in Eq. (4.1)). Indeed, effective theories always have different ultraviolet (UV) structure from the full theories to which they are matched. For example, in SCET, there are $\frac{1}{\varepsilon^2}$ UV poles at 1-loop in dimensional regularization, while in full QCD, one only ever has $\frac{1}{\varepsilon}$ poles. In fact, these double poles allow for the resummation of Sudakov double logarithms in SCET using the renormalization group. We also know that one does not have to distinguish soft from collinear momenta in

loops when using Eq. (4.1): the overcounting is compensated for by the vacuum matrix elements in the denominator of this equation. Thus, we have good reason to believe that subtractions similar to the denominator factors in Eq. (4.1) can be added to this formula to allow for unrestricted phase-space integrals.

Removing the overcounting of soft and collinear momenta has been addressed in the traditional approach to factorization, for certain observables [43, 110, 129]. There, the soft limit of collinear momenta is compensated for with eikonal jet functions [72]. In SCET, the overcounting can be formally avoided by not including the zero-momentum bin in any of the collinear sectors [59]. This exclusion translates into a subtraction diagram-by-diagram. This zero-bin subtraction is necessary in SCET because the same soft-collinear momentum region in QCD is represented by multiple fields in the effective theory (similar overcounting is present in other effective theories, such as NRQCD). In [97, 108, 109] the two prescriptions were shown to be equivalent. Alternatively, in the method-of-regions approach to SCET [49, 50, 130, 131] the overcounting is sidestepped through careful consideration of the analytic properties of the contributions from different sectors. We briefly review these approaches and contrast them with our approach in Section 4.3.3.

The formulation of factorization in [3] and [4] and Eq. (4.1) is intermediate between traditional QCD and SCET. It provides a precise formulation of factorization purely in terms the fields in full QCD, but has a factorized form with a natural effective field theory interpretation. It is based on the observation of Freedman and Luke [51] that the unwieldy Feynman rules of SCET can be avoided and the effective Lagrangian taken simply as the direct sum of $N + 1$ copies of the QCD Lagrangian,

corresponding to N collinear sectors and a soft sector. The formulation in [3] and [4] can be thought of as a generalization of the Freedman-Luke proposal, equivalent but simpler at leading power, and that addresses the soft-collinear overlap of virtual momenta. In this chapter, we extend the formulation so that phase-space integrations can be done without explicit cutoffs on the momenta of various sectors.

There are two main results in this chapter. First, in Section 4.2, we show how the specification of which sector a gluon belongs to can be removed at the amplitude level. More precisely, suppose we have an amplitude $\mathcal{M}(p_1, \ldots, p_n, q_1 \cdots q_m)$ with n hard momenta and m other momenta in QCD. We show how an approximation to $\mathcal{M}$ which we call $\mathcal{M}_{\text{sub}}$ can be derived with the property that when any of the q_i become soft or collinear to any of the p_i, $\mathcal{M}_{\text{sub}}$ agrees with $\mathcal{M}$ at leading power. That is, one does not have to specify which sector the q_i belong to – the matrix element is correct no matter what. While $\mathcal{M}_{\text{sub}}$ is not a factorized product of matrix elements, it is the sum of factorized products of matrix elements of fields and Wilson lines. Each term in this product is simpler than full QCD. Thus such a subtracted matrix element may be integrable analytically and therefore provide a useful basis for a subtraction scheme in fixed-order QCD.

The second result, in Section 4.3, is a derivation of how at the amplitude-squared level factorization can be preserved and phase-space cutoffs removed for certain inclusive event shapes. Although the result of this section agrees with the eikonal-jet function subtraction method of traditional QCD (which is itself equivalent to SCET), we believe our derivation elucidates some subtleties and makes the procedure more systematic. In addition, we present explicit 1-loop formulas for various relevant soft

and jet functions, with and without cutoffs and with different regulators. These formulas demonstrate which objects are infrared safe, cutoff-dependent, and well-defined. Section 4.3.3 contrasts our approach with previous approaches. We conclude in Section 4.4.

4.2 Factorization at the amplitude level

We begin by quickly reviewing the notation and main results of Chs. 2 and 3. These chapters showed that factorization holds for massless particles whose momenta are either soft or collinear to one of N directions n_j^μ. States with particles of these momenta are written as $\langle X_1 \cdots X_N; X_s|$. The hard scale (such as the center-of-mass energy) is denoted as Q and scaling parameters λ_j are defined each collinear sector and λ_s for the soft sector. Momenta in each collinear sector scale as

$$\langle X_j| = \langle \dots, q_j, \dots| \quad \Longrightarrow \quad \frac{1}{Q}(n_j \cdot q_j, \bar{n}_j \cdot q_j, q_j^\perp) \sim (\lambda_j^2, 1, \lambda_j) \tag{4.2}$$

and momenta in the soft sector scale like

$$\langle X_s| = \langle \dots, k_s, \dots| \quad \Longrightarrow \quad \frac{1}{Q}(n_j \cdot k_s, \bar{n}_j \cdot k_s, k_s^\perp) \sim (\lambda_s, \lambda_s, \lambda_s), \quad \forall j \tag{4.3}$$

For simplicity, assume the scattering process under consideration is the decay of a heavy particle mediated by an operator $\mathcal{O}$ in QED (to avoid cumbersome color indices of QCD). Then, the factorization formula takes the form of Eq. (4.1):

$$\langle X_1 \cdots X_N; X_s| \, \mathcal{O} \, |0\rangle \;\cong\; \mathcal{C}_\mathcal{O}(S_{ij}) \, \frac{\langle X_1| \, \bar{\psi} W_1 \, |0\rangle}{\langle 0| \, Y_1^\dagger W_1 \, |0\rangle} \, \cdots \, \frac{\langle X_N| \, W_N^\dagger \psi \, |0\rangle}{\langle 0| \, W_N^\dagger Y_N \, |0\rangle} \; \langle X_s| \, Y_1^\dagger \cdots Y_N \, |0\rangle$$

Here $\mathcal{C}_\mathcal{O}(S_{ij})$ is a finite function of the large products of the net momentum in each jet, $S_{ij} = P_i \cdot P_j$; it does not depend on the small power-counting parameters, λ_j of

λ_s. The Wilson lines, $W_j^\dagger$ and $Y_j^\dagger$, are defined in QCD as follows:

$$Y_j^\dagger = P\Bigg\{ \exp\left[ig \int_0^\infty ds\, n_j \cdot A(x + s\, n_j)\, e^{-\varepsilon s} \right] \Bigg\} \tag{4.4}$$

and

$$W_j^\dagger = P\Bigg\{ \exp\left[ig \int_0^\infty ds\, t_j \cdot A(x + s\, t_j)\, e^{-\varepsilon s} \right] \Bigg\} \tag{4.5}$$

where t_j^μ are some lightlike directions assumed not collinear to their associated n_j^μ. The $P\{\}$ denotes path ordering; in QED the path ordering is trivial and the electromagnetic charge is $e = -g$. Eq. (4.1) is an equality at leading power in all of λ_j and λ_s separately. For many applications, such as for thrust, one takes $\lambda_j^2 = \lambda_s$ for all j; in the SCET literature, this power counting is referred to as SCET_I [47]. For recoil sensitive observables like jet broadening, one takes $\lambda_j = \lambda_s$ as in SCET_II [111]. The factorization in Eq. (4.1) holds for any relative scaling.

The important physics contained in Eq. (4.1) is that each factor on the right-hand side represents a different factorized sector: the Wilson coefficient, $\mathcal{C}_\mathcal{O}(S_{ij})$, represents all of the hard physics and must be IR-insensitive. Each collinear sector is represented by the ratio $\langle X_j |\, W_j^\dagger \psi\, | 0 \rangle \,/\, \langle 0 |\, W_j^\dagger Y_j\, | 0 \rangle$ and contains only n_j-collinear IR divergences. Finally, the soft sector is fully described by the matrix element, $\langle X_s |\, Y_1^\dagger \cdots Y_N\, | 0 \rangle$, which contains all of the soft divergences of the full amplitude on the left-hand side of Eq. (4.1).

One attractive feature of Eq. (4.1) is that each matrix element is constructed out of full-theory operators and evaluated using the full-theory Lagrangian; there are no additional subtractions/prescriptions needed, just simple QCD/QED Feynman rules. Moreover, the power counting is a consequence only of the scaling of the external momenta in the states $\langle X_1 \cdots X_N; X_s |\, \mathcal{O}\, | 0 \rangle$. An obvious fact with important

repercussions is that Eq. (4.1) is not valid when any of the momenta in a given sector does not obey the scaling that is associated with that sector. Consequently, one cannot, for example, integrate over the entire phase space of one of the external momenta in Eq. (4.1) because it would enter the scaling regime of other sectors.

Therefore, when calculating cross sections by squaring Eq. (4.1) one can either integrate over the phase space $d\Pi_{X_j}$ with cutoffs in the integrals restricting each integral to be within the collinear region, or one can try to extend the integrations to the entire phase space and perform a subtraction that gets rid of the errors that we introduced by extending $d\Pi_{X_j}$ to the entire phase space. Introducing cutoffs to integrals is incredibly tedious and produces new scales in the effective theory that obscure factorization (as shown explicitly in Section 4.3). The subtraction procedure is the only reasonable way forward. We next discuss subtractions at the amplitude level, and discuss subtractions at the cross section level in Section 4.3.

4.2.1 Example subtractions

Consider the case of a $q\bar{q}g$ final state, with quark momenta p_1^μ and p_2^μ in different directions and the gluon momentum q^μ. Suppose we want to integrate over the gluon momenta inclusively. We can do so using Eq. (4.1) if when $q \parallel p_1$ we use

$$\mathcal{M}_1(p_1, p_2, q) \equiv \frac{\langle p_1; q| \bar{\psi} W_1 |0\rangle}{\langle 0| Y_1^\dagger W_1 |0\rangle} \frac{\langle p_2| W_2^\dagger \psi |0\rangle}{\langle 0| W_2^\dagger Y_2 |0\rangle} \langle 0| Y_1^\dagger Y_2 |0\rangle \ , \tag{4.6}$$

if $q \parallel p_2$, we use

$$\mathcal{M}_2(p_1, p_2, q) \equiv \frac{\langle p_1| \bar{\psi} W_1 |0\rangle}{\langle 0| Y_1^\dagger W_1 |0\rangle} \frac{\langle p_2; q| W_2^\dagger \psi |0\rangle}{\langle 0| W_2^\dagger Y_2 |0\rangle} \langle 0| Y_1^\dagger Y_2 |0\rangle \ , \tag{4.7}$$

and if q is soft, we use

$$\mathcal{M}_s(p_1, p_2, q) \equiv \frac{\langle p_1 | \, \bar{\psi} W_1 \, | 0 \rangle}{\langle 0 | \, Y_1^\dagger W_1 \, | 0 \rangle} \frac{\langle p_2 | \, W_2^\dagger \psi \, | 0 \rangle}{\langle 0 | \, W_2^\dagger Y_2 \, | 0 \rangle} \langle q | \, Y_1^\dagger Y_2 \, | 0 \rangle \tag{4.8}$$

However we split up the integration regions (say with a soft energy cutoff Λ and cone radius R) the dependence on the split (on Λ and R) will drop out at leading power when all three contributions are added. Nevertheless, it would be nice to have an expression that we could simply integrate over q without ever introducing Λ and R in the first place.

To proceed, we first examine the consequences of soft-collinear factorization for the operator $\mathcal{O}_{\bar{\psi}W} = \bar{\psi} W_1$ (rather than a local QCD operator like $\bar{\psi}\psi$). The all-orders proof of factorization in [4] applies to $\mathcal{O}_{\bar{\psi}W}$. In particular, if we have a state with momenta $p_1 \cdots p_n$ all of which are collinear to each other as well as momenta $q_1 \cdots q_m$ all of which are soft, then

$$\langle p_1 \cdots p_n; q_1 \cdots q_m | \, \bar{\psi} W_1 \, | 0 \rangle \cong C_{\bar{\psi}W} \, \langle p_1 \cdots p_n | \, \bar{\psi} W_1 \, | 0 \rangle \, \frac{\langle q_1 \cdots q_m | \, Y_1^\dagger W_1 \, | 0 \rangle}{\langle 0 | \, Y_1^\dagger W_1 \, | 0 \rangle} \tag{4.9}$$

for some $C_{\bar{\psi}W}$. To determine $C_{\bar{\psi}W}$, we note that $C_{\bar{\psi}W}$ does not depend on how the momentum in the collinear and soft sectors are distributed; this equation holds for any $n > 0$ and any $m \geq 0$. In particular, if we take $m = 0$ then the two sides are identical (and agree at leading power) if and only if $C_{\bar{\psi}W} = 1$. Thus we must have $C_{\bar{\psi}W} = 1$ for any states.

As a special case, Eq. (4.9) implies that for one collinear and one soft momentum

$$\frac{\langle p_1; q | \, \bar{\psi} W_1 \, | 0 \rangle}{\langle 0 | \, Y_1^\dagger W_1 \, | 0 \rangle} \overset{q \text{ soft}}{\cong} \frac{\langle p_1 | \, \bar{\psi} W_1 \, | 0 \rangle}{\langle 0 | \, Y_1^\dagger W_1 \, | 0 \rangle} \frac{\langle q | \, Y_1^\dagger W_1 \, | 0 \rangle}{\langle 0 | \, Y_1^\dagger W_1 \, | 0 \rangle} \tag{4.10}$$

Similarly, applying the general factorization formula to $\mathcal{O} = Y_1^\dagger Y_2$, we get

$$\langle q | \, Y_1^\dagger Y_2 \, | 0 \rangle \overset{q \parallel p_1}{\cong} \frac{\langle q | \, Y_1^\dagger W_1 \, | 0 \rangle}{\langle 0 | \, Y_1^\dagger W_1 \, | 0 \rangle} \times \langle 0 | \, Y_1^\dagger Y_2 \, | 0 \rangle \tag{4.11}$$

In this case one can see that the Wilson coefficient is 1 to all orders by using the proof in [4] that the factorization theorem is independent of the collinear Wilson-line direction, t_1, and then choosing $t_1^\mu = n_2^\mu$, so that $W_1 = Y_2$.

With these results, we can now analyze the following all-loop-order subtracted matrix element:

$$\begin{aligned}\mathcal{M}_{\text{sub}}(p_1,p_2,q) \equiv &\left\{\frac{\langle p_1;q|\,\bar\psi W_1\,|0\rangle}{\langle 0|\,Y_1^\dagger W_1\,|0\rangle} - \frac{\langle p_1|\,\bar\psi W_1\,|0\rangle}{\langle 0|\,Y_1^\dagger W_1\,|0\rangle}\frac{\langle q|\,Y_1^\dagger W_1\,|0\rangle}{\langle 0|\,Y_1^\dagger W_1\,|0\rangle}\right\}\frac{\langle p_2|\,W_2^\dagger\psi\,|0\rangle}{\langle 0|\,W_2^\dagger Y_2\,|0\rangle}\,\langle 0|\,Y_1^\dagger Y_2\,|0\rangle \\ &+\frac{\langle p_1|\,\bar\psi W_1\,|0\rangle}{\langle 0|\,Y_1^\dagger W_1\,|0\rangle}\left\{\frac{\langle p_2;q|\,\bar\psi W_2\,|0\rangle}{\langle 0|\,Y_2^\dagger W_2\,|0\rangle} - \frac{\langle p_2|\,\bar\psi W_2\,|0\rangle}{\langle 0|\,Y_2^\dagger W_2\,|0\rangle}\frac{\langle q|\,Y_2^\dagger W_2\,|0\rangle}{\langle 0|\,Y_2^\dagger W_2\,|0\rangle}\right\}\langle 0|\,Y_1^\dagger Y_2\,|0\rangle \\ &+\frac{\langle p_1|\,\bar\psi W_1\,|0\rangle}{\langle 0|\,Y_1^\dagger W_1\,|0\rangle}\frac{\langle p_2|\,W_2^\dagger\psi\,|0\rangle}{\langle 0|\,W_2^\dagger Y_2\,|0\rangle}\,\langle q|\,Y_1^\dagger Y_2\,|0\rangle \quad (4.12)\end{aligned}$$

If we take q soft, then neither of the first two lines contribute by Eq. (4.10), and the result is given by the third line which is the correct leading power matrix element $\mathcal{M}_s$. When $q \parallel p_1$, then neither term in the second line is IR sensitive and the subtraction term in the first line (which is IR-sensitive) is canceled by collinear limit of the third line, using Eq. (4.11). Thus, only the first term on the first line contributes at leading power in this limit, in agreement with $\mathcal{M}_1$. The analogous argument works for the $q \parallel p_2$ limit. We conclude that $\mathcal{M}_{\text{sub}}(p_1,p_2,q)$ agrees with full QCD at leading power for any q. Thus, we can integrate $\mathcal{M}_{\text{sub}}$ over phase space without splitting the soft and collinear sectors.

To be explicit, we can evaluate Eq. (4.12) in perturbation theory. At tree-level,

$$\begin{aligned}\mathcal{M}(p_1,p_2,q) \overset{\text{tree}}{=} &\,\bar u(p_1)\left\{\left(\frac{-g\not\epsilon_q(\not p_1+\not q)}{2p_1\cdot q}+\frac{gt_1\cdot\epsilon_q}{t_1\cdot q}\right)-\left(\frac{-gn_1\cdot\epsilon_q}{n_1\cdot q}+\frac{gt_1\cdot\epsilon_q}{t_1\cdot q}\right)\right\}v(p_2) \\ &+\bar u(p_1)\left\{\left(\frac{g(\not p_2+\not q)\not\epsilon_q}{2p_2\cdot q}+\frac{-gt_2\cdot\epsilon_q}{t_2\cdot q}\right)-\left(\frac{-gt_2\cdot\epsilon_q}{t_2\cdot q}+\frac{gn_2\cdot\epsilon_q}{n_2\cdot q}\right)\right\}v(p_2) \\ &+\bar u(p_1)\left(\frac{-gn_1\cdot\epsilon_q}{n_1\cdot q}+\frac{gn_2\cdot\epsilon_q}{n_2\cdot q}\right)v(p_2) \quad (4.13)\end{aligned}$$

where each term in round brackets corresponds to one of the matrix elements containing the gluon, and thereby each satisfies the Ward identity separately. From the explicit expression in Eq. (4.13) it is easy to check that each soft and collinear limit works out exactly as stated in the paragraph after Eq. (4.12). It can also be seen that the t_j dependent terms cancel out completely as do the soft terms containing n_j at this order, leaving:

$$\mathcal{M}_{\text{sub}}(p_1,p_2,q) \overset{\text{tree}}{=} \bar{u}(p_1)\left(\frac{-g\not{\epsilon}_q(\not{p}_1+\not{q})}{2p_1\cdot q}+\frac{g(\not{p}_2+\not{q})\not{\epsilon}_q}{2p_2\cdot q}\right)v(p_2) \overset{\text{tree}}{=} \mathcal{M}(p_1,p_2,q) \quad (4.14)$$

So the the full matrix element of QED is reproduced exactly in this case. Of course, for more complex calculations we expect $\mathcal{M}$ to only reproduce the full-theory matrix element at leading power, rather than be exactly equal to it.

4.2.2 General amplitude-level subtraction

The generalization of Eq. (4.12) for arbitrary collinear and soft sectors is

$$\begin{aligned}\langle X_1\cdots X_N;X_s;q|\,\mathcal{O}\,|0\rangle \cong_{\text{IR}} &\frac{\langle X_1|\,\bar{\psi}W_1\,|0\rangle}{\langle 0|\,Y_1^\dagger W_1\,|0\rangle}\cdots\frac{\langle X_N|\,W_N^\dagger\psi\,|0\rangle}{\langle 0|\,W_N^\dagger Y_N\,|0\rangle}\,\langle X_s,q|\,Y_1^\dagger\cdots Y_N\,|0\rangle \\ &+\sum_{i=1}^{N}\frac{\langle X_1|\,\bar{\psi}W_1\,|0\rangle}{\langle 0|\,Y_1^\dagger W_1\,|0\rangle}\cdots\left\{\frac{\langle X_i,q|\,W_i^\dagger\psi\,|0\rangle}{\langle 0|\,W_i^\dagger Y_i\,|0\rangle}\right\}^{q}_{\substack{\text{soft}\\ \text{sub}}}\cdots\frac{\langle X_N|\,W_N^\dagger\psi\,|0\rangle}{\langle 0|\,W_N^\dagger Y_N\,|0\rangle}\,\langle X_s|\,Y_1^\dagger\cdots Y_N\,|0\rangle\end{aligned} \quad (4.15)$$

where the $\{\}^{q}_{\substack{\text{soft}\\ \text{sub}}}$ notation means the operator matrix element corresponding to having subtracted the $q\to$ soft limit. To be explicit, we can use the notation $\mathcal{S}(q)$ as in [4]

for the leading order contribution in the $q \to$ soft limit. Then

$$\begin{aligned}\left\{\frac{\langle X_i, q|\, W_i^\dagger \psi\,|0\rangle}{\langle 0|\, W_i^\dagger Y_i\,|0\rangle}\right\}_{\substack{q\\ \text{soft}\\ \text{sub}}} &\equiv \frac{\langle X_i, q|\, W_i^\dagger \psi\,|0\rangle}{\langle 0|\, W_i^\dagger Y_i\,|0\rangle} - \left(\frac{\langle X_i, q|\, W_i^\dagger \psi\,|0\rangle}{\langle 0|\, W_i^\dagger Y_i\,|0\rangle}\right)_{\mathcal{S}(q)} \\ &= \frac{\langle X_i, q|\, W_i^\dagger \psi\,|0\rangle}{\langle 0|\, W_i^\dagger Y_i\,|0\rangle} - \frac{\langle X_i|\, W_i^\dagger \psi\,|0\rangle\, \langle q|\, W_i^\dagger Y_i\,|0\rangle}{\langle 0|\, W_i^\dagger Y_i\,|0\rangle^2}\end{aligned} \tag{4.16}$$

This subtracted quantity is exactly the same as what was used in Eq. (4.12) and vanishes at leading power in the $q \to$ soft limit by Eq. (4.10). Eq. (4.15) is a sum of factorized expressions which agrees at leading power with full QCD in any soft or collinear limit of q.

To generalize to multiple gluons or quarks with momenta q_i, the analogous formula is easiest to define recursively. For example, adding a second gluon to Eq. (4.15), we can either place it in the soft matrix element, or in a collinear matrix element. If it is in the collinear matrix element, we must subtract off the soft limit. Thus we get a sum of terms:

$$\begin{aligned}\langle X_1 \cdots X_N; X_s; q_1, q_2|\, \mathcal{O}\,|0\rangle \cong_{\text{IR}} &\frac{\langle X_1|\, \bar{\psi} W_1\,|0\rangle}{\langle 0|\, Y_1^\dagger W_1\,|0\rangle} \cdots \frac{\langle X_N|\, W_N^\dagger \psi\,|0\rangle}{\langle 0|\, W_N^\dagger Y_N\,|0\rangle}\, \langle X_s, q_1, q_2|\, Y_1^\dagger \cdots Y_N\,|0\rangle \\ &+ \sum_{i=1}^N \cdots \left\{\frac{\langle X_i, q_1|\, W_i^\dagger \psi\,|0\rangle}{\langle 0|\, W_i^\dagger Y_i\,|0\rangle}\right\}_{\substack{q_1\\ \text{soft}\\ \text{sub}}} \cdots \langle X_s, q_2|\, Y_1^\dagger \cdots Y_N\,|0\rangle \\ &+ \sum_{i=1}^N \cdots \left\{\frac{\langle X_i, q_2|\, W_i^\dagger \psi\,|0\rangle}{\langle 0|\, W_i^\dagger Y_i\,|0\rangle}\right\}_{\substack{q_2\\ \text{soft}\\ \text{sub}}} \cdots \langle X_s, q_1|\, Y_1^\dagger \cdots Y_N\,|0\rangle \\ &+ \sum_{i,j=1}^N \cdots \left\{\frac{\langle X_i, q_1|\, W_i^\dagger \psi\,|0\rangle}{\langle 0|\, W_i^\dagger Y_i\,|0\rangle}\right\}_{\substack{q_1\\ \text{soft}\\ \text{sub}}} \cdots \left\{\frac{\langle X_j, q_2|\, W_j^\dagger \psi\,|0\rangle}{\langle 0|\, W_j^\dagger Y_j\,|0\rangle}\right\}_{\substack{q_2\\ \text{soft}\\ \text{sub}}} \cdots \langle X_s|\, Y_1^\dagger \cdots Y_N\,|0\rangle\end{aligned} \tag{4.17}$$

where the $\cdots$ represent the other collinear matrix elements which do not contain any q's. In the last line, when $i = j$ the soft subtraction must be done iteratively to ensure that the subtraction mitigates the soft enhancement in any order of limits of q_1 and

q_2 going soft. That is,

$$\frac{\langle X_j, q_1, q_2|\, W_j^\dagger \psi\,|0\rangle}{\langle 0|\, W_j^\dagger Y_j\,|0\rangle}\bigg|_{\substack{q_1,q_2\\ \text{soft}\\ \text{sub}}} \equiv \frac{\langle X_j, q_1, q_2|\, W_j^\dagger \psi\,|0\rangle}{\langle 0|\, W_j^\dagger Y_j\,|0\rangle} - \left(\frac{\langle X_j, q_1, q_2|\, W_j^\dagger \psi\,|0\rangle}{\langle 0|\, W_j^\dagger Y_j\,|0\rangle}\right)_{\mathcal{S}(q_1,q_2)} - \left(\frac{\langle X_j, q_1, q_2|\, W_j^\dagger \psi\,|0\rangle}{\langle 0|\, W_j^\dagger Y_j\,|0\rangle} - \left(\frac{\langle X_j, q_1, q_2|\, W_j^\dagger \psi\,|0\rangle}{\langle 0|\, W_j^\dagger Y_j\,|0\rangle}\right)_{\mathcal{S}(q_1,q_2)}\right)_{\mathcal{S}(q_1)} - \left(\frac{\langle X_j, q_1, q_2|\, W_j^\dagger \psi\,|0\rangle}{\langle 0|\, W_j^\dagger Y_j\,|0\rangle} - \left(\frac{\langle X_j, q_1, q_2|\, W_j^\dagger \psi\,|0\rangle}{\langle 0|\, W_j^\dagger Y_j\,|0\rangle}\right)_{\mathcal{S}(q_1,q_2)}\right)_{\mathcal{S}(q_2)} \tag{4.18}$$

where $\mathcal{S}(q_1, q_2)$ means taking the leading-power expression in the $q_1, q_2 \to$ soft limit simultaneously and, therefore, does not drop q_1 with respect to q_2 or vice-versa. Note that, as always, we can write the soft limits in terms of amplitudes with Wilson lines using the factorization theorem of Eq. (4.1). For example,

$$\left(\frac{\langle X_j, q_1, q_2|\, W_j^\dagger \psi\,|0\rangle}{\langle 0|\, W_j^\dagger Y_j\,|0\rangle}\right)_{\mathcal{S}(q_1,q_2)} = \frac{\langle X_j|\, W_j^\dagger \psi\,|0\rangle}{\langle 0|\, W_j^\dagger Y_j\,|0\rangle}\frac{\langle q_1, q_2|\, W_j^\dagger Y_j\,|0\rangle}{\langle 0|\, W_j^\dagger Y_j\,|0\rangle} \tag{4.19}$$

where we know that the Wilson coefficient will always be 1 to all orders by the argument given after Eq. (4.9).

That these subtractions will always work follows using the arguments of Ch. 3. In particular, the "coloring algorithm" in Section 3.6 of that chapter is exactly the recursive soft subtraction procedure indicated by Eqs. (4.12), (4.15)–(4.18). As with the algorithm in [4], the soft limit of any subset of the q's in the $\{\}^{q_1\cdots q_m}_{\substack{\text{soft}\\ \text{sub}}}$ matrix elements are power suppressed, and they should correspondingly be colored blue. With this knowledge, it is easy to check that Eq. (4.17) agrees in the IR: when $q_1, q_2 \to$ soft, all of the $\{\}^{q_i}_{\substack{\text{soft}\\ \text{sub}}}$ matrix elements are power suppressed and only the top line survives, which gives the correct answer. When $q_1 \parallel p_j$ and $q_2 \to$ soft, say, the bottom two lines are power suppressed and the $\mathcal{S}(q_1)$-subtracted term cancels with the top line, leaving only the one term that matches the full-factorized formula in this

limit. Similarly, all other limits can be simply checked. The pattern of subtractions with more than two gluons follows exactly as with the coloring algorithm stated in generality in [4].

The procedure outlined in this section produces amplitudes which can be computed as a sum of factorized terms. These amplitudes, which are a new result, reproduce all of the leading-power IR-sensitive limits of the full-QCD amplitudes, at all-loop order. Each factor in each term in the sum involves matrix elements of fields and Wilson lines that are universal and simpler than the factors in the full QCD amplitude. Given these properties, an interesting application of the matrix elements derived in this section might be towards subtraction procedures for QCD calculations at NNLO or beyond. One application of subtraction methods is to split an amplitude into a universal IR-sensitive piece that is simple enough to integrate analytically and a piece that is IR-finite which could be integrated numerically [132–136]. The amplitudes presented in this section could be a candidate for such a procedure at any order in perturbation theory and for any number of external particles.

4.3 Factorization for distributions

Despite having many strengths, amplitudes as in Eq. (4.15), are no longer factorized: they cannot be written as a single product of terms with the same external states (in this case the collinear sectors and the soft sector are tangled). When the amplitudes are squared, the interference effects between various terms in the sum contribute at leading power, so they must all be included. Thus, while one *can* integrate over the momenta q_j without overcounting the infrared-sensitive region, the separa-

tion between soft and collinear contributions is no longer manifest. Moreover, it is not clear how the large logarithms associated with the leading-power IR sensitivity can be resummed using such amplitudes.

Fortunately, for certain observables, one can perform subtractions differently so that factorization is preserved at the cross-section level. In this section, we discuss a class of factorizing observables. Namely, we discuss observables whose measurement function, that is, the mapping from the final-state momenta to the observable, is linear in the soft and collinear momenta. These observables include many e^+e^- event shapes, such as thrust [7–9, 137, 138], angularities [72, 139, 140] heavy jet mass [10], the C parameter [141–143] and jet broadening [144–148]. Many hadron collider observables are also in this class [16], such Drell-Yan near threshold [149], deep inelastic scattering as $x \to 1$ [101], direct photon production [17,150], W/Z + jet [18,19,151], jet mass [23, 24], or $t\bar{t}$ production near the hadronic threshold [104,152] as well as N-(sub)jettiness [6, 26, 153].

Factorization at the cross-section level for observables in this class has been understood already by traditional QCD and by Soft-Collinear Effective Theory (see above references). The overcounting of soft and collinear integration regions is also well-understood in both approaches, and the two approaches have already been shown to be equivalent [97, 108, 109]. Unfortunately, it is challenging to extract from the literature which aspects of the removal of overcounting have been rigorously proven (in either approach) and which aspects are simply assumed. Moreover, the overcounting in phase-space integrals has not been addressed at all in the effective field theory formulation with full-theory fields [51], [3], [4]. The goal of this section is to give a

self-contained proof that the overcounting induced by removing phase-space cutoffs can be completely compensated for. We thereby demonstrate a form of factorization that holds exactly at leading power at the cross-section level with no phase space cutoffs.

4.3.1 Factorization for thrust

For concreteness and simplicity, we begin our discussion with thrust, the paradigmatic observable whose distribution factorizes. Thrust, T, is defined as [137]

$$T \equiv \frac{\sum_j |\vec{p}_j \cdot \vec{n}|}{\sum_j |\vec{p}_j|} \tag{4.20}$$

where $\vec{n}$ is the thrust axis, defined to maximize T. The region where factorization holds is where $\tau = 1 - T \ll 1$. Then

$$\tau \cong 1 - \sum_j \frac{1}{Q} |\vec{p}_j \cdot \vec{n}| = \frac{1}{2Q} \sum_j \Omega_\tau(p_j) \tag{4.21}$$

where Q is the center of mass energy and $\Omega_\tau(p)$ is the measurement function for thrust:

$$\Omega_\tau(p) = p^- \theta(p^+ - p^-) + p^+ \theta(p^- - p^+) \tag{4.22}$$

where $p^+ = n \cdot p$ and $p^- = \bar{n} \cdot p$.

Note that τ has the property that it is linear in the momenta: each particle momentum contributes additively to thrust, independent of the other momenta in the final state $\langle X|$. In particular, if we decompose $\langle X|$ into soft, collinear and hard momenta, then we can compute the contribution to thrust from each sector separately and just add the results. In other words, linearity implies

$$\delta\Big(\tau - \frac{1}{2Q}\Omega_\tau(p_X)\Big) = \delta\Big(\tau - \frac{1}{2Q}p_s - \frac{1}{2Q}p_1 - \frac{1}{2Q}p_2 - \frac{1}{2Q}p_{\rm h}\Big) \tag{4.23}$$

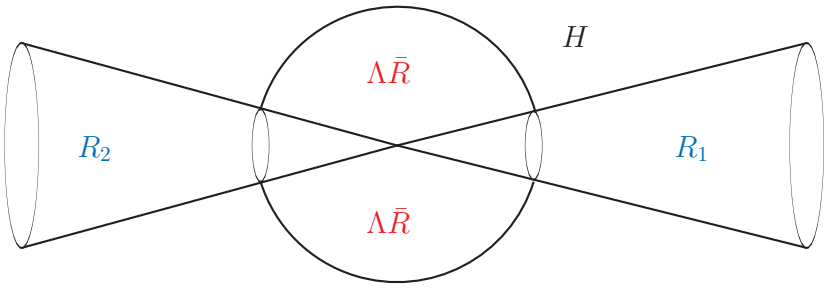

Figure 4.1: Mutually exclusive sectioning of phase space into j-collinear, soft and hard momentum labelled by R_j, $\Lambda\overline{R}$ and H, respectively. In explicit formulas in this chapter, R is treated as a rapidity variable: $R = \tan^2\frac{\theta}{2}$, with θ the opening angle of the cone.

where p_s is the sum of $\Omega_\tau(k)$ over the soft momenta, p_1 and p_2 the sum over collinear momenta in each direction and p_h the sum over the remaining momenta. Writing the argument of the δ-function as a sum lets us turn products of matrix elements into convolutions.

To be concrete let us place the momenta into sectors using hard cuts: we draw cones of angular size R around the $\vec{n}$ and $-\vec{n}$ collinear directions and a ball of size Λ around the origin; anything in the cones but not the ball is collinear, $\langle X_j|$, anything in the ball but not the cones is soft, $\langle X_s|$. For later convenience, we include the soft-collinear radiation, which is in both the ball and the a cone, in the collinear sector (we could equally well have put it in the soft sector). Anything not in the cone or ball is called hard, $\langle X_H|$. This breakdown of phase space is shown in Fig 4.1.

Consider the thrust distribution in full QCD mediated by the operator $\mathcal{O} = \bar{\psi}\gamma^\mu\psi$. That is,

$$\frac{d\sigma}{d\tau} = \sum_X \int d\Pi_X |\langle X|\mathcal{O}|0\rangle|^2 \delta\Big(\tau - \frac{1}{2Q}\Omega_\tau(p_X)\Big) \tag{4.24}$$

where the sum is over all possible final states $\langle X|$ and the normalization and momentum-

conserving δ-function are left implicit.

When τ is small, only states of the form $\langle X| = \langle X_1| \langle X_2| \langle X_s|$ contribute at leading power in τ. With the hard phase-space cuts in place, the factorization formula at the amplitude level, Eq. (4.1) along with Eq. (4.23), immediately generates a factorization formula for the thrust distribution:

$$\frac{d\sigma}{d\tau} \cong H \times S^{\Lambda\overline{R}} \otimes J^{R_1} \otimes J^{R_2} \tag{4.25}$$

Here $H = |\mathcal{C}|^2$ refers to the hard function (the square of the Wilson coefficient in the factorization formula). J^{R_1} and J^{R_2} are jet functions with restricted phase-space integrals:

$$J^{R_1}(\tau) = \sum_{X_1} \int d\Pi_{X_1} \left| \frac{\langle X_1| \bar{\psi} W_1 |0\rangle}{\langle 0| Y_1^\dagger W_1 |0\rangle} \right|^2 \delta\big(\tau - p^+_{X_1}\big) \tag{4.26}$$

with X_1 the set of states all of whose momenta are within an angular distance R of the n^μ direction. Note that we have modified the measurement function from $\Omega_\tau(p)$ in Eq. (4.22) to simply p^+. This is allowed since all the momenta in the cone necessarily have $p^- > p^+$ so the step functions in Eq. (4.22) can be evaluated explicitly. Analogously, the jet function, J^{R_2}, will have the measurement function replaced by p^-. Lastly, $S^{\Lambda\overline{R}}$ is the phase-space restricted soft function

$$S^{\Lambda\overline{R}}(\tau) = \sum_{X_s} \int d\Pi_{X_s} \left| \langle X_s| Y_1^\dagger \cdots Y_N |0\rangle \right|^2 \delta\Big(\tau - \frac{1}{2Q}\Omega_\tau(p_{X_s})\Big) \tag{4.27}$$

Here the states have momenta which are not collinear, that is, they are an angular distance greater than R from all jets, and they have energy less than Λ.

The equivalence in Eq. (4.25) holds at leading power in τ only if R and Λ are small enough so that the collinear radiation is collinear and the soft radiation is soft. More precisely, it holds at leading power in R and Λ, meaning that the two

sides my differ by terms of order R or order Λ which vanish as $R \to 0$ and $\Lambda \to 0$. Since the operators entering the soft and jet function are different, we do not expect the R dependence to cancel exactly between them; the factorization theorem only guarantees that it vanish at leading power.

We suspect it may be pedagogically useful to examine explicit expressions for $S^{\Lambda\overline{R}}$ and J^R. To distinguish UV divergences from IR divergences we include an off-shellness regulator ω for the IR: namely, we take the outgoing external fermion lines to have an offshellness of $Q^2\omega$. Consequently, the propagator in Y_j will look like

$$\frac{n_j^\mu}{n_j \cdot k} \to \frac{p_j^\mu}{p_j \cdot k + \frac{Q^2\omega}{2}} \tag{4.28}$$

We further analytically continue to $d = 4 - 2\varepsilon$ dimensions for the UV. Details of the intermediate steps are given in the Appendix of [5]. For the unrenormalized jet function at finite R, we find

$$\begin{aligned} J^{R_j}(\tau) \cong \delta(\tau) + \frac{\alpha_s C_F}{2\pi}\left(\frac{\mu^2}{Q^2}\right)^\varepsilon \Bigg\{ & \delta(\tau)\left(\frac{2}{\varepsilon^2} + \frac{3}{2\varepsilon} + \frac{7}{2} + \frac{\pi^2}{6}\right) \\ & + \delta(\tau)\left(-\frac{2}{\varepsilon}\ln\omega - 2\ln\omega\ln R + 2\ln^2\omega + \mathcal{O}(R)\right) - \left(\frac{3}{2} - 2\ln R\right)\left[\frac{1}{\tau}\right]_+ - 2\left[\frac{\ln\tau}{\tau}\right]_+ \Bigg\} \end{aligned} \tag{4.29}$$

This expression includes both the real and virtual contributions to $\langle X_1|\,\bar{\psi}W_1\,|0\rangle$ and the purely virtual contributions to $\langle 0|\,Y_1^\dagger W_1\,|0\rangle$ in Eq. (4.26). Note that it has $\frac{1}{\varepsilon^2}$ UV poles, which come from the virtual graphs. It also has an overlapping UV-IR singularity (the $\frac{1}{\varepsilon}\ln\omega$ term on the second line). This singularity, which cannot be removed through local counterterms, comes from loops involving the Wilson lines which go to infinite energy collinear to one of the Wilson line directions. The $\log R$ dependence in Eq. (4.29) comes from the soft-collinear region of the restricted phase-space integral. Indeed, it cannot come from the collinear-but-not soft region, since at

arbitrarily small τ, the radiation is forced arbitrarily close to the jet axis and must be a finite distance from the cone boundary. In the soft-collinear region, the radiation can be soft but an angular distance R from the axis, so there can be R dependence at leading power in τ. That the $\ln R$ dependence comes from only the soft-collinear region is to be expected if it is to be completely canceled by the soft function.

The soft function outside the cones with finite Λ is

$$\begin{aligned} S^{\Lambda\overline{R}}(\tau) = \delta(\tau) + C_F \frac{\alpha_s}{\pi} \left(\frac{\mu^2}{Q^2}\right)^{\varepsilon} \Bigg\{ \delta(\tau) \left(-\frac{1}{\varepsilon^2} - \frac{7\pi^2}{12} + \frac{2}{\varepsilon} \ln\omega + 2\ln\omega \ln R - 2\ln^2\omega + \mathcal{O}(R) \right) \\ - \left[\frac{2}{\tau} \ln R \right]_+ \Bigg\} \theta\Big(\Lambda - \frac{\tau}{R}\Big) \\ + C_F \frac{\alpha_s}{\pi} \left(\frac{\mu^2}{Q^2}\right)^{\varepsilon} \left\{ \delta(\tau) \left[-\frac{1}{\varepsilon^2} - \frac{\pi^2}{4} - 2\left(-\frac{1}{\varepsilon} \ln\omega + \ln\omega \ln\frac{\Lambda}{Q} + \frac{1}{2}\ln^2\omega \right) \right] - \left[\frac{2}{\tau} \ln\frac{\tau Q}{\Lambda} \right]_+ \right\} \theta\Big(\frac{\tau}{R} - \Lambda\Big) \end{aligned} \tag{4.30}$$

This function also has an incomplete cancellation between the real and virtual contributions. In particular, the virtual includes the soft-collinear region which is excluded from the real emission. Note that the Λ dependence is entirely subleading power in τ: for small τ, the θ function in the third line in Eq. (4.30) vanishes and the other θ function evaluates to unity. The R dependence is not subleading power as $\tau \to 0$. There are also $\mathcal{O}(R)$ terms not shown here but written out in Eq. (**??**). We will come back to the cancellation of the R dependence among the two jet functions and the soft function shortly.

Convolving Eq. (4.29) for each jet with Eq. (4.30) we get

$$\begin{aligned} &S^{\Lambda\overline{R}} \otimes J^{R_1} \otimes J^{R_2} \\ &\cong \delta(\tau) + C_F \frac{\alpha_s}{\pi} \left(\frac{\mu^2}{Q^2}\right)^{\varepsilon} \left\{ \delta(\tau) \left(\frac{1}{\varepsilon^2} + \frac{3}{2\varepsilon} + \frac{7}{2} - \frac{5\pi^2}{12} + \mathcal{O}(R) \right) - \frac{3}{2} \left[\frac{1}{\tau}\right]_+ - 2 \left[\frac{\ln\tau}{\tau}\right]_+ \right\} \end{aligned} \tag{4.31}$$

Note that the Λ dependence has dropped out completely, and the R dependence which is singular as $R \to 0$ has also dropped out. It is not hard to verify that this result agrees with the full-theory result for thrust at leading power, up to the coefficient of $\delta(\tau)$ which is corrected by the hard function.

While the factorization formula for thrust in Eq. (4.25) works, it has numerous flaws. On the practical side, it is difficult to use because of the phase-space cuts. On the conceptual side, the cuts introduce additional scales into the soft and jet functions which frustrate factorization and resummation. The most serious flaw, however, is that the jet and soft functions are not individually infrared safe: they each have infrared divergences which cancel only when combined, as we saw with the explicit example above. These divergences come from an incomplete cancellation between the real-emission graphs, which have phase-space restrictions, and the virtual graphs, which do not. We could attempt to put phase-space cuts on the virtual graphs as well. However, it is more logical to try to remove the phase-space cuts from the real-emission contributions to the jet and soft functions, since this would simplify their calculation and removes the spurious scales.

First we remove Λ. This is quite simple. Only the soft function depends on Λ. By our definition, $S^{\Lambda\overline{R}}$ in Eq. (4.25) only integrates over the soft-but-not-collinear region of phase space. The phase-space region outside of the cones but with energy

$\Lambda < E < \infty$ does not contribute at all at leading power in τ. So we can simply define a new soft function by including also this region:

$$S^{\overline{R}} \cong S^{\Lambda\overline{R}} \tag{4.32}$$

where $S^{\overline{R}} = S^{(\Lambda=\infty)\overline{R}}$ has no cutoff on energy in the soft function. This equivalence can be verified at order α_s in the Appendix of [5], where the entire Λ dependence is subleading power in τ, as observed above. Explicitly,

$$\begin{aligned} S^{\overline{R}}(\tau) = \delta(\tau) + C_F \frac{\alpha_s}{\pi} \left(\frac{\mu^2}{Q^2}\right)^{\varepsilon} \Bigg\{ & \delta(\tau) \left[-\frac{1}{\varepsilon^2} - \frac{7\pi^2}{12} \right] \\ & - 2\delta(\tau) \left[-\frac{1}{\varepsilon} \ln\omega - \ln\omega \ln R + \ln^2\omega + \mathcal{O}(R) \right] - \left[\frac{2}{\tau} \ln R \right]_+ \Bigg\} \end{aligned} \tag{4.33}$$

Note that $S^{\overline{R}}$ is identical to the coefficient of $\theta(\Lambda - \frac{\tau}{R})$ in Eq. (**??**). One might have imagined that taking $\Lambda \to \infty$ would introduce new UV poles. However, radiation in $\overline{R}$, say in the right hemisphere, at a given τ must have $k^+ = Q\tau$ and $k^- < \frac{1}{R} k^+ = Q\frac{\tau}{R}$, so the energy $E = \frac{1}{2}(k^+ + k^-) < \frac{Q\tau}{2}(1 + \frac{1}{R})$ of all radiation contributing to $S^{\overline{R}}$ at fixed τ is in fact bounded from above so there are no new UV divergences. Thus, we now have

$$\frac{d\sigma}{d\tau} \cong H \times S^{\overline{R}} \otimes J^{R_1} \otimes J^{R_2} \tag{4.34}$$

with no Λ dependence on either side. Keep in mind that this equivalence is still valid only as $R \to 0$: there are power corrections in R on the right-hand side.

Removing the R dependence is more subtle, since the R dependence in both the soft and jet functions is relevant at leading power in τ and since the dependence on R in both functions is singular as $R \to 0$. To remove it, we need a subtraction. To construct the subtraction, first recall that the general amplitude-level factorization

proof in [4] applies to any operator, including one composed of Wilson lines. In particular, collinear factorization for a Wilson-line operator implies

$$S \cong S^{\overline{R}} \otimes J_{\text{eik}}^{R_1} \otimes J_{\text{eik}}^{R_2} \tag{4.35}$$

where $S = S^{\overline{R=\infty}}$ has no angular or energy restriction and the **eikonal jet function** is defined as

$$J_{\text{eik}}^{R_1}(\tau) = \sum_{X_1} \int d\Pi_{X_1} \left| \frac{\langle X_1 | \, Y_1^\dagger W_1 \, | 0 \rangle}{\langle 0 | \, Y_1^\dagger W_1 \, | 0 \rangle} \right|^2 \delta(\tau - p_{X_1}^+) \tag{4.36}$$

The eikonal jet function differs from the jet function in Eq. (4.26) in that $Y_1^\dagger$ replaces the field $\bar{\psi}$. Note that the measurement function in the eikonal jet function is the power-expanded version, $\delta(p - p^+)$, rather than $\Omega_\tau(p)$. This is consistent with Eq. (4.35) since the phase space in the eikonal jet function is restricted to be in a cone.

Explicitly, to order α_s, we find

$$J_{\text{eik}}^{R_j}(\tau) = \delta(k) + \frac{\alpha_s C_F}{2\pi} \left(\frac{\mu^2}{Q^2} \right)^\varepsilon \left\{ \delta(\tau) \left[\frac{2\pi^2}{3} - \frac{2}{\varepsilon} \ln \omega - 2 \ln \omega \ln R + 2 \ln^2 \omega + \mathcal{O}(R) \right] \right.$$
$$\left. + \left(\frac{2}{\varepsilon} + 2 \ln R \right) \left[\frac{1}{\tau} \right]_+ - 4 \left[\frac{\ln \tau}{\tau} \right]_+ \right\} \tag{4.37}$$

Comparing Eq. (4.37) to Eq. (4.29), we see that the ω and R dependence in $J_{\text{eik}}^{R_j}$ is the same as that in J^{R_j}. This is expected, since the only IR-sensitive difference between the two is in the collinear-but-not-soft region of $\langle X_1 | \, Y_1^\dagger W_1 \, | 0 \rangle$ and $\langle X_1 | \, \bar{\psi} W_1 \, | 0 \rangle$. In this region, there is a complete cancellation of real and virtual graph for both functions, hence both are IR-finite. Note also that there are no $\frac{1}{\varepsilon^2}$ poles in the eikonal jet function. These double UV poles in the regular jet function come from virtual graphs. In the eikonal jet function, the virtual graphs in the numerator and denominator of

Eq. (4.36) are identical and hence cancel in the ratio to order α_s. The lack of $\frac{1}{\varepsilon^2}$ poles also implies that there are no Sudakov double logs in the eikonal jet function.

Now, if we convolve both sides of Eq. (4.25) with the eikonal jet functions and use Eq. (4.32) and Eq. (4.35), we get

$$\frac{d\sigma}{d\tau} \otimes J^{R_1}_{\text{eik}} \otimes J^{R_2}_{\text{eik}} \cong H \times S \otimes J^{R_1} \otimes J^{R_2} \tag{4.38}$$

At this point, no object in this leading-power equivalence depends on Λ and the R dependence on both sides is only in the jet functions and eikonal jet functions. We still must have R small though, since there are power corrections in R on both sides.

Finally, we want to remove the R-dependence completely. Let us call a jet function with no restriction on R an **inclusive jet function** and denote it by J^j. Removing the R introduces additional unphysical singularities collinear to the Wilson-line direction t_j which are not regulated with the off-shellness regulator. We must introduced another regulator for these singularities, so we use the Δ-regulator [154], δ_j, which shifts the eikonal propagators as:

$$\frac{1}{t_j \cdot k} \to \frac{1}{t_j \cdot k + \delta_j (t_j \cdot p_j)} \tag{4.39}$$

To order α_s we find for the inclusive jet function

$$\begin{aligned} J^j(\tau) = \delta(\tau) + \frac{\alpha_s C_F}{2\pi} \left(\frac{\mu^2}{Q^2}\right)^{\varepsilon} \Bigg\{ & \delta(\tau) \left(\frac{2}{\varepsilon^2} + \frac{3}{2\varepsilon} + \frac{7}{2} - \frac{\pi^2}{6} \right) \\ & + \delta(\tau) \left(-\frac{2}{\varepsilon} \ln \omega + 2 \ln \omega \ln \delta_j + \ln^2 \omega \right) - \left(2 \ln \delta_j + \frac{3}{2} \right) \left[\frac{1}{\tau} \right]_+ \Bigg\} \end{aligned} \tag{4.40}$$

Similarly, for the inclusive eikonal jet function we find

$$\begin{aligned} J^j_{\text{eik}}(\tau) = \delta(\tau) + \frac{\alpha_s C_F}{2\pi} \left(\frac{\mu^2}{Q^2}\right)^{\varepsilon} \Bigg\{ & \delta(\tau) \left[\frac{\pi^2}{3} - \frac{2}{\varepsilon} \ln \omega + 2 \ln \omega \ln \delta_j + \ln^2 \omega \right] \\ & + \left(\frac{2}{\varepsilon} - 2 \ln \delta_j \right) \left[\frac{1}{\tau} \right]_+ - 2 \left[\frac{\ln \tau}{\tau} \right]_+ \Bigg\} \end{aligned} \tag{4.41}$$

Note that the δ_j dependence associated with the Wilson line direction is identical in the two inclusive jet functions.

Next, note that since $\overline{R_j}$ does not contain the jet direction the only leading-power contributions to the jet function from this region are soft.[1] Thus, we can apply the general amplitude-level factorization theorem to the operator $\bar{\psi}W_j$ to get

$$J^j \;\cong\; J^{R_j} \otimes J^{\overline{R_j}}_{\text{eik}} \tag{4.42}$$

This equation can be verified at 1-loop by comparing Eq. (4.40) with the combination of Eqs. (4.29), (4.37) and (4.41). Similarly,

$$J^j_{\text{eik}} \;\cong\; J^{R_j}_{\text{eik}} \otimes J^{\overline{R_j}}_{\text{eik}} \tag{4.43}$$

Therefore, convolving both sides of Eq. (4.38) with $J^{\overline{R_1}}_{\text{eik}}$ and $J^{\overline{R_2}}_{\text{eik}}$ gives

$$\frac{d\sigma}{d\tau} \otimes J^1_{\text{eik}} \otimes J^2_{\text{eik}} \cong H \times S \otimes J^1 \otimes J^2 \tag{4.44}$$

In this final form, all the dependence on Λ or R has been explicitly removed.

Finally, we want to isolate $\frac{d\sigma}{d\tau}$ from Eq. (4.44). To do this, we use that convolutions map to products in Laplace space. Taking the Laplace transform, Eq. (4.44) translates to

$$\int d\tau \frac{d\sigma}{d\tau} e^{-\nu\tau} \;\cong\; H\, \frac{\widetilde{S}(\nu)\widetilde{J}^1(\nu)\widetilde{J}^2(\nu)}{\widetilde{J}^1_{\text{eik}}(\nu)\widetilde{J}^2_{\text{eik}}(\nu)} \tag{4.45}$$

This form is in agreement with previously known expressions in the literature [72,97].

[1] One might be concerned about collinear singularities associated with the Wilson-line direction t_j^μ. However, since the measurement function forces $p\cdot n = \tau$, at small τ radiation cannot be collinear to both t_j^μ and the jet direction n^μ. Thus, radiation collinear to t_j^μ cannot contribute at leading power.

4.3.2 Jet broadening

The above discussion shows how the phase-space cutoffs separating collinear and soft radiation as well as the UV phase-space cutoff can be removed in the factorization formula for a particular observable (thrust). The derivation easily generalizes to many other observables. The key general property that was used is that the vanishing limit of the observable forces the phase space into the N-jet configuration at leading power. This allows the factorization theorem in Eq. (4.1) to be used to factorize the matrix-element squared in the full distribution. It also ensures that the dependence on the phase-space cutoffs is power suppressed, once the eikonal jet functions are included. For observables whose measurement function is not linear in each sector, the integrals will not be a simple convolution.

For a marginally different example, consider jet broadening [144–148]. (Total) jet broadening acting on a state $|X\rangle$ with particles of momenta p_j^μ has the eigenvalue

$$b(X) = \frac{1}{2Q} \sum_j \Omega_b(p_j), \qquad \Omega_b(p) = |\vec{p}_\perp| \tag{4.46}$$

where $\vec{p}_\perp$ are the components of the 3-momenta of the particles transverse to the thrust axis.

In the SCET literature, jet broadening is considered a SCET_II observable because soft emissions which are hard enough to recoil against collinear emissions contribute to jet broadening at leading power, while they are subleading power for thrust. More explicitly, for thrust only the small component of momentum $p^+ = n \cdot p$ contributes (for particles going in the n hemisphere). Thus collinear momenta, with $(p^-, p^+, p^\perp) \sim Q(1, \lambda, \lambda^2)$ and soft momenta with $p \sim Q\lambda^2$ contribute at the same order. Soft momenta scaling like $p \sim Q\lambda$ give a power-suppressed contribution to thrust.

For jet broadening, $p_\perp$ is measured. So collinear momenta contribute $p_\perp \sim Q\lambda$ and therefore soft momenta scaling like $p \sim Q\lambda$ are relevant at leading power making jet broadening a $\mathrm{SCET_{II}}$ observable.

From the point of view of the factorization as set up in [3] and [4], the soft scaling is unrelated to the collinear scaling. That is, the amplitude-level factorization formula, Eq. (4.1) holds for any relationship between the soft-scaling parameter, λ_s, and the collinear-scaling parameter, λ_c. $\mathrm{SCET_I}$ corresponds to $\lambda_s = \lambda_c^2$ and $\mathrm{SCET_{II}}$ to $\lambda = \lambda_c$. The relevant implication of the soft and collinear momenta having $p_\perp$ components of the same order is that configurations where soft particles recoil against collinear particles must be accounted for in the factorization theorem. The result is that the factorization formula has the form

$$\frac{d\sigma}{db} = H \int db_s db_1 db_2 d^2p_1^\perp d^2\vec{p}_2^\perp J^1(b_1, \vec{p}_1^\perp) J^2(b_2, \vec{p}_2^\perp) S(b_s, -\vec{p}_1^\perp, -\vec{p}_2^\perp) \delta(b - b_s - b_1 - b_2) \tag{4.47}$$

We can write this heuristically as

$$\frac{d\sigma}{db} \cong H \times J^1 \otimes J^2 \otimes S \tag{4.48}$$

with the understanding that $\otimes$ for jet broadening refers to the double convolution in Eq. (4.47).

With phase-space restrictions, these jet functions are given by

$$J^{R_1}(b, \vec{p}^\perp) = \sum_{X_1} \int d\Pi_{X_1} \left| \frac{\langle X_1 | \, \bar{\psi} W_1 \, | 0 \rangle}{\langle 0 | \, Y_1^\dagger W_1 \, | 0 \rangle} \right|^2 \delta\Big(b - b(X_1)\Big) \delta(Q - p_{X_1}^+) \delta(\vec{p}_\perp - \vec{p}_{X_1}^\perp) \tag{4.49}$$

and the soft function by

$$S^{\Lambda\overline{R}}(b,\vec{p}_1^{\,\perp},\vec{p}_2^{\,\perp}) = \sum_{X_s}\int d\Pi_X \left|\langle X_s|\, Y_1^\dagger Y_2\,|0\rangle\right|^2 \delta\Big(b-b(X_s)\Big)\left[\delta(\vec{p}_1^{\,\perp}-\vec{p}^{\,1}_{X_s})+\delta(\vec{p}_2^{\,\perp}-\vec{p}^{\,2}_{X_s})\right] \tag{4.50}$$

where $\vec{p}^{\,1}_{X_s}$ is the net $\perp$ momenta in the left hemisphere and $\vec{p}^{\,2}_{X_s}$ is the net $\perp$ momenta in the right hemisphere. As with thrust, these phase-space restricted functions will have overlapping UV-IR divergences and unwieldy dependence on the cutoffs R and Λ. However, as with thrust, we can convolve both sides of Eq. (4.48) with eikonal jet functions to get a factorization formula with only objects with no phase space cutoffs. The result in Laplace space is

$$\int db \frac{d\sigma}{db} e^{-\nu b} \cong H \int \mathrm{d}^2 x_L^\perp \mathrm{d}^2 x_R^\perp \, \frac{\widetilde{J}(x_L^\perp,\nu)\,\widetilde{J}(x_R^\perp,\nu)\,\widetilde{S}(x_L^\perp,x_R^\perp,\nu)}{\widetilde{J}_{\rm eik}(x_L^\perp,\nu)\,\widetilde{J}_{\rm eik}(x_R^\perp,\nu)} \tag{4.51}$$

Here, ν is the Laplace-conjugate variable to b and $x_1^\perp$ and $x_2^\perp$ are the Laplace conjugate variables to $p_1^\perp$ and $p_2^\perp$ respectively.

4.3.3 Comparison to other approaches

We have seen how phase-space cutoffs can be removed for certain inclusive observables if the double counting in the soft-collinear region is removed with an eikonal jet function. In this section, we would like to emphasize some conceptual differences in our derivation and previous ones and contrast with the literature.

First of all, it is easy to compare our results to those in traditional QCD, where the eikonal jet function first appeared. The final factorization formulas are identical. One difference is that in the early literature the eikonal jet functions were subtracted from the soft function rather than the jet function. From the point of view of the final

formula, there is no difference. However, conceptually our analysis makes it clear that the eikonal jet function should be subtracted from the jet function rather than the soft function. Indeed, the soft function is by itself infrared finite while the naive inclusive jet function (without the subtraction) is not. As shown explicitly in Eq. (4.40), the infrared divergences do not cancel between the real and virtual graphs for the jet function. With the subtraction the jet function is a well-defined and infrared safe object. The fact that the subtraction is more naturally applied in the collinear sector was also appreciated in [97].

The comparison to SCET is perhaps more illuminating than the comparison to traditional QCD. In the early days of SCET, calculations were mostly done in dimensional regularization (DR) and the overlapping of soft and collinear phase-space regions were not much discussed. In retrospect, it is easy to see why the correct answers result in DR without a subtraction: the eikonal jet functions, as in Eq. (4.36), give scaleless integrals in DR and thus formally vanish and can be ignored.

It is natural to be somewhat uncomfortable with setting scaleless but IR and UV divergent integrals to zero in DR. The mathematical justification notwithstanding, it is dangerous from a practical point of view if one hopes to extract an anomalous dimension from the poles in the jet and soft functions at $d = 4$. The only way it will work is if the object one computes is infrared finite. For infrared finite objects, all the poles are by definition UV. So setting $\frac{1}{\varepsilon_{\rm UV}} - \frac{1}{\varepsilon_{\rm IR}} = 0$ has no effect. As we have shown, the subtracted inclusive jet function is IR finite, so practically, one can ignore the subtraction in DR. Morally, though, to do this one must be able to show that the jet function is IR finite. Without the subtraction it is not. In this respect, the

success of SCET in pure DR was somewhat accidental.

The missing subtractions were understood in the classic paper on zero-bin subtraction by Manohar and Stewart [59]. These authors showed the the proper derivation of the effective Lagrangian for SCET involves binning the momenta into collinear momenta in different directions and soft momenta. The zero bin in each collinear sector should be formally excluded. In [59] it was shown that this exclusion amounts to the subtraction diagram-by-diagram of the soft-limit of the collinear momenta. In [97,108,109], this subtraction procedure was shown to be equivalent to the eikonal jet function subtraction of traditional QCD.

A somewhat different perspective comes from the method-of-regions multipole-expansion approach to SCET [49, 50, 130], as recently reviewed in [131]. In this approach, the soft-collinear subtraction and the extension of the soft integrals to $\Lambda = \infty$ are not discussed or needed. The basis of the argument is that the non-analytic dependence on the observable in each region is independent of the possible phase-space cutoffs. Since all the physics is in this non-analytic dependence, one can remove the cutoffs without consequence. For more details, see [130, 131].

4.4 Conclusion

In this chapter we have presented two new results. First, we have given a recursive formula for constructing amplitudes which agree with full QCD at leading power to all-loop order in any soft and collinear limit. The subtracted amplitudes we describe are matrix elements of fields and Wilson lines. Unlike with the amplitude-level factorization formula in [4], one does not have to specify whether the particles are soft or collinear ahead of time: the subtracted matrix elements will be correct in any limit. Although the amplitudes appear simpler than in full QCD (for example, the only interference effects from different directions involve gluons emitted off Wilson lines), it remains to be seen whether they can be integrated simply to provide a productive subtraction scheme. In our derivation of this formula, extensive use was made of the proof of factorization in [4].

Second, we showed how phase-space cutoffs can be removed when integrating a factorized amplitude squared against the measurement function for certain inclusive observables. Removing the cutoffs does two things: it overcounts the soft-collinear region and adds UV divergences to the phase-space integrals. These two effects can be compensated for by integrating the full QCD distribution against an eikonal jet function. This convolution can be easily disentangled, at least for thrust, jet broadening and angularities. This extends the results of amplitude-level factorization from [3] and [4] to the level of observables.

In our presentation, we have included explicit 1-loop expressions for soft and jet functions with cutoffs and for the eikonal jet function in a regularization scheme which separates UV from IR. These expressions confirm generally the qualitative analyses

that we have presented of the UV and IR structure of the integrals.

Although our final factorization formulas are not new, we believe our derivation is systematic and rigorous. We hope that the step-by-step procedure we have presented will be useful in future studies of factorization, where subtleties abound.

Chapter 5

Precision jet-substructure calculation

5.1 Introduction

The Large Hadron Collider (LHC) is exploring a new regime where the collision energy far exceeds the masses of known standard model particles. At such energies, heavy particles such as W/Z bosons and top quarks are often produced with large Lorentz boost factors, which leaves their hadronic decay products collimated into a single energetic "fat jet". Jet substructure techniques extract information from these fat jets to distinguish boosted heavy objects from the QCD background of jets initiated by light quarks and gluons. Examples of variables defined for this purpose include planar flow [155,156], jet angularities [156], pull [157], N-subjettiness [26,158], dipolarity [159], and angular correlations [160], with applications to boosted Higgs bosons [161], tops [155, 162], Ws [163] and quark versus gluon discrimination [164], along with many beyond the standard model applications (see [165, 166] for recent reviews). Jet substructure measurements are underway at the LHC [167, 168], but to

date, studies of the analyzing power of substructure variables have been limited by the use of leading-log shower Monte Carlo simulations. If higher-order QCD computations were available, one could use them to directly compare to experiments or test the accuracy of Monte Carlo simulations.

In this chapter, which follows the author and collaborators' paper [6], we develop a framework for performing jet substructure computations analytically, in the limit where the boosted object of interest has a large momentum Q. We find a mapping between global e^+e^- event shapes—which have been calculated to high precision—and jet substructure variables in the large Q limit, treating finite jet size, initial state radiation (ISR), and underlying event (UE) as $1/Q$ corrections. Concretely, we consider the jet substructure observable N-subjettiness $\mathcal{T}_N$ [26], which is the subjet version of the global event shape N-jettiness [153]. The ratio $\mathcal{T}_N/\mathcal{T}_{N-1}$ is a robust probe for N-prong decays [169], and compares favorably to other methods for boosted object identification.

Here, we focus on 1- and 2-subjettiness ($\mathcal{T}_1$ and $\mathcal{T}_2$), which are relevant for LHC searches involving W/Z and Higgs bosons. We compute the distribution for the ratio $\mathcal{T}_2/\mathcal{T}_1$ from $Z \to q\bar{q}$ decays to next-to-next-to-next-to-leading-log ($\mathrm{N^3LL}$) order, using ingredients from higher-order calculations of the classic e^+e^- thrust event shape [8, 9, 137, 138, 170–172]. From a calculational point of view, the use of this ratio is crucial, since it has a finite limit when $Q \to \infty$. We will show that our full subjet distribution is equal to the global distribution generated by the Z decay products, up to $1/Q$ power-suppressed corrections. The dominant hadronization corrections cause a shift which is encoded in a single Q-independent parameter. We compare

our substructure calculation to PYTHIA 8.150 [173] tune 4C and also use PYTHIAto demonstrate that the effects from the jet boundary and from external radiation (i.e. ISR and UE) are suppressed by $1/Q$, only entering at the 5% level for $Q \gtrsim 400\,\text{GeV}$.

5.2 Factorization formula for the cross section

We begin by considering a fat jet of size R (clustered with anti-k_T [174]) in a pp collision event. This jet should contain most of the Z decay products as well as some ISR/UE contamination. The jet momentum is $P_J^\mu = \sum_{j\in J} p_j^\mu$, where j runs over the four-vectors p_j^μ within the jet J. The jet boost Q is defined as $Q \equiv |\vec{P}_J|$. To calculate N-(sub)jettiness, we must specify a distance measure [26, 153, 169, 175], and we use the geometric measure

$$\mathcal{T}_N \equiv \min_{n_1,n_2,\ldots,n_N} \sum_{j\in J} \min\{n_1\cdot p_j, n_2\cdot p_j, \ldots, n_N\cdot p_j\}. \tag{5.1}$$

Here, $n_i^\mu = (1,\hat{n}_i)$ are lightlike axes defined by the overall minimization. The minimum inside the sum partitions the jet's constituents into subjet regions $J_1,\ldots,J_N$, defined by the axes n_i^μ. For the N-jettiness event shape, J is replaced by the entire event.

For 1-subjettiness, $\mathcal{T}_1 = \min_n \sum_{j\in J} n\cdot p_j$, which can also be written as the small component of the fat-jet momentum, $\mathcal{T}_1 = P^+ \equiv n\cdot P_J$. If the jet contained all the Z decay products and nothing else, $\mathcal{T}_1$ would depend only on the Z boson momentum P_Z^μ as:

$$\widehat{\mathcal{T}}_1 \equiv P_Z^+ = \sqrt{Q^2+m_Z^2} - Q. \tag{5.2}$$

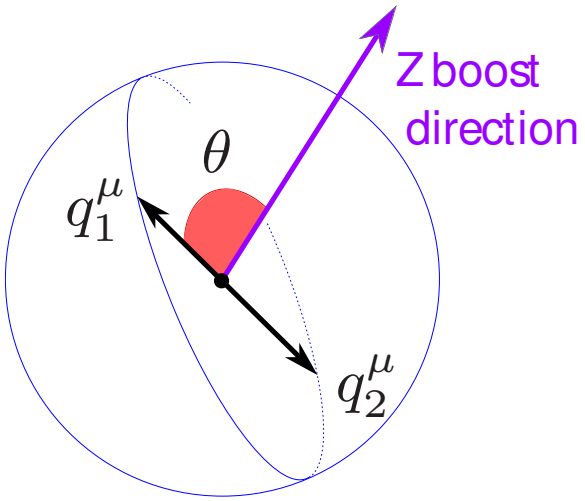

Figure 5.1: Kinematics of boosted Z decay.

Thus, the difference

$$\Delta\tau \equiv \mathcal{T}_1 - \widehat{\mathcal{T}}_1 \tag{5.3}$$

measures how much the Z is incorrectly reconstructed. We will use $\Delta\tau$ to correct for ISR/UE contamination.

Turning to 2-subjettiness, we first calculate the ratio $\mathcal{T}_2/\mathcal{T}_1$ including only the Z decay products, and then discuss how other effects can be systematically included. The distribution for the Z decay products is easily determined by boosting the Z rest frame distribution. At leading order, Z decays to a $q\bar{q}$ pair which go off back-to-back in the rest frame, at an angle θ (the *helicity angle*) with respect to the boost axis as in Fig. 5.1. For simplicity, we treat the Z as unpolarized with a flat θ distribution, but one could easily integrate over a different θ distribution, for example for Ws coming from top decays [162]. In the boosted frame, the Z momentum P_Z^μ and the

two daughter-quark momenta q_1^μ and q_2^μ are

$$\begin{aligned} P_Z^\mu &= \Big\{E_Q, 0, 0, Q\Big\}, \\ q_1^\mu &= \frac{1}{2}\Big\{E_Q - Q\cos\theta, -m_Z\sin\theta, 0, Q - \cos\theta E_Q\Big\}, \\ q_2^\mu &= \frac{1}{2}\Big\{E_Q + Q\cos\theta, m_Z\sin\theta, 0, Q + \cos\theta E_Q\Big\}, \end{aligned} \tag{5.4}$$

with $E_Q = \sqrt{m_Z^2 + Q^2}$. The quark energies are $E_1 = \frac{1}{2}(E_Q - Q\cos\theta)$ and $E_2 = \frac{1}{2}(E_Q + Q\cos\theta)$.

For the relevant small $\mathcal{T}_2$ region, the subjet directions from the minimization in (5.1) can be aligned with the leading-order quark directions [153]. Thus, we can take

$$n^\mu = (1, 0, 0, 1)\,, \qquad n_1^\mu = \frac{1}{E_1}q_1^\mu\,, \qquad n_2^\mu = \frac{1}{E_2}q_2^\mu\,, \tag{5.5}$$

where n^μ is the $\mathcal{T}_1$ axis and n_1^μ and n_2^μ are the $\mathcal{T}_2$ axes. In terms of the subjet masses m_i and energies E_i,

$$\mathcal{T}_2 = P_1^+ + P_2^+ \simeq \frac{m_1^2}{2E_1} + \frac{m_2^2}{2E_2}. \tag{5.6}$$

In the large Q limit, $E_1 \sim Q\sin^2(\theta/2)$, $E_2 \sim Q\cos^2(\theta/2)$, and $\mathcal{T}_1 \sim m_Z^2/(2Q)$, while m_i are Q independent. Thus the distribution of the ratio $\mathcal{T}_2/\mathcal{T}_1$ asymptotes to a fixed Q-independent result.

Now let us consider how the scaling with Q is affected when $\mathcal{T}_2/\mathcal{T}_1$ is considered in a realistic environment, such as at the LHC. A measurement of $\mathcal{T}_2/\mathcal{T}_1$ includes effects from having a finite jet boundary and from including radiation from elsewhere in the event. The jet boundary R identifies a Q-independent phase space region about the jet axis. As $Q \to \infty$, the phase space for the Z decay products to land outside of the cone falls as $1/Q$. Hence, the jet boundary is at most a $1/Q$ correction to $\mathcal{T}_2/\mathcal{T}_1$. The same conclusion holds if R is defined with a jet algorithm other than anti-k_T.

Next consider radiation not coming from the Z decay (i.e. ISR/UE). Since $\mathcal{T}_N$ depends linearly on p_j^μ in (5.1), both $\mathcal{T}_1$ and $\mathcal{T}_2$ will be distorted by (different) shifts due to this contaminating radiation. If we require the fat-jet mass to be close to m_Z, then the shifts will scale as $\mathcal{T}_N$, giving at most an $\mathcal{O}(Q^0)$ distortion of $\mathcal{T}_2/\mathcal{T}_1$. To turn this into a $1/Q$ distortion, note that the distribution of contaminating radiation is smooth over the fat jet, and at large Q,

$$n_{1,2}^\mu = n^\mu + \frac{m_Z}{Q}\Big\{ -\cot\frac{\theta}{2}, \tan\frac{\theta}{2}\Big\}\hat{e}_x^\mu + \mathcal{O}\Big(\frac{1}{Q^2}\Big), \tag{5.7}$$

where $\hat{e}_x^\mu = (0,1,0,0)$. Comparing $n\cdot p_j$ and $\min\{n_1\cdot p_j, n_2\cdot p_j\}$, both $\mathcal{T}_1$ and $\mathcal{T}_2$ will be shifted in the *same* way up to $1/Q$ corrections. Hence we can remove the leading effect of contamination with $\Delta\tau$ from (5.3), by defining

$$\tau_{2/1} \equiv \frac{\mathcal{T}_2 - \Delta\tau}{\mathcal{T}_1 - \Delta\tau}. \tag{5.8}$$

$\tau_{2/1}$ has two important properties: first, it is close to $\mathcal{T}_2/\mathcal{T}_1$ since $\tau_{2/1} = \mathcal{T}_2/\mathcal{T}_1$ if only the exact Z decay products are included; second, it is insensitive to jet contamination up to $1/Q$ corrections. It is crucial that the $\Delta\tau$ correction be made experimentally on an event-by-event basis; if only the $\mathcal{T}_2/\mathcal{T}_1$ distribution is measured, then the contamination will *not* be a $1/Q$ correction. The subtraction can be improved further by replacing $\Delta\tau$ with $\Delta\tau' \equiv \Delta\tau(1 - \frac{\pi}{2}m_Z/Q)$ in the numerator of (5.8); the additional factor accounts for the average fractional difference between $\mathcal{T}_2$ and $\mathcal{T}_1$ for uncorrelated soft radiation. The above logic is also appropriate for event pileup.

To compute the $\tau_{2/1}$ spectrum at leading order in $1/Q$, we calculate $\mathcal{T}_2/\mathcal{T}_1$ assuming only the Z decay products are included in the fat jet. We then average over the angle θ. Using the correspondence with 2-jettiness, the factorization formula for

$\mathcal{T}_2/\mathcal{T}_1$ is [153]

$$\frac{1}{\sigma_0}\frac{d\sigma}{d\tau_{2/1}} = H\int\frac{d\cos\theta}{2}\int ds_1 ds_2 dk_1 dk_2\, S(k_1,k_2,\{n_i\},\mu) \\ \times J(s_1,\mu)J(s_2,\mu)\,\delta\Big(\tau_{2/1}-\frac{k_1+k_2}{\widehat{\mathcal{T}}_1}-\frac{s_1E_2+s_2E_1}{2E_1E_2\widehat{\mathcal{T}}_1}\Big), \tag{5.9}$$

where σ_0 is the tree-level cross-section given by the Z decay rate. Here $H = H(m_Z,\mu)$, $J(s_i,\mu)$, and $S(k_1,k_2,\{n_i\},\mu)$ are respectively the $Z\to q\bar{q}$ hard function, inclusive jet function, and 2-jettiness soft function. H and J are known at $\mathcal{O}(\alpha_s^2)$ [176, 177]. For simplicity, we consider the narrow width limit, neglecting $\mathcal{O}(\Gamma_Z/m_Z)$ corrections. We also neglect non-singular corrections at $\mathcal{O}(\alpha_s)$. These contribute less than 5% in the peak of the $\tau_{2/1}$ distribution and can be included following [9, 138].

We now show that the 2-jettiness soft function S can be related to the hemisphere soft function $S_{\rm hemi}$—relevant for thrust and heavy jet mass—which is known perturbatively to $\mathcal{O}(\alpha_s^2)$ [121, 122]. The soft function is

$$S(k_1,k_2,n_1\cdot n_2,\mu,\Lambda) \equiv \frac{1}{N_c}\sum\nolimits_{X_s}\delta(k_1-n_1\cdot P_s^1) \\ \times\delta(k_2-n_2\cdot P_s^2)\,\langle 0|\,\overline{Y}_{n_2}^T Y_{n_1}\,|X_s\rangle\,\langle X_s|\,Y_{n_1}^\dagger\overline{Y}_{n_2}^*\,|0\rangle\,, \tag{5.10}$$

where the Y's are light-like Wilson lines and $P_s^{1,2}$ are the momenta of the subjets $J_{1,2}$ in the state $|X_s\rangle$. Rotational invariance implies that the subjet directions only appear in the combination $n_1\cdot n_2$, and the argument $\Lambda\equiv\Lambda_{\rm QCD}$ is a reminder of nonperturbative corrections contained in S. The hemisphere case corresponds to $n_1\cdot n_2 = 2$, so that $S_{\rm hemi}(k_L,k_R,\mu,\Lambda) = S(k_L,k_R,2,\mu,\Lambda)$. From (5.1), the partitioning into regions of 2-subjettiness is invariant under a common rescaling of the subjet direction, $n_1\to\beta n_1$ and $n_2\to\beta n_2$. So (5.10) satisfies

$$S(k_1,k_2,n_1\cdot n_2,\mu,\Lambda) = \beta^2 S(\beta k_1,\beta k_2,\beta^2 n_1\cdot n_2,\mu,\Lambda).$$

Choosing

$$\beta = \beta_\theta = \sqrt{\frac{2}{n_1 \cdot n_2}} = \frac{\sqrt{m_Z^2 + Q^2 \sin^2\theta}}{m_Z}, \tag{5.11}$$

we find

$$\begin{aligned} S(k_1, k_2, n_1 \cdot n_2, \mu, \Lambda) &= \beta_\theta^2 \, S\left(\beta_\theta k_1, \beta_\theta k_2, 2, \mu, \Lambda\right) \\ &= S_{\text{hemi}}\left(k_1, k_2, \mu/\beta_\theta, \Lambda/\beta_\theta\right) , \end{aligned} \tag{5.12}$$

where we have rescaled all dimensionful arguments by β_θ^{-1} and used the fact that S has mass dimension -2.

When $k_i \gg \Lambda/\beta_\theta$, the leading nonperturbative correction to S_{hemi} is equivalent to a shift [97, 178, 179], $k_i \to k_i - \Phi/\beta_\theta$, where $\Phi \sim \Lambda$ is Q-independent. Since $\mathcal{T}_2$ in (5.1) is not identical to thrust for massive hadrons, we cannot use the value found in [138]. All the objects in (5.9) have known renormalization group equations, so we can sum large logarithms of $\tau_{2/1}$ up to N^{3}LL (with a Padé approximation for the small contribution of the four-loop cusp anomalous dimension). Thus for $\tau_{2/1} \gg 2\Lambda/(\widehat{\mathcal{T}}_1 \beta_\theta)$ we have

$$\begin{aligned} \frac{1}{\sigma_0}\frac{d\sigma}{d\tau_{2/1}} &= \widehat{\mathcal{T}}_1^2 \int \frac{d\cos\theta}{2} H(m_Z, \mu_H) U_H(m_Z, \mu_H, \mu_J) \\ &\times \int dz_s \, ds_1 ds_2 J\big(s_1, \mu_J\big) J\big(s_2, \mu_J\big) S_\tau\Big(\widehat{\mathcal{T}}_1 z_s, \frac{\mu_S}{\beta_\theta}, \alpha_s(\mu_S)\Big) \\ &\times U_S^\tau\Big(\widehat{\mathcal{T}}_1 \tau_{2/1} - \frac{2\Phi}{\beta_\theta} - \frac{s_1}{2E_1} - \frac{s_2}{2E_2} - \widehat{\mathcal{T}}_1 z_s, \frac{\mu_J}{\beta_\theta}, \frac{\mu_S}{\beta_\theta}\Big). \end{aligned} \tag{5.13}$$

Here S_τ is the perturbative thrust soft function, and H, J, and S_τ are fixed-order expansions in $\alpha_s(\mu_H)$, $\alpha_s(\mu_J)$, and $\alpha_s(\mu_S)$ respectively. U_H and U_S^τ are evolution kernels which sum $\alpha_s^i \ln^j \tau_{2/1}$ terms. See [9] for details.

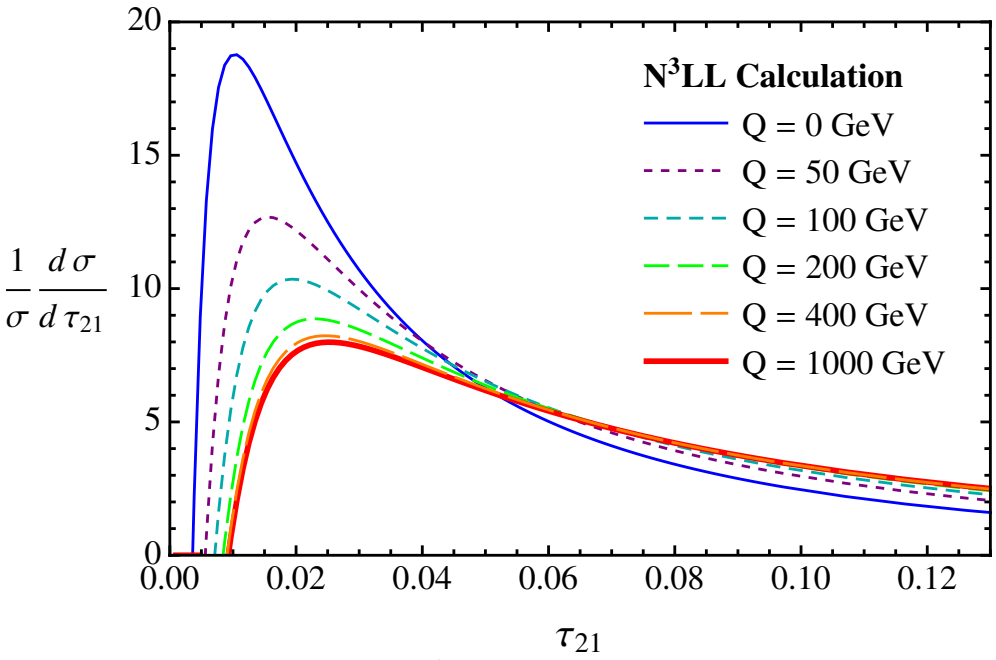

Figure 5.2: Results of the N^{3}LL analytic calculation for $\tau_{2/1}$ with $\Phi = 0$. The distribution saturates for $Q \gtrsim 400$ GeV.

The natural scale choices are

$$\mu_H = m_Z, \qquad \mu_J = \mu_Q \sqrt{\tau_{2/1}}, \qquad \mu_S = \mu_Q \, \tau_{2/1}. \tag{5.14}$$

Here $\mu_Q = \widehat{\mathcal{T}}_1 \sqrt{1 + Q^2/(2m_Z^2)}$ is an average over θ of $\widehat{\mathcal{T}}_1 \beta_\theta$ which appears in the large logarithms. For $Q = 0$ one has $\mu_Q = m_Z$, while for $Q \to \infty$ one has $\mu_Q = m_Z/(2\sqrt{2})$. We perform the $s_{1,2}$ and z_s integrations in (5.13) analytically and the θ integral numerically.

5.3 Results

Results for the $\tau_{2/1}$ distribution for various Q are shown in Fig. 5.2. As anticipated, the curves rapidly approach a fixed distribution at large Q.

In Fig. 5.3 we show a comparison to a "baseline" PYTHIA distribution, where the

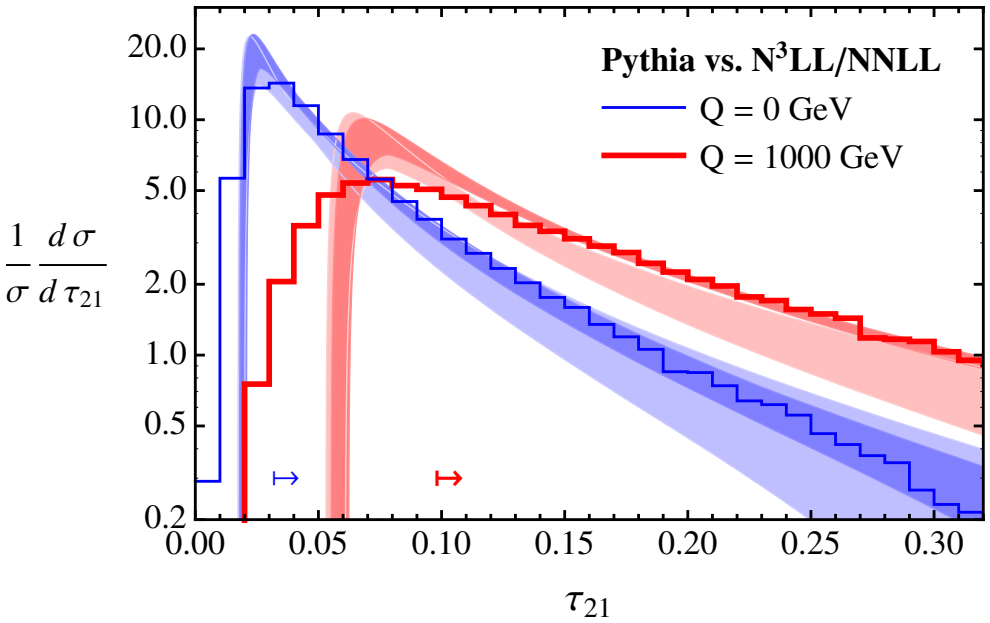

Figure 5.3: Comparison of theory prediction (bands) for $\tau_{2/1}$ to baseline PYTHIA(histograms). The heavier (lighter) band is N^{3}LL (NNLL), with widths given by factor of two variations of the hard, jet, and soft scales. Here, $\Phi = 700$ MeV. Arrows indicate the approximate range of validity of (5.13).

effects of hadronization are included but the Z width, finite cone size, and ISR/UE contamination have been turned off. For this comparison we fix $\Phi = 700$ MeV to match the peak of the $Q = 0$ PYTHIAdistribution, which allows us to compute the distribution for all $Q \neq 0$. In the tail of the distribution, there is excellent quantitative agreement. The accuracy of PYTHIA's tail is somewhat artificial since it was tuned to closely related e^+e^- thrust data at $Q = 0$. Predictions in the peak region require additional nonperturbative corrections, which could be included following [138].

In Fig. 5.4, we show the effect of a finite $R = 1.0$ cone and jet contamination in PYTHIA, restricting our attention to jets whose mass is within a 10 GeV window of m_Z. At large Q, the effect of an $R = 1.0$ cone is quite mild. While ISR/UE give a large distortion to $\mathcal{T}_2/\mathcal{T}_1$, this is successfully corrected in $\tau_{2/1}$ by the $\Delta\tau$ in (5.8).

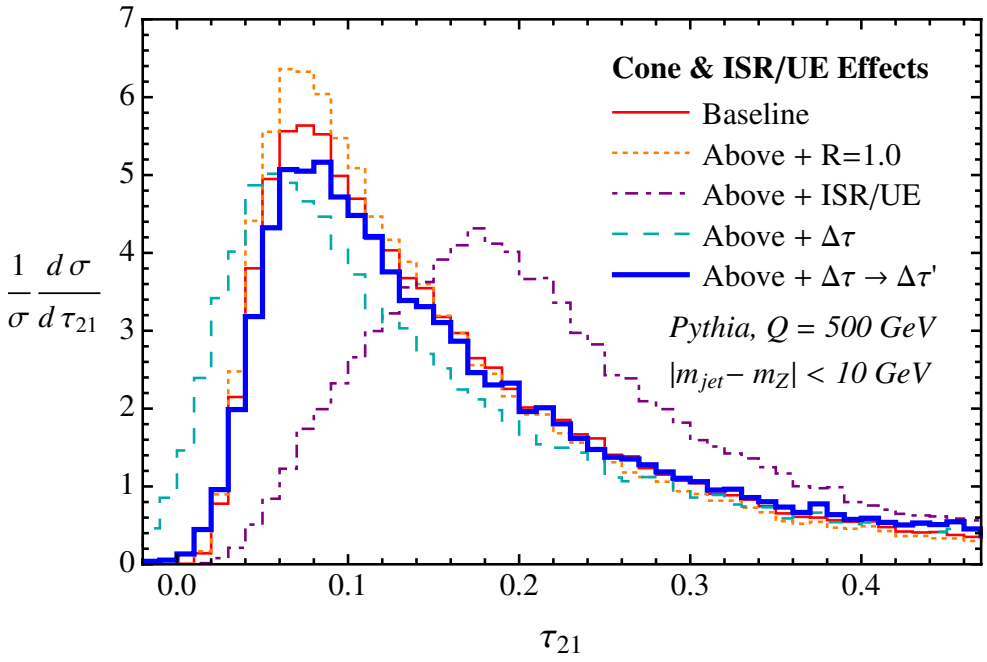

Figure 5.4: Effect of finite jet cone and ISR/UE in PYTHIA. The $\Delta\tau'$ correction mitigates ISR/UE jet contamination.

With the $\Delta\tau \to \Delta\tau'$ replacement we do even better. Using $\Delta\tau'$ for $Q = 1000\,\text{GeV}$, the PYTHIA$\tau_{2/1}$ distribution with $R = 1.0$/ISR/UE is indistinguishable at the 2% level from the baseline distribution shown in Fig. 5.3. Thus our analytic result agrees very well with the full PYTHIAdistribution.

We use PYTHIA to verify that the effects we have neglected in our calculation are indeed $1/Q$ suppressed. In Fig. 5.5, we plot the Kolmogorov-Smirnov D-statistic between the baseline PYTHIA distribution and PYTHIA as finite cone and ISR/UE effects are reinstated, as a function of Q. The D-statistic measures the maximum fractional difference between the cumulant $\tau_{2/1}$ distributions. Both finite cone and ISR/UE effects fall off as $1/Q$, and the corrections are $\lesssim 5\%$ for $Q \gtrsim 400$ GeV.

In the above calculation, we neglected the finite width of the Z boson, which

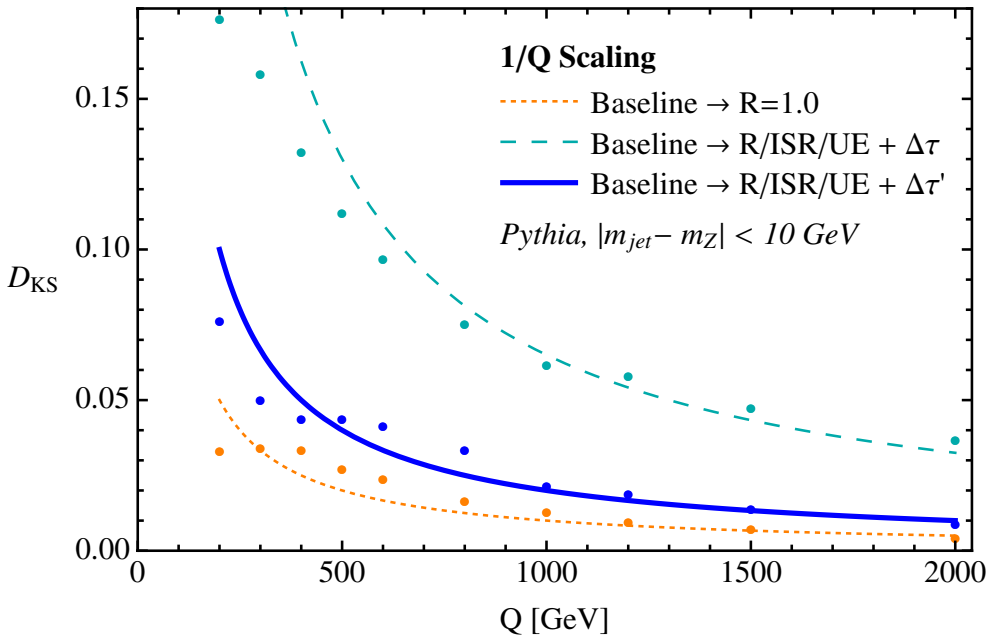

Figure 5.5: Fractional effect of adding finite cone and ISR/UE to the PYTHIA baseline distribution. With the $\Delta\tau'$ correction, these effects are smaller than 5% for $Q \gtrsim 400$ GeV, and scale as $1/Q$ as expected.

leads to $\mathcal{O}(\Gamma_Z/m_Z)$ corrections that are independent of Q. As shown in Fig. 5.6, finite width has only a small effect on the baseline distribution. Including $\Delta\tau$ yields a larger effect, since (5.3) assumed that all deviations from the Z pole were due to jet contamination and not Γ_Z. Nevertheless, we see in Fig. 5.6 that $\Delta\tau'$ still mitigates the effect of ISR/UE. Though beyond the scope of this letter, one can directly calculate $\tau_{2/1}$ with finite width effects.

It is interesting to explore analytically the Q dependence of our $d\sigma/d\tau_{2/1}$ (dropping cone and ISR/UE effects and taking $\Phi = 0$) by considering two extreme cases. In the Z rest frame $Q = 0$, $d\sigma/d\tau_{2/1}$ is equal to thrust $d\sigma/d\tau$. In the $Q \to \infty$ limit, $d\sigma/d\tau_{2/1}$ depends logarithmically on $\tau_{2/1}$ multiplied by various functions of the

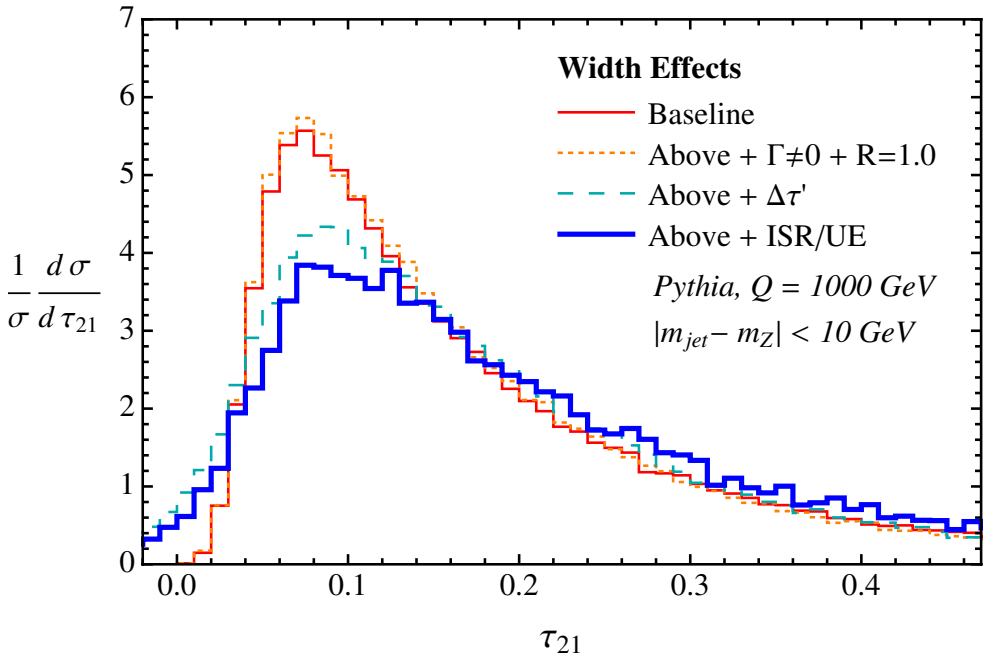

Figure 5.6: Effect of finite Z width.

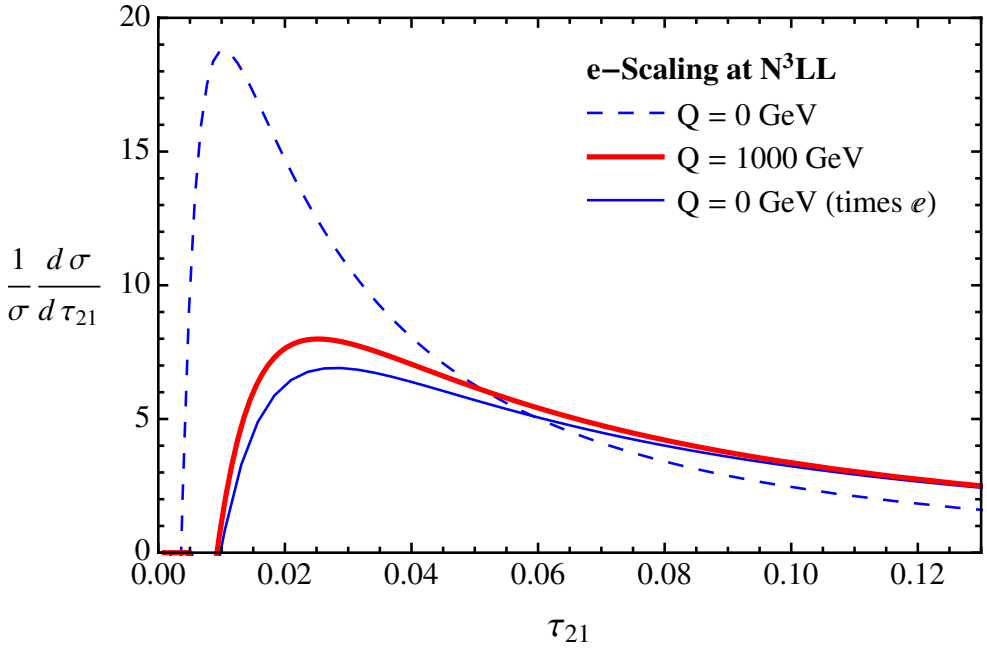

Figure 5.7: e-scaling between $Q = 0$ (thrust) and $Q = \infty$.

helicity angle θ. Isotropically averaging over θ, these logarithms behave as

$$\int \frac{d\cos\theta}{2}\, \log^n\left(\tau \sin^2\frac{\theta}{2}\right) = \log^n \frac{\tau}{e} + \mathcal{O}\big(\log^{n-2}\tau\big). \tag{5.15}$$

Thus, up to NLL order, the $Q \to \infty$ distribution is related to thrust by scaling by a factor of $e = 2.718...$,

$$\left.\frac{d\sigma}{d\tau_{2/1}}\right|_{Q\to\infty} = \frac{1}{e}\frac{d\sigma}{d\tau}(\tau = \tau_{2/1}/e)\,. \tag{5.16}$$

This is demonstrated in Fig. 5.7.

5.4 Conclusions

Our technique of treating the jet boundary and external radiation as $1/Q$ corrections can be readily generalized to color neutral objects with N-prong decays, and the known NNLL ingredients for the N-jettiness event shape [175] are a starting point for the calculation of N-subjettiness. It can also be used to compute the distribution of individual subjet masses m_i, which are directly accessible with the N-jettiness factorization theorem. Another straightforward generalization would be to incorporate massive final state quarks as in $H \to b\bar{b}$. To treat colored objects like boosted top quarks (or to calculate the QCD background from light quark and gluon jets) requires understanding the effect of final-state radiation on substructure observables, and we anticipate that expanding about the $Q \to \infty$ limit will be fruitful in that context as well.

Chapter 6

Conclusions

We have stated a precise formulation of factorization relevant to jet formation in collider physics and proven it at tree level in Ch. 2 and at all-loop order in Ch. 3. In Ch. 4 we showed how it can be used to calculate cross sections in terms of universal and completely factorized functions, whose renormalization group evolution can be used to sum large logarithms. These three chapters provide and rigorously justify a formalism for high-precision calculations in particle collisions. In Ch. 5 we apply this to a jet-substructure observable, 2-subjettiness, which can be used to discriminate jets based on the physics that seeded them. We calculate 2-subjettiness to next-to-next-to-next-to-leading logarithmic resummation accuracy, which shows how highly precise calculations can be done using factorization.

With the LHC starting up again this year, and decades of precision QCD ahead of it, now is the time to thoroughly understand factorization, the foundation of precision calculations. It seems increasingly likely that the next decade of particle collider physics will not witness new physics discoveries, but will be a decade of pinning down

Standard Model coupling constants and refining our understand of the phenomenology of QCD. We hope that the results presented in this thesis will be built upon and help in the endeavor to understand the rich structure of QCD and the Standard Model.

Bibliography

[1] Georges Aad *et al.*, Phys.Lett. **B716**, 1 (2012).

[2] Serguei Chatrchyan *et al.*, Phys.Lett. **B716**, 30 (2012).

[3] Ilya Feige and Matthew D. Schwartz, Phys.Rev. **D88**, 065021 (2013).

[4] Ilya Feige and Matthew D. Schwartz, Phys.Rev. **D90**, 105020 (2014).

[5] Ilya Feige, Matthew D. Schwartz, and Kai Yan, (2015).

[6] Ilya Feige, Matthew D. Schwartz, Iain W. Stewart, and Jesse Thaler, Phys.Rev.Lett. **109**, 092001 (2012).

[7] S. Catani, L. Trentadue, G. Turnock, and B.R. Webber, Nucl.Phys. **B407**, 3 (1993).

[8] Matthew D. Schwartz, Phys.Rev. **D77**, 014026 (2008).

[9] Thomas Becher and Matthew D. Schwartz, JHEP **0807**, 034 (2008).

[10] Yang-Ting Chien and Matthew D. Schwartz, JHEP **1008**, 058 (2010).

[11] Thomas Becher and Guido Bell, JHEP **1211**, 126 (2012).

[12] Jui-Yu Chiu, Ambar Jain, Duff Neill, and Ira Z. Rothstein, JHEP **1205**, 084 (2012).

[13] Daniel de Florian and Massimiliano Grazzini, Phys.Lett. **B674**, 291 (2009).

[14] Valentin Ahrens, Thomas Becher, Matthias Neubert, and Li Lin Yang, Phys.Lett. **B698**, 271 (2011).

[15] Nikolaos Kidonakis and George F. Sterman, Nucl.Phys. **B505**, 321 (1997).

[16] Eric Laenen, Gianluca Oderda, and George F. Sterman, Phys.Lett. **B438**, 173 (1998).

[17] Thomas Becher and Matthew D. Schwartz, JHEP **1002**, 040 (2010).

[18] Thomas Becher, Christian Lorentzen, and Matthew D. Schwartz, Phys.Rev. **D86**, 054026 (2012).

[19] Thomas Becher, Christian Lorentzen, and Matthew D. Schwartz, Phys.Rev.Lett. **108**, 012001 (2012).

[20] Nikolaos Kidonakis and Richard J. Gonsalves, Phys.Rev. **D87**, 014001 (2013).

[21] Matteo Cacciari, Michal Czakon, Michelangelo Mangano, Alexander Mitov, and Paolo Nason, Phys.Lett. **B710**, 612 (2012).

[22] Valentin Ahrens, Andrea Ferroglia, Matthias Neubert, Ben D. Pecjak, and Li Lin Yang, Phys.Lett. **B703**, 135 (2011).

[23] Yang-Ting Chien, Randall Kelley, Matthew D. Schwartz, and Hua Xing Zhu, Phys.Rev. **D87**, 014010 (2013).

[24] Mrinal Dasgupta, Kamel Khelifa-Kerfa, Simone Marzani, and Michael Spannowsky, JHEP **1210**, 126 (2012).

[25] Teppo T. Jouttenus, Iain W. Stewart, Frank J. Tackmann, and Wouter J. Waalewijn, (2013).

[26] Jesse Thaler and Ken Van Tilburg, JHEP **1103**, 015 (2011).

[27] Stefano Catani and Massimiliano Grazzini, Nucl.Phys. **B570**, 287 (2000).

[28] R. Keith Ellis, Howard Georgi, Marie Machacek, H. David Politzer, and Graham G. Ross, Phys.Lett. **B78**, 281 (1978).

[29] R. Keith Ellis, Howard Georgi, Marie Machacek, H. David Politzer, and Graham G. Ross, Nucl.Phys. **B152**, 285 (1979).

[30] D. Amati, R. Petronzio, and G. Veneziano, Nucl.Phys. **B140**, 54 (1978).

[31] D. Amati, R. Petronzio, and G. Veneziano, Nucl.Phys. **B146**, 29 (1978).

[32] Zvi Bern, Lance J. Dixon, David C. Dunbar, and David A. Kosower, Nucl.Phys. **B425**, 217 (1994).

[33] Zvi Bern, Vittorio Del Duca, William B. Kilgore, and Carl R. Schmidt, Phys.Rev. **D60**, 116001 (1999).

[34] Zoltan Nagy and Davison E. Soper, JHEP **0309**, 055 (2003).

[35] Lance J. Dixon, Lorenzo Magnea, and George F. Sterman, JHEP **0808**, 022 (2008).

[36] Thomas Becher and Matthias Neubert, Phys.Rev.Lett. **102**, 162001 (2009).

[37] Einan Gardi and Lorenzo Magnea, JHEP **0903**, 079 (2009).

[38] B.I. Ermolaev, M. Greco, and S.I. Troyan, Eur.Phys.J. **C72**, 1953 (2012).

[39] Ruth Britto, Freddy Cachazo, Bo Feng, and Edward Witten, Phys.Rev.Lett. **94**, 181602 (2005).

[40] Nima Arkani-Hamed *et al.*, (2012).

[41] Stephen B. Libby and George F. Sterman, Phys.Rev. **D18**, 3252 (1978).

[42] George F. Sterman, Phys.Rev. **D17**, 2773 (1978).

[43] John C. Collins, Davison E. Soper, and George F. Sterman, Adv.Ser.Direct.High Energy Phys. **5**, 1 (1988).

[44] John C. Collins, Davison E. Soper, and George F. Sterman, Nucl.Phys. **B308**, 833 (1988).

[45] L.D. Landau, Nucl.Phys. **13**, 181 (1959).

[46] Christian W. Bauer, Sean Fleming, and Michael E. Luke, Phys.Rev. **D63**, 014006 (2000).

[47] Christian W. Bauer, Sean Fleming, Dan Pirjol, and Iain W. Stewart, Phys.Rev. **D63**, 114020 (2001).

[48] Christian W. Bauer, Dan Pirjol, and Iain W. Stewart, Phys.Rev. **D65**, 054022 (2002).

[49] M. Beneke, A.P. Chapovsky, M. Diehl, and T. Feldmann, Nucl.Phys. **B643**, 431 (2002).

[50] M. Beneke and T. Feldmann, Phys.Lett. **B553**, 267 (2003).

[51] Simon M. Freedman and Michael Luke, Phys.Rev. **D85**, 014003 (2012).

[52] Simon M. Freedman, (2013).

[53] Yang-Ting Chien, Matthew D. Schwartz, David Simmons-Duffin, and Iain W. Stewart, Phys.Rev. **D85**, 045010 (2012).

[54] Randall Kelley and Matthew D. Schwartz, Phys.Rev. **D83**, 045022 (2011).

[55] Iain W. Stewart, Frank J. Tackmann, and Wouter J. Waalewijn, PoS **LL2012**, 058 (2012).

[56] Stefano Catani, Daniel de Florian, and German Rodrigo, JHEP **1207**, 026 (2012).

[57] D.R. Yennie, Steven C. Frautschi, and H. Suura, Annals Phys. **13**, 379 (1961).

[58] B.I. Ermolaev and Victor S. Fadin, JETP Lett. **33**, 269 (1981).

[59] Aneesh V. Manohar and Iain W. Stewart, Phys.Rev. **D76**, 074002 (2007).

[60] Steven Weinberg, Phys.Rev. **135**, B1049 (1964).

[61] Christian W. Bauer, Oscar Cata, and Grigory Ovanesyan, (2008).

[62] Guido Altarelli and G. Parisi, Nucl.Phys. **B126**, 298 (1977).

[63] Christian W. Bauer and Matthew D. Schwartz, Phys.Rev. **D76**, 074004 (2007).

[64] Christian W. Bauer and Matthew D. Schwartz, Phys.Rev.Lett. **97**, 142001 (2006).

[65] S. Coleman and R.E. Norton, Nuovo Cim. **38**, 438 (1965).

[66] John C. Collins and George F. Sterman, Nucl.Phys. **B185**, 172 (1981).

[67] Ashoke Sen, Phys.Rev. **D24**, 3281 (1981).

[68] Ashoke Sen, Phys.Rev. **D28**, 860 (1983).

[69] John C. Collins and Davison E. Soper, Nucl.Phys. **B193**, 381 (1981).

[70] Sunil Mukhi and George F. Sterman, Nucl.Phys. **B206**, 221 (1982).

[71] Nikolaos Kidonakis, Gianluca Oderda, and George F. Sterman, Nucl.Phys. **B525**, 299 (1998).

[72] Carola F. Berger, Tibor Kucs, and George F. Sterman, Phys.Rev. **D68**, 014012 (2003).

[73] George F. Sterman and Maria E. Tejeda-Yeomans, Phys.Lett. **B552**, 48 (2003).

[74] S. Mert Aybat, Lance J. Dixon, and George F. Sterman, Phys.Rev. **D74**, 074004 (2006).

[75] V.N. Gribov and L.N. Lipatov, Sov.J.Nucl.Phys. **15**, 438 (1972).

[76] L.N. Lipatov, Sov.J.Nucl.Phys. **20**, 94 (1975).

[77] Yuri L. Dokshitzer, Sov.Phys.JETP **46**, 641 (1977).

[78] Howard Georgi and H. David Politzer, Phys.Rev. **D9**, 416 (1974).

[79] D.J. Gross and Frank Wilczek, Phys.Rev. **D9**, 980 (1974).

[80] G. Curci, W. Furmanski, and R. Petronzio, Nucl.Phys. **B175**, 27 (1980).

[81] W. Furmanski and R. Petronzio, Phys.Lett. **B97**, 437 (1980).

[82] S. Moch, J.A.M. Vermaseren, and A. Vogt, Nucl.Phys. **B688**, 101 (2004).

[83] Guido Altarelli, R. Keith Ellis, and G. Martinelli, Nucl.Phys. **B157**, 461 (1979).

[84] Zvi Bern and Gordon Chalmers, Nucl.Phys. **B447**, 465 (1995).

[85] David A. Kosower, Nucl.Phys. **B552**, 319 (1999).

[86] A. Bassetto, M. Ciafaloni, and G. Marchesini, Phys.Rept. **100**, 201 (1983).

[87] Stefano Catani and Massimiliano Grazzini, Nucl.Phys. **B591**, 435 (2000).

[88] Claude Duhr and Thomas Gehrmann, Phys.Lett. **B727**, 452 (2013).

[89] Ye Li and Hua Xing Zhu, JHEP **1311**, 080 (2013).

[90] S. Catani, B.R. Webber, and G. Marchesini, Nucl.Phys. **B349**, 635 (1991).

[91] S. Catani and L. Trentadue, Nucl.Phys. **B327**, 323 (1989).

[92] Roberto Bonciani, Stefano Catani, Michelangelo L. Mangano, and Paolo Nason, Phys.Lett. **B575**, 268 (2003).

[93] A. Bassetto, M. Ciafaloni, G. Marchesini, and Alfred H. Mueller, Nucl.Phys. **B207**, 189 (1982).

[94] F. Fiorani, G. Marchesini, and L. Reina, Nucl.Phys. **B309**, 439 (1988).

[95] M. Dasgupta and G.P. Salam, Phys.Lett. **B512**, 323 (2001).

[96] A. Banfi, G. Marchesini, and G. Smye, JHEP **0208**, 006 (2002).

[97] Christopher Lee and George F. Sterman, Phys.Rev. **D75**, 014022 (2007).

[98] George F. Sterman, (1994).

[99] John Collins, (2011).

[100] Jr. Grammer, G. and D.R. Yennie, Phys.Rev. **D8**, 4332 (1973).

[101] Aneesh V. Manohar, Phys.Rev. **D68**, 114019 (2003).

[102] Miguel Garcia-Echevarria, Ahmad Idilbi, and Ignazio Scimemi, Phys.Rev. **D84**, 011502 (2011).

[103] Valentin Ahrens, Thomas Becher, Matthias Neubert, and Li Lin Yang, Eur.Phys.J. **C62**, 333 (2009).

[104] Valentin Ahrens, Andrea Ferroglia, Matthias Neubert, Ben D. Pecjak, and Li Lin Yang, JHEP **1009**, 097 (2010).

[105] Thomas Becher, Matthias Neubert, and Ben D. Pecjak, JHEP **0701**, 076 (2007).

[106] Randall Kelley and Matthew D. Schwartz, Phys.Rev. **D83**, 033001 (2011).

[107] Christian W. Bauer, Bjorn O. Lange, and Grigory Ovanesyan, JHEP **1107**, 077 (2011).

[108] Ahmad Idilbi and Thomas Mehen, Phys.Rev. **D76**, 094015 (2007).

[109] Ahmad Idilbi and Thomas Mehen, Phys.Rev. **D75**, 114017 (2007).

[110] John C. Collins, Adv.Ser.Direct.High Energy Phys. **5**, 573 (1989).

[111] Christian W. Bauer, Sean Fleming, Dan Pirjol, Ira Z. Rothstein, and Iain W. Stewart, Phys.Rev. **D66**, 014017 (2002).

[112] Zvi Bern, Vittorio Del Duca, and Carl R. Schmidt, Phys.Lett. **B445**, 168 (1998).

[113] A. Gehrmann-De Ridder, T. Gehrmann, E.W.N. Glover, and G. Heinrich, JHEP **0711**, 058 (2007).

[114] James Currie, E.W.N. Glover, and Steven Wells, JHEP **1304**, 066 (2013).

[115] Vittorio Del Duca, Alberto Frizzo, and Fabio Maltoni, Nucl.Phys. **B568**, 211 (2000).

[116] Mrinal Dasgupta, Alessandro Fregoso, Simone Marzani, and Gavin P. Salam, JHEP **1309**, 029 (2013).

[117] Randall Kelley, Matthew D. Schwartz, and Hua Xing Zhu, (2011).

[118] Kamel Khelifa-Kerfa, JHEP **1202**, 072 (2012).

[119] Jonathan R. Walsh and Saba Zuberi, (2011).

[120] Randall Kelley, Matthew D. Schwartz, Robert M. Schabinger, and Hua Xing Zhu, Phys.Rev. **D86**, 054017 (2012).

[121] Andrew Hornig, Christopher Lee, Iain W. Stewart, Jonathan R. Walsh, and Saba Zuberi, JHEP **1108**, 054 (2011).

[122] Randall Kelley, Matthew D. Schwartz, Robert M. Schabinger, and Hua Xing Zhu, Phys.Rev. **D84**, 045022 (2011).

[123] Randall Kelley, Jonathan R. Walsh, and Saba Zuberi, JHEP **1209**, 117 (2012).

[124] Matthew D. Schwartz and Hua Xing Zhu, (2014).

[125] Andrew J. Larkoski, Ian Moult, and Duff Neill, (2015).

[126] Simon Caron-Huot, (2015).

[127] Kamel Khelifa-Kerfa and Yazid Delenda, (2015).

[128] F. Bloch and A. Nordsieck, Phys.Rev. **52**, 54 (1937).

[129] Ratindranath Akhoury, Michael G. Sotiropoulos, and George F. Sterman, Phys.Rev.Lett. **81**, 3819 (1998).

[130] M. Beneke and Vladimir A. Smirnov, Nucl.Phys. **B522**, 321 (1998).

[131] Thomas Becher, Alessandro Broggio, and Andrea Ferroglia, (2014).

[132] Simone Alioli and Jonathan R. Walsh, JHEP **1403**, 119 (2014).

[133] S. Frixione, Z. Kunszt, and A. Signer, Nucl.Phys. **B467**, 399 (1996).

[134] Zoltan Kunszt and Davison E. Soper, Phys.Rev. **D46**, 192 (1992).

[135] S. Catani and M.H. Seymour, Nucl.Phys. **B485**, 291 (1997).

[136] A. Gehrmann-De Ridder, T. Gehrmann, and E.W. Nigel Glover, JHEP **0509**, 056 (2005).

[137] Edward Farhi, Phys.Rev.Lett. **39**, 1587 (1977).

[138] Riccardo Abbate, Michael Fickinger, Andre H. Hoang, Vicent Mateu, and Iain W. Stewart, Phys.Rev. **D83**, 074021 (2011).

[139] Carola F. Berger and George F. Sterman, JHEP **0309**, 058 (2003).

[140] Andrew Hornig, Christopher Lee, and Grigory Ovanesyan, JHEP **0905**, 122 (2009).

[141] G. Parisi, Phys.Lett. **B74**, 65 (1978).

[142] John F. Donoghue, F.E. Low, and So-Young Pi, Phys.Rev. **D20**, 2759 (1979).

[143] André H. Hoang, Daniel W. Kolodrubetz, Vicent Mateu, and Iain W. Stewart, (2015).

[144] Paul E.L. Rakow and B.R. Webber, Nucl.Phys. **B191**, 63 (1981).

[145] R. Keith Ellis and B.R. Webber, Conf.Proc. **C860623**, 74 (1986).

[146] S. Catani, G. Turnock, and B.R. Webber, Phys.Lett. **B295**, 269 (1992).

[147] Jui-yu Chiu, Ambar Jain, Duff Neill, and Ira Z. Rothstein, Phys.Rev.Lett. **108**, 151601 (2012).

[148] Thomas Becher, Guido Bell, and Matthias Neubert, Phys.Lett. **B704**, 276 (2011).

[149] Thomas Becher, Matthias Neubert, and Gang Xu, JHEP **0807**, 030 (2008).

[150] Nikolaos Kidonakis and J.F. Owens, Int.J.Mod.Phys. **A19**, 149 (2004).

[151] Richard J. Gonsalves, Nikolaos Kidonakis, and Agustin Sabio Vera, Phys.Rev.Lett. **95**, 222001 (2005).

[152] Nikolaos Kidonakis, Phys.Part.Nucl. **45**, 714 (2014).

[153] Iain W. Stewart, Frank J. Tackmann, and Wouter J. Waalewijn, Phys.Rev.Lett. **105**, 092002 (2010).

[154] Jui-yu Chiu, Andreas Fuhrer, Andre H. Hoang, Randall Kelley, and Aneesh V. Manohar, Phys.Rev. **D79**, 053007 (2009).

[155] Jesse Thaler and Lian-Tao Wang, JHEP **0807**, 092 (2008).

[156] Leandro G. Almeida *et al.*, Phys.Rev. **D79**, 074017 (2009).

[157] Jason Gallicchio and Matthew D. Schwartz, Phys.Rev.Lett. **105**, 022001 (2010).

[158] Ji-Hun Kim, Phys.Rev. **D83**, 011502 (2011).

[159] Anson Hook, Martin Jankowiak, and Jay G. Wacker, (2011).

[160] Martin Jankowiak and Andrew J. Larkoski, JHEP **1106**, 057 (2011).

[161] Jonathan M. Butterworth, Adam R. Davison, Mathieu Rubin, and Gavin P. Salam, Phys.Rev.Lett. **100**, 242001 (2008).

[162] David E. Kaplan, Keith Rehermann, Matthew D. Schwartz, and Brock Tweedie, Phys.Rev.Lett. **101**, 142001 (2008).

[163] Yanou Cui, Zhenyu Han, and Matthew D. Schwartz, Phys.Rev. **D83**, 074023 (2011).

[164] Jason Gallicchio and Matthew D. Schwartz, Phys.Rev.Lett. **107**, 172001 (2011).

[165] A. Abdesselam *et al.*, Eur.Phys.J. **C71**, 1661 (2011).

[166] A. Altheimer *et al.*, J.Phys. **G39**, 063001 (2012).

[167] Serguei Chatrchyan *et al.*, JHEP **1209**, 029 (2012).

[168] Georges Aad *et al.*, JHEP **1205**, 128 (2012).

[169] Jesse Thaler and Ken Van Tilburg, JHEP **1202**, 093 (2012).

[170] S. Catani, G. Turnock, B.R. Webber, and L. Trentadue, Phys.Lett. **B263**, 491 (1991).

[171] Gregory P. Korchemsky and George F. Sterman, Nucl.Phys. **B555**, 335 (1999).

[172] Sean Fleming, Andre H. Hoang, Sonny Mantry, and Iain W. Stewart, Phys.Rev. **D77**, 074010 (2008).

[173] Torbjorn Sjostrand, Stephen Mrenna, and Peter Z. Skands, Comput.Phys.Commun. **178**, 852 (2008).

[174] Matteo Cacciari, Gavin P. Salam, and Gregory Soyez, JHEP **0804**, 063 (2008).

[175] Teppo T. Jouttenus, Iain W. Stewart, Frank J. Tackmann, and Wouter J. Waalewijn, Phys.Rev. **D83**, 114030 (2011).

[176] T. Matsuura, S.C. van der Marck, and W.L. van Neerven, Nucl.Phys. **B319**, 570 (1989).

[177] Thomas Becher and Matthias Neubert, Phys.Lett. **B637**, 251 (2006).

[178] Yuri L. Dokshitzer and B.R. Webber, Phys.Lett. **B404**, 321 (1997).

[179] Andre H. Hoang and Iain W. Stewart, Phys.Lett. **B660**, 483 (2008).